

Study, Design and Fabrication of 3D Carbon Electrodes for Cell Separation Using Dielectrophoresis

THESIS

Submitted in the partial fulfillment of the requirements for the degree of
DOCTOR OF PHILOSOPHY

by

**PARIDHI PURI
(2012PHXF0422P)**

Under the Supervision of

Dr. SACHIN ULHASRAO BELGAMWAR

Department of Mechanical Engineering
Birla Institute of Technology & Science Pilani, Pilani Campus
Pilani– 333 031 (Rajasthan)

Co- Supervision

Prof. NITI NIPUN SHARMA

Department of Mechanical Engineering
School of Automobile, Mechanical & Mechatronics Engineering
Manipal University, Jaipur – 303 007 (Rajasthan)



BITS Pilani
Pilani | Dubai | Goa | Hyderabad

**BIRLA INSTITUTE OF TECHNOLOGY & SCIENCE
PILANI – 333 031 (RAJASTHAN) INDIA**

2020

Dedicated

to

my parents

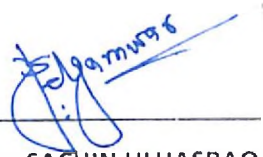
my in-laws & my husband 'Vijay'

BIRLA INSTITUTE OF TECHNOLOGY AND SCIENCE, PILANI

CERTIFICATE

This is to certify that the thesis entitled **Study, Design and Fabrication of 3D Carbon Electrodes for Cell Separation Using Dielectrophoresis** and submitted by **Paridhi Puri** ID No **2012PHXF0422P** for award of Ph.D. of the Institute embodies original work done by him/her under my supervision.

Signature of the Supervisor: _____



Name in capital letters : Dr. SACHIN ULHASRAO BELGAMWAR

Designation : Assistant Professor
Department of Mechanical Engineering
Birla Institute of Technology and Science
PILANI-333031

Date: 24/01/2020

Signature of the Co-supervisor: _____



Name in capital letters : PROF. NITI NIPUN SHARMA

Designation : Pro-President
Department of Mechanical Engineering
Manipal University, JAIPUR-303007

Date: 24/01/2020

ACKNOWLEDGEMENT

This thesis would not have been possible without the support of many people. Many thanks to my supervisor **Dr. Sachin U. Belgamwar** and my co-supervisor **Prof. N.N. Sharma**, for the guidance and support they has provided throughout the course of this research. Their advices have been inspiring and motivating, and the words of encouragement have always been a strong support especially in difficult moments.

I am immensely thankful to **Prof. Souvik Bhattacharyya**, Vice-Chancellor, BITS-Pilani; **Prof. Sudhirkumar Barai**, Director, BITS-Pilani, Pilani Campus. I express my gratitude to **Prof. Srinivas Krishnaswamy** (Dean, Academic Graduate Studies & Research Division); **Prof. Jitendra Panwar** (Associate Dean, Academic Graduate Studies & Research Division); BITS-Pilani, Pilani Campus for their constant and official support and encouragement.

My sincere thanks to **Prof. Mani Sankar Dasgupta** (Head of the Department, Mechanical Engineering), **Dr. Prabhat N. Jha** (Head of the Department, Biological Science) for his support during completion of the research work. I am grateful to the entire faculty and staff of Mechanical Engineering Department for their kind support and assistance.

I thanks **Prof. Kuldip Singh Sangwan** (Chief, Central Placement Unit); Doctoral Research Committee (DRC); my Doctoral Advisory Committee (DAC) members; who gave their precious time to provide suggestions that immensely helped in improving the quality of my PhD thesis.

I would also like to express my gratitude to all the technical staff, especially to Sh. Yadav and Sh. Ashok for providing me the electrical equipment and support.

I am immensely grateful to **Prof. K.N. Bhat**, Visiting Professor, Indian Institute of Science, Bangalore for allowing me to use the MEMS fabrication facility. I express my gratitude to **Dr. Ajay Agarwal** (Sr. Principal Scientist, Coordinator, Smart Sensors Area, & Head of Nano Biosensors Group at CSIR-Central Electronics Engineering Research) for lending me the syringe pump, because of which I was able to finish my all experimental work. I also

thank **Dr. Jaspreet Singh** (Dead of MEMS Fabrication Division, SCL, Mohali) for allowing me to use MEMS fabrication facility.

My endless thanks to my friends **Dr. Neha Arora, Ms. Shivani Nain, Dr. Tamalika B. Ms. Ritika Sharma, Ms. Vidushi Asati, Ms. Zaiba Khan, Ms. Chetna Sangwan, Dr. Rahul Prajesh** and my aunty **Mrs. Neelam Bhatia** who endured this long process with me, always offering support and care.

I would like to thanks **Mr. Santosh Kumar Saini** (Academic Under-graduate Studies Division) for his help in assembling of my thesis.

Finally, I would like to thanks my lovable family, my sister **Ms. Suvidhi Puri** and my brother **Mr. Kapil Puri** and my in-laws for their everlasting support and care through my life. In particular I must acknowledge my husband **Dr. Vijay Kumar** a deepest gratitude for his understanding, endless patience and encouragement for completion of my thesis.

Paridhi Puri

Biological sample analysis is a costly and time-consuming process. It involves highly trained technicians operating large and expensive instruments in a temperature and dust controlled environment. In the world of rising healthcare cost, the drive towards a more cost-effective solution calls for a point-of-care device that performs accurate analyses of human blood samples. To achieve this goal, today's bulky laboratory instruments need to be scaled down and integrated on a single microchip of only a few square centimeters or millimeters in size.

Dielectrophoresis (DEP), a phenomenon where particles are manipulated by non-uniform electric fields, stands to feature prominently in the point-of-care device. An original device that enhances DEP effect through novel geometry of the electrodes is presented. When activated with sinusoidal waveforms, the novel shaped electrodes generate non uniform bands of electric fields on the surface of the microchip. With these bands of electric fields, particles can be separated and eluted out. Experimental results showing the collection, separation, and transportation of yeast cells are presented. With capabilities for high throughput cell trapping, the novel microchip device delivers substantial improvements over the existing DEP designs. The research presented here explores the novel electrode geometry in cell trapping fabricated using an inexpensive screen printing technique.

Chapter 1 introduces the problem statement and discusses in detail about the phenomenon of DEP along with the governing equations. The motivation of the present work is also discussed at the end of the chapter.

Chapter 2, provides an overview of the state-of-the-art of different 2D and 3D metal and carbon electrode structures used in various dielectrophoretic microfluidic devices. Detail review of various electrode types fabricated with convention lithography and pyrolysis techniques and non-conventional screen printing method is carried out and arranged chronologically to study the evolution of carbon electrodes. At the end the scope of the present work towards realizing a cost effective and high throughput method is discussed.

Chapter 3, we present the simulation results to provide us a better understanding of the particle behaviour in the proposed channel. Since, the heart of any DEP device is a set of

electrodes producing a high gradient electric field that drives particles by DEP, therefore some of the commonly used electrode designs have been simulated using COMSOL and the field gradient results have been compared.

Chapter 4. details the fabrication of C-Serpentine electrodes that are fabricated using gold and conventional micro-fabrication technology. We have also discussed the steps involved in preparing sample of viable and non-viable yeast cells. Followed are the test results that are obtained in trapping of both the cell populations.

Chapter 5. elaborates the fabrication of carbon electrodes. The principal component, i.e the microelectrodes, were constructed via screen printing process. The fabrication of DEP device entirely of glass is discussed in detail. The biocompatibility of the conductive carbon ink is also tested.

Finally conclusion for all experimental work is given in Chapter 6 with scope for future work.

CONTENTS	Page No.
Acknowledgement	i-ii
Abstract	iii-iv
Table of Contents	v-ix
List of Figures	x-xiii
List of Tables	xiv-xv
List of Abbreviations	xvi-xvii
List of Symbols	xviii
CHAPTER 1 Introduction	1-16
1.1 General Introduction	1
1.2 Dielectrophoresis	4
1.3 Theory	5
1.4 Dielectrophoretic microfluidic devices	10
1.5 Motivation	10
<i>References</i>	13
CHAPTER 2 Literature Review	17-74
2.1 General Introduction	17
2.2 Metal Electrodes	18
2.2.1 Two dimensional 2D planar electrodes	18
2.2.1.1. Pin electrode	18
2.2.1.2 Interdigitated electrodes	20
2.2.1.3. Castellated electrodes	26
2.2.1.4. Polynomial electrodes	29
2.2.1.5 Angled or Slanted electrodes	33
2.2.1.6. Other planar designs	35
2.2.2 Three Dimensional 3D Electrodes	39
2.2.2.1 Top-Bottom electrode pattern	39
2.2.2.2 Extruded electrodes	42

CONTENTS	Page No.
2.2.2.3 Sidewall patterned electrodes	44
2.3 Carbon electrodes	45
2.3.1 C-MEMS	46
2.3.1.1 Three dimensional 3D carbon electrodes	49
2.3.2 Screen Printing	54
2.4 Gaps in Existing Research and Investigations	57
2.5 Organization of the Thesis	59
<i>References</i>	61
CHAPTER 3 Dielectrophoresis Modeling	75-96
3.1 General Introduction	75
3.2 Various Electrode Geometries and Their Electric Field Simulations	76
3.3 Simulation in Circular Geometry	80
3.3.1 Effect of variation in channel width	83
3.3.2 Effect of variation in channel height	84
3.4 C-Serpentine Geometry	85
3.4.1 Electric field distribution	86
3.4.2 Effect of variation in channel width	87
3.4.3 Effect of variation in channel height	88
3.5 MATLAB Modeling	89
3.6 Conclusion	93
<i>References</i>	95
CHAPTER 4 Dielectrophoretic Trapping with Microfabricated Gold Electrodes	97-136
4.1 General Introduction	97
4.2 Experimental Details	98
4.2.1 Mask design	98
4.2.2 Fabrication details	98

CONTENTS	Page No.
4.2.2.1 Cleaning and sample preparation	99
4.2.2.2 Thermal oxidation	101
4.2.2.3 Gold deposition	101
4.2.2.4 Lithography	101
4.2.2.5 Cr/Au etching	102
4.2.2.6 SU-8 coating and microchannel patterning	103
4.2.2.7 Channel closing with glass substrate	103
4.2.2.8 Chrome patterning	104
4.2.2.9 Glass dicing and drilling	105
4.2.2.10 Bonding of both substrates	105
4.2.2.11 Wire bonding	106
4.2.3 Yeast Cells	107
4.2.3.1. The science of yeast cells	107
4.2.3.2 Sample preparation	108
4.3 Testing and Characterization of the DEP Device	111
4.4. Results and Discussion	113
4.4.1 Dead cells	114
4.4.2 Live cells	116
4.4.3 Mixture of live and dead cell	117
4.5 Device Efficiency	118
4.5.1 Adding methylene blue dye	119
4.5.2. Dilution of sample	119
4.5.3. Preparing the hemocytometer	119
4.5.4. Counting yeast cells in the centre square of cytometer	119
4.5.4.1. Counting dead and live cells (Input)	120
4.5.4.2 Counting input cell density in cell mixture	123
4.5.4.3 Counting dead and live cells (Output)	123

CONTENTS	Page No.
4.5.4.3.1 Dead cells	123
4.5.4.3.2 Live cells	127
4.5.4.4 Estimation of Cell Viability	130
4.5.4.5. Cell Mixture	132
4.6 Conclusions	133
<i>References</i>	136
CHAPTER 5 Dielectrophoretic Trapping with Printed Carbon Electrodes	137-168
5.1 General Introduction	137
5.2. Conductive Carbon Inks	139
5.3 Experimental Details	140
5.3.1 Mask design	141
5.3.2 Fabrication details	142
5.3.2.1 Cleaning and substrate preparation	142
5.3.2.2 Carbon electrode printing	143
5.3.2.3 SU-8 coating and patterning	145
5.3.2.4 Chrome patterning on top glass substrate	146
5.3.2.5 Chrome etching	146
5.3.2.6 Glass dicing and drilling	147
5.3.2.7 Bonding of both substrates	148
5.3.2.8 Wire bonding	149
5.3.2.9 Cell preparations	149
5.4 Testing and Characterization of the DEP Device	149
5.5. Results and Discussion	150
5.5.1. Electrical characterization	151
5.5.2 Dead cells	152
5.5.3 Live cells	152
5.5.4 Mixture of live and dead cells	153

CONTENTS	Page No.
5.6 Device Efficiency	155
5.6.1 Counting dead cells (Output)	155
5.6.2 Counting live cells (Output)	158
5.6.3 Viability test	161
5.6.4 Counting cells in mixture	162
5.7 Biocompatibility Test of Carbon Ink	164
5.8 Conclusions	165
<i>References</i>	167
CHAPTER 6 Overall Conclusion and Future Scope	169-172
6.1 Overall Conclusion	169
6.2 Future Scope	172
Appendix I	173-177
Appendix II	178-190
Appendix III	191
List of Publications	192-193
Brief biography of the Candidate	194
Brief biography of the Supervisor	195
Brief biography of the Co-Supervisor	196

Figure No.	Title	Page No.
1.1	Kidney “Natural Filtering Organ	2
1.2	Schematic of the polarization of a spherical particle in a dielectric medium in a uniform and non uniform electric field	9
2.1	Classification of electrodes	18
2.2	Pin electrodes (a) Pin-plate configuration, (b) Pin-pin configuration	19
2.3	Interdigitated electrode	20
2.4	Castellated electrodes (a) Off-Set configuration (b) Set configuration	26
2.5	Polynomial electrode	30
2.6	Angled electrode	33
2.7	Other planar designs (a) Curved electrodes, (b) Electrode array, (c) Triangular electrode, (d) Dot electrodes, (e) Trapezoidal electrode.	36
2.8	Pie chart representation of various 2D electrode configurations	39
2.9	Top-Bottom patterned electrodes	40
2.10	Extruded gold electrode post	43
2.11	Sidewall patterned electrode	44
2.12	C-MEMS process flow (a) Spin coating of photoresist of desired thickness (b) Exposure to UV light to pattern the resist (c) Photoresist pyrolysis (d) Carbon posts	47
2.13	Carbon electrode posts	49
2.14	Schematic of screen printing technique	54
2.15	Pie chart representation of 3D electrode geometries reported in DEP	57
3.1	Different electrode geometries (a) Saw tooth electrodes (Set), (b) Saw tooth electrodes (Offset), (c) Castellated electrodes (Set), (d) Castellated electrodes (Offset), (e) Bell shaped electrodes (Set), (f) Bell shaped electrodes (Offset), (g) Circular electrode	76
3.2	Electric gradient distribution in Set type electrode geometry (a) Saw tooth, (b) Circular electrode, (c) Rectangular electrode (d) Bell shaped electrode	77
3.3	Electric gradient distribution in Off-set electrode geometry (a) Saw tooth, (b) Circular electrode, (c) Rectangular electrode (d) Bell shaped electrode	78
3.4	(a) Circular channel geometry, (b) $Re[K]$ as a function of frequency (SET-A) $\sigma_p=0.95$, (SET-B) $\sigma_p=0.01$	80
3.5	Particles with (a) p-DEP (b) n-DEP behavior	82

List of Figures

Figure No.	Title	Page No.
3.6	Stepwise representation of particle separation of two sets of particles	82
3.7	Particle separation in circular channel of different widths (a) 1mm, (b) 500 μm and (c) 200 μm	83
3.8	Particle separation in circular channel of different heights (a) 20 μm , (b) 15 μm and (c) 10 μm	84
3.9	C-Serpentine device schematic diagram	85
3.10	(a) Electric field gradient distribution (b) Expanded view	86
3.11	Particle separation in C-Serpentine channel of different widths (a) 1mm, (b) 500 μm and (c) 200 μm	87
3.12	Particle separation in C-Serpentine of different heights (a) 20 μm , (b) 15 μm and (c) 10 μm	88
3.13	Two-shell model of a yeast cell.	89
3.14	Plot of $\text{Re}[K(\omega)]$ vs. frequency for live yeast cells	92
3.15	Plot of $\text{Re}[K(\omega)]$ vs. frequency for dead yeast cells	92
4.1	Mask Layout of DEP Device (a) Mask#1 Electrode Mask (a) Mask#2 Microchannel Mask.	99
4.2	Schematic cross section view of the fabrication flow of gold electrode based DEP device	100
4.3	Gold Electrode (a) Pattern after developing, (b) Pattern after gold etching, (c) Complete fabricated gold electrode	102
4.4	SU-8 pattern DEP device	103
4.5	Chrome pattern on glass substrate	104
4.6	Glass bond DEP device (a) Air trapping in the channel (b) Glass bonded sample with no air traps	106
4.7	Fabricated DEP Device (a) With Inlet/Outlet fabrication (b) Wire bonded fabricated device.	107
4.8	Diagrammatic representation of <i>Saccharomyces Cerevisiae</i>	107
4.9	Cell preparation (a) Adding 1gm yeast in to YPD nutrient media (b) Media after addition of yeast.	109
4.10	Incubation of yeast cells at 30°C for overnight	110
4.11	Turbid media, with yeast cells at bottom, (b) Pallet of yeast cells in 280 mM mannitol	110
4.12	(a) Heat treatment to yeast cells and (b) Dead cells stained with methylene blue	111

Figure No.	Title	Page No.
4.13	Experimental set-up	112
4.14	Hemocytometer (a) Sample loading (b) Counting chambers (c) Zoomed view of centre square	113
4.15	Streaming and trapping of the dead cells in microchannel	115
4.16	Live cells trapping in microchannel	116
4.17	Clausius-Mossotti plot of Live (green) and Dead (blue line) yeast cells	117
4.18	(a) Trapping of dead cells at 350 kHz, (b) Trapping of live cells at 700 kHz	118
4.19	Hemocytometer centre square	120
4.20	Microscopic view of dead and live yeast cells at five different chambers in hemocytometer	121
4.21	Cells under microscope at 10X and 40X view	124
4.22	Microscopic view of dead cells in five different chambers of hemocytometer	125
4.23	Dead cells: Efficiency per run	127
4.24	Microscopic view of live cells in five different chambers of hemocytometer	128
4.25	Live cells: Efficiency per run	130
5.1	Composition of conductive inks	140
5.2	Mask Layout of DEP Device (a) Mask#1 Electrode Mask (b) Mask#2 Microchannel Mask.	142
5.3	Schematic cross section view of the fabrication flow of carbon electrode based DEP device	144
5.4	(a) Screen printing machine (b) Stencil mask pattern (c) Conductive carbon ink	145
5.5	Devices with SU-8 microchannels	146
5.6	Chrome patterning on glass substrate	147
5.7	Drilled glass substrates	147
5.8	Glass bonded DEP device with inlet/outlet holes	148
5.9	Wire bonded carbon DEP device	149
5.10	Experimental Set-up	150
5.11	Resistance measurement using four probe IV-CV system	151
5.12	Dead cell trapping in carbon DEP device	152

List of Figures

Figure No.	Title	Page No.
5.13	Live cell trapping in carbon DEP device	153
5.14	Trapping of cells in mixture	154
5.15	Microscopic view of dead cells in five different chambers of hemocytometer	156
5.16	Dead cells: Efficiency per run	158
5.17	Microscopic view of live cells in five different chambers of hemocytometer	159
5.18	Live cells: Efficiency per run	161
5.19	(a) Control, (b) Test (c,d) Growth after 14 hrs, (e,f) 20 hrs, (g,h) 25 hrs	165

Table No.	Title	Page No.
3.1	Electric field gradient for different electrode configuration with 5 Vp-p actuation voltage (the distance between electrodes was 200 μm)	80
3.2	Simulation parameters	81
3.3	The values of the radius (r), electric conductivity (σ), and permittivity (ϵ) for each layer of live and dead yeast cells	90
4.1	Dead and live cells count (Input)	120
4.2	Live and dead cell count in cell mixture (Input)	123
4.3	Dead cells count (Output)	124
4.4	Device efficiency using dead cells	126
4.5	Live cells count (Output)	127
4.6	Device efficiency for each run with live cells	129
4.7	Trapped cell count	131
4.8	Percentage of viable cells	131
4.9	Cell count at 350 kHz	132
4.10	Device efficiency for each run	132
4.11	Cell count at 700 kHz	133
4.12	Device efficiency for each run	133
5.1	Dimensions of different screen printed carbon test structures	141
5.2	Test structures and their resistance value	151
5.3	Dead cell count in different runs	155
5.4	Cell density and device efficiency in different runs	157
5.5	Live cell count in different runs	158
5.6	Cell density and device efficiency in different runs	160
5.7	Trapped cell count	161
5.8	Percentage of viable cells	162
5.9	Cell count in each run (300 kHz)	162
5.10	Device efficiency for each run	163

List of Tables

Table No.	Title	Page No.
5.11	Cell count in each run (700 kHz)	163
5.12	Device efficiency for each run (700 kHz)	164

List of Abbreviations

Abbreviations	Explanation
Ass	Avg. number of cells in small square of hemocytometer
AC	Alternating Current
CM factor	Clausius-mossotti factor
CNC	Computer numerical control
C-MEMS	Carbon-MEMS
C-DEP	Carbon- Dielectrophoresis
CAN	Ceric ammonium nitrate
DEP	Dielectrophoresis
DNA	Deoxyribonucleic acid
DACS	Dielectrophoresis assisted cell sorting
DC	Direct current
DI water	De-ionized water
DF	Dilution factor
ESC's	Embryonic stem cells
E.coli	Escherichia coli
FEA	Finite element analysis
HSV-1	Herpes simplex virus type 1
HDMS	Hexamethyldisilazane
LOC	Lab on a chip
MEMS	Microelectromechanical systems
MWCNTs	Multi walled carbon nanotubes
MB	Methylene blue
MEK	Methyl ethyl ketone
μ TAS	Micro total analysis system
n-DEP	Negative Dielectrophoresis
NEMS	Nanoelectromechanical systems
p-DEP	Positive Dielectrophoresis
PDMS	Polydimethylsiloxane

List of Abbreviations

PCR	Polymerize chain reaction
PS	Polystyrene
Re[K]	Real component of clausius mossotti factor
RNA	Ribonucleic acid
rRNA	Ribosomal ribonucleic acid
RBCs	Red blood cells
RF gel	Resorcinol formaldehyde gel
rpm	Revolutions per minute
SWNTs	Single walled carbon nanotubes
SAM	Self assembled monolayer
TMV	Tobacco mosaic virus
2D	Two dimensional
3D	Three dimensional
UV	Ultraviolet
V _{ss}	Volume of small square of hemocytometer
WBCs	White blood cells
YPD	Yeast extract, peptone and dextrose

Symbols	Explanation
a	radius of particle
ϵ_m	permittivity of medium
ϵ_p	permittivity of particle
E_{rms}	root mean square of electric field
ϵ_m^*	complex permittivity of medium
ϵ_p^*	complex permittivity of particle
ω	frequency of applied electric field
σ_m	conductivity of medium
σ_p	conductivity of particle
σ_m^*	complex conductivity of medium
σ_p^*	complex conductivity of particle
V_{p-p}	peak to peak voltage of applied signal
F_{DEP}	dielectrophoretic force
E	electric field
V	voltage
d	distance between electrodes
Q	flow rate
A	channel area
ϵ_1^*	complex permittivity of cell wall
ϵ_2^*	complex permittivity of cell membrane
ϵ_3^*	complex permittivity of nucleus
r_1	radius of cell wall
r_2	radius of cell membrane
r_3	radius of nucleus

1.1 General Introduction

Nature around us exemplifies itself with constitution of problems of extremities and in providing their amazing simple solution. For example, when too many nutrients are available in the sea, phytoplanktons may grow out of control and can cause harmful algal blooms. These blooms can produce extremely toxic compounds that have harmful effect on fishes, mammals, and even humans. Also, rapid plankton growth in sea water is a sign of excess carbon dioxide loading. Difficulty to this extreme has a simple solution i.e. the sea creatures like shrimps, snails, and jellyfish act as filter feeders which means that they feed by filtering the planktons out of the water through slits in their membranes. This helps in maintaining a balance in the ecosystem. Let us take another very interesting example from human body that is of kidneys which acts as a natural dialyzing organ in the body and helps in filtering toxins and waste from the bloodstream. As shown in Figure 1.1, the dirty blood enters the kidneys through renal artery (red in colour, as shown in Figure 1.1) and passes through the structure of the kidneys called as superfilters or nephrons where the waste products and excess water is separated from the blood stream. After filtration, the pure blood with only the essential nutrients is send back to the body through renal vein (blue in colour, as shown in Figure 1.1) and the waste is sent out from the kidneys through ureter tubes.

This function of the kidneys is vital to life because the blood that enters the kidney has a great variety of materials in it. Some minerals are essential to human life, while others are harmful to life. If the harmful elements remain in blood, they would cause illness or even death. Blood passing through the kidneys is dialyzed to separate essential compounds from harmful compounds. But, sometimes a person's kidney may be damaged by disease or physical injury and they are no longer able to dialyze blood properly. In this case, we try to mimic natural dialyzing mechanism using artificial means i.e. by using a dialyzing machine. This helps a person to live a little longer. In nature also, many compounds and elements aren't found in their pure form, but are found as part of mixtures. However, scientific research in cellular and molecular biology as

well as diagnostics and therapy in clinical practices often requires a large number of single-type cells. Thus, rapid and high-throughput cell sorting and separation from complex, heterogeneous mixtures are strongly desirable. Unfortunately, conventional techniques that are used for separation such as flow cytometry or fluorescence-activated cell sorting suffer restrictions in popularization due to their high cost, bulky instrumentation, and complicated operation (for example, immunolabeling).

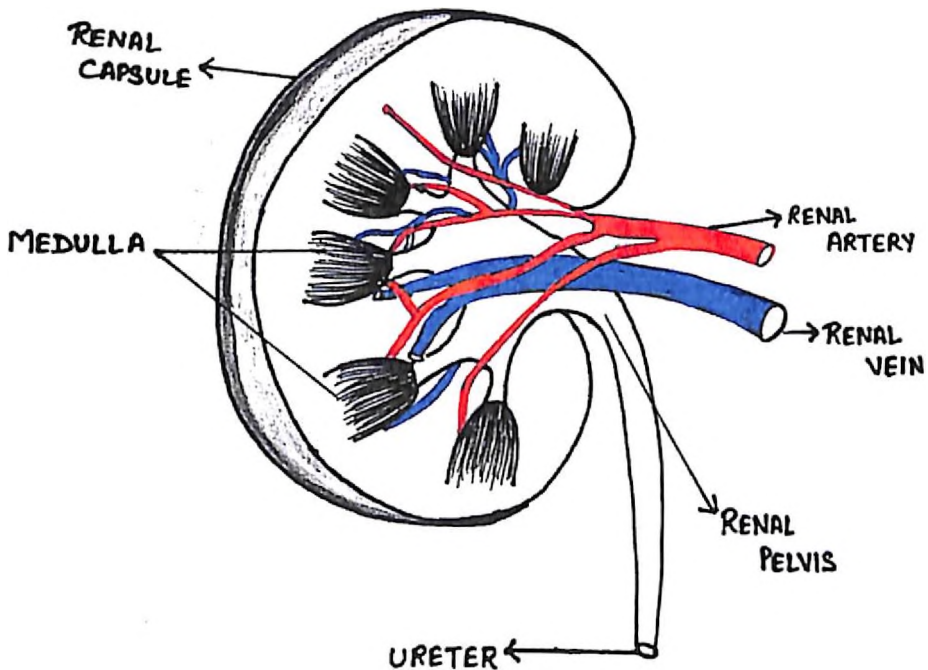


Figure 1.1: Kidney “Natural Filtering Organ”

A promising alternative lies in the lab-on-a-chip systems that works on a microfluidic scale and utilize a multitude of inherent cellular properties to isolate different cell populations. In 1958, scientists developed the first trial silicon chip [1], by arranging a huge number of microscopic transistors onto a single silicon chip, which lead to remarkable improvements in all aspects of technology. This also led to the *Information Revolution*. Later on, researchers found that mechanical devices can also be miniaturized and batch fabricated, promising the same benefits to the mechanical world, which results in the strong trend towards miniaturizing equipment for chemical analysis and synthesis until today [2]. The obvious advantages are lower cost consumption, shorter response time, less pollution, better process control *etc.* This trend is strengthened by the development of lithography based microtechnology, which fabricates laboratory

functions on a single chip of only few millimeters to centimeter in size. This is the *Lab-on-a-chip* (LOC) concept, and is often indicated as *Micro Total analysis system* (μ TAS) as well. Recently, as nanotechnology progresses, research in LOC systems is extended towards fluid handling of nanoparticles as single-walled carbon nanotubes (SWNTs), proteins, DNA and virus [3]–[6].

Today cell manipulation instruments are prevalent in all facilities that deal with biological samples (biosamples). However, even the most advanced laboratory today is still depended on large and expensive instruments that deal with biosamples in bulk. Macroscale cell manipulations have some very prohibitive disadvantages for example, dealing with large sample size requires large and expensive testing instruments that only a few laboratories can afford and also it requires large sample size which is a limitation when dealing with biological fluids. Therefore, the automation of miniaturized instruments will mean a boon to health network.

As one of the earliest applications of microfluidic devices, separation, manipulation and deposition of cells and particles with small size differences, constantly attract great research interest in analytical chemistry. Various strategies based on different principles are employed, for example, mechanical (filters [7] , micropipettes etc), magnetical [8], optical [9] and electrical (electro-osmosis, electrophoresis, dielectrophoresis) [10] separation methods. Each method has its own advantages and disadvantages and is therefore suitable for certain application field. Traditional cell separation methods that include using filters, micropipettes and centrifuges are dependent on size and density of the cells. These types of separation methods are often associated with some disadvantages, such as low precision, separation for a long time, complicate to operate and a larger effect on cell activity. Other separation methods like electrophoresis, fluorescence and magnetic activated cell sorting, requires the cells to be charged or modified with some magnetic and fluorescent material. Attachments on the cell produced in the preprocessing of separation are difficult to be removed and greatly influence the cell activity. In addition, the complex operations can only be completed by some sophisticated equipments such as hydrocyclone and flow cytometry instrument, which make it expensive and inaccessible. There are two commonly implemented methodologies amongst the electrical systems that can be incorporated in microfluidics devices. The most common one is known as electrophoresis, that uses electric fields to

control the motions of charged particles and the other is known as dielectrophoresis (DEP), that utilizes non-uniform electric fields to manipulate self-polarizable particles. In this work, we have focused our research on DEP associated microfluidic systems. There are several advantages associated when DEP is used for particle manipulations. First of all, DEP utilizes non-uniform electric field to manipulate self-polarized particles; therefore, particles require no prior treatments before performing any investigations. Second, DEP forces are precisely controlled using applied electric fields that can be adjusted by tuning the amplitudes, frequencies and phases of the applied electric potentials and enables accurate controlling of particles. Also, the magnitudes and directions of DEP forces, which are related to the particles properties, are suitable to be employed for manipulating particles in varying applications, such as sorting and trapping. In addition, DEP-microfluidic systems are low cost experimental platforms that can be conveniently fabricated.

Interestingly, DEP device miniaturization has been beneficial in improving the effectiveness of DEP. Devices with microscale electrodes allows for production of more pronounced non-uniform electric fields. Since, high fields can be generated by use of low voltage power supplies instead of high voltage power supplies, safety is improved. The sheer size of early DEP devices having machined electrodes produced appreciable heating, particularly in aqueous solutions, due to the high voltages needed to accomplish dielectrophoresis [11].

The thesis will begin by discussing the basic principles of DEP, and why it is the manipulation method best suited for the cell clinics chip. Various electrode geometries used for performing Dielectrophoresis will also be discussed. Finally, we will conclude the introduction by giving a brief motivation for undertaking this study. In this dissertation, each chapter begins with a literature review that frames the work relevant to that chapter; therefore this will not be included in the introduction as it is typically done.

1.2 Dielectrophoresis

The term Dielectrophoresis originated from the word Electrophoresis, but does not require a particle to be charged. DEP is a separation phenomenon in which particles are segregated or separated according to their interaction with a non-uniform electric field. A non-uniform electric field is generated by using electrodes of appropriate geometry or by

placing insulating posts between the pair of electrodes. Unlike electrophoresis where only dc voltages are used, either an ac signal or a dc voltage can be employed in DEP to distinguish different particles in a sample. By changing the frequency of the applied signal, a dipole moment is induced in a particle and causes the particle to experience a positive dielectrophoretic movement or a negative dielectrophoretic movement and thereby allowing it to move into a region of high potential or low potential respectively. The term DEP was first used to describe the motion of particles in non-uniform fields by Pohl [12]. Some initial devices used by Pohl to generate the non-uniform electric fields were fabricated by placing a wire in the center of a glass tube in which another wire was wrapped along the inner wall of the glass tube [13]. These devices required high potentials and were limited to analysis of particles 1 μm in diameter or larger due to joule heating effects which led to brownian movement that countered DEP force [11].

DEP is an established technique for particle manipulation. Although first demonstrated in the 1950s, it was not until the development of miniaturization techniques in the 1990s that DEP became a popular research field. The 1990s saw an abundance of DEP publications using microfabricated metal electrode arrays to sort a wide variety of cells. The concurrent development of microfluidics enabled devices for flow management and better understanding of the interaction between hydrodynamic and electrokinetic forces.

Several different modes of microchip based DEP exist. These modes include focusing/trapping DEP [14]–[16], isotropic DEP [17], traveling wave DEP [18]–[21], and DEP field-flow fractionation [22]–[24]. In this thesis we will focus on “conventional or affinity” DEP in the microchip format: trapping of particles in devices that utilize C-serpentine electrodes fabricated using metal and screen printed conducting carbon paste.

1.3 Theory

A force is experienced by a particle when placed inside a non-uniform electric field generated by the electrodes [25], [26]. This non-uniform electric field will create the necessary imbalanced force on the suspended particle inside the microchannel. This imbalanced force induces a dipole moment inside the particle, which can be used to move or manipulate a particle as long as the electric field is non-homogeneous.

However, if the electric field is uniform, a dipole moment will be induced in the particle but it will not move because the force experienced on the opposite sides of the particle will be exactly identical. Charged particles too will experience a dipole and will move to their respective pole if the frequency of the applied potential is at or near zero, but will otherwise oscillate along with the applied frequency [27]. For conventional DEP, the DEP force experienced by a particle inside a non-uniform electric field can be approximated by Equation (1.1). [28]:

$$F_{dep} = 2\pi a^3 \epsilon_m R_e[K] \nabla E_{rms}^2 \quad (1.1)$$

where a is the radius of the particle, E_{rms} is the root mean square applied electric field, ϵ_m is the permittivity of the medium. Equation (1.1) implies that the DEP force depends on a variety of parameters, such as particle size, the permittivities and conductivities of the particle and suspending medium, and the spatial non-uniformity of the electric field. $R_e[K]$ is the real component of Clausius-Mossotti factor (CM) which is represented as :-

$$[K] = \frac{\epsilon_p^* - \epsilon_m^*}{\epsilon_p^* + 2\epsilon_m^*} \quad (1.2)$$

where ϵ_p^* and ϵ_m^* are the complex permittivity's of particle and medium respectively defined in equation (1.3) and (1.4)

$$\epsilon_p^* = \epsilon_p - j \frac{\sigma_p}{\omega} \quad (1.3)$$

$$\epsilon_m^* = \epsilon_m - j \frac{\sigma_m}{\omega} \quad (1.4)$$

where σ_p and σ_m are the conductivity of the particle and the medium respectively, and ω is the angular frequency of the applied electric field. Moreover, the CM factor plays an important role in the DEP force, which represents the dielectric properties of the DEP environment from the contribution of the particle and suspending medium. It also shows that the DEP effect depends on the frequency of external electric fields, which is considered to be an excellent feature of this phenomenon. If the particle is more polarizable than the suspending medium ($\text{Re}[K(\omega)] > 0$), then the particle is pushed towards the region of strong electric field, and such a motion is termed positive DEP (p-DEP). In contrast, if the suspending medium is more polarizable than the particle ($\text{Re}[K(\omega)] < 0$), then the motion of the particle is away from the region of strong

electric field, which is called negative DEP (n-DEP). A useful solution for $Re[K]$ which illustrates its dependency on applied field is given as [28].

$$Re[k] = \frac{\varepsilon_p - \varepsilon_m}{\varepsilon_p + 2\varepsilon_m} + \frac{3(\varepsilon_m \sigma_p - \varepsilon_p \sigma_m)}{\tau_{MW} (\sigma_p + 2\sigma_m)^2 (1 + \omega^2 \tau_{MW}^2)} \quad (1.5)$$

where τ_{MW} is the Maxwell-Wagner charge relaxation time and it is given as [28]

$$\tau_{MW} = \left(\frac{\varepsilon_p + \varepsilon_m}{\sigma_p + 2\sigma_m} \right) \quad (1.6)$$

The CM factor expressed as equation (1.2) is valid only for homogeneous spherical particles. The frequency dependence of the DEP force is shown by investigating the CM factor of a homogeneous spherical particle; that is, Equation (1.2). The factor can vary from -0.5 (i.e. $\varepsilon_p^* \ll \varepsilon_m^*$) to $+1$ (i.e. $\varepsilon_p^* \gg \varepsilon_m^*$), which means a positive DEP force can be twice as strong as a negative DEP force. Moreover, at low and high frequency limits, the CM factor is reduced to the following forms, respectively:

$$K(\omega) = \frac{\sigma_p - \sigma_m}{\sigma_p + 2\sigma_m} \quad \text{for } \omega \rightarrow 0 \quad (1.7)$$

$$K(\omega) = \frac{\varepsilon_p - \varepsilon_m}{\varepsilon_p + 2\varepsilon_m} \quad \text{for } \omega \rightarrow \infty \quad (1.8)$$

Therefore, at low frequencies, the DEP force depends on the conductive properties of the particle and the suspending medium, while the permittivity values govern the DEP effect at high frequencies. At intermediate frequencies, both the dielectric and conductive properties of the particle and suspending medium determine the magnitude and polarity of the DEP force. The particle's DEP response may be varied by changing the frequency of the applied electric fields: at a range of frequencies, the particle experiences a positive DEP, while it exhibits a negative DEP response in another range of frequencies. The point where the response switches from p-DEP to n-DEP, or from n-DEP to p-DEP, is called the crossover frequency. At this frequency, the complex permittivity of the particle is equal to that of suspending medium, and the DEP force will be zero ($Re[K(\omega)] = 0$). The shift of the crossover frequency can be achieved by changing the permittivity and conductivity of the particle and suspending medium.

Determination of the type of dielectrophoretic moment a particle will experience, can be accomplished by calculating $Re[K(\omega)]$ using Equation (1.5). The real portion of the CM factor will dictate whether the dielectrophoretic force on a particle will be positive or negative. The CM factor is frequency dependent because it is determined from the frequency dependent complex permittivities of the particle and the medium [26], [29], [30]. As such, by constructing a plot of the real component of the CM factor as a function of frequency it is possible to estimate the frequency ranges in which a particle will exhibit positive DEP and negative DEP. Careful selection of the suspending medium (and more specifically its conductivity) can be used to increase the selectivity in discriminating between different analytes as stated in the CM factor. The effects of conductivity of the medium have been studied by several researchers [31]–[36]. Green and Morgan observed these behaviors for the study of latex spheres [31]. Huang and Pethig showed that by altering the conductivity of the solution and maintaining other conditions constant it was possible to cause a change in the DEP behavior of yeast cells [32]. Also, a detailed study by Pethig in 2016 [37], summarizes his analysis on DEP progress in various application fields since 2000-2016.

In brief, the DEP force on a particle suspended in a dielectric medium depends on the effective polarisability of the particle, a value which is related to the difference between the complex permittivities of the particle and the suspending medium. The effective polarisability can be either positive or negative so that the resulting force is either towards high field regions or towards low field regions respectively. The polarization of a sphere in an electric field and the difference between positive and negative DEP are shown schematically in Figure 1.2. If a particle with polarization greater than that of medium is placed in a uniform electric field as shown in Figure 1.2(a1), there is no net movement because the forces on the charges in the dipole tends to balance each other as they are equal and opposite. However if the same particle is placed in a non-uniform electric field as shown in Figure 1.2(a2), the particle will move towards a high electric field area showcasing p-DEP behavior as there is an imbalance in the force on the charges in a dipole. Similarly, if a particle with polarization less than that of medium is placed in a uniform electric field as shown in Figure 1.2(b1), there is no net movement because the forces on the charges in the dipole tends to balance each other as they are equal and opposite. However if the same particle is placed in a non-uniform electric field as shown in Figure 1.2(b2), the particle will move towards a low electric field area

showcasing n-DEP behavior as there is an imbalance in the force on the charges in a dipole.

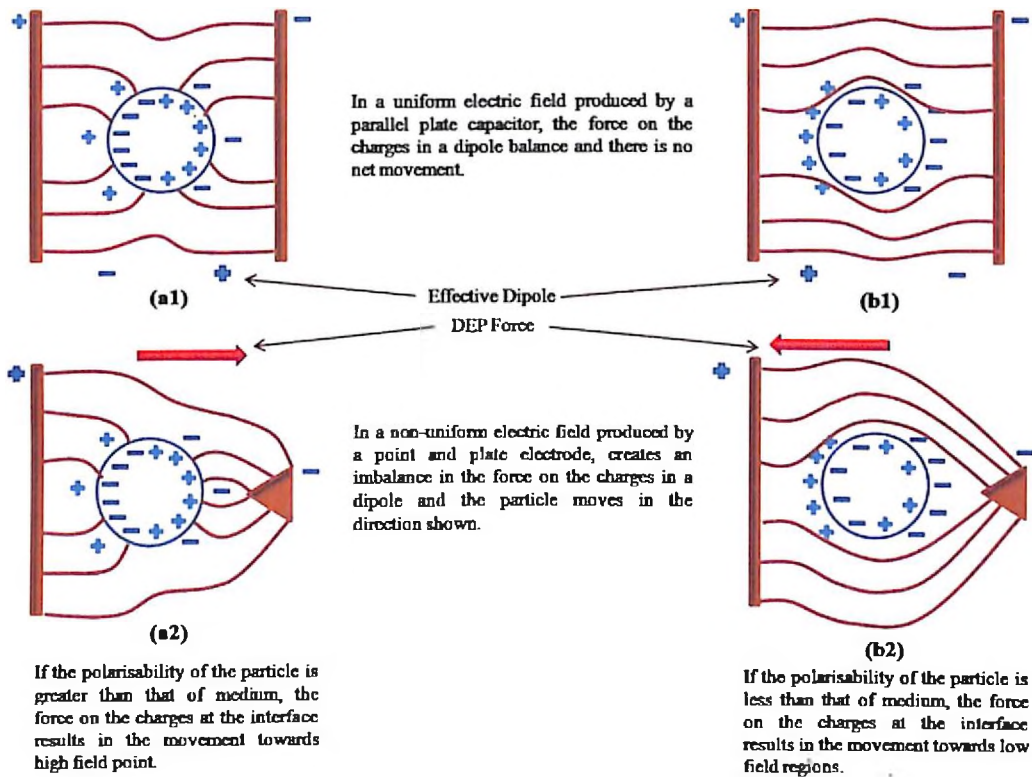


Figure 1.2: Schematic of the polarization of a spherical particle in a dielectric medium in a uniform and non uniform electric field. The case of the particle with polarisability greater than the medium polarisability is shown on the left and the case where particle polarisability is less than that of medium is shown on the right. Both cases are detailed with the relative amount of charge on either side of the particle/medium interface, the effective dipole and the direction of the dielectrophoretic force

The magnitude and the direction of the dielectrophoretic force depends on the particle permittivity and conductivity, the medium permittivity and conductivity and the field strength and frequency. The fact that the DEP force is dependent on such a variety of parameters, makes DEP a powerful tool for particle, especially in biological particle, characterisation, manipulation and separation [38].

1.4 Dielectrophoretic Microfluidic Devices

The non-uniform electric field required to build up the DEP effect is generated by either the electrode or electrodeless i.e insulator based DEP devices. In case of insulator DEP, the non-uniformity is created by means of the specially designed structures inside the microchannel such as hurdles or obstacles. Besides embedding insulating obstacles in a straight microchannel, a variety of curved microchannels have also been used to manipulate particles. Xuan's group developed a serpentine channel, where the electric field becomes non-uniform at each U-turn, with the maximum and minimum values obtained at the inner and outer corner, respectively. This design has been used to: focus polystyrene particles [39], [40] and cells [41]; to separate polystyrene particles based on size [42], [43] and dielectrophoretic response [40]; and to separate yeast cells from *E. coli* [41] and polystyrene particles [42] Consequently, dielectrophoretic microdevices with different configurations and structures of microelectrodes and insulators have been successfully used to manipulate and separate particles. Since there are no electrodes inside the device, therefore these devices are robust, chemically inert and very simple in terms of fabrication [44]. However, these devices require a high voltage supply to generate sufficient DEP force which may lead to serious Joule heating effects inside the channel. On the other hand, electrode based DEP devices, do not require high driving voltage since the electric field is produced by electrodes that are embedded inside the microchannel. The electrode based DEP has been reported to manipulate and isolate colorectal cancer HCT116 cells from the mixture with human embryonic kidney 293 HEK293 and *E. coli* cells [45], to isolate and separate human cancer cells [46], trapping and sorting of tobacco mosaic virus (TMV) and herpes simplex virus (HSV) [15], trapping cells and silica beads [47], immobilization of lamda-DNA molecules [48], concentrating embryonic stem cells (ESCs) [49], sorting nano-[50] and microparticles [51], clones of mouse melanoma B16F10 cells [52], separating cancer cells from blood [53] [54] separating dormant *Mycobacterium smegmatis* from live and dead *M. smegmatis* [55] have also been reported.

1.5 Motivation

As discussed in the previous section, from last few decades the technique of Dielectrophoresis have been investigated with various methods and are reported in literature. The DEP devices employing metal electrodes to generate non-uniform electric field have been explored widely. The fabrication of these metal electrodes requires a

complicated and an expensive technique of electroplating, that often restricts the yield and results in more expensive devices. The prime reason for advancing attempts in fabricating metal electrodes DEP devices is because the metal patterning technology is fully matured and developed in the area of MEMS. However, the high fabrication cost cannot contribute to the mass production of disposable chips. Therefore, recently the interest has been expressed in Carbon-MEMS technique in order to fabricate cost effective DEP devices that are also disposable.

For fabrication of carbon electrodes various carbon precursors are used. Carbonizable polymers are widely available and high-quality ones are typically much less expensive than metals such as gold and platinum used in thin film metal electrode fabrication. The polymer can be shaped using any suitable low cost technique such as photolithography, CNC (computer numerical control) machining, moulding and embossing. No expensive and complex equipment such as metal evaporators or metal sputters are required. In addition, while working with bio-particles, fouling of the metal electrodes (i.e. sample electrolysis) may distort the operation of AC-DEP devices. One of the possible solutions is to employ carbon electrode because carbon has a much wider electrochemical stability window than metals commonly used in thin film electrode fabrication such as gold and platinum, and affords higher applied voltages in a given solution without electrolyzing it. Besides, the use of carbon electrodes yields other advantages including excellent biocompatibility, mechanical properties and chemical inertness in almost all solvents/electrolytes. There is growing literature on the subject but interestingly there had been few attempts made towards fabricating carbon electrodes with other techniques except pyrolysis or C-MEMS. In our opinion, however, C-MEMS is still complicated and time-consuming in terms of operation conditions. Another alternative way to fabricate carbon electrodes needs to be exploited urgently. This quest had been the guiding factor for the present work.

The available literature though contain volumes on use of carbon electrodes fabricated by pyrolysis of negative resist, few attempts have been made towards the realization of 3D carbon structures using screen printing technique. Towards this intent, we present a comprehensive review in Chapter 2 and frame specific problem statements. In Chapter 3, device modeling is presented. In Chapter 4 we present fabrication and investigation on efficiency of gold DEP device for cell trapping. In Chapter 5, we have given the

fabrication details of carbon based DEP device along with its testing. Finally in Chapter 6 we give conclusions and scope for future work.

References:

- [1] H. Helvajian and S. W. Janson, *Microengineering space systems*. 1999.
- [2] G. E. Karniadakis and A. Beskok. *Micro flows: Fundamentals & Simulation*. Springer, 2001.
- [3] H. Morgan and N. G. Green, "Dielectrophoretic manipulation of rod-shaped viral particles," *J. Electrostat.*, vol. 42, no. 3, pp. 279–293, 1997.
- [4] J. Kadaksham, P. Singh, and N. Aubry. "Manipulation of particles using dielectrophoresis," *Mech. Res. Commun.*, vol. 33, no. 1, pp. 108–122, 2006.
- [5] M. Dimaki and P. Bøggild, "Dielectrophoresis of carbon nanotubes using microelectrodes: a numerical study," *Nanotechnology*, vol. 15, no. 8, pp. 1095–1102, 2004.
- [6] R. Krupke, F. Hennrich, H. Lohneysen, and M. Kappes, "Separation of Metallic from Semiconducting Single-Walled Carbon Nanotubes.," *Science (80-)*, vol. 301, no. 5631, pp. 344–347, 2003.
- [7] T. Ryll, G. Dutina, A. Reyes, J. Gunson, L. Krummen, and T. Etcheverry. "Performance of small-scale CHO perfusion cultures using an acoustic cell filtration device for cell retention: characterization of separation efficiency and impact of perfusion on product quality.," *Biotechnol. Bioeng.*, vol. 69, no. 4, pp. 440–449, 2000.
- [8] K. E. McCloskey, J. J. Chalmers, and M. Zborowski, "Magnetic Cell Separation : Characterization of Magnetophoretic Mobility," *Anal. Chem.*, vol. 75, no. 24, pp. 6868–6874, 2003.
- [9] V. V. Tuchin, "A clear vision for laser diagnostics (review)," *IEEE J. Sel. Top. Quantum Electron.*, vol. 13, no. 6, pp. 1621–1628, 2007.
- [10] A. R. Minerick, R. Zhou, P. Takhistov, and H.-C. Chang, "Manipulation and characterization of red blood cells with alternating current fields in microdevices," *Electrophoresis*, vol. 24, no. 21, pp. 3703–3717, 2003.
- [11] B. Zimmerman *et al.*, "Formation of focal adhesion-stress fibre complexes coordinated by adhesive and non-adhesive surface domains," in *IEEE proceedings of nanobiotechnology*. 2004, vol. 151, no. 2, pp. 207–211.
- [12] H. A. Pohl, "The motion and precipitation of suspensoids in divergent electric fields," *J. Appl. Phys.*, vol. 22, no. 7, pp. 869–871, 1951.
- [13] H. A. Pohl and C. E. Plymale, "Continuous Separations of Suspensions by Nonuniform Electric Fields in Liquid Dielectrics," *J. Electrochem. Soc.*, vol. 170, no. 5, pp. 390–396, 1960.
- [14] B. H. Lapizco-Encinas, B. A. Simmons, E. B. Cummings, and Y. Fintschenko, "Dielectrophoretic Concentration and Separation of Live and Dead Bacteria in an Array of Insulators," *Anal. Chem.*, vol. 76, no. 6, pp. 1571–1579, 2004.
- [15] H. Morgan, M. P. Hughes, and N. G. Green, "Separation of submicron bioparticles by dielectrophoresis.," *Biophys. J.*, vol. 77, no. 1, pp. 516–525, 1999.
- [16] Y. Huang, S. Joo, M. Duhon, M. Heller, B. Wallace, and X. Xu,

- “Dielectrophoretic cell separation and gene expression profiling on microelectronic chip arrays,” *Anal. Chem.*, vol. 74, no. 14, pp. 3362–3371, 2002.
- [17] Y. Li and K. V. I. S. Kaler, “Dielectrophoretic fluidic cell fractionation system,” *Anal. Chim. Acta*, vol. 507, no. 1, pp. 151–161, 2004.
- [18] L. Pin, Z. Xiaolu, and J. Aimin, “Design of a micro manipulation device for cell microinjection,” *Microsyst. Technol.*, pp. 1–10, 2016.
- [19] L. Cui and H. Morgan, “Design and fabrication of travelling wave dielectrophoresis structures,” *J. Micromechanics Microengineering*, vol. 10, no. 1, p. 72, 2000.
- [20] H. Morgan, I. A. Garcia, B. David, G. N. G, and R. Antonio, “The dielectrophoretic and travelling wave forces generated by interdigitated electrode arrays : analytical solution using Fourier series,” *J. Phys. D. Appl. Phys.*, vol. 34, no. 10, pp. 1553–1561, 2001.
- [21] L. YY, L. U, L. YJ, W. MS, and Y. PC, “A Modified Travelling Wave Dielectrophoretic Method for the Measurement of the Imaginary Part of the Clausius-Mossotti Factor Using Dual Frequency Operation,” *J. Mech.*, vol. 30, no. 06, pp. 651–660, 2014.
- [22] X. B. Wang, J. Yang, Y. Huang, J. Vykoukal, F. F. Becker, and P. R. C. Gascoyne, “Cell separation by dielectrophoretic Field- Flow-fractionation,” *Anal. Chem.*, vol. 72, no. 4, pp. 832–839, 2000.
- [23] B. Roda *et al.*, “Field-flow fractionation in bioanalysis: A review of recent trends,” *Anal. Chim. Acta*, vol. 635, no. 2, pp. 132–143, 2009.
- [24] A. Ieng K. Lao, Y. K. Lee, and I. M. Hsing, “Mechanistic investigation of nanoparticle motion in pulsed voltage miniaturized electrical field flow fractionation device by in situ fluorescence imaging,” *Anal. Chem.*, vol. 76, no. 10, pp. 2719–2724, 2004.
- [25] H. A. Pohl, *Dielectrophoresis: the behavior of neutral matter in nonuniform electric fields*, Vol 80. Cambridge: Cambridge university press, 1978.
- [26] T. B. Jones, *Electromechanics of particles*. Cambridge Univ. Press, Cambridge., 1995.
- [27] A. D. Goater and R. Pethig, “Electrorotation and dielectrophoresis,” *Parasitology*, vol. 117, no. 07, pp. 177–189, 1999.
- [28] C. F. Gonzalez and V. T. Remcho, “Harnessing dielectric forces for separations of cells , fine particles and macromolecules,” *J. Chromatogr. A*, vol. 1079, no. 1–2, pp. 59–68, 2005.
- [29] M. P. Hughes, “Strategies for dielectrophoretic separation in laboratory-on-a-chip systems,” *Electrophoresis*, vol. 23, no. 16, pp. 2569–2582, 2002.
- [30] L. Benguigui and I. J. Lin, “More about the dielectrophoretic force,” *J. Appl. Phys.*, vol. 53, no. 2, pp. 1141–1143, 1982.
- [31] N. G. Green and H. Morgan, “Dielectrophoretic investigations of sub-micrometre latex spheres,” *J. Phys. D. Appl. Phys.*, vol. 30, no. 18, pp. 2626–2633, 1997.
- [32] Y. Huang and R. Pethig, “Electrode design for negative dielectrophoresis,” *Meas.*

- Sci. Technol.*, vol. 2, no. 12, pp. 1142–1146, 1991.
- [33] A. W.M., S. H.P., and Z. U. “Surface Conductance and Other Properties of Latex Particles Measured by Electrorotation,” *J. Phys. Chem.*, vol. 91, no. 19, pp. 5093–5098, 1987.
- [34] N. G. Green and H. Morgan, “Dielectrophoresis of Submicrometer Latex Spheres. I. Experimental Results,” *J. Phys. Chem. B*, vol. 103, no. 1, pp. 41–50, 1999.
- [35] Y. Huang, X.-B. Wang, R. Holzel, F. F. Becker, and P. R. C. Gascoyne, “Electrorotational studies of the cytoplasmic dielectric properties of Friend murine erythroleukaemia cells,” *Phys. Med. Biol.*, vol. 40, no. 11, pp. 1789–1806, 1995.
- [36] Y. Huang, X. B. Wang, F. F. Becker, and P. R. C. Gascoyne, “Membrane changes associated with the temperature-sensitive P85 gag-mos-dependent transformation of rat kidney cells as determined by dielectrophoresis and electrorotation,” *Biochim. Biophys. Acta - Biomembr.*, vol. 1282, no. 1, pp. 76–84, 1996.
- [37] R. Pethig, “Review—Where Is Dielectrophoresis (DEP) Going?,” *J. Electrochem. Soc.*, vol. 164, no. 5, pp. B3049–B3055, 2017.
- [38] N. Abd Rahman, F. Ibrahim, and B. Yafouz, “Dielectrophoresis for Biomedical Sciences Applications: A Review,” *Sensors*, vol. 17, no. 3, pp. 449–475, 2017.
- [39] J. Zhu, T. R. J. Tzeng, G. Hu, and X. Xuan, “DC dielectrophoretic focusing of particles in a serpentine microchannel,” *Microfluid. Nanofluidics*, vol. 7, no. 6, pp. 751–756, 2009.
- [40] C. Church, J. Zhu, J. Nieto, G. Keten, E. Ibarra, and X. Xuan, “Continuous particle separation in a serpentine microchannel via negative and positive dielectrophoretic focusing,” *J. Micromechanics Microengineering*, vol. 20, no. 6, pp. 065011–065016, 2010.
- [41] C. Church, J. Zhu, G. Wang, T. R. J. Tzeng, and X. Xuan, “Electrokinetic focusing and filtration of cells in a serpentine microchannel,” *Biomicrofluidics*, vol. 3, no. 4, pp. 044109–044118, 2009.
- [42] J. Zhu, R. C. Canter, G. Keten, P. Vedantam, T. R. J. Tzeng, and X. Xuan, “Continuous-flow particle and cell separations in a serpentine microchannel via curvature-induced dielectrophoresis,” *Microfluid. Nanofluidics*, vol. 11, no. 6, pp. 743–752, 2011.
- [43] C. Church, J. Zhu, and X. Xuan, “Negative dielectrophoresis-based particle separation by size in a serpentine microchannel,” *Electrophoresis*, vol. 32, no. 5, pp. 527–531, 2011.
- [44] C.-F. Chou *et al.*, “Electrodeless dielectrophoresis of single- and double-stranded DNA,” *Biophys. J.*, vol. 83, no. 4, pp. 2170–2179, 2002.
- [45] F. Yang *et al.*, “Dielectrophoretic separation of colorectal cancer cells,” *Biomicrofluidics*, vol. 4, no. 1, p. 13204, Jan. 2010.
- [46] M. Alshareef *et al.*, “Separation of tumor cells with dielectrophoresis-based microfluidic chip,” *Biomicrofluidics*, vol. 7, no. 1, p. 011803, 2013.
- [47] Q. Ramadan, V. Samper, D. Poenar, Z. Liang, C. Yu, and T. M. Lim, “Simultaneous cell lysis and bead trapping in a continuous flow microfluidic

- device." *Sensors Actuators B Chem.*, vol. 113, no. 2, pp. 944–955, 2006.
- [48] W. A. Germishuizen *et al.*, "Selective dielectrophoretic manipulation of surface-immobilized DNA molecules," *Nanotechnology*, vol. 14, no. 8, pp. 896–902, 2003.
- [49] S. Agarwal, A. Sebastian, L. M. Forrester, and G. H. Markx, "Formation of embryoid bodies using dielectrophoresis," *Biomicrofluidics*, vol. 6, no. 2, p. 024101, 2012.
- [50] N. . Green and H.Morgan, "Separation of submicrometre particles using a combination of dielectrophoretic and electrohydrodynamic forces." *J. Phys. D. Appl. Phys.*, vol. 31, no. 7, p. L25, 1998.
- [51] R. Pethig, Y. Huang, X. Wang, and J. P. H. Burt, "Positive and negative dielectrophoretic collection of colloidal particles using interdigitated castellated microelectrodes," *J. Phys. D. Appl. Phys.*, vol. 25, no. 5, pp. 881–888, May 1992.
- [52] A. C. Sabuncu, J. A. Liu, S. J. Beebe, and A. Beskok, "Dielectrophoretic separation of mouse melanoma clones," *Biomicrofluidics*, vol. 4, no. 2, p. 021101, 2010.
- [53] P. R. C. Gascoyne, X. Wang, Y. Huang, and F. F. Becker, "Dielectrophoretic Separation of Cancer Cells from Blood," *IEEE Trans. Ind. Appl.*, vol. 33, no. 3, pp. 670–678, 1997.
- [54] F. F. Becker, X.-B. Wang, Y. Huang, R. Pethig, J. Vykoukal, and P. R. C. Gascoyne, "Separation of human breast cancer cells from blood by differential dielectric affinity," *Proc. Natl. Acad. Sci.*, vol. 92, no. 3, pp. 860–864, 1995.
- [55] K. Zhu, A. S. Kaprelyants, E. G. Salina, and G. H. Markx, "Separation by dielectrophoresis of dormant and nondormant bacterial cells of *Mycobacterium smegmatis*," *Biomicrofluidics*, vol. 4, no. 2, p. 022809, 2010.

2.1 General Introduction

The potential of the DEP phenomenon for cell separation has been discussed in the previous chapter. Researchers have often investigated the dielectrophoretic identification and separation methods (DEP) since Pohl introduced this phenomenon in the 1950s [1]. The main reasons that have made DEP one of the long lasting cell characterization and separation methods are: (i) DEP preserves the viability, cultivability, genetic and phenotypic properties of the cells [2]; (ii) DEP employs the intrinsic dielectric properties of the cells [3]; (iii) DEP is contact-free and low cost [4]. However, implementation of a dielectrophoretic force on a sample requires a non-uniform electric field that creates volumes of different electric field magnitudes across the sample where particles can be selectively positioned according to their dielectric phenotype and different experimental parameters. This non uniform electric field is generated by the electrodes. Therefore, electrodes form the heart of any DEP device.

Various 2D and 3D electrodes geometries for application in DEP have been reported in literature. So far, metals and carbon have been the most reported material for forming electrodes in various DEP devices. This chapter discusses in detail various 2D and 3D metal and carbon electrode configuration available in literature. A hierarchical classification of various electrode configurations discussed in this chapter is shown in Figure 2.1. This chapter aims to provide a clear and concise understanding of DEP and highlighting the aspects relevant to the current study related to these materials. This review provides an overview of the state-of-the-art of different 2D and 3D electrode structures used in various dielectrophoretic microdevices aimed based on the extensive literature review which is presented in the following section.

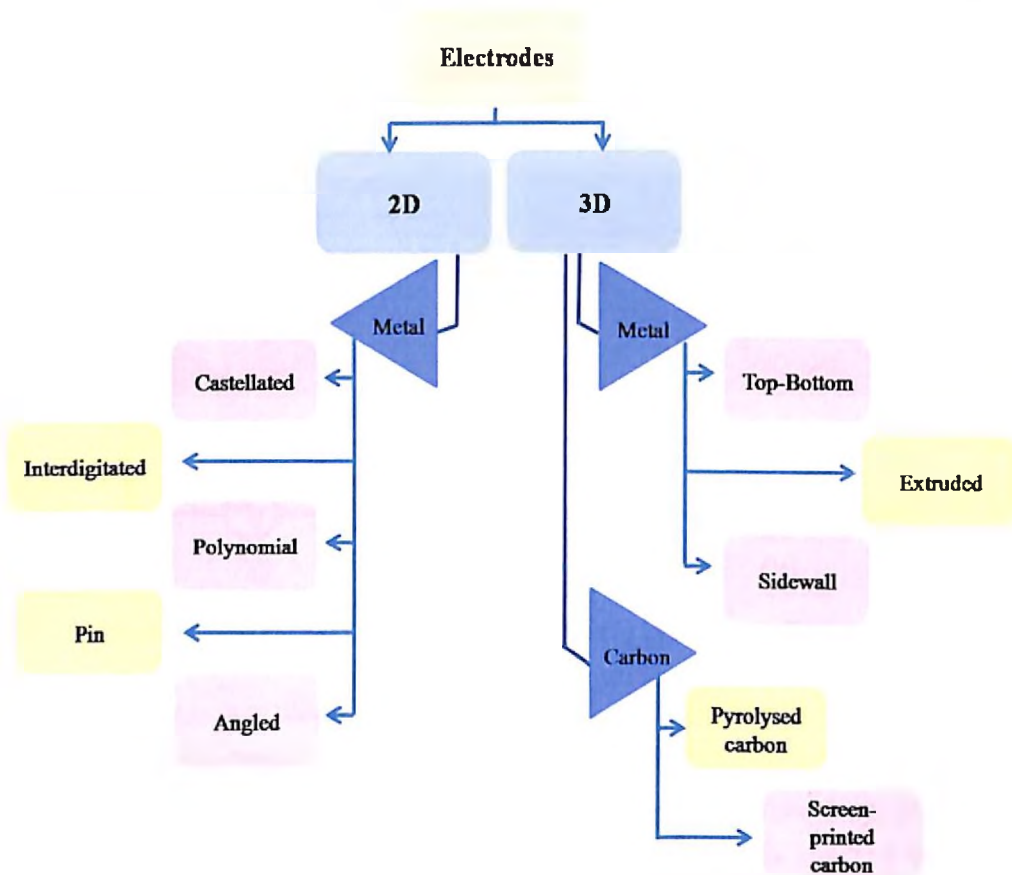


Figure 2.1: Classification of electrodes

2.2 Metal Electrodes

2.2.1 Two Dimensional 2D Planar Electrodes

Traditionally, spatial non-uniformity is generated by applying AC electric field via microelectrode arrays patterned within microchannels. A wide variety of electrode based DEP microdevices have been developed, fabricated, and successfully employed to manipulate and separate bioparticles (i.e. DNA, proteins, bacteria, viruses, mammalian and yeast cells). The 2D microelectrodes of different geometries, such as polynomial, castellated, interdigitated, slanted and curved have been discussed in detail below.

2.2.1.1 Pin electrode

Pin electrode configuration marks the start of DEP experiments by Pohl. Some of the work reported in literature using this configuration is described below. A simple arrangement of pin-plate electrode configuration is shown in Figure 2.2(a) where a

stainless steel wire (red colour) faces a stainless steel plate (blue colour) and the pin-pin electrode configuration is shown in Figure 2.2 (b), in which two wires are placed at some distance with each other and the rounded pin tips acts as cell separation spheres.

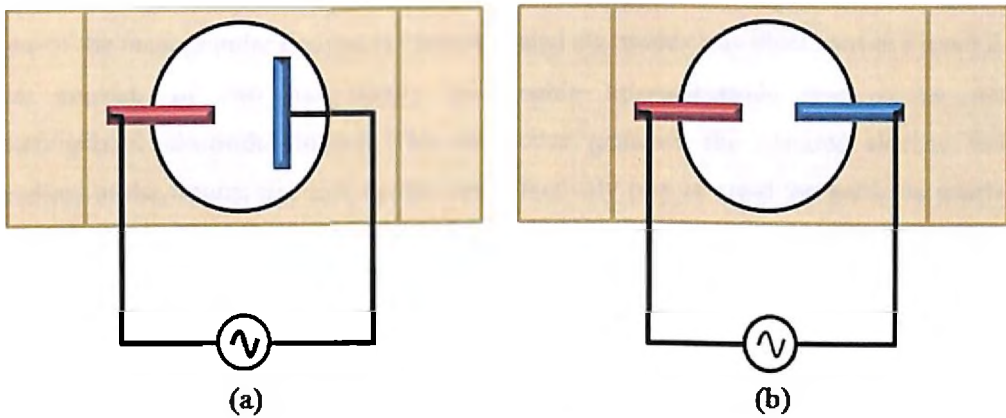


Figure 2.2: (a) Pin-plate configuration [5], (b) Pin-pin configuration [6]

DEP phenomenon was first reported by Pohl et al in 1966 [5] and he introduced the application of high frequency electric fields to cause selective DEP of yeast cells in an aqueous media. The dielectrophoretic cell consisted of pin and plate electrode made of stainless steel and on application an ac signal of 30 Vrms or more and 2.55 MHz, live cells gathered at pin electrodes. In his succeeding work in 1971 [6] Pohl presented a detailed study of yeast cells using a simple pin-pin electrode system made of platinum and applying high frequency alternating fields one observes that the collectability of cells at an electrode tip, i.e. in the region of the most intense field. This electrode configuration minimizes the wien effect unlike pin-plate configuration (i.e increase in ionic mobility or conductivity of electrolytes at high potential gradient). This cell collection depends upon physical parameters such as the field strength, field uniformity, frequency, cell suspension concentration, its conductivity; and upon the time of collection. The yield of cells collected is also observed to depend upon biological factors such as the colony age, thermal treatment of the cells, irradiation with ultraviolet light, and chemical poisons.

However in 1989, Masuda et al [7] were one of the first groups to use DEP in an LOC device. They designed a “fluid integrated circuit,” which was used to manipulate cells and separate them into different outlets using parallel wire configuration capable of handling cells in batches. The proposed tool enabled automated single cell manipulation

and device miniaturization by combining multiple cell-handling components, such as micropumps and cell-fusion electrodes, onto one substrate.

2.2.1.2 Interdigitated electrodes

One of the most popular designs is “interdigitated electrodes”, as illustrated in Figure 2.3 that consists of two individually addressable microelectrode array strips with interdigitated electrode fingers. The electrodes generate the greatest electric field gradient at the fingers tip, and, hence, can effectively trap or repel the particles nearby. Some of the groundbreaking work using this electrode geometry is detailed below:

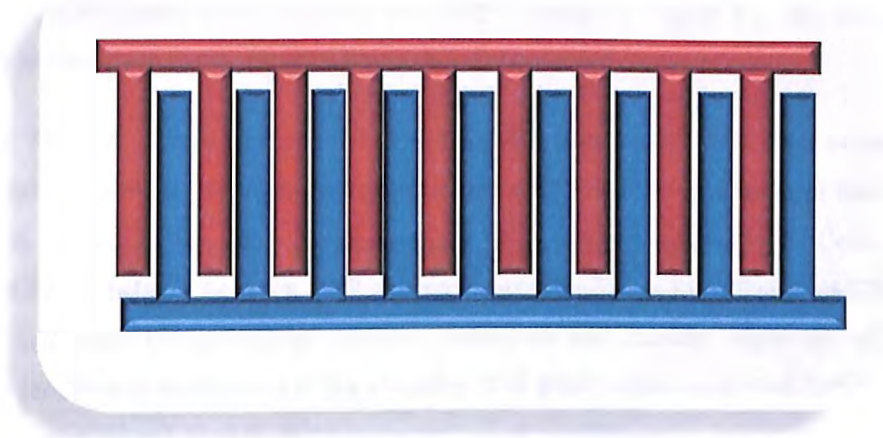


Figure 2.3: Interdigitated electrode

In 1996 Schnelle et al [8], proposed a method to prevent the electrodes from particle adhesion. For this, they investigated the influence of insulating layers on the ability of interdigitated electrodes to repel particles from surfaces, using both high-frequency alternating and traveling-electric fields. Also some electrode arrays were coated with thin dielectric layers to improve stability. The results show that many types of particles (e.g. Sephadex and latex spheres between 0.1 and 100 μm in diameter) and living cells can be repelled by the n-DEP forces induced by ac or traveling electric fields, at frequencies up to 200 MHz, in aqueous solutions.

Suehiro and group in 1999 [9], described a new detection method of biological particles suspended in liquid medium by using a dielectrophoretic impedance measurement. The impedance method is technically much easier than the optical method because it employs only electrical signals and does not need an optical measuring system also it can

characterize smaller particles or cells, which are not suitable for optical monitoring. The particles were trapped on a micro-electrode array by p-DEP and possess electrical impedance depending on their dielectric properties as well as their geometric form in the electrode array. By monitoring the transient variation of the circuit impedance, it is possible to detect the particles and quantitatively evaluate their concentration in suspension. In succeeding work in 2003 [10], they proposed the use of electropermeabilization phenomenon to increase the sensitivity of dielectrophoretic impedance method as the detection of lower bacteria concentration took longer. Therefore electropermeabilization was coupled with DEP to allow easy detection of lower bacteria concentration. It was experimentally confirmed that the electropermeabilization could increase the DEP impedance signal by two orders of magnitude relative to the conventional one.

In 2000, Wang et al [11], reported the separation of breast cancer cells from normal T-lymphocytes and from CD34+ hematopoietic stem cells, also the separation of the major leukocyte subpopulations, and the enrichment of leukocytes from blood. Cells were levitated by the balance between DEP and sedimentation forces to different equilibrium heights and were transported at differing velocities and thereby separated when a velocity profile was established in the chamber. The purity after separation for different cells employed ranged from 92-99% under optimized conditions.

In series of work, Li et al in 2002 [12], reported the separation of live and dead cells of *Listeria innocua*. The separation was achieved by applying an ac signal of 1V and 10 KHz frequency. They managed to achieve a separation efficiency of 90% using interdigitated electrodes by using an ac signal of 50 kHz frequency. Also in 2005, Li et al [13] successfully achieved the separation and trapping of different biological cells (polystyrene beads, yeast, spores and bacteria) in dynamic flows. Finite element modeling on the holding forces for both n-DEP and p-DEP is also presented. Asbury et al in 2002 [14], demonstrated the trapping of DNA molecules and proposed two quantitative methods for measuring the efficiency of DEP in DNA trapping. For the first time, Auerswald et al in 2003 [15] gave a quantitative data for analyzing the maximum allowed flow velocities in DEP retaining devices for polystyrene beads and red blood cells using platinum electrodes.

Suzuki et al in 2004 [16], fabricated 2D micropatterns of microparticles on a non conductive glass support using n-DEP. The advantages of using DEP for patterning are that pre patterning of the substrates is unnecessary and the assembly of microparticles, including biological cells, occurs rapidly. To avoid the disintegration of particles when AC field is removed he introduced the use of crosslinking agents where the patterned microparticles were covalently bound. In his succeeding work in 2007 [17] he introduced the use of conductive Indium Tin Oxide layer at the bottom that creates various electric field gradients. The present procedure is substantially simple, rapid, and highly reproducible method for fabrication of particle arrays unlike SAM (Self-assembled monolayer). Also here they suggested the use of cross-linker, succinimidyl 4-(p-maleimidophenyl)-butyrate (SMPB) to avoid aggregation of particles and a random reaction between the activated substrate and particles, causing a degradation of the patterning precision unlike the previous study.

Sjoberg in 2005 [18], used DEP to concentrate few live bacterial cells into an extremely small volume of 400 pl in the fabricated microdevice followed by impedance measurement of microbial activity. This effectively increases the cell concentration close to the impedance electrodes without increasing the number of cells, thus eliminating the need to amplify the bacterial population by long culture enrichment, and reducing the total assay time. Lagally et al [19], integrated continuous flow with electrokinetic technology for rapidly increasing the concentration of bacteria integrated with genetic analysis. To define a chamber volume around a set of microelectrodes the device uses PDMS microvalves. By closing the microvalves after trapping bacterial cells in the sample, the volume is greatly reduced and therefore it enhances the locally detectable concentration of genetic material. The microsystem utilizes an optical molecular beacon to lyse the bacteria and to conduct rapid sequence-specific hybridization to detect the presence of 16S ribosomal RNA from *Escherichia coli* cells. This work is the first of its kind that pursues on-chip concentration followed by direct, on-chip genetic detection.

Yang et al in 2006 [20], developed a novel multifunctional device for selective capturing of *Listeria monocytogenes* using oxide covered Pt electrodes. The device couples DEP with antibody recognition to capture only the target cells. They achieved 90% trapping of cells when 20 Vp-p and 1 MHz signal was applied, indicating the effectiveness of DEP in trapping foodborne pathogenic bacterial cells. Gadish et al [21] fabricated a particle

microconcentrator based on DEP and chaotic mixer. This microconcentrator was used to concentrate beads and *B.subtilis* spores. It was observed that the chaotic mixer increased the capture efficiency significantly by suitably arranging the grooves in the mixer and using optimal interdigitated electrode geometry.

Li et al in 2007 [22], proposed a device prototype for DEP based continuous cell sorting and purification of live and dead yeast cells. The device had three distinct regions for cell focusing, separation and cell collection. Under isomotive DEP field conditions, they observed and quantified the p-DEP and n-DEP motion and deflections of yeast cells in different regions of the frequency. Crews et al [23], developed an equation to calculate the electric gradient term above interdigitated electrodes, which is a function of the width and gaps of the electrode, the applied voltage and the height above the electrode surface. By understanding the effect that the dimensions of the electrodes have on DEP force, micro-fluidic devices can be designed to produce the most effective dielectrophoretic effect on the biological samples.

In 2008 Park et al [24], proposed a theoretical model to predict the AC electrokinetic motion of microparticles, which were validated by parametric experiments of colloid particles, including polystyrene and gold particles, and *C. sporogenes* bacterial spores, with interdigitated electrodes. Vykoukal et al [25] proposed a dielectrophoretic microseparator with a flex interdigitated electrode array to enrich stem cells from enzyme-digested adipose tissue, which was fabricated using a novel, scalable and low-cost hybrid flex-circuit method.

Mernier and group in 2009 [26] were the first to fabricate a device integrating both cell sorting and counting abilities, based on DEP and coulter counting technique respectively. The combination of these two methods allowed sorting and determination of the percentage of living and dead cells for viability studies of cell samples. Park et al [27], developed a novel negative DEP based microfluidic device for trapping colloidal particles from high-conductivity media. The electrodes consist of interdigitated positive and negative electrodes with repeated patterns of square blocks. An electric potential well is created inside these patterns isolated by strong electric field between the positive and negative electrodes, this enabled trapping of cells at specific attachment sites. Negative DEP trapping of latex spheres was investigated using solution of different conductivities.

Henning et al in 2010 [28], determined the dielectrophoretic properties of DNA by measuring the capacitance change between the interdigitated electrodes. This method allowed an uncomplicated, automatic acquisition of the dielectrophoretic properties of submicroscopic objects without the need for labeling protocols or optical accessibility.

In 2011 Giraud et al [29], demonstrated for the first time the DEP collection and repulsion of subunits of *E. coli* rRNA using microelectrodes. The DEP responses were measured as a function of the strength and frequency of an applied non-uniform electric field. Using microfabricated interdigitated electrodes and the total internal reflection fluorescence microscopy technique, positive and negative DEP behavior of rRNA subunits was observed.

Narayanan Unni et al in 2012 [30], demonstrated the trapping and characterization of *Cryptosporidium* and *Giardia* cells using a microfluidic experimental setup. The two cells used in the study vary in shape as *Cryptosporidium* is spherical and *Giardia* cells are spheroidal. In this study, the experimental setup is based on the integration of microfluidics within a microfabricated electrode set, with potentially easy integration into lab-on-a-chip systems.

A new DEP method to estimate the cell dielectric properties by measuring capture voltage spectrum where the DEP force and Stokes drag force are balanced was introduced by Wu et al in 2013 [31]. Dielectric properties of less explored colon cancer cells were measured experimentally under different medium conductivities. It was observed that, cell interior permittivity and conductivity are insensitive to the change of medium conductivity. Shin et al [32][33], used DEP for the isolation of different cancer cells under panel NCI-60 cells by allowing continuous-flow sorting of cells to achieve throughputs $>10^6$ nucleated cells/min. The authors were the first to detail all the operational stages of a continuous flow DEP field flow fractionation system that is capable of processing 10 ml clinical specimens in less than 1 hr.

In 2014, Zhang et al [34] proposed a novel idea of DEP inertial microfluidics. The device had interdigitated electrodes patterned on glass slide and square serpentine channel in PDMS. The device used vertical DEP force to levitate particles in equilibrium position to the channel centre. The proposed hybrid device possesses the advantages of both DEP

and inertial microfluidic devices, working in a high-throughput manner as well as having precise controllability in real-time.

In 2017, Alazzam et al [35], introduced a novel electrode arrangement with interdigitated electrodes that protruded slightly into the separation chamber creating strong electric field along one of the sidewall. The author is the first to report the continuous separation of cancer cells from normal blood cells using this particular arrangement of electrodes. Also the separation of cells occurs in lateral direction and is therefore independent of gravity, making the separation quick and easy. The effectiveness of the proposed microfluidic device in separating viable cells is demonstrated using a mixture of green fluorescent protein labeled MDAMB-231 cancer cells and normal blood cells. Separation of MDA-MB-231 was performed at an applied AC signal of 15 Vp-p and 40 kHz. The separation accuracy and purity were found to be 100% and around $81 \pm 6.2\%$, respectively. Wang et al [36], detailed the design and implementation of bacteria impedance detection microsystem that is integrated with enrichment system on a microfluidic chip with microelectrodes, an impedance detection circuit, a signal control and a conduct circuit and related software. The device demonstrated pDEP enrichment of E.coli cells and it's in situ impedance detection. Sadeghian et al [37] elaborated a microfluidic actuator with gold interdigitated electrode patterns to separate white blood cells (k562-cells) from polystyrene particles. They performed an optimization by using COMSOL Multiphysics 5, and according to their results, geometric parameters such as pitch, width to pitch ratio, and channel height are important because the gradient of the generated electric field depends on these factors. Efficiency of recovery was 93% with 100% of purity at 7.5 Vp-p and 800 MHz. It was concluded that in their interdigitated electrode array the electrodes-pitch should be as close as possible. The channel must have a minimum height, and the voltage should be as high as possible but avoiding cell damage to achieve cell separation.

In 2018, Adams et al [38], reported the separation of neural stem and progenitor cells based on its capacitance using three different DEP based microfluidics devices. Among the three electrode configuration large capacity electrode array with interdigitated gold electrode provided higher throughput and better enrichment potential.

2.2.1.3 Castellated electrodes

Another very popular electrode design is of castellated structure. Castellated electrodes as shown in Figure 2.4 consist of two individually addressable array of electrodes (red and blue) with castellations along its length. Castellated electrodes can be used either in off-set or set configuration as shown in Figure 2.4(a) and (b) respectively. In this electrode, the high field gradient is at the tip of the castellations and the low field gradient exists in the wells present between two adjacent electrode fingers. Some of the work that utilized this geometry is discussed in detail below:

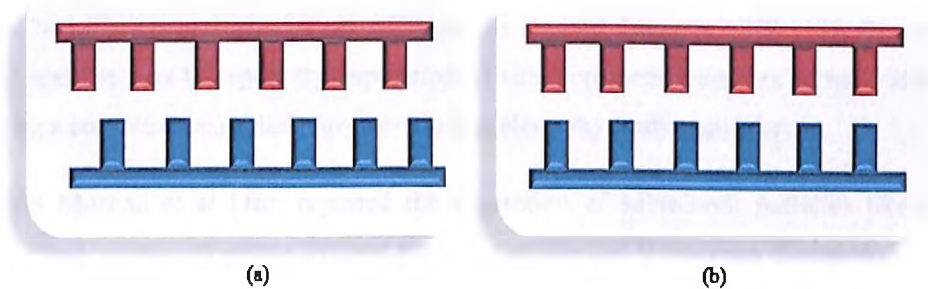


Figure 2.4: Castellated electrodes (a) Off-Set configuration (b) Set configuration

Pethig et al in 1992 [39], demonstrated the DEP behavior using interdigitated castellated electrodes for yeast cells and a theoretical explanation is presented in terms of the electric field patterns generated by the electrodes. The authors report the formation of diamond shaped aggregates on the electrode surface at 500 Hz, which is not so clearly understood.

A similar work like that of Pethig [39] on separation of yeast cells was reported by Markx et al in 1994 [40]. Known mixtures of viable and heat-treated yeast cells were separated and selectively isolated using p-DEP and n-DEP forces generated by microelectrodes. They reported that the separation efficiency can be increased by dilution of the initial cell suspension.

In 1995, Becker et al [41], reported that the dielectric characteristics of cultured breast cancer cells are significantly different from those of blood cells. This difference is exploited using dielectric affinity column to remove tumor cells from dilute blood.

A similar kind of work was reported by Gascoyne et al in 1997 [42], where they demonstrated the use of differential DEP forces for the separation of several different cancerous cell types from blood in a dielectric affinity column having microelectrodes on

the bottom wall. On application of ac signal, the resulting DEP force, influence the rate of elution of cells from the chamber. For tumor to normal cell ratios as low as $1:3 \times 10^5$ efficient removal of cancer cells from normal cells was observed. Later in 2002 [43], they applied DEP for the isolation of malaria infected cells from blood using a low conductivity suspension medium. To manipulate cells, DEP forces were typically produced by applying alternating (AC) electric fields of 10 kHz to 100 MHz and 5Vp-p. Green et al [44], was the first to report the separation of population of nanoparticles into two subpopulations on the basis of their dielectric properties. The results indicate that carboxylate modified latex spheres experienced p-DEP under 20 MHz range and n-DEP above 20 MHz range when 1Vp-p AC signal is applied. Later in 1998 [45], Green and group was the first to report the separation of submicrometre particles of two different sizes by a combination of dielectrophoretic and electrohydrodynamic forces.

In 1999 Morgan et al [46], reported the separation of submicron particles like latex spheres and viruses according to their dielectric properties. It has been demonstrated that with an appropriate electrode array and a suitable electric field and frequency, separation of particles can be accomplished.

Ramadan et al in 2006 [47], reported DNA isolation by simultaneous cell lysis and trapping by electroporation and DEP respectively. The same lysis electrode pattern has been used for trapping silica beads that are known to bind selectively to DNA. Also to avoid common issues like cell lysate clogging, cell-cell agglomeration, and cell sedimentation the authors adopted the use of continuous flow. Rajaraman et al [48] reported four fabrication technologies to make low cost DEP devices that can be used for manipulation, separation and enrichment of particles, nanowires and microorganisms. All the techniques proposed are simple, rapid and inexpensive with minimum use of clean room facility making use of titanium as adhesion promoter and gold as electrode layer.

In 2007, Tai et al [49], reported a biochip capable of cell separation and nucleus collection utilizing DEP forces in a microfluidic system comprising of micropumps and microvalves, operating in an automatic format. The device had castellated gold electrodes and was operated at 15Vp-p and 16 MHz frequency. Experimental data show that viable and non-viable cells (human lung cancer cell, A549-luc-C8) can be successfully separated and collected using the developed microfluidic platform. The separation accuracy, depending on the DEP operating mode used, of the viable and non-

viable cells are measured to be 84 and 81%, respectively. In addition, after cell lysis, the nucleus can be also collected using a similar scheme.

In 2008 Choi et al [50], proposed a new oocyte selection method based on DEP as an objective criterion. Under the applied ac biased condition, a particular group of oocytes that showed movement had a better developmental potential than the group of oocytes that stayed, representing a higher rate of blastocyst formation. These results demonstrate that the difference in dielectrophoretic velocity can be used to establish an objective criterion for the selection of oocytes.

In 2009, Zhang et al [51], employed DEP for the separation of nano and micro structures i.e multi walled CNT's and polystyrene microparticles in stationary liquid. MWCNT's were successfully separated from polystyrene microparticles for frequencies over 100 kHz, also the particle behaviour at different frequencies were characterized and analyzed. Yasukawa et al [52], proposed a novel way of separation by DEP to control the position of microparticles within the fluid flow based on its size and utilizing castellated microelectrode array with different width and gaps. Separation of the fluid stream of two particles where the 3 μ m-diameter particles were seen flowing through the narrow castellation gap and 10 μ m-diameter particles were flowing through wider gap on application of 20 Vp-p and 2 MHz AC signal.

Sabuncu et al in 2010 [53], explored the ability of DEP to differentiate between two malignant cells of the same origin, which differ from each other by small changes in their melanin content. The study showed that the difference in the melanin content of these clones is most likely responsible for the differences in their crossover frequency. Zhu et al [54], performed DEP experiments to separate dormant cells from active and dead *Mycobacterium smegmatis* bacterial cells. Cells were selectively concentrated onto the submerged electrode array and the UV absorbance of the cell suspension was measured giving insight as to what cells are being selectively removed. Suehiro et al. [55] utilized the DEP-trapped CNTs as gas sensors to detect NO₂ and NH₃. They also trapped *E. coli* on a microelectrode by the help of multiwalled CNTs attached to the end of the microelectrodes.

In 2012 Agarwal et al [56], described the application of p-DEP in the formation of embryoid bodies (i.e 3D aggregates of pluripotent stem cells). DEP offers advantage

over natural aggregation methods by guiding cells to a predefined location, both short and long distance cells can be manipulated, and easy device control. The results indicate significantly faster embryoid body formation than conventional culture-based methods, which typically takes 2–3 days.

In 2014, Du et al [57], presented a novel method i.e DEP stretching, that exploits DEP to cause deformation in healthy human red blood cells and malaria infected red blood cells. By determining the DEP force versus deformation (i.e stretch ratio) at different frequencies, the authors were able to distinguish between healthy and unhealthy cells in the suspension. Nouse et al [58] reported the use of castellated electrode arrays based on a microfluidic DEP-assisted cell sorting (DACS) to differentiated and enriched the stem cells by applying different frequencies.

Hallfors et al in 2016 [59] reported a similar kind of work as that of Du et al in 2014 except that here the DEP force versus deformation is studied at different applied voltages. The force induced through DEP acts against the elastic force of the cell, causing lengthening and slimming of the cell. The change in dimensions due to deformation under DEP is measured under a microscope, and when compared to DEP force applied, can provide useful information about the mechanical properties of cell.

Chen et al in 2018 [60], designed a microfluidics platform integrated with DEP trap and fluorescence observation for trapping of *S.oneidensis* cells. PDMS passivation layers with holes for varying sizes and castellated gold electrode array aided trapping of different quantity and length of bacteria in holes.

2.2.1.4 Polynomial electrodes

Polynomial electrodes are a set of four electrodes that produce a quadrupole geometry where the electrodes are offset by 180 degrees as illustrated in Figure 2.5. In parabolic geometries, the potential gradient expands radially from the center of the device towards the electrode surface. Some of the work that utilize polynomial electrode geometry are discussed below:

Polynomial electrode design was first introduced by Huang et al in 1991 [61]. They demonstrated that the particles can be directed into the central location, and slightly

levitated above the plane, of these electrodes by a negative DEP force. At this central location the gradient of electric field is zero, and so no DEP force can be exerted.



Figure 2.5: Polynomial electrode

Wang et al 1993 [62], presented a detailed study on determining the potential energy surfaces created by polynomial and castellated electrodes. The two electrode geometries were also tested for selective trapping and release of viable and non-viable yeast cells, erythrocytes and bacteria using p-DEP and n-DEP. It was inferred from their study that the yeast cells trapped in wells under the action of n-DEP can be more easily removed from the electrode structure than those trapped under p-DEP.

Similar kind of work as that of Huang in 1991 on polynomial electrodes using yeast cells was reported by Marx et al in 1994 [63]. The electrode system was deposited on microscopic glass slide and was primarily used to check the positive and negative DEP behavior of yeast cells before actual physical separation on other electrode geometry.

Watarai and group in 1997 [64], was the first to realize the DEP behavior of single polystyrene particle with a hyperbolic quadrupole microelectrode. Mathematical analysis of DEP migration of single cell in non uniform electric field is also presented.

In 1998 Hughes et al [65], presented the frequency dependent dielectrophoretic behavior of herpes simplex virus type 1 (HSV-1) in microfabricated electrode arrays. HSV-1 viruses suspended in mannitol solution of conductivity 5mS/m, exhibit p-DEP below 4.5 MHz and n-DEP at higher frequencies.

In 1999, Morgan et al [46], achieved trapping and sorting of tobacco mosaic virus (TMV) and herpes simplex virus (HSV) type 1 in a polynomial electrode. This design

generates high electric fields along the edges of the electrode, and a low electric field at the center. Therefore, an HSV-1 experiencing n-DEP is trapped at the center of the electrode array, while TMV experiencing p-DEP is collected at the electrode edge.

Tsukahara et al in 2000 [66], studied the behavior of single polystyrene-carboxylate microparticles and polystyrene microparticles using polynomial microelectrodes. The DEP motion of polystyrene particles was studied in different acidic medium i.e HCl, KCl, KOH, tetrabutylammonium chloride. They found out that the migration velocity of polystyrene particles is enhanced for the p-DEP under acidic conditions. In their succeeding work in 2003, Tsukahara and group [67] extended the DEP study from single polystyrene microparticles to microbioparticles such as yeast cells and DNA molecules. They concluded that the DEP force is exerted not on the intrinsic volume of the particle. but on the total volume including the intrinsic volume and the volume of the dynamic diffusion cloud formed around charged particles. Green et al [68] reported sub-micrometre particle dynamics under the influence of dielectrophoretic and electrohydrodynamic forces. They reported that charge double layer effects are most important in low conductivity media typically at frequencies in the low kHz range where they can cause a p-DEP force to be exerted on a particle of otherwise low polarisability.

In 2002, Ratanachoo et al [69], studied the time and dose response of human leukemia cells in response to various toxicants that changes the cell morphology and physiology significantly. The method uses the measurement of the DEP cross-over frequency vs. the conductivity of the suspending medium to deduce the cell dielectric properties. Changes in cross-over frequency are indicative not only of the specific cellular responses to drug or chemical agent exposures but also of the ability of microscale DEP methods to detect such exposures.

In 2003, Asokan et al [70], demonstrated two dimensional manipulation of proteins using DEP trapping technique. They reported that actin filaments of length greater than 1 μm can be successfully trapped at high electric field areas with field strengths of 1.5×10^6 V/m.

In 2004, Zheng et al [71] used polynomial electrode geometry fabricated for positioning of DNA and proteins on a chip by DEP. There's was the first group to measure, the conductance of DNA and proteins trapped between two electrodes using

DEP by in situ monitoring the impedance change of the DNA and protein solutions in both solution and dry states.

Du et al in 2008 [72], demonstrated that the use of the present quadrupole electrode design to achieve superfast and long-range trapping of DNA molecules with ac fields. The trapping is the result of collaborative effects of AC electroosmotic flow focusing, dipolar attraction between polarized DNA molecules, and DEP. Beck et al [73], presented the ability to rapidly detect individual bacterial spores via electrical measurements. The magnitude of the electrical response when an individual spore enters a gap between two planar microelectrodes is used to discriminate between different *Bacillus* species. Measurement of the electrical response of individual spores provides a way to discriminate between different bacterial spores that can be used in conjunction with additional separation and identification methods.

In 2009, Jang et al [74] reported the use of alternating current electrothermal effect induced flow and n-DEP force for guiding and trapping of single particle. Manipulation of particle motion using AC electrothermal flow to target trap is modeled numerically. Manipulation and trapping of the latex beads and HeLa cells in physiological media was demonstrated in the diagonal, vertical, and horizontal directions and the particle velocities were analyzed. It was observed that velocities increase with increasing distance from the electrodes and higher applied voltages.

In 2011 Chung et al [75], presented a simple, and sensitive method to detect the antibiotic susceptibility of *E. coli* via measuring the changes in the DEP behavior and the elongation rate caused by the antibiotic treatment. The dielectric properties and shapes of bacteria, which are drug sensitive, are changed by treating with different antibiotics concentration; thus, the viability of bacteria can be distinguished. The DEP approach was used to observe the change in dielectric properties of bacteria after the antibiotic treatment and to fix bacteria on the focal plane for scaling analysis.

In 2016, Tanaka et al [76] was the first to report the use of dielectrophoresis to manipulate the single- particle passage through a solid-state pore in transverse direction. The solid state pore consisted of four Pt electrode which creates a trap field when supplied with AC voltage. It was anticipated that the transverse field effects can be strengthened by using a low salt concentration solution that provides more

extensive electric field distributions inside pore channels. Menachery et al [77] used quadruple geometry to dielectrophoretically characterize the two phenotypic variants of small cell lung cancer cells. Mixed population of two phenotypic variant cells was fractionated by flowing the cells through the chamber at a flow rate of 50 nl/s while applying a 3Vp-p, 40 kHz AC to the electrodes. They concluded the ability of DEP to selectively sort cell types with subtle phenotypic differences.

In 2017 Amico et al [78], developed a system with combined membraneless microfluidic dialysis and DEP to achieve label-free isolation and concentration of bacteria from whole blood. DEP force was created using a co-planar quadrupole microelectrode geometry embedded at the bottom of the channel. E.coli cells were separated from normal blood cells by applying a frequency between 0.5-30 MHz. For the enrichment of bacteria from blood co-planar planar electrodes were used. The total trapping efficiency for E.coli was $79\pm 3\%$ and Staphylococcus aureus was $78\pm 2\%$.

2.2.1.5 Angled or slanted electrodes

This category of electrodes as shown in Figure 2.6 consists of a pair or an array of microfabricated electrodes that are at an angle to the flow direction. This geometry offers an easy alternative to other planar electrode designs as it generates sufficiently strong electric field to realize DEP. Some of the authors that have utilized this geometry is discussed in detail below:

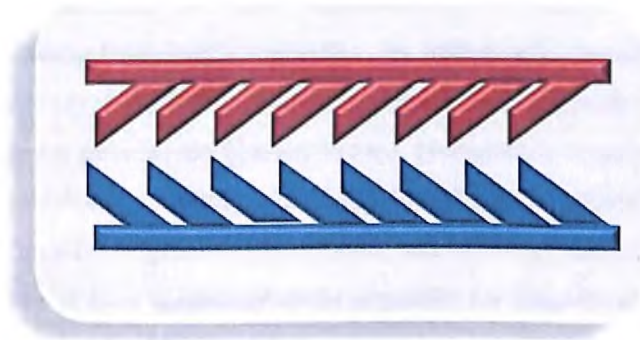


Figure 2.6: Angled electrodes

In 2006, Karlj et al [79] used an array of angled interdigitated electrodes to dielectrophoretically separate polystyrene particles by size. Polystyrene particles suspended in aqueous solution flow continuously across an electrode array and

experience transverse DEP force that depends on particle size. Larger particles are deflected more than smaller particles, and consequently, particles suspensions are separated by size into different transverse positions as they flow down the length of the device. It was concluded that reduction in the electrode spacing and channel height would make it possible to generate stronger electric field gradients and separate mixtures of smaller particles with good efficiency.

In 2007 Fatoyinbo et al [80], described the use of DEP for isolating and concentrating bacterial spores in a solution containing diesel particulate matter. They reported the use of gold interdigitated electrodes that were angled at 45° to the flow. The results show 99% removal of diesel particulate matter from bacterial spores by retaining particle matter on the electrodes by p-DEP.

Kim et al in 2008 [81], for the first time proposed a novel approach to specifically label multiple cells with unique synthetic dielectrophoretic tags i.e polystyrene beads of different diameter that modulate the complex permittivities of the labeled cells, allowing them to be sorted with high purity using DEP. The DEP chip employed microfabricated gold angled electrodes to create the necessary repulsive force inside the channel. The results demonstrate approximate 1000-fold enrichment of multiple bacterial target cell types in a single-pass separation. Pommer et al [82], used DEP phenomenon to separate platelets from whole blood in a continuous flow. Cytometry analysis revealed that a single pass through the device yields a high purity of platelets approx 95%. Vahey and Voldman [83] demonstrated the first implementation of microfluidic equilibrium separation method using Isodielectric separation, for sorting cells based upon electrically distinguishable phenotypes. DEP is used to force cell to a point in the conductivity gradient where the net polarization charges is zero. Isodielectric separation offers many advantages as the device is continuous-flow, capable of parallel separations of multiple subpopulations from a heterogeneous background, and label-free method. Han et al [84], presented a continuous flow dielectrophoretic separator for laterally separating red and white blood cells. They reported the fabrication of converging and diverging electrode design to perform separation. Experimental results showed that the divergent type of microseparator can continuously separate out 87% of the RBCs and 92.1% of the WBCs from dilute whole blood. While the convergent type of microseparator could separate out 93.6% of the RBCs and 76.9% of the WBCs.

experience transverse DEP force that depends on particle size. Larger particles are deflected more than smaller particles, and consequently, particles suspensions are separated by size into different transverse positions as they flow down the length of the device. It was concluded that reduction in the electrode spacing and channel height would make it possible to generate stronger electric field gradients and separate mixtures of smaller particles with good efficiency.

In 2007 Fatoyinbo et al [80], described the use of DEP for isolating and concentrating bacterial spores in a solution containing diesel particulate matter. They reported the use of gold interdigitated electrodes that were angled at 45° to the flow. The results show 99% removal of diesel particulate matter from bacterial spores by retaining particle matter on the electrodes by p-DEP.

Kim et al in 2008 [81], for the first time proposed a novel approach to specifically label multiple cells with unique synthetic dielectrophoretic tags i.e polystyrene beads of different diameter that modulate the complex permittivities of the labeled cells, allowing them to be sorted with high purity using DEP. The DEP chip employed microfabricated gold angled electrodes to create the necessary repulsive force inside the channel. The results demonstrate approximate 1000-fold enrichment of multiple bacterial target cell types in a single-pass separation. Pommer et al [82], used DEP phenomenon to separate platelets from whole blood in a continuous flow. Cytometry analysis revealed that a single pass through the device yields a high purity of platelets approx 95%. Vahey and Voldman [83] demonstrated the first implementation of microfluidic equilibrium separation method using Isodielectric separation, for sorting cells based upon electrically distinguishable phenotypes. DEP is used to force cell to a point in the conductivity gradient where the net polarization charges is zero. Isodielectric separation offers many advantages as the device is continuous-flow, capable of parallel separations of multiple subpopulations from a heterogeneous background, and label-free method. Han et al [84], presented a continuous flow dielectrophoretic separator for laterally separating red and white blood cells. They reported the fabrication of converging and diverging electrode design to perform separation. Experimental results showed that the divergent type of microseparator can continuously separate out 87% of the RBCs and 92.1% of the WBCs from dilute whole blood. While the convergent type of microseparator could separate out 93.6% of the RBCs and 76.9% of the WBCs.

Alazzam et al in 2011 [85], was the first to propose a method for continuous flow separation of circulating malignant cells from blood using deflector DEP and interdigitated comb electrodes. Malignant cells were separated from the blood to a daughter channel using two pairs of Cr interdigitated comb electrodes that were positioned convergent and divergent to the flow force that raises the separation speed. Kuczenski et al [86], utilized pairs of angled microelectrodes to continuous flow and separate E. coli cells from RBC. The results illustrate that the device is capable of a five-fold larger microbe concentration in the target analyte stream compared to the waste stream at a continuous sample flow rate of 35 $\mu\text{l/h}$.

In 2013 Yang et al [87], successfully manipulated and isolated prostate cancer cells from colorectal cancer cells. Prostate cells were deflected to the side channel by n-DEP and were therefore got separated. The separation chip was made using transparent acrylic plastic substrates with a pair of indium tin oxide thin film electrodes that were angled at 45° on the bottom surface. DEP spectra of the prostate cancer cell and the colorectal cancer cell were measured in media with different conductivity. Effect of parameters such as flow rate and applied voltage has been investigated as well. Similar kind of work using same electrode design was reported by Alshareef et al [88] for separating breast cancer cells from colorectal cancer cells.

Song et al in 2015 [89], fabricated and presented a continuous flow microfluidic device for sorting of stem cells and osteoblast cells. The device had oblique interdigitated electrode array spanning the entire channel with an inclined angle of 45° with respect to flow direction. Experimental results with stem cells and osteoblasts were carried out at different flow rates, and clear separation of the two populations was achieved. Collection efficiency up to 92% and 67% for stem cells and osteoblasts, respectively, along with purity up to 84% and 87% was obtained.

2.2.1.6 Other planar designs

Few other electrode configuration as shown in Figure 2.7, like curved, triangular, dot and trapezoidal electrode configurations have also been reported by few researchers and are discussed in detail below:

In 1998 Cheng et al [90], for the first time reported the use of DEP for separation of cervical carcinoma cells from normal blood cells using an array of addressable electrode

array in a check board pattern. The advantage of this configuration is that the addressing pattern of the electrodes can be configured in many different ways unlike the fixed patterns of hard-wired electrodes. Also this was the only report so far of DEP being performed on a silicon chip as opposed to glass slides. It was observed during the separation process that no convective movement of cells was seen in contrast to what one might see with a glass slide based DEP device.

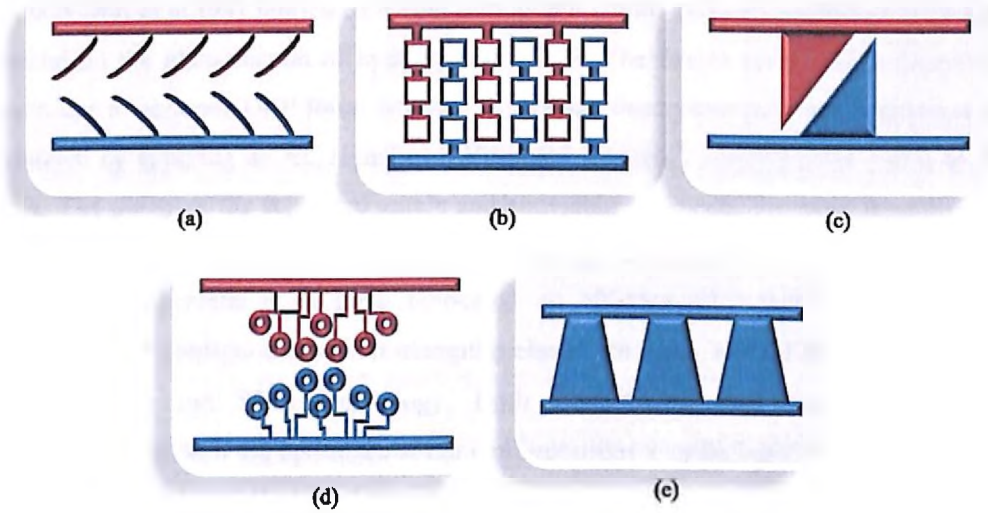


Figure 2.7: (a) Curved electrodes, (b) Electrode array, (c) Triangular electrode, (d) Dot electrodes, (e) Trapezoidal electrode.

In 2003 Frenea et al [91], proposed a design composed of high-density electrode array dedicated to the parallel positioning of single living cells using n-DEP. Several electrode shapes (circular, square and clover leaf shapes) arrays were evaluated and compared in terms of cell focusing capabilities. Field calculations tend to show that the circular electrode shape array may enhance the collection of particles. Suehiro et al [92], demonstrated continuous separation and recovery of yeast cells suspended in water using a DEP filter. The DEP filter consisted of an electrode system of copper films filled up with many glass beads. These glass beads modify the electric field distribution in the electrode system so that strong DEP force is generated on their surfaces. It was experimentally confirmed that the DEP filter could continuously eliminate yeast cells suspended in water as the cell density decreased from 10^6 to 10^1 cells/ml in about 1hr.

Gray et al in 2004 [93], presented a novel microfabricated device to actively trap thousands of single mammalian cells in alignment with a planar microelectrode array of gold. Cell confinement to the electrodes was accomplished by aligning a pattern of cell-adhesive regions with the electrode array, surrounded by a non-adhesive coating. Thus, after trapping with DEP, cells attached to the adhesive pattern and remained aligned to the electrodes. The proposed device achieved cell registration efficiency of $70\pm 1\%$.

In 2005 Doh et al [94] fabricated a high throughput continuous cell separation chip that worked on the phenomenon of hydrodynamic DEP. The device uses three asymmetric electrodes to generate DEP force. Mixture of live and dead yeast cells was continuously separated by applying an AC signal of 8 Vp-p and frequency ranging from 1 kHz to 10 MHz. The purity of the separated viable and nonviable yeast cells has been measured in the range of 95.9–97.3 and 64.5–74.3%, respectively, at the mixture flow-rates of 0.1–1 $\mu\text{l}/\text{min}$. Nieuwenhuis et al [95], fabricated an efficient DEP particle sorter. Four different sorter configurations with triangular electrodes were realized in chips based on silicon, glass, and SU-8 technology. Both experimental and simulation results demonstrate that with the optimized sorter configurations very high performance gains of +200%. Holzel et al [96], demonstrated the trapping of single protein molecule by using an array of sharp triangular nanoelectrodes to create very strong electric field gradient. Trapping of the protein molecule was observed on applying sinusoidal signal of 10 Vrms and 1 MHz. Choi et al [97], for the first time proposed the use of planar trapezoidal electrode array for DEP particle separation and analysis by n-DEP. The work studies the effect of flow rate on focusing performance, the electrode number on separation performance, and separation of beads.

In 2009 Khoshmanesh et al [98], developed a device for performing dielectrophoretic manipulation of particles using novel curved electrodes that formed a funnel. This geometry gradually introduces the DEP field to the particle flow and hence avoiding turbulent shock. The channel is fabricated from PDMS and the pair of five curved electrodes made of gold is on the glass substrate. The performance of the system was assessed with microspheres of 1, 5 and 12 μm in diameters. In his series of work in 2010 [99], the authors modified the curved channel by changing the width of the microchannel to 600 μm from 1000 μm that was used in the previous study. Smaller width microchannel, decreased the volume of the redundant sections of the micro-channel,

which in turn increased the performance of the system by allowing particles to experience DEP forces more efficiently.

In 2010, Koklu et al [100], fabricated a microfluidic device for capturing bacterial spores and polystyrene particles from high conductivity media. They utilized an interdigitated array of planar square electrode design fabricated onto glass slide with PDMS layer on top. On application of ac signal of 10 Vp-p and 10 MHz frequency, polystyrene beads experienced n-DEP and got trapped in shallow chambers in the centre of each square electrode.

Young et al in 2012 [101], fabricated a device for single cell lysis using electro-osmotic flow and DEP force. Electro-osmotic flow was used to drive the cell to the specific area while varying the frequency (1 Hz-1 MHz) lead to lysis of the cells. The electrode for cell lysis is a triangular palladium (Pd) electrode with a sharp tip fabricated onto a glass substrate. On application of 15 V and 400 kHz cell lysis was observed. The overall successful rate of cell tracking, positioning, and lysis was 80%.

In 2013 Yafouz et al [102] described the microarray dot electrode, a promising electrode geometry to characterize and manipulate cells via DEP. The protocol for fabricating planar microelectrodes using photolithography has also been described to demonstrate that it is a fast and cost-effective process.

In 2018, Chen et al [103], developed a microfluidic chip integrated with DEP technique, hole array structures and fluorescence to trap, detect and count *S. oneidensis* multi cells. The gold coplanar microelectrode array was fabricated on glass substrate along with a micro hole array layer, and the microfluidic channel was made in PDMS. The results demonstrate that the amount of bacteria correlated with the hole sizes. The microfluidic platform provided a rapid and effective bacteria trap and cell level measurements.

which in turn increased the performance of the system by allowing particles to experience DEP forces more efficiently.

In 2010, Koklu et al [100], fabricated a microfluidic device for capturing bacterial spores and polystyrene particles from high conductivity media. They utilized an interdigitated array of planar square electrode design fabricated onto glass slide with PDMS layer on top. On application of ac signal of 10 Vp-p and 10 MHz frequency, polystyrene beads experienced n-DEP and got trapped in shallow chambers in the centre of each square electrode.

Young et al in 2012 [101], fabricated a device for single cell lysis using electro-osmotic flow and DEP force. Electro-osmotic flow was used to drive the cell to the specific area while varying the frequency (1 Hz-1 MHz) lead to lysis of the cells. The electrode for cell lysis is a triangular palladium (Pd) electrode with a sharp tip fabricated onto a glass substrate. On application of 15 V and 400 kHz cell lysis was observed. The overall successful rate of cell tracking, positioning, and lysis was 80%.

In 2013 Yafouz et al [102] described the microarray dot electrode, a promising electrode geometry to characterize and manipulate cells via DEP. The protocol for fabricating planar microelectrodes using photolithography has also been described to demonstrate that it is a fast and cost-effective process.

In 2018, Chen et al [103], developed a microfluidic chip integrated with DEP technique, hole array structures and fluorescence to trap, detect and count *S. oneidensis* multi cells. The gold coplanar microelectrode array was fabricated on glass substrate along with a micro hole array layer, and the microfluidic channel was made in PDMS. The results demonstrate that the amount of bacteria correlated with the hole sizes. The microfluidic platform provided a rapid and effective bacteria trap and cell level measurements.

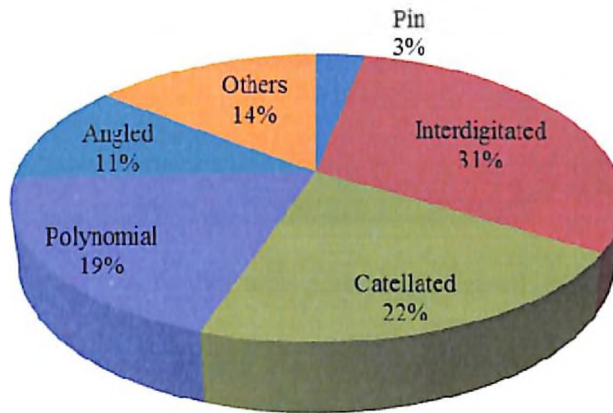


Figure 2.8: Pie chart representation of various 2D electrode configurations

A pie chart representation of different 2D electrode geometries is shown in Figure 2.8. The pie chart shows the percentage contribution of each of the electrode geometry in the field of DEP. It is inferred from our study that the interdigitated electrode configuration is most widely explored as it constitutes 31% of the total pie chart.

2.2.2 Three Dimensional 3D Electrodes

Compared to 2D planar electrodes that are commonly patterned on the bottom of the microchannel, 3D electrodes includes the top-bottom electrodes patterned inside the microchannel, extruded electrodes and electrodes that are patterned on channel sidewalls. 3D electrode designs increase the region where effective DEP takes place, allowing the improvement of microsystem efficiency. Also, it avoids the problem of particle adhesion on the surface of electrode or channel walls that occurred in dielectrophoretic devices with 2D electrodes.

2.2.2.1 Top-bottom electrode pattern

One of the simplest approach to overcome the limitations offered by 2D planar electrodes is to use a pair of electrodes on the floor and ceiling of the microchannel as shown in Figure 2.9. This electrode arrangement helps in extending the electric field to a much greater distance inside the microchannel thereby allowing better control over particle manipulation. Some of the work using this geometry is discussed in detail below:

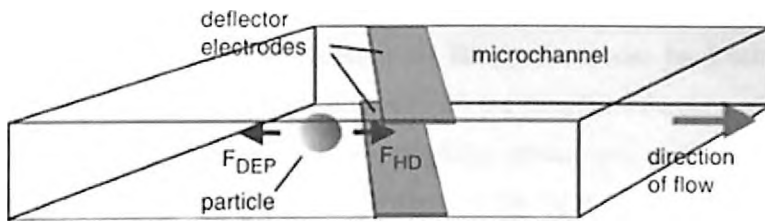


Figure 2.9: Top-Bottom patterned electrodes [104]

In 2003 Durr et al [105], fabricated a 3D DEP based device with deflector structures inside the channel to separate latex particles according to their size. Various microfluidic devices have been developed comprising pairs of electrodes extending into fluid channels on both top and bottom side of the microfluidic channels. Electrodes were aligned under angles varying from 0 to 75° with respect to the direction of flow. Similar 3D DEP geometry with deflector structure was used by Kentsch et al [104] for the separation of micro and submicrometer beads. The authors also fabricated a novel NanoVirDirect system that is a combination of dielectrophoretic deflector arrays, funnels and field-cages integrated in a microfluidic device.

In 2005 Park et al [106], reported the use of asymmetric 3D electrodes for efficient cell separation system using DEP. Compared with the typical 3D-microelectrode system, a continuously varied electric field was generated in the present 3D-asymmetric microelectrode system, and this field induced dielectrophoretic forces with more variation. A mixed cell suspension of mouse P19 embryonic carcinoma cells and RBCs was successfully separated when a sinusoidal potential of 8 V_{p-p} and 5 MHz was applied. The purities of the separated cells were 81.5±7.6% and 94.1±4.3% for P19 EC cells and RBCs, respectively.

In 2006 Chen et al [107] fabricated a DEP device with pairs of microelectrode structures on the top and bottom sides of the microchannel to separate particles based on n-DEP and hydrodynamic force. This geometry led to the formation of DEP gates between the top and bottom electrodes with high-frequency AC voltage. Behavior of microparticles such as polystyrene beads or cells carried by a laminar flow past the electrodes were studied. Depending on the relative strength of the DEP force and hydrodynamic force acting on the particles, the particles can either penetrate the gates or settle by the gates. The 3D electrodes allowed for higher holding force, higher operating flow rates allowed

and more stable particle movements. In his succeeding work in 2007 Chen et al [108] used the pair of top and bottom electrode pair, but the electrodes used were now open ended (i.e the top or bottom electrode do not touch the opposite microchannel wall). The separation of the particles was achieved by taking advantages of their differences in traveling velocities in the flow under the effects of the DEP and hydrodynamic forces. The particles running along the flow will exhibit two types of movements: penetrating the barrier or moving along the electrode edges, depending on the relative strength of the DEP force and hydrodynamics force on the particles. The proposed 3D electrode configuration overcomes the problems encountered in the planar electrodes such as particle adhesion at walls. Grom et al [109], successfully demonstrated the trapping of Hepatitis-A particles by means of a combination of electrohydrodynamic flow and dielectrophoretic forces. The microsystem consisted of a pair of polynomial electrodes of platinum, with each set on upper and lower half's of the microfluidic channel such that it formed a field cage structure

In 2007, Cheng et al [110] reported for the first time an integrated 3D DEP chip for continuous filtering, focusing, sorting, trapping and detection of bacteria using 3D DEP forces and surface enhanced raman scattering. The 3D electrode produce gates that utilize different n-DEP mobilities of the bacteria and other particles in a high-conductivity buffer to manipulate them within the channel. Yasukawas et al [111] proposed new immunosensing method and reported the development of an integrated microfluidic system for immunoassays using antibody-modified polystyrene particles. The system used a caged area surrounded by n-DEP generated electric barriers that capture microparticles modified with anti mouse immunoglobulins. The model system described demonstrated that the n-DEP device allows a full immunoassay to be completed in 40 min.

In 2012 Imasato et al [112], reported the separation of leukemia cells from blood using DEP. For performing experiments they have considered two types of electrode location, "flooring electrodes" and "ceiling electrodes". The results show that the abnormal cells may be detected by using the magnitude difference of the DEP forces. Leukocytes were separated from erythrocytes by DEP at 60 MHz, 10 Vp-p and leukemia cells were separated from the normal leukocytes (Mononuclear) at 37 kHz, 14 Vp-p.

Li et al in 2013 [113] proposed an integrated array consisting of three units: a funnel-shaped focusing unit, a straight aligning unit, and a crescent-shaped trapping unit, which

was used to concentrate different-sized polystyrene microparticles and yeast cells, separate polystyrene particles based on size, and separate 5 μm polystyrene particles from yeast cells based on dielectric properties. The authors present the threshold voltages required for successfully trapping varying-sized particles, along with the effects of applied voltage and flow rate on the cell-trapping efficiency. Li et al [114], investigated the integration of hydrodynamic, DC electroosmotic, DC electrophoretic, and AC dielectrophoretic forces in microchannels and developed a high-throughput Lab-on-a-chip device. The proposed device allows the integration of trapping, release and separation functions and operates in several channels in parallel. The device was tested for capturing polystyrene particle, yeast cells, and E-coli, and also for separation of live and dead yeast cells. Hamada et al [115], proposed a device for simultaneous concentration and detection of bacteria. The device uses a set of planar gold electrodes first to concentrate cells by n-DEP followed by its detection using p-DEP. Yunus et al [116], fabricated a device for continuous flow through separation of colloidal particles. For particle separation an innovative design for a double-sided aligned electrode array is presented. The electrodes were fabrication onto a pyrex glass substrate with platinum as electrode material. They were able to achieve separation efficiency of 99.9% of latex spheres.

2.2.2.2 Extruded electrodes

DEP with top-bottom electrodes helps in improving the trapping efficiency, but the alignment and bonding of the top and bottom electrodes is difficult. This has prevented many DEP techniques from adapting this configuration. Employing extruded microelectrodes as shown in Figure 2.10 (reported by Voldman [117]) is another method to improve the particle manipulation efficiency. Extruded electrodes unlike the planar ones cover more height of the microchannel. This arrangement of electrode increases the volume where particles experience a strong DEP effect. Some of the work using this configuration is discussed in detail below:

In Voldman et al in 2002 [117] and 2003 [118], demonstrated the dielectrophoretic trapping of beads using microfabricated gold posts excited in a quadrupolar fashion fabricated on glass substrate. The extruded electrode structures were designed in such a way that they can strongly hold particles against flow. The results show the greatly increased strength of the new trap i.e 100 times as compared to the planar trap. In the

former year trapping of HeLa cells was reported whereas latter includes the trapping of polystyrene particles.

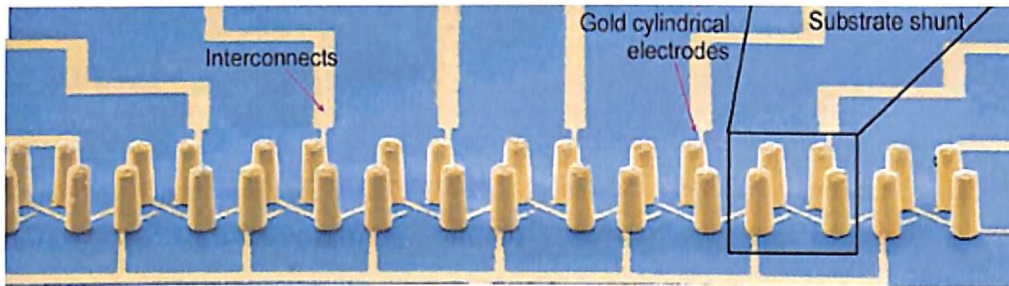


Figure 2.10: Extruded gold electrode posts [117]

In 2004 Hunt et al [119], developed a device for trapping and positioning of particles using gold micropost matrix electrodes (50 nm height), where each of the posts could be energized individually. The device showed trapping and positioning of a single yeast cell when a post was energized with 10 V and 10 MHz frequency.

In 2008 Iliescu et al [120], proposed a bidirectional separation method using DEP and 3D electrode pillars with square cross section. The device was successfully tested for the separation of viable and non-viable yeast cells. By applying an electric field the two populations are separated in different locations according to their electrical properties and are simultaneous flushed out by flowing fresh buffer solution.

In their succeeding work in 2009, Iliescu et al [121] used a field-flow method for separating particle populations in a DEP chip with asymmetric 3D electrodes under continuous flow. Electrode arrays consisted of an array of thick and thin square cross sectional pillars to generate an increased gradient of electric field in the vertical plane that can levitate the particles experiencing n-DEP. The separation method consists of trapping one population using p-DEP in the plane of the thin electrode, while the other population is levitated using n-DEP and flowed out. Separation of live and dead yeast cells is achieved with an efficiency of around 90%.

In 2017 Zaman et al [122], proposed an efficient method for trapping nano-particles using DEP assisted plasmonic traps. The plasmonic trap consists of a C-shaped engraving on a gold base, a gold nanopillar and an indium tin oxide plate. A polystyrene sphere of radius 150 nm was selected as the nanoparticle. In the proposed technique, AC voltage is applied first to draw the nanoparticle near the nanopillar due to DEP then the

voltage is turned off and the laser is turned on, so that the optical force from the C structure can pull the particle and trap it. It is found that the proposed scheme shows a significant increase in particle trapping probability.

2.2.2.3 Sidewall patterned electrodes

Apart from top-bottom patterned electrodes and extruded electrodes, few authors have also used sidewall patterned electrodes for DEP applications. A set of interdigitated electrodes embedded in the sidewall of the microchannel is shown in Figure 2.11 [123]. However these electrodes are not necessarily made from metals but from other materials like conducting PDMS or Silicon. The details of work using this electrode configuration are described below:

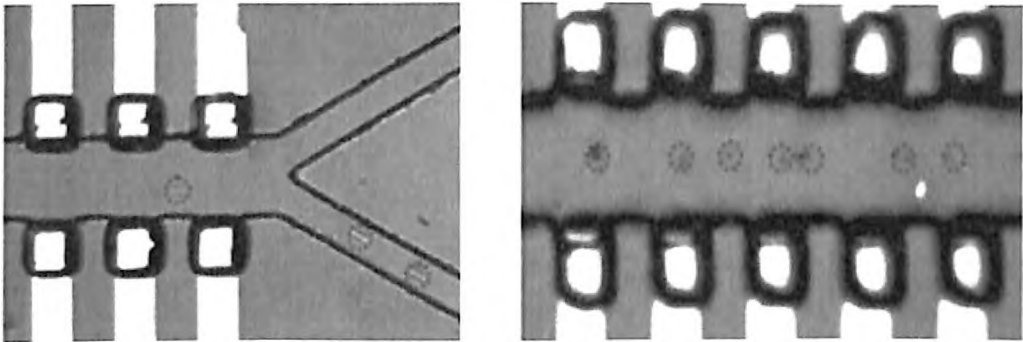


Figure 2.11: Sidewall interdigitated electrode [123]

In 2007, Tay et al [124] presented a DEP device with highly doped silicon, which acted both as channel wall and electrodes simultaneously. This dual purpose 3D DEP device maximizes the channel volume where the particles experience useful DEP force, therefore improving the trapping efficiency of particles. Also, the joule heating effects are 8–10 times lower than in the planar 2D structure, making the device suitable for use in biological applications. The device was tested with yeast cells and the results show that even at high flow rate of 1 ml/min, the 3D silicon electrodes can still achieve a trapping efficiency of more than 60%. Yu et al [125] reported a similar study on DEP except that they reported the use of triangular channel walls instead of semicircular ones as used by Tay et al. Wang et al [123] presented a novel DEP switching with 3D sidewall electrodes. A set of interdigitated electrodes in the sidewall of the microchannel generates n-DEP force that repels beads/cells from the sidewall making it to switch from one outlet to the other. The switching depends on

the set of electrodes energized. Experimental results for switching biological cells and polystyrene microbeads to multiple outlets (up to 5) have been achieved.

DEP separation of cells in microfluidic channel by dual frequency coupling using the same geometry [123] has been reported by Wang et al in 2009 [126]. Cetin et al [127], presented a novel device for the continuous separation of 5 and 10 μm latex particles and yeast cells from white blood cells. The DEP device had two asymmetric electrodes embedded along the channel wall to generate a non-uniform electrical field in the y-direction.

In 2010 Lewpiriyawong et al [128] developed a PDMS based microfluidic device for continuous sorting and separation of microparticles by size using AC DEP with 3D conducting PDMS composites as sidewall electrodes. The composite was synthesized by mixing silver powders with PDMS gel. The capability of PDMS-based microfluidic device was demonstrated for continuously sorting and separating 10 and 15 μm , and 5 from 10 μm particles respectively. In their succeeding work in 2011, Lewpiriyawong et al [129] demonstrated the use of 3D conducting PDMS composite side wall electrode for the separation of live yeast and bacterial cells from similar-size latex particles as well as live yeast cells from dead yeast cells. The separation efficiency of 97% was achieved in all cases.

2.3 Carbon Electrodes

Most of the work in DEP relies on the use of metal microelectrodes contained in a flow channel to induce non-uniform electric field [130]. However, 3D metal electrodes were able to increase the throughput of the DEP device by extending the electric field along the channel height but there are still some issues that need to be addressed. The use of metal microelectrodes in direct contact with the sample severely restricts the magnitude of the applied voltages as one must prevent sample electrolysis. Unfortunately, the fabrication of 3D metal electrodes quickly turns complicated and expensive as it typically requires the use of metal electroplating which often limits the yield and results in more expensive devices. In order to overcome the above mentioned issues, 3D carbon electrodes have recently been used in DEP devices.

The carbon micro/nano electromechanical systems techniques is one of the most cost effective methods for fabrication of high aspect ratio carbon structures. Carbon

microstructures originated thousands of years ago when the first attempt of making charcoal succeeded. As early as 1970s, an attempt has been reported on pyrolysis of carbon polymer precursors like polyacrylonitrile, polyimide and phenol formaldehyde that resulted in amorphous carbon structures. For applications involving direct contact of the electrodes with the sample solution, carbon electrodes have an edge over metal electrodes. For example, the possibility of sample electrolysis is reduced because carbon has a much larger electrochemical stability window [131], [132] than metals. Carbon when compared to the commonly used metals in thin film electrode fabrication such as gold and platinum affords higher applied voltages in a given solution without electrolyzing it [133]. This fact only applies when comparing bare materials, and improvements have been reported to metal electrodes to maximize performance. Few authors have also detailed the use of hydrogel coated metal electrodes [134], [135]. Such hydrogel coatings can be applied to any electrode material and not only to metals and could bring a significant improvement to the field in general. It is also observed that the properties of carbon electrodes are very similar to glassy carbon [136]. The use of carbon electrodes also have other advantages like: (a) excellent biocompatibility [137]–[139], (b) chemically very inert in almost all solutes/electrolytes [140], (c) excellent mechanical properties [141], and (d) low fouling rate [142][143], (e) resistant to corrosive environment. Also some efforts have already been reported to remove or reduce fouling problems that are associated with carbon electrodes in many electrochemical experiments [144]. Recently 3D form of carbon that is metallic and stable under ambient pressure and temperature conditions has also been discovered [145].

Carbon microstructures are fabricated by using a well known Carbon MEMS (C-MEMS) or resist pyrolysis technique. The section below details the C-MEMS process along with its contribution in the field of DEP.

2.3.1 C-MEMS

C-MEMS or carbonization [139] refers to a fabrication technique where glass-like carbon is obtained by converting microstructure to nanostructures that have been patterned using photolithography, molding, embossing or any other suitable patterning technique, followed by its pyrolysis in an inert atmosphere.

The process of carbonization or C-MEMS, combines different polymers patterning techniques followed by its pyrolysis at elevated temperatures (1100°C) to derive glass-like carbon structures. Pyrolysis is the typical process for fabrication of the carbon structures which is realized in an inert atmosphere at high temperatures, including a hard baking step and a carbonization bake step. Specifically, when a polymer precursor is pyrolyzed, it results in the removal of volatile impurities and leaving new C-C bonds. Typical process for fabricating the C-MEMS is shown in flow schematic in Figure 2.12.

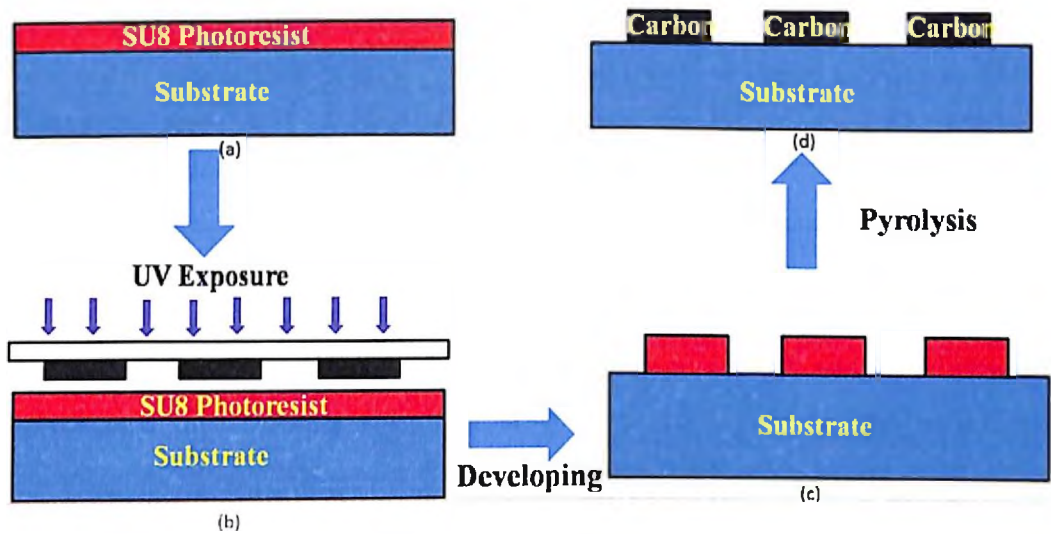


Figure 2.12: C-MEMS Process flow (a) Spin coating of photoresist of desired thickness (b) Exposure to UV light to pattern the resist (c) Photoresist pyrolysis (d) Carbon posts.

The micromaching process starts with spin coating a layer of photoresist on to a substrate (e.g. Silicon wafer) to form a uniform photoresist layer as shown in Figure 2.12(a) ranging from few 100nm to few mm in thickness, depending upon the spin speed and the type of resist used. The resist is then micro-patterned using a variety of methods: conventional tool machining, molding, stamping, photolithography etc to cross-link the resist as shown in Figure 2.12(b). Then using a photoresist developer high aspect ratio resist structures are obtained as shown in Figure 2.12(c). These structures are then pyrolyzed in a non-reactive atmosphere to obtain carbon structures as shown in Figure 2.12(d). During pyrolysis the photoresist (epoxy) decompose into volatile components, such as water, carbon dioxide, carbon mono-oxide and methane leaving solid residue rich in carbon [146]. Although some shrinkage occurs, but the geometry is largely preserved during carbonization because the shrinkage is isometric. To maintain

the structure isometric, it is necessary to heat the structure below its glass transition temperature [147].

A lot of work has been done towards fabricating and characterizing 2D films and carbon structures in various applications. Some of them are discussed in chronological order below:

Kim et al in 1998 [148], presented that carbon film electrodes prepared at temperatures greater than or equal to 700°C showed electrochemical behavior similar to that of glassy carbon. Ranganathan et al in 2000 [136] studied the effects of various atmosphere on the shrinkage of positive resist films. The results show that the extend of the shrinkage depends upon the oxygen content in the furnace. Singh et al in 2002 [149] fabricated carbon structures using negative photoresist (SU-8 and photosensitive polyimide) and compared those with the structures formed by positive photoresist (AZ4330). Park et al in 2005 [150] discussed about the electrical characteristics and shrinkage of various thickness (1.5-25µm) carbon films derived from SU-8 and AZ P4620, at different temperatures (600-1000°C). NAKA et al in 2005 [151] presented the design and fabrication of pyrolyzed polymers (photosensitive polyimide) micro bridge structures as a typical MEMS structure used for sensor and actuator. They also formed thin films of electron beam resist (SAL-601 SR-2, Rohm & Hass), and studied the change in its thickness and resistivity, further he also detailed the fabrication of an array of micro pillars using pyrolyzed Parylene-C. Burckel et al in 2009 [152] reported a robust fabrication method to create lithographically defined porous pyrolyzed carbon electrodes (from negative resist NR-7) and characterized the electrochemical properties of metal nanoparticles on these electrodes. Sharma et al in 2010 [153] demonstrated a novel and facile method for micro-fabrication of a variety of surface patterns and sub-surface micro-structures, such as channels, in carbon by employing micro-molding of an aqueous resorcinol-formaldehyde (RF) gel, followed by its drying and pyrolysis under optimized conditions to ensure isotropic shrinkage and minimal pattern distortion and cracking. Min Jin et al in 2011 [154] presented a facile and effective route to develop a supported pyrolysis method that employed a coating of Silica shell on SU-8 structures. The Silica shell on the SU-8 structures provided effective mechanical support to resist pattern distortion or collapse during subsequent large mass loss at high temperature. The carbon electrodes so obtained had sufficiently high conductivity so that they can be used as

electrodes in variety of applications. Sharma and Madou in 2012 [139] detailed the fabrication methodologies for carbon-MEMS and carbon-NEMS devices and strategies for their surface modification for biocompatibility and bio-sensing. They also detailed about wide variety of carbon precursor materials that can be patterned with a wide variety of tools to yield lengths from a few nanometers to a hundred microns.

There is a growing literature on C-MEMS, but to the best of our knowledge these 2D carbon structures has not been applied to the field of DEP. Although 3D carbon structures fabricated using pyrolysis process have found use in DEP. Some of the groundbreaking work using 3D pyrolysed carbon electrodes is described below:

2.3.1.1 Three dimensional 3D carbon electrodes

3D carbon structures fabricated by resist pyrolysis have been reportedly used in DEP applications. The advantage of using photoresist as a starting material is that it can be patterned by photolithography easily, and can also be molded into wide variety of repeatable shapes and structures thus making it possible to fabricate high aspect ratio structures as well as complex polymer micromechanical and microfluidic structures [155]. Moreover different temperature treatment of photoresist results in different resistivities, electrical and mechanical properties [150] that can widely be exploited. Figure 2.13 shows pyrolysed carbon post of different shapes [156].

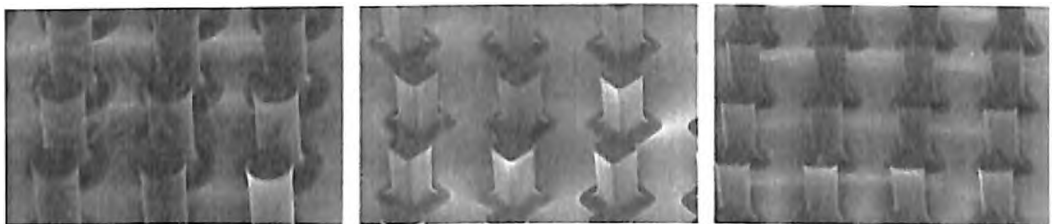


Figure 2.13: Carbon electrode posts [156]

Wang et al in 2005 [133], developed a novel fabrication process to fabricate high aspect ratio carbon structures. The structures were fabricated using two step pyrolysis process with SU-8 photoresist. Different substrates used for the photoresist pyrolysis were (1) bare Si, (2) $\text{Si}_3\text{N}_4(2000)/\text{Si}$ and (3) $\text{SiO}_2(5000)/\text{Si}$. Two kinds of positive photoresists-SPI827 and AZ4620, as well as a negative tone photoresist, SU-8 100, were used in this study. Iron (III) oxide nanopowder was mixed into SU-8 100 as one way to modify the SU-8 100 photoresist properties. By carefully controlling the lithography processing

parameters and the heating conditions, a variety of complex 3D C-MEMS structures by resist pyrolysis at 900°C in forming gas environment, a high-aspect C-MEMS posts and also suspended carbon wires, bridges, plates, and self-organized posts (carbon flowers) and ribbons (networks), were fabricated.

In 2008, Duarte et al [157], presented the fluid-dynamic and electromagnetic characterization of an array of 3D electrodes to be used in high throughput and high efficiency carbon DEP device. Finite Element Analysis (FEA) was conducted to model flow velocity and electric fields established by polarized high aspect ratio carbon cylinders, and planar carbon connecting leads, immersed in a water-based medium. SU-8 posts (130µm high and 50µm diameter) were fabricated in a two-step photolithography sequence and were then carbonized by pyrolysis at 900°C in nitrogen/forming gas environment leading to carbon structure array with features 60µm high post electrodes. Experimental results show continuous enrichment of viable yeast by p-DEP focusing. Another novel research work has been reported by Duarte et al [158], where a high throughput multi-stage, multi-frequency filter and separation device based on carbon DEP is presented. Two carbon arrays of 20x5 electrode, each made by pyrolysing SU-8. Carbon posts are 70 µm high with 25 µm in diameter. Microchannel of 600 µm width and 100 µm high has been fabricated using pressure sensitive double sided tape. First array trapped viable yeast cells when energized with 10 Vp-p and 5 MHz, while the second array trapped non-viable cells when energized with 500 kHz signal. Lee et al [159], presented two methods for fabricating multi-level 3D SU-8 microstructures. First technique involves a combination of multiple coating and exposures, whereas second method involved a dose modulation technique to control cross-linking thicknesses. Freestyle, freestanding carbon microstructures were fabricated by heating 3D SU-8 microstructures between 600-1000°C in a nitrogen atmosphere. Carbon structures from positive resist AZ 9260 were also fabricated and compared to those of SU-8.

In 2010, Jaramillo et al [160] used 3D carbon-electrode DEP chip to trap and release bacterial cells. The carbon electrodes were made using SU-8 as polymer precursor and was heat treated at 900°C in nitrogen/forming gas environment. The flow through channel (with cross section 600-µm wide and 100-µm height) was cut from pressure-sensitive double-sided adhesive and adhered to a piece of drilled polycarbonate. The channel is then aligned around the carbon electrode array and sealed against the

silicon/silicon dioxide substrate using a mechanical press. Carbon posts on interdigitated fingers when actuated with a sinusoidal signal of 10 Vp-p and frequencies ranging from 100 kHz to 30 MHz showed trapping of E.coli cells. Another interesting and novel research in the field of C-MEMS was reported by Duarte et al [161] [162] where 3D carbon electrodes were integrated with CD based centrifugal platform. SU-8 was used as polymer precursor and was pyrolysed at 900°C in inert environment to yield carbon. Two different heights (40-70µm) of carbon electrodes are used in this study. The CD based centrifugal platform was used to implement a DEP-enabled active filter to trap particles of interest. They studied the impact of electrode height, DEP chip misalignment and particle sedimentation on filter efficiency. The propose method offers advantages in terms of footprint, cost, robustness and practicality.

In 2011 Duarte et al [156], presented the fabrication of carbon electrodes on a transparent fused silica substrate. The use of a transparent substrate greatly improves the versatility of carbon-DEP devices and makes them more amenable for integration with other systems. also it is significantly cheaper than other high-temperature transparent materials such as sapphire. SU-8 was used as polymer precursor for carbon and was heat treated at 900°C in environment of nitrogen. The fabricated electrodes were then used for applications like particle positioning, high-throughput filtering and cell focusing using p-DEP.

In their succeeding work in 2012, Duarte et al [163], detailed different fabrication techniques that can boost the development of practical DEP devices to be used in different settings such as clinical cell sorting and infection diagnosis, industrial food safety, and enrichment of particle populations for drug development. Microfabrication of DEP devices has been critically reviewed in this work in terms of complexity, cost, and throughput.

In 2013, Jaramillo et al [164], presented the use of carbon electrode DEP system, in removing PCR inhibitors from a sample. They reported the capturing of viable yeast cells present in natural samples, purify them from any contaminants and finally recover them from the carbon-DEP chip. 3D carbon posts were obtained by pyrolysis of SU-8 at 900°C in nitrogen atmosphere. The height of the electrodes is 90 ± 10 µm while the diameter of the electrodes and the spacing between them is 58 µm. The total number of electrodes in the array is 2730. Fluidic network is build using pressure sensitive double

sided tape. The use of frequencies between 5 and 10 MHz and 20 Vp-p maximizes the amount of cells trapped. When frequencies below 2 MHz were used, large numbers of cells were washed out from the chip thus reducing yield. Duarte et al [165] was the first to report that carbon electrodes can be used for the manipulation and trapping of biomolecules such as DNA. SU-8 precursor structure was fabricated on a transparent fused silica substrate and then carbonized by heating to 900°C in nitrogen atmosphere. The geometry consisted of an array of planar interdigitated fingers connected to large connection pads; 3D electrodes were fabricated on top of each of the interdigitated fingers. They also compared the numerical and experimental results quantitatively and observed that the simulation results thus correlate well with the experimental results.

Another interesting and novel research in the field of C-MEMS was reported again by Duarte et al in 2014 [166], detailed the application of carbon electrodes as an active filter for trapping and purification of selected particles. The electrodes made by pyrolysing SU-8 pillars that were made on SU-8 interdigitated fingers and carbonizing them at 900°C in nitrogen environment. However the microfluidic channel was fabricated out of pressure sensitive double sided adhesive and aligning it to the channel inlet and outlet that were drilled in polycarbonate. They also proposed a multi-stage carbon DEP device, with five different sets of electrode array embedded in the channel. Each of the five sets of electrodes have different shapes, sizes and gaps in between them and can be polarized individually. Such system could significantly decrease the cost and time of common diagnostic assays in clinical and environmental applications. Elitas et al [167], used 3D carbon-electrode arrays for DEP-based separation of intact cells from damaged cells, and also reported the procedure to purify intact cells from cultures of *Mycobacterium smegmatis* treated with isoniazid, an anti-tuberculosis drug. Glass-like carbon electrodes were manufactured on a transparent fused silica substrate by pyrolysis of SU-8 structures at 900°C in nitrogen/forming gas environment. The array, of up to 2730 posts, features an intercalated geometry. Electrode dimensions in the devices were: 50 µm diameter by 100 µm height. A microfluidic channel, was fabricated in double-sided pressure-sensitive adhesive and polycarbonate, is then manually positioned around the electrode array. Electric fields with frequencies between 1 and 10 MHz induce a p-DEP behavior on the intact *M. smegmatis* cells, thus attracting them to the surfaces of the electrodes. The use of frequencies less than 500 kHz leads to strong n-DEP forces, as a result of which the

bacteria are repelled by the electrodes and they accumulate in the weak electric field regions.

Pilloni et al in 2016 [168], proposed a novel design which utilizes individually addressable planar and 3D carbon micro electrodes produced by the pyrolysis (at 900°C in nitrogen) of a common photoresist SU-8. The electrodes were demonstrated to manipulate the particles in 3D space by using DEP force. Islam et al [169], performed DEP enrichment of yeast cells using carbon electrodes. Carbon post microelectrodes on intercalated rows were prepared by pyrolysing SU-8 at 1000°C in nitrogen environment, and the flow channel was made from double sided pressure sensitive aligned to the electrode array. An enrichment of 154.2 ± 23.7 times was achieved when the sample flow rate was 10 $\mu\text{l}/\text{min}$ and the cells were suspended in low electrically conductive media that maximizes DEP trapping. The experimental trapping efficiency was found to be close to 100% for the cell concentration 10^2 – 10^4 cells/ml. Further Islam et al [170], reported that upon increasing the flow rate up to 30 $\mu\text{l}/\text{min}$, the enrichment dropped down to 18.4 ± 4 folds due to the increase of drag force, though the enriched concentration around 10^4 cells/ml was achieved. Davila et al [171], proposed the use of square wave to improve the trapping efficiency of 3D carbon based DEP devices. Computational modeling was performed to calculate the DEP force generated by both square and sine signal waveforms and the trapping efficiency was then determined experimentally. The DEP device was fabricated by pyrolysing SU-8 posts at 1000°C and then sealed with pressure sensitive double sided tape to form flow channel. The carbon electrode array features posts of 50 μm diameter and 100 μm height. Experimental results show that the trapping efficiency using square signals is as much as double as that obtained when using sinusoidal signals. Duarte et al [172], presented a detailed review highlighting the challenges in the field of carbon based DEP. The use of 3D electrodes over more traditional planar ones is emphasized as a way to increase the throughput of DEP devices.

In 2017, Yiltizhan et al [173], reported the dielectrophoretic separation and characterization of live and dead monocytes using 3D carbon-electrodes. Carbon electrodes were prepared by two-step photolithography process of SU-8 photoresist on a silicon wafer. Microelectrodes were carbonized by heat treatment to 1000°C in a nitrogen atmosphere. The 3D carbon-DEP chip has 218 intercalated rows of electrodes

for a total of 3161 electrodes with 100 μm height and 50 μm diameter. A 1.8mm-wide, 3.2cm-long channel was cut from a 127 μm -thick double-sided pressure sensitive adhesive and adhered to a previously drilled polycarbonate. This arrangement was then manually positioned around the carbon-electrode array and sealed using a rolling press. It was observed that when the electric field was 20 Vp-p–300 kHz, the viable monocytes exhibited p-DEP while nonviable cells remained unresponsive. Hassan et al [174], detailed investigation on the improvement and characterization of carbon electrodes obtained from negative epoxy based photoresist SU-8 with a pyrolysis process at 1100°C in N_2 . The influence of pyrolysis parameters such as heating rate and dwell time at the maximum temperature was investigated. It was observed that the resistivity value decreased when the dwell time at the highest temperature was increased. Also, for faster temperature ramps there is increased mass loss due to evaporation of organic compounds and consequently a more prominent decrease in final film thickness.

2.3.2 Screen Printing

Another well known technique for making carbon electrodes is screen printing technique. Screen printing is a cost effective way of depositing thin films on to a plane surface. Screen printing is also called a stencil method. This technology was originally developed for the production of miniature, robust and above all cheap electronic circuitry. For disposable chemical sensors, recent industrial experience indicates that screen printing is a good alternative to a high cost Si technology. The following section details the process of screen printing along with its contribution in DEP.

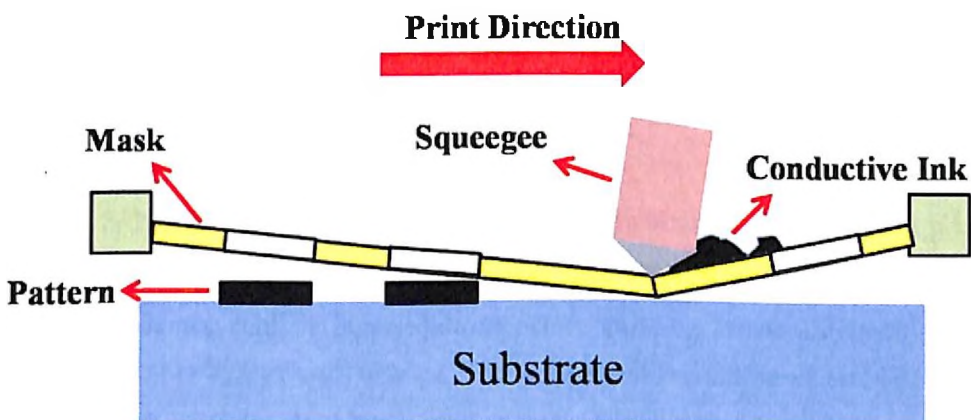


Figure 2.14: Schematic of screen printing technique

In the screen printing technique [175], a paste or an ink is pressed onto a substrate through openings on a screen with required mesh size as shown in Figure 2.14. The paste consists of a mixture of material of interest, an organic binder and a solvent. The organic vehicle determines the flow property of the paste. The bonding agent provides adhesion of particles to one another and to the substrate. The active particles make the ink a conductor, a resistor or an insulator. The pattern in the screen emulsion is transferred onto the substrate by forcing paste through the mass openings with the squeegee. In the first step, paste is put down on the screen, then the squeegee lowers and pushes the screen onto a substrate, forcing the paste through the openings in the screen during its horizontal motion. During the last step, the screen snaps back, the thick film paste which adheres between the screening frame and the substrate shears, and the printed pattern is formed on the substrate. The resolution of the process depends on the openings in the screen and the nature of the pastes. For difficult to print pastes, a shadow mask may complement the process, such as a metal foil with openings. However the resolution of this method is very inferior. Finally after printing the wet print is allowed to dry, this removes the solvent from the paste. Currently, synthetic threads are commonly used in the screen printing process. The most popular mesh in general use is made of polyester. There are special use mesh materials of nylon and stainless steel available to the screen printer. There are also different types of mesh size which will determine the outcome and look of the finished design on the material.

Although not new, having being in existence for over many years, it is only in the last few years or so that Screen printing technology have found use in printing carbon electrode for microfluidics applications like DEP [176], and electrochemical biosensors [177]. Some of the innovative work utilizing screen printing technology in this field of DEP is discussed below:

Zhu et al in 2015 [178], fabricated a microfluidic chip via inexpensive screen printing method. Carbon paste, instead of metals, was used to print interdigitated electrodes which were constructed by layer-by-layer screen printing process. The commercial carbon paste (ED 423SS, ACHESON, USA) was first printed on clean glass surface to form interdigitated carbon electrodes of three different configurations via a semi-automatic screen printer and a 400 mesh stencil. After curing at 130°C for 10 min to harden carbon paste, UV curable dielectric paste (YB-1300) was repeatedly printed

and exposed to UV light for 5 min to form micro-fluidic channels. The depth of the channels was controlled at ca.50 μm . Finally, a PDMS polymer film with inlet and outlet ports was exposed to O_2 plasma, pressed on the top of the microfluidic channels and then heated in an oven at 80°C for 1h. To demonstrate its dielectrophoretic separation performance, yeast cells, were trapped and separated from a mixed suspension with polystyrene microspheres. The results show that high capture rate and separation efficiency (94-96%) can be achieved under optimized conditions.

The limitation offered by the device proposed by Zhu et al in 2015 was the long exposure time of cells of interest to the high electric field gradient and high fluid-shear force imposed on cells, leading to the decrease in cell viability. Therefore Lin et al in 2016 [179], improved the DEP device by screen-printing 3D sidewall electrodes so as to realize continuous-flow cell and particle sorting and separation and thus enhance the cell viability dramatically by reducing their exposure time to the electric field. Also, they proposed and validated a semi-empirical formula to simplify the complicated calculation and plotting of DEP spectra. Carbon electrodes were fabricated by screen printing carbon paste (ED423SS) onto a glass substrate. After heating at 130°C for 10 min to cure the carbon electrodes, UV curable dielectric paste (YB-1300) was printed using another stencil and then exposed to UV light for 5 min to form the microchannel. The thickness of channels and electrodes were controlled at ca. 25–30 μm . Finally, a flat polydimethylsiloxane (PDMS) layer with an inlet port and three outlet ports was sealed onto the glass slide using O_2 plasma. The performance of a screen-printed continuous flow microfluidic DEP device was evaluated using a suspension containing polystyrene (PS) microspheres and erythrocytes is used as the biosample. The results show that a high sorting efficiency (93%) can be achieved.

A pie chart representation of different 3D electrode geometries is shown in Figure 2.15. The pie chart shows the percentage contribution of each of the electrode geometry in the field of DEP. It is inferred from our study that the pyrolysed carbon electrodes have been widely explored as it constitutes 42% of the total pie chart. While, the fabrication of 3D carbon structures using screen printing technique is the least investigated in the field of DEP.

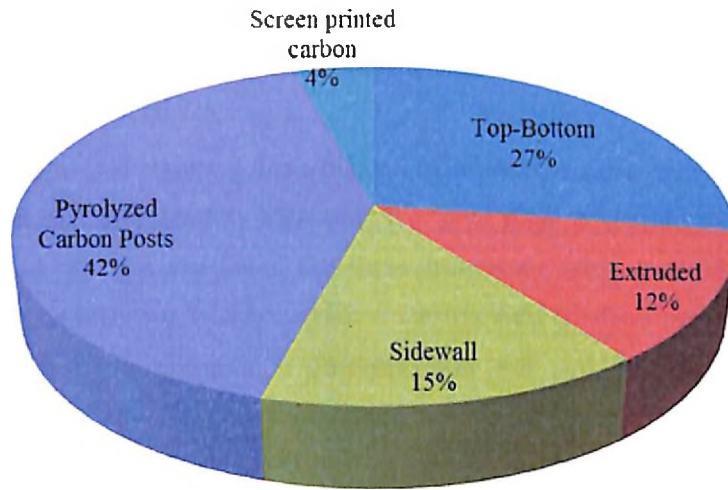


Figure 2.15: Pie chart representation of 3D electrode geometries reported in DEP

2.4 Gaps in Existing Research and Investigations

Numerous electrode designs and materials have been studied to achieve the DEP phenomena. Most of the research work is oriented towards the use of metal electrodes for cell trapping and manipulation using DEP. From the literature review, still a few significant gaps exist in studies on DEP phenomena using metal and carbon electrodes. A few of them are figured out and addressed in this thesis and are detailed below:

1. The majority of the research work has been done on the use of 2D and 3D metal electrodes for DEP cell trapping. As we know that DEP is a short range phenomenon and addressing all the particles flowing inside the channel becomes a challenge in case of 2D electrodes. The use of 3D electrodes is able to increase the throughput of the device by increasing the effective cell trapping region inside the channel, yet there remain critical issues to be addressed. For example, the patterning of metal requires the use of expensive clean room facility like: lithography, sputtering, evaporation etc., which are not widely accessible. Also, the process turns even more complicated and expensive if 3D electrode structures are to be fabricated. Therefore there is the need to explore an inexpensive and reliable alternative to gold for fabricating 3D electrodes.

Proposed Solution- Recently, carbon electrodes have been proposed as a good and reliable alternative to metal electrode but the use of carbon electrode has not been much

investigated in literature. Therefore, in this research work, we are proposing the use of carbon as an electrode material for cell trapping using DEP technique.

2. Different electrode designs e.g. inter-digitated, castellated, angular, polynomial etc have been proposed and discussed in literature. We have done a comprehensive study on various electrode designs and found that these designs are often associated with issues like stagnation regions and locally amplified electric field gradient points due to sharp turns, making it more sensitive to contamination and cell damage. Therefore, an electrode design free from the above mentioned issues needs to be investigated.

Proposed Solution- A simple curved or C-serpentine shaped design in which the non-uniform electric field is extended throughout the channel will provide a better protection against cell damage and stagnation regions. Therefore C-serpentine structure that serves both as electrode and microchannel wall is proposed in this study.

3. For various MEMS devices, gold has always been a material of choice because of its fully grown fabrication technology and its biocompatibility. From the literature review, it was found that the gold electrode based DEP device with serpentine design has not been investigated exhaustively.

Proposed Solution- The present study aims to show a detailed fabrication of simple C-serpentine structure and its testing for dielectrophoretic cell trapping. Also, the performance of the fabricated gold electrode based DEP device is compared with that of fabricated carbon electrode DEP device.

4. Carbon is also a widely used material in microfluidic area which is less investigated in literature for DEP applications. The fabrication of carbon DEP devices compare advantageously with metallization because it does not require high vacuum, expensive metal and expensive infrastructure. One of the commonly reported methods to fabricate carbon electrodes is by photoresist pyrolysis at 900-1100°C. However, the pyrolyzation method used for fabricating carbon structures is a long process, requires high temperature and is associated with an inevitable phenomenon of polymer shrinkage. The shrinkage of the precursor structure during pyrolysis is an important challenge in C-DEP, because it reduces the mechanical stability of the electrodes and also widens the gap between them.

Proposed Solution- Stenciling a conductive material on to a substrate could prove to be a more straightforward solution or an easy alternative to pyrolysis process. So, we

propose the use of screen printed carbon electrode with serpentine design for cell trapping in our study. In addition, we have proposed, the sealing of carbon DEP device using glass, instead of PDMS, which not only reduce the leakage problem but also improves the device performance.

Based on the existing knowledge and gaps in research, following objectives were designed:

1. Simulation study of various electrode schemes to conclude about the most appropriate design.
2. Fabrication and testing of gold electrode DEP device for cell trapping.
3. Fabrication of screen printed carbon electrode for DEP devices.
4. Comparative study on trapping efficiency of both gold and carbon electrode devices.

2.5 Organization of the Thesis

Dielectrophoresis (DEP) has become a vital tool for cell manipulation and characterization due to its non-invasiveness. It is very useful in the trend towards point-of-care systems. Currently, most efforts are focused on using DEP in biomedical applications, such as the spatial manipulation of cells, the selective separation or enrichment of target cells, high-throughput molecular screening, biosensors and immunoassays. A significant amount of research on DEP has produced a wide range of microelectrode configurations. Much literature has concluded that the use of carbon electrodes provides more cost effective and more durable DEP devices than metal electrodes. More efficient devices not only needs to be constructed from a low cost material but also from inexpensive fabrication techniques. The electrodes fabricated using screen printing of conductive carbon paste suggests a most easiest and cost effective way to fabricate DEP devices.

In Chapter 3, we present the modeling and simulation to provide us a better understanding of the particle behaviour in the proposed channel. Since, the heart of any DEP device is a set of electrodes producing a high gradient electric field that drives particles by DEP, therefore some of the commonly used electrode designs have been simulated using COMSOL and the field gradient results have been compared.

In Chapter 4, details the fabrication of C-Serpentine electrodes that are fabricated using gold and conventional micro-fabrication technology. We have also discussed the steps

involved in preparing sample of viable and non-viable yeast cells. Followed are the test results that are obtained in trapping of both the cell populations.

In Chapter 5, elaborates the fabrication of carbon electrodes. The principal component, i.e. the microelectrodes, were constructed via screen printing process. The fabrication of DEP device entirely of glass is discussed in detail. The biocompatibility of the conductive carbon ink is also tested.

Finally conclusion for all experimental work is given in Chapter 6 with scope for future work.

References

- [1] H. A. Pohl, "The motion and precipitation of suspensoids in divergent electric fields," *J. Appl. Phys.*, vol. 22, no. 7, pp. 869–871, 1951.
- [2] M. Elitas, R. Martinez-Duarte, N. Dhar, J. D. McKinney, and P. Renaud, "Dielectrophoresis-based purification of antibiotic-treated bacterial subpopulations," *Lab Chip*, vol. 14, no. 11, pp. 1850–1857, 2014.
- [3] J. Yang, Y. Huang, X. Wang, X.-B. Wang, F. F. Becker, and P. R. Gascoyne, "Dielectric properties of human leukocyte subpopulations determined by electrorotation as a cell separation criterion," *Biophys. J.*, vol. 76, no. 6, pp. 3307–3314, 1999.
- [4] G. P. RC and V. Jody, "Particle separation by dielectrophoresis," *Electrophoresis*, vol. 23, no. 13, pp. 1973–1983, 2002.
- [5] H. A. Pohl and H. Ira, "Separation of Living and dead cells by Dielectrophoresis," *Science (80-.)*, vol. 152, no. 3722, pp. 647–649, 1966.
- [6] H. A. Pohl and J. S. Crane, "Dielectrophoresis of Cells," *Biophys. J.*, vol. 11, no. 9, pp. 711–727, 1971.
- [7] S. Masuda, M. Washizu, and T. Nanba, "Novel Method of Cell Fusion in Field Constriction Area in Fluid Integrated Circuit," *IEEE Trans. Ind. Appl.*, vol. 25, no. 4, pp. 732–737, 1989.
- [8] T. Schnelle, T. Mu, A. Voigt, K. Reimer, B. Wagner, and G. Fuhr, "Adhesion-Inhibited Surfaces . Coated and Uncoated Interdigitated Electrode Arrays in the Micrometer and Submicrometer Range," *Langmuir*, vol. 12, no. 3, pp. 801–809, 1996.
- [9] J. Suehiro, R. Yatsunami, and R. Hamada, "Quantitative estimation of biological cell concentration suspended in aqueous medium by using dielectrophoretic impedance measurement method," *J. Phys. D. Appl. Phys.*, vol. 32, no. 21, p. 2814, 1999.
- [10] J. Suehiro, M. Shutou, T. Hatano, and M. Hara, "High sensitive detection of biological cells using dielectrophoretic impedance measurement method combined with electroporabilization," *Sensors Actuators B Chem.*, vol. 96, no. 1–2, pp. 144–151, 2003.
- [11] X. B. Wang, J. Yang, Y. Huang, J. Vykoukal, F. F. Becker, and P. R. C. Gascoyne, "Cell separation by dielectrophoretic Field- Flow-fractionation," *Anal. Chem.*, vol. 72, no. 4, pp. 832–839, 2000.
- [12] H. Li and R. Bashir, "Dielectrophoretic separation and manipulation of live and heat-treated cells of *Listeria* on microfabricated devices with interdigitated electrodes," *Sensors Actuators, B Chem.*, vol. 86, no. 2, pp. 215–221, 2002.
- [13] L. Haibo, Y. Zheng, D. Akin, and R. Bashir, "Characterization and modeling of a microfluidic dielectrophoresis filter for biological species," *J.*

- Microelectromechanical Syst.*, vol. 14, no. 1, pp. 103–112, 2005.
- [14] J. P. H. Burt, R. Pethig, P. R. C. Gascoyne, and F. F. Becker, “Dielectrophoretic characterisation of Friend murine erythroleukaemic cells as a measure of induced differentiation,” *Biochim. Biophys. Acta (BBA)-General Subj.*, vol. 1034, no. 1, pp. 93–101, 1990.
- [15] J. Auerswald and H. F. Knapp, “Quantitative assessment of dielectrophoresis as a micro fluidic retention and separation technique for beads and human blood erythrocytes,” *Microelectron. Eng.*, vol. 67, pp. 879–886, 2003.
- [16] M. Suzuki, T. Yasukawa, Y. Mase, D. Oyamatsu, H. Shiku, and T. Matsue, “Dielectrophoretic Micropatterning with Microparticle Monolayers Covalently Linked to Glass Surfaces,” *Langmuir*, vol. 20, no. 25, pp. 11005–11011, 2004.
- [17] M. Suzuki, T. Yasukawa, H. Shiku, and T. Matsue, “Negative dielectrophoretic patterning with colloidal particles and encapsulation into a hydrogel,” *Langmuir*, vol. 23, no. 7, pp. 4088–4094, 2007.
- [18] R. Gomez-Sjoberg, D. T. Morissette, and R. Bashir, “Impedance microbiology-on-a-chip: Microfluidic bioprocessor for rapid detection of bacterial metabolism,” *J. Microelectromechanical Syst.*, vol. 14, no. 4, pp. 829–838, 2005.
- [19] E. T. Lagally, S.-H. Lee, and H. T. Soh, “Integrated microsystem for dielectrophoretic cell concentration and genetic detection,” *Lab Chip*, vol. 5, no. 10, pp. 1053–1058, 2005.
- [20] L. Yang *et al.*, “A multifunctional micro-fluidic system for dielectrophoretic concentration coupled with immuno-capture of low numbers of *Listeria monocytogenes*,” *Lab Chip*, vol. 6, no. 7, pp. 896–905, 2006.
- [21] N. Gadish and J. Voldman, “High-Throughput Positive-Dielectrophoretic Bioparticle Microconcentrator,” *Anal. Chem.*, vol. 78, no. 22, pp. 7870–7876, 2006.
- [22] Y. Li, C. Dalton, H. J. Crabtree, G. Nilsson, and K. V. Kaler, “Continuous dielectrophoretic cell separation microfluidic device,” *Lab Chip*, vol. 7, no. 2, pp. 239–248, 2007.
- [23] N. Crews, J. Darabi, P. Voglewede, F. Guo, and A. Bayoumi, “An analysis of interdigitated electrode geometry for dielectrophoretic particle transport in microfluidics,” *Sensors Actuators B Chem.*, vol. 125, no. 2, pp. 672–679, 2007.
- [24] S. Park and A. Beskok, “Alternating Current Electrokinetic Motion of Colloidal Particles on Interdigitated Microelectrodes,” *Anal. Chem.*, vol. 80, no. 8, pp. 2832–2841, 2008.
- [25] J. Vykoukal, D. M. Vykoukal, S. Freyberg, E. U. Alt, and P. R. C. Gascoyne, “Enrichment of putative stem cells from adipose tissue using dielectrophoretic field-flow fractionation,” *Lab Chip*, vol. 8, no. 8, pp. 1386–1393, 2008.
- [26] G. Mernier, N. Piacentini, R. Tornay, N. Buffi, and P. Renaud, “Label-free

- Sorting and Counting of Yeast Cells for Viability Studies,” in *Procedia Chemistry*, 2009, vol. 1, no. 1, pp. 385–388.
- [27] S. Park, M. Koklu, and A. Beskok, “Particle Trapping in High-Conductivity Media with Electrothermally Enhanced Negative Dielectrophoresis,” *Anal. Chem.*, vol. 81, no. 6, pp. 2303–2310, 2009.
- [28] A. Henning, F. F. Bier, and R. Hölzel, “Dielectrophoresis of DNA : Quantification by impedance measurements.,” *Biomicrofluidics*, vol. 4, no. 2, p. 022803, 2010.
- [29] G. Giraud *et al.*, “Dielectrophoretic manipulation of ribosomal RNA,” *Biomicrofluidics*, vol. 5, no. 2, p. 024116, 2011.
- [30] H. Narayanan Unni *et al.*, “Characterization and separation of Cryptosporidium and Giardia cells using on-chip dielectrophoresis,” *Biomicrofluidics*, vol. 6, no. 1, p. 012805, 2012.
- [31] L. Wu, L.-Y. Lanry Yung, and K.-M. Lim, “Dielectrophoretic capture voltage spectrum for measurement of dielectric properties and separation of cancer cells,” *Biomicrofluidics*, vol. 6, no. 1, p. 014113, 2012.
- [32] S. Shim, K. Stenke-Hale, J. Noshari, F. F. Becker, and P. R. C. Gascoyne, “Dielectrophoresis has broad applicability to marker-free isolation of tumor cells from blood by microfluidic systems,” *Biomicrofluidics*, vol. 7, no. 1, p. 011808, 2013.
- [33] S. Shim *et al.*, “Antibody-independent isolation of circulating tumor cells by continuous-flow dielectrophoresis,” *Biomicrofluidics*, vol. 7, no. 1, p. 011807, 2013.
- [34] J. Zhang, S. Yan, G. Alici, N.-T. Nguyen, D. Di Carlo, and W. Li, “Real-time control of inertial focusing in microfluidics using dielectrophoresis (DEP),” *Rsc Adv.*, vol. 4, no. 107, pp. 62076–62085, 2014.
- [35] A. Alazzam, B. Mathew, and F. Alhammadi, “Novel microfluidic device for the continuous separation of cancer cells using dielectrophoresis,” *J. Sep. Sci.*, vol. 40, no. 5, pp. 1193–1200, 2017.
- [36] R. Wang, Y. Xu, H. Liu, J. Peng, J. Irudayaraj, and F. Cui, “An integrated microsystem with dielectrophoresis enrichment and impedance detection for detection of Escherichia coli,” *Biomed. Microdevices*, vol. 19, no. 2, p. 34, 2017.
- [37] H. Sadeghian, Y. Hojjat, and M. Soleimani, “Interdigitated electrode design and optimization for dielectrophoresis cell separation actuators,” *J. Electrostat.*, vol. 86, pp. 41–49, 2017.
- [38] T. N. G. Adams, A. Y. L. Jiang, P. D. Vyas, and L. A. Flanagan, “Separation of neural stem cells by whole cell membrane capacitance using dielectrophoresis,” *Methods*, vol. 133, no. 2018, pp. 91–103, 2018.
- [39] R. Pethig, Y. Huang, X. Wang, and J. P. H. Burt, “Positive and negative dielectrophoretic collection of colloidal particles using interdigitated castellated

- microelectrodes." *J. Phys. D. Appl. Phys.*, vol. 25, no. 5, p. 881, 1992.
- [40] G. H. Markx, M. S. Talary, and R. Pethig, "Separation of viable and non-viable yeast using dielectrophoresis," *J. Biotechnol.*, vol. 32, no. 1, pp. 29–37, 1994.
- [41] F. F. Becker, X.-B. Wang, Y. Huang, R. Pethig, J. Vykoukal, and P. R. C. Gascoyne, "Separation of human breast cancer cells from blood by differential dielectric affinity," *Proc. Natl. Acad. Sci.*, vol. 92, no. 3, pp. 860–864, 1995.
- [42] P. R. C. Gascoyne, X. Wang, Y. Huang, and F. F. Becker, "Dielectrophoretic Separation of Cancer Cells from Blood," *IEEE Trans. Ind. Appl.*, vol. 33, no. 3, pp. 670–678, 1997.
- [43] P. Gascoyne, C. Mahidol, M. Ruchirawat, J. Satayavivad, P. Watcharasit, and F. F. Becker, "Microsample preparation by dielectrophoresis: isolation of malaria.." *Lab Chip*, vol. 2, no. 2, pp. 70–75, 2002.
- [44] N. Green and H. Morgan, "Dielectrophoretic separation of nanoparticles," *J. Phys. D. Appl. Phys.*, vol. 30, no. 11, p. L41, 1997.
- [45] N. . Green and H.Morgan, "Separation of submicrometre particles using a combination of dielectrophoretic and electrohydrodynamic forces," *J. Phys. D. Appl. Phys.*, vol. 31, no. 7, p. L25, 1998.
- [46] H. Morgan, M. P. Hughes, and N. G. Green, "Separation of submicron bioparticles by dielectrophoresis.," *Biophys. J.*, vol. 77, no. 1, pp. 516–525, 1999.
- [47] Q. Ramadan, V. Samper, D. Poenar, Z. Liang, C. Yu, and T. M. Lim, "Simultaneous cell lysis and bead trapping in a continuous flow microfluidic device," *Sensors Actuators B Chem.*, vol. 113, no. 2, pp. 944–955, 2006.
- [48] S. Rajaraman, H. (Moses) Noh, P. J. Hesketh, and D. S. Gottfried, "Rapid, low cost microfabrication technologies toward realization of devices for dielectrophoretic manipulation of particles and nanowires," *Sensors Actuators B Chem.*, vol. 114, no. 1, pp. 392–401, Mar. 2006.
- [49] C. Tai, S. Hsiung, C. Chen, T. Mei-Lin, and L. Gwo-Bin, "Automatic microfluidic platform for cell separation and nucleus collection," *Biomed. Microdevices*, vol. 9, no. 4, pp. 533–543, 2007.
- [50] W. Choi, J. Kim, D. Lee, K. Lee, D. Koo, and J. Park, "Dielectrophoretic oocyte selection chip for in vitro fertilization," *Biomed. Microdevices*, vol. 10, no. 3, pp. 337–345, 2008.
- [51] C. Zhang, K. Khoshmanesh, F. T. Lopez, A. Mitchell, W. Wlodarski, and Z. K. Klantar, "Dielectrophoretic separation of carbon nanotubes and polystyrene microparticles," *Microfluid. Nanofluidics*, vol. 7, no. 5, pp. 633–645, 2009.
- [52] T. Yasukawa, M. Suzuki, H. Shiku, and T. Matsue, "Control of the microparticle position in the channel based on dielectrophoresis," *Sensors Actuators B Chem.*, vol. 142, no. 1, pp. 400–403, 2009.

- [53] A. C. Sabuncu, J. A. Liu, S. J. Beebe, and A. Beskok. "Dielectrophoretic separation of mouse melanoma clones." *Biomicrofluidics*, vol. 4, no. 2, p. 021101, 2010.
- [54] K. Zhu, A. S. Kaprelyants, E. G. Salina, and G. H. Markx, "Separation by dielectrophoresis of dormant and nondormant bacterial cells of *Mycobacterium smegmatis*," *Biomicrofluidics*, vol. 4, no. 2, p. 022809, 2010.
- [55] J. Suehiro, "Fabrication and characterization of nanomaterial-based sensors using dielectrophoresis." *Biomicrofluidics*, vol. 4, no. 2, p. 022804, 2010.
- [56] S. Agarwal, A. Sebastian, L. M. Forrester, and G. H. Markx, "Formation of embryoid bodies using dielectrophoresis," *Biomicrofluidics*, vol. 6, no. 2, p. 024101, 2012.
- [57] E. Du, M. Dao, and S. Suresh, "Quantitative biomechanics of healthy and diseased human red blood cells using dielectrophoresis in a microfluidic system," *Extrem. Mech. Lett.*, vol. 1, no. 2014, pp. 35–41, 2014.
- [58] J. L. Nourse *et al.*, "Membrane Biophysics Define Neuron and Astrocyte Progenitors in the Neural Lineage," *Stem Cells*, vol. 32, no. 3, pp. 706–716, 2014.
- [59] N. G. Hallfors, F. Alhammedi, and A. Alazzam, "Deformation of Red Blood Cells under Dielectrophoresis." in *Bio-engineering for Smart Technologies (BioSMART), 2016 International Conference on. IEEE*, 2016, pp. 1–3.
- [60] X. Chen *et al.*, "Microfluidic dielectrophoresis device for trapping , counting and detecting *Shewanella oneidensis* at the cell level," *Biosens. Bioelectron.*, vol. 99, no. 2018, pp. 416–423, 2018.
- [61] Y. Huang and R. Pethig, "Electrode design for negative dielectrophoresis," *Meas. Sci. Technol.*, vol. 2, no. 12, pp. 1142–1146, 1991.
- [62] X.-B. Wang, Y. Huang, J. P. H. Burt, G. H. Markx, and R. Pethig, "Selective dielectrophoretic confinement of bioparticles in potential energy wells." *J. Phys. D. Appl. Phys.*, vol. 26, no. 8, pp. 1278–1285, 1993.
- [63] G. H. Markx, Y. Huang, X. Zhou, and R. Pethig, "Dielectrophoretic characterization and separation of micro-organisms," *Microbiology*, vol. 140, no. 3, pp. 585–591, 1994.
- [64] H. Watarai, T. Sakamoto, and S. Tsukahara, "In situ measurement of dielectrophoretic mobility of single polystyrene microparticles," *Langmuir*, vol. 13, no. 8, pp. 2417–2420, 1997.
- [65] M. P. Hughes, H. Morgan, F. J. Rixon, J. P. H. Burt, and R. Pethig, "Manipulation of herpes simplex virus type 1 by dielectrophoresis," *Biochim. Biophys. Acta (BBA)-General Subj.*, vol. 1425, no. 1, pp. 119–126, 1998.
- [66] S. Tsukahara, T. Sakamoto, and H. Watarai, "Positive dielectrophoretic mobilities of single microparticles enhanced by the dynamic diffusion cloud of ions," *Langmuir*, vol. 16, no. 8, pp. 3866–3872, 2000.

- [67] S. Tsukahara and H. Watarai, "Dielectrophoresis of microbioparticles in water with planar and capillary quadrupole electrodes.," *IEE Proc. Nanobiotechnol.*, vol. 150, no. 2, pp. 59–65, 2003.
- [68] N. Green, A. Ramos, and H. Morgan, "Ac electrokinetics: a survey of sub-micrometre particle dynamics," *J. Phys. D. Appl. Phys.*, vol. 33, no. 6, pp. 632–641, 2000.
- [69] K. Ratanachoo, P. R. C. Gascoyne, and M. Ruchirawat, "Detection of cellular responses to toxicants by dielectrophoresis," *Biochim. Biophys. Acta - Biomembr.*, vol. 1564, no. 2, pp. 449–458, 2002.
- [70] S. B. Asokan, L. Jawerth, R. L. Carroll, R. E. Cheney, S. Washburn, and R. Superfine, "Two-dimensional manipulation and orientation of actin-myosin systems with dielectrophoresis," *Nano Lett.*, vol. 3, no. 4, pp. 431–437, 2003.
- [71] L. Zheng, J. P. Brody, and P. J. Burke, "Electronic manipulation of DNA, proteins, and nanoparticles for potential circuit assembly," *Biosens. Bioelectron.*, vol. 20, no. 3, pp. 606–619, 2004.
- [72] J. Du, Y. Juang, J. Wu, and H. Wei, "Long-range and superfast trapping of DNA molecules in an ac electrokinetic funnel," *Biomicrofluidics*, vol. 2, no. 4, p. 044103, 2008.
- [73] J. D. Beck, L. Shang, B. Li, M. S. Marcus, and R. J. Hamers, "Discrimination between Bacillus Species by Dielectrophoretically Positioned Spores," *Anal. Chem.*, vol. 80, no. 10, pp. 3757–3761, 2008.
- [74] L.-S. Jang, P.-H. Huang, and K.-C. Lan, "Single-cell trapping utilizing negative dielectrophoretic quadrupole and microwell electrodes," *Biosens. Bioelectron.*, vol. 24, no. 12, pp. 3637–3644, 2009.
- [75] C. Chung, I.-F. Cheng, W.-H. Yang, and H.-C. Chang, "Antibiotic susceptibility test based on the dielectrophoretic behavior of elongated Escherichia coli with cephalixin treatment," *Biomicrofluidics*, vol. 5, no. 2, p. 021102, 2011.
- [76] S. Tanaka *et al.*, "Tailoring particle translocation via dielectrophoresis in pore channels," Nature Publishing Group, 2016.
- [77] A. Menachery *et al.*, "Dielectrophoretic characterization and separation of metastatic variants of small cell lung cancer cells," *UNE*, vol. 13, p. 15, 2016.
- [78] L. Amico, N. Ajami, J. Adachi, P. Gascoyne, and J. Petrosino, "Isolation and concentration of bacteria from blood using microfluidic membraneless dialysis and dielectrophoresis," *Lab Chip*, vol. 17, no. 7, pp. 1340–1348, 2017.
- [79] J. G. Kralj, M. T. W. Lis, M. A. Schmidt, and K. F. Jensen, "Continuous Dielectrophoretic Size-Based Particle Sorting," *Anal. Chem.*, vol. 78, no. 14, pp. 5019–5025, 2006.
- [80] H. O. Fatoyinbo, M. P. Hughes, S. P. Martin, P. Pashby, and F. H. Labeed, "Dielectrophoretic separation of Bacillus subtilis spores from environmental

- diesel particles." *J. Environ. Monit.*, vol. 9, no. 1, pp. 87–90, 2007.
- [81] U. Kim, J. Qian, S. A. Kenrick, P. S. Daugherty, and H. T. Soh, "Multitarget Dielectrophoresis Activated Cell Sorter," *Anal. Chem.*, vol. 80, no. 22, pp. 8656–8661, 2008.
- [82] M. S. Pommer *et al.*, "Dielectrophoretic separation of platelets from diluted whole blood in microfluidic channels," *Electrophoresis*, vol. 29, no. 6, pp. 1213–1218, 2008.
- [83] M. D. Vahey and J. Voldman, "An Equilibrium Method for Continuous-Flow Cell Sorting Using Dielectrophoresis," *Anal. Chem.*, vol. 80, no. 9, pp. 3135–3143, 2008.
- [84] K.-H. Han and A. B. Frazier, "Lateral-driven continuous dielectrophoretic microseparators for blood cells suspended in a highly conductive medium," *Lab Chip*, vol. 8, no. 7, pp. 1079–1086, 2008.
- [85] A. Alazzam, I. Stiharu, R. Bhat, and A.-N. Megueditchian, "Interdigitated comb-like electrodes for continuous separation of malignant cells from blood using dielectrophoresis," *Electrophoresis*, vol. 32, no. 11, pp. 1327–1336, 2011.
- [86] R. S. Kuczynski, H. Chang, and A. Revzin, "Dielectrophoretic microfluidic device for the continuous sorting of *Escherichia coli* from blood cells," *Biomicrofluidics*, vol. 5, no. 3, p. 032005, 2011.
- [87] F. Yang, X. Yang, H. Jiang, W. M. Butler, and G. Wang, "Dielectrophoretic Separation of Prostate Cancer Cells," *Technol. Cancer Res. Treat.*, vol. 12, no. 1, pp. 61–70, 2013.
- [88] M. Alshareef *et al.*, "Separation of tumor cells with dielectrophoresis-based microfluidic chip," *Biomicrofluidics*, vol. 7, no. 1, p. 011803, 2013.
- [89] H. Song *et al.*, "Continuous-flow sorting of stem cells and differentiation products based on dielectrophoresis," *Lab Chip*, vol. 15, no. 5, pp. 1320–1328, 2015.
- [90] J. Cheng, E. L. Sheldon, L. Wu, M. J. Heller, and J. P. O'Connell, "Isolation of cultured cervical carcinoma cells mixed with peripheral blood cells on a bioelectronic chip," *Anal. Chem.*, vol. 70, no. 11, pp. 2321–2326, 1998.
- [91] F. M., S. P. Faure, B. Le Pioufle, P. Coquet, and H. Fujita, "Positioning living cells on a high-density electrode array by negative dielectrophoresis," *Mater. Sci. Eng. C*, vol. 23, no. 5, pp. 597–603, 2003.
- [92] J. Suehiro, Guangbin, M. Imamura, and M. Hara, "Dielectrophoretic Filter for Separation and Recovery of Biological Cells in Water," *IEEE Trans. Ind. Appl.*, vol. 39, no. 5, pp. 1514–1521, 2003.
- [93] D. S. Gray, J. L. Tan, J. Voldman, and C. S. Chen, "Dielectrophoretic registration of living cells to a microelectrode array," *Biosens. Bioelectron.*, vol. 19, no. 7, pp. 771–780, Feb. 2004.

- [94] I. Doh and Y. Cho, "A continuous cell separation chip using hydrodynamic dielectrophoresis (DEP) process," *Sensors Actuators A Phys.*, vol. 121, no. 1, pp. 59–65, 2005.
- [95] J. H. Nieuwenhuis, A. Jachimowicz, P. Svasek, and M. J. Vellekoop, "Optimization of Microfluidic Particle Sorters Based on Dielectrophoresis," *IEEE Sens. J.*, vol. 5, no. 5, pp. 810–816, 2005.
- [96] H. Ralph, N. Calander, Z. Chiragwandi, M. Willander, and F. F. Bier, "Trapping Single Molecules by Dielectrophoresis," *Phys. Rev. Lett.*, vol. 95, no. 12, p. 128102, 2005.
- [97] S. Choi and J. Park, "Microfluidic system for dielectrophoretic separation based on a trapezoidal electrode array," *Lab Chip*, vol. 5, no. 10, pp. 1161–1167, 2005.
- [98] K. Khoshmanesh *et al.*, "Dielectrophoretic manipulation and separation of microparticles using curved microelectrodes," *Electrophoresis*, vol. 30, no. 21, pp. 3707–3717, 2009.
- [99] K. Khoshmanesh *et al.*, "Size based separation of microparticles using a dielectrophoretic activated system.," *J. Appl. Phys.*, vol. 108, no. 3, p. 034904, 2010.
- [100] M. Koklu, S. Park, S. D. Pillai, and A. Beskok, "Negative dielectrophoretic capture of bacterial spores in food matrices," *Biomicrofluidics*, vol. 4, no. 3, p. 034107, 2010.
- [101] C. Young, J. Hsieh, and C. Ay, "Development of an Integrated Chip for Automatic Tracking and Positioning Manipulation for Single Cell Lysis," *Sensors*, vol. 12, no. 3, pp. 2400–2413, 2012.
- [102] B. Yafouz, N. A. Kadri, and F. Ibrahim, "Microarray Dot Electrodes Utilizing Dielectrophoresis for Cell Characterization," *Sensors*, vol. 13, no. 7, pp. 9029–9046, 2013.
- [103] X. Chen *et al.*, "Microfluidic dielectrophoresis device for trapping , counting and detecting *Shewanella oneidensis* at the cell level," *Biosens. Bioelectron.*, vol. 99, pp. 416–423, 2018.
- [104] J. Kentsch *et al.*, "Microdevices for separation , accumulation , and analysis of biological micro- and nanoparticles," *IEE Proceedings-nanobiotechnology*, vol. 150, no. 2, pp. 82–89, 2003.
- [105] M. Durr, J. Kentsch, T. Muller, T. Schnelle, and M. Stelzle, "Microdevices for manipulation and accumulation of micro-and nanoparticles by dielectrophoresis," *Electrophoresis*, vol. 24, no. 4, pp. 722–731, 2003.
- [106] J. Park, B. Kim, S. K. Choi, S. Hong, S. H. Lee, and K. Il Lee, "An efficient cell separation system using 3D-asymmetric microelectrodes," *Lab Chip*, vol. 5, no. 11, pp. 1264–1270, 2005.
- [107] D. F. Chen, H. Du, and W. H. Li, "A 3D paired microelectrode array for

- accumulation and separation of microparticles," *J. Micromechanics Microengineering*, vol. 16, no. 7, pp. 1162–1169, 2006.
- [108] D. Chen and H. Du, "A dielectrophoretic barrier-based microsystem for separation of microparticles," *Microfluid. Nanofluidics*, vol. 3, no. 5, pp. 603–610, 2007.
- [109] F. Grom, J. Kentsch, T. Müller, T. Schnelle, and M. Stelzle, "Accumulation and trapping of hepatitis A virus particles by electrohydrodynamic flow and dielectrophoresis," *Electrophoresis*, vol. 27, no. 7, pp. 1386–1393, 2006.
- [110] I.-F. Cheng and H.-C. Chang, "An integrated dielectrophoretic chip for continuous bioparticle filtering, focusing, sorting, trapping and detecting," *Biomicrofluidics*, vol. 1, no. 2, p. 021503, 2007.
- [111] T. Yasukawa, M. Suzuki, T. Sekiya, H. Shiku, and T. Matsue, "Flow sandwich-type immunoassay in microfluidic devices based on negative dielectrophoresis," *Biosens. Bioelectron.*, vol. 22, no. 11, pp. 2730–2736, 2007.
- [112] H. Imasato, T. Yamakawa, and M. Eguchi, "Separation of Leukemia Cells from Blood by Employing Dielectrophoresis," *Intell. Autom. Soft Comput.*, vol. 18, no. 2, pp. 139–152, 2012.
- [113] M. Li, S. Li, W. Cao, W. Li, W. Wen, and Gursel Alici, "Improved concentration and separation of particles in a 3D dielectrophoretic chip integrating focusing, aligning and trapping," *Microfluid. Nanofluidics*, vol. 14, no. 3–4, pp. 527–539, 2013.
- [114] S. Li, M. Li, K. Bougat-Robin, W. Cao, and I. Y. Y. Chau, "High-throughput particle manipulation by hydrodynamic, electrokinetic, and dielectrophoretic effects in an integrated microfluidic chip," *Biomicrofluidics*, vol. 7, no. 2, p. 024106, 2013.
- [115] R. Hamada, H. Takayama, Y. Shonishi, L. Mao, M. Nakano, and J. Suehiro, "A rapid bacteria detection technique utilizing impedance measurement combined with positive and negative dielectrophoresis," *Sensors Actuators, B Chem.*, vol. 181, pp. 439–445, 2013.
- [116] N. A. Yunus, H. Nili, and N. G. Green, "Continuous separation of colloidal particles using dielectrophoresis," *Electrophoresis*, vol. 34, no. 7, pp. 969–978, 2013.
- [117] J. Voldman, M. L. Gray, M. Toner, and M. A. Schmidt, "A microfabrication-based dynamic array cytometer," *Anal. Chem.*, vol. 74, no. 16, pp. 3984–3990, 2002.
- [118] J. Voldman, M. Toner, M. L. Gray, and M. A. Schmidt, "Design and analysis of extruded quadrupolar dielectrophoretic traps," *J. Electrostat.*, vol. 57, no. 1, pp. 69–90, 2003.
- [119] T. Hunt, H. Lee, and R. Westervelt, "Addressable micropost array for the dielectrophoretic manipulation of particles in fluid," *Appl. Phys. Lett.*, vol. 85, no. 26, pp. 6421–6423, 2004.

- [120] C. Iliescu, L. Yu, F. E. H. Tay, and B. Chen, "Bidirectional field-flow particle separation method in a dielectrophoretic chip with 3D electrodes," *Sensors Actuators B Chem.*, vol. 129, no. 1, pp. 491–496, 2008.
- [121] C. Iliescu, G. Tresset, and G. Xu, "Dielectrophoretic field-flow method for separating particle populations in a chip with asymmetric electrodes," *Biomicrofluidics*, vol. 3, no. 4, p. 044104, 2009.
- [122] M. A. Zaman, P. Padhy, P. C. Hansen, and L. Hesselink, "Dielectrophoresis-assisted plasmonic trapping of dielectric nanoparticles," *Phys. Rev. A*, vol. 95, no. 2, p. 023840, 2017.
- [123] L. Wang, L. A. Flanagan, N. L. Jeon, E. Monuki, and A. P. Lee, "Dielectrophoresis switching with vertical sidewall electrodes for microfluidic flow cytometry," *Lab Chip*, vol. 7, no. 9, pp. 1114–1120, 2007.
- [124] F. E. H. Tay, L. Yu, A. J. Pang, and C. Iliescu, "Electrical and thermal characterization of a dielectrophoretic chip with 3D electrodes for cells manipulation," *Electrochim. Acta*, vol. 52, no. 8, pp. 2862–2868, 2007.
- [125] L. Yu, C. Iliescu, G. Xu, and F. E. H. Tay, "Sequential field-flow cell separation method in a dielectrophoretic chip with 3D electrodes," *J. microelectromechanical Syst.*, vol. 16, no. 5, pp. 1120–1129, 2007.
- [126] L. Wang, J. Lu, S. A. Marchenko, E. S. Monuki, L. A. Flanagan, and A. P. Lee, "Dual frequency dielectrophoresis with interdigitated sidewall electrodes for microfluidic flow-through separation of beads and cells," *Electrophoresis*, vol. 30, no. 5, pp. 782–791, 2009.
- [127] B. Cetin, Y. Kang, Z. Wu, and D. Li, "Continuous particle separation by size via AC-dielectrophoresis using a lab-on-a-chip device with 3-D electrodes," *Electrophoresis*, vol. 30, no. 5, pp. 766–772, 2009.
- [128] N. Lewpiriyawong, C. Yang, and Y. C. Lam, "Continuous sorting and separation of microparticles by size using AC dielectrophoresis in a PDMS microfluidic device with 3-D conducting PDMS composite electrodes," *Electrophoresis*, vol. 31, no. 15, pp. 2622–2631, 2010.
- [129] N. Lewpiriyawong, K. Kandaswamy, C. Yang, V. Ivanov, and R. Stocker, "Microfluidic characterization and continuous separation of cells and particles using conducting poly(dimethyl siloxane) electrode induced alternating current-dielectrophoresis," *Anal. Chem.*, vol. 83, no. 24, pp. 9579–9585, 2011.
- [130] M. Li and R. K. Anand, "Cellular dielectrophoresis coupled with single-cell analysis," *Anal. Bioanal. Chem.*, pp. 2499–2515, 2018.
- [131] D. Sun, L. Zhu, and G. Zhu, "Glassy carbon ceramic composite electrodes," *Anal. Chim. Acta*, vol. 564, no. 2, pp. 243–247, Apr. 2006.
- [132] N. E. Hebert, B. Snyder, R. L. McCreery, W. G. Kuhr, and S. A. Brazill, "Performance of Pyrolyzed Photoresist Carbon Films in a Microchip Capillary Electrophoresis Device with Sinusoidal Voltammetric Detection," *Anal. Chem.*,

- vol. 75, no. 16, pp. 4265–4271, 2003.
- [133] C. Wang, G. Jia, L. H. Taherabadi, and M. J. Madou, “A Novel Method for the Fabrication of High-Aspect Ratio C-MEMS Structures.” *J. Microelectromechanical Syst.*, vol. 14, no. 2, pp. 348–358, 2005.
- [134] A. Sonnenberg, J. Y. Marciniak, R. Krishnan, and M. J. Heller, “Dielectrophoretic isolation of DNA and nanoparticles from blood.,” *Electrophoresis*, vol. 33, no. 16, pp. 2482–90, Aug. 2012.
- [135] R. Krishnan, B. D. Sullivan, R. L. Mifflin, S. C. Esener, and M. J. Heller, “Alternating current electrokinetic separation and detection of DNA nanoparticles in high-conductance solutions.,” *Electrophoresis*, vol. 29, no. 9, pp. 1765–74, May 2008.
- [136] S. Ranganathan, R. McCreery, S. M. Majji, and M. Madou, “Photoresist-Derived Carbon for Microelectromechanical Systems and Electrochemical Applications,” *J. Electrochem. Soc.*, vol. 147, no. 1, pp. 277–282, 2000.
- [137] H. Xu, K. Malladi, C. Wang, L. Kulinsky, M. Song, and M. Madou, “Carbon post-microarrays for glucose sensors.,” *Biosens. Bioelectron.*, vol. 23, no. 11, pp. 1637–1644, Jun. 2008.
- [138] M. Blazewicz, “Carbon materials in the treatment of soft and hard tissue injuries,” *Eur. cells Mater.*, vol. 2, pp. 21–29, 2001.
- [139] M. Madou and S. Sharma, “Micro and nano patterning of carbon electrodes for bioMEMS,” *Bioinspired, Biomim. Nanobiomaterials*, vol. 1, no. 4, pp. 252–265, Aug. 2012.
- [140] S. Yamada and H. Sato, “Some physical properties of glassy carbon,” *Nature*, vol. 193, pp. 261–262, 1962.
- [141] W. V. Kotlensky and H. E. Martens, “Tensile properties of glassy carbon to 2900C,” *Nature*, vol. 206, pp. 1276–1247, 1965.
- [142] G. T. Teixidor *et al.*, “Carbon microelectromechanical systems as a substratum for cell growth.,” *Biomed. Mater.*, vol. 3, no. 3, pp. 034116–034124, Sep. 2008.
- [143] K. Kinoshita, *Carbon: electrochemical and physicochemical properties*. 1988.
- [144] P. Takmakov *et al.*, “Carbon Microelectrodes with a Renewable Surface,” *Anal. Chem.*, vol. 82, no. 5, pp. 2020–2028, 2010.
- [145] Sathya Achia Abraham, “2013 - 3D carbon goes metallic,” 2013. [Online]. Available: http://news.vcu.edu/article/Threedimensional_carbon_goes_metallic.
- [146] C. Wang and M. Madou, “From MEMS to NEMS with carbon.,” *Biosens. Bioelectron.*, vol. 20, no. 10, pp. 2181–2187, Apr. 2005.
- [147] R. Kostecki, B. Schnyder, D. Alliata, X. Song, K. Kinoshita, and R. Kotz, “Surface studies of carbon films from pyrolyzed photoresist,” *Thin Solid Films*.

- vol. 396. no. 1, pp. 36–43, 2001.
- [148] J. Kim, X. Song, K. Kinoshita, M. Madou, and R. White, “Electrochemical Studies of Carbon Films from Pyrolyzed Photoresist,” *J. Electrochem. Soc.*, vol. 145, no. 7, pp. 2314–2319, 1998.
- [149] A. Singh, J. Jayaram, M. Madou, and S. Akbar, “Pyrolysis of Negative Photoresists to Fabricate Carbon Structures for Microelectromechanical Systems and Electrochemical Applications,” *J. Electrochem. Soc.*, vol. 149, no. 3, pp. 78–83, 2002.
- [150] B. Y. Park, L. Taherabadi, C. Wang, J. Zoval, and M. J. Madou, “Electrical Properties and Shrinkage of Carbonized Photoresist Films and the Implications for Carbon Microelectromechanical Systems Devices in Conductive Media,” *J. Electrochem. Soc.*, vol. 152, no. 12, pp. 136–143, 2005.
- [151] K. Naka and S. Konishi, “Design and Fabrication of Pyrolyzed Polymer Micro and Nano Structures,” 2005.
- [152] D. B. Burckel *et al.*, “Lithographically defined porous carbon electrodes.,” *Small*, vol. 5, no. 24, pp. 2792–2796, Dec. 2009.
- [153] C. S. Sharma, A. Verma, M. M. Kulkarni, D. K. Upadhyay, and A. Sharma, “Microfabrication of carbon structures by pattern miniaturization in resorcinol-formaldehyde gel.,” *ACS Appl. Mater. Interfaces*, vol. 2, no. 8, pp. 2193–2197, Aug. 2010.
- [154] W. M. Jin and J. H. Moon. “Supported pyrolysis for lithographically defined 3D carbon microstructures,” *J. Mater. Chem.*, vol. 21, no. 38, pp. 14456–14460, 2011.
- [155] P. Abgrall, S. Charlot, R. Fulcrand, L. Paul, A. Boukabache, and A.-M. Gué, “Low-stress fabrication of 3D polymer free standing structures using lamination of photosensitive films,” *Microsyst. Technol.*, vol. 14, no. 8, pp. 1205–1214, May 2008.
- [156] R. Martinez-Duarte, P. Renaud, and M. J. Madou, “A novel approach to dielectrophoresis using carbon electrodes.,” *Electrophoresis*, vol. 32, no. 17, pp. 2385–2392, Sep. 2011.
- [157] R. Martinez-Duarte, S. Cito, E. Collado-arredondo, S. O. Martinez, and M. J. Madou, “Fluido-Dynamic and Electromagnetic Characterization of 3D Carbon Dielectrophoresis with Finite Element Analysis,” in *Proceedings of NSTI Nanotech*, 2008, pp. 265–268.
- [158] R. Martinez-Duarte, J. Andrade-Roman, S. . Martinez, and M. Madou, “A High Throughput Multi-Stage, Multi-Frequency Filter and Separation Device Based on Carbon Dielectrophoresis,” *NSTI-Nanotech*, vol. 3, no. 2008, pp. 316–319, 2008.
- [159] J. A. Lee, S. W. Lee, K.-C. Lee, S. Il Park, and S. S. Lee, “Fabrication and characterization of freestanding 3D carbon microstructures using multi-exposures and resist pyrolysis,” *J. Micromechanics Microengineering*, vol. 18, no. 3, pp. 035012–035022, Mar. 2008.

- [160] M. D. C. Jaramillo, E. Torrents, R. Martínez-Duarte, M. J. Madou, and A. Juárez, "On-line separation of bacterial cells by carbon-electrode dielectrophoresis.." *Electrophoresis*, vol. 31, no. 17, pp. 2921–2928, Sep. 2010.
- [161] R. Martinez-Duarte, R. a Gorkin, K. Abi-Samra, and M. J. Madou, "The integration of 3D carbon-electrode dielectrophoresis on a CD-like centrifugal microfluidic platform.," *Lab Chip*, vol. 10, no. 8, pp. 1030–1043, Apr. 2010.
- [162] R. Martinez Duarte, "Label-free cell sorting using carbon-electrode dielectrophoresis and centrifugal microfluidics," University of California, Irvine, 2010.
- [163] R. Martinez-Duarte, "Microfabrication technologies in dielectrophoresis applications-A review," *Electrophoresis*, vol. 33, no. 21, pp. 3110–3132, 2012.
- [164] M. D. C. Jaramillo, R. Marti, M. Huttener, P. Renaud, E. Torrents, and A. Juarez, "Increasing PCR sensitivity by removal of polymerase inhibitors in environmental samples by using dielectrophoresis," *Biosens. Bioelectron.*, vol. 43, pp. 297–303, 2013.
- [165] R. Martinez-Duarte, F. Camacho-Alanis, P. Renaud, and A. Ros, "Dielectrophoresis of lambda-DNA using 3D carbon electrodes.," *Electrophoresis*, vol. 34, no. 7, pp. 1113–1122, Apr. 2013.
- [166] R. Martinez-Duarte, "Carbon-electrode Dielectrophoresis for Bioparticle Manipulation," *ECS Trans.*, vol. 61, no. 7, pp. 11–22. 2014.
- [167] M. Elitas, R. Martinez-duarte, N. Dhar, J. D. Mckinney, and P. Renaud, "Dielectrophoresis-based purification of antibiotic- treated bacterial subpopulations," *Lab Chip*, vol. 14, no. 11, pp. 1850–1857, 2014.
- [168] O. Pilloni, J. L. Benítez Benítez, L. F. Olguin, C. A. Palacios-Morales, and L. Oropeza-Ramos, "Micro Device for Bio-Particle Positioning in a 3D space based on Carbon MEMS and Dielectrophoretic Forces," *ECS Trans.*, vol. 72, no. 31, pp. 17–24, 2016.
- [169] M. Islam, R. Natu, M. F. Larraga-Martinez, and R. Martinez-Duarte, "Enrichment of diluted cell populations from large sample volumes using 3D carbon-electrode dielectrophoresis," *Biomicrofluidics*, vol. 10, no. 3, p. 033107, 2016.
- [170] M. Islam, R. Natu, M. F. Larraga-martinez, G. Contreras-Davila, and R. Martinez-Duarte, "3D Carbon-Electrode Dielectrophoresis for Enrichment of a Small Cell Population from A Large Sample Volume," *ECS Trans.*, vol. 72, no. 1, pp. 97–103, 2016.
- [171] G. Contreras-Davila, J. I. Gomez-Quinones, V. H.Perez-Gonzalez, and R. Martinez-Duarte, "Assessing the Advantages of Using Square Wave Signals for Particle Trapping in Carbon-Electrode Dielectrophoresis," *ECS Trans.*, vol. 72, no. 1, pp. 105–114, 2016.
- [172] R. Martinez-duarte, "Fabrication challenges and perspectives on the use of carbon-electrode dielectrophoresis in sample preparation," *IET nanobiotechnology*, vol.

- 11, no. 2, pp. 127–133, 2016.
- [173] Y. Yildizhan, N. Erdem, M. Islam, R. M. Duarte, and M. Elitas, “Dielectrophoretic Separation of Live and Dead Monocytes Using 3D Carbon-Electrodes,” *Sensors*, vol. 17, no. 11, p. 2691, 2017.
- [174] Y. M. Hassan *et al.*, “High temperature SU-8 pyrolysis for fabrication of carbon electrodes,” *J. Anal. Appl. Pyrolysis*, vol. 125, no. November 2016, pp. 91–99, 2017.
- [175] M. J. Madou, *Fundamentals of Microfabrication: The Science of Miniaturization*, Second edi. CRC press, 2002.
- [176] D. Christopher, L. Julian, and W. A. R., “Printed Microfluidics,” *Adv. Funct. Mater.*, vol. 27, no. 11, pp. 1604824–1604835, 2017.
- [177] K. Yamanaka, M. delanji C.Vestergaard, and E. Tamiya, “Printable Electrochemical Biosensors : A Focus on Screen-Printed Electrodes and Their Applications,” *Sensors*, vol. 16, no. 10, p. 1761, 2016.
- [178] H. Zhu, X. Lin, Y. Su, H. Dong, and J. Wu, “Screen-printed microfluidic dielectrophoresis chip for cell separation,” *Biosens. Bioelectron.*, vol. 63, pp. 371–378, 2015.
- [179] X. Lin, J. Yao, H. Dong, and X. Cao, “Effective Cell and Particle Sorting and Separation in Screen-Printed Continuous-Flow Microfluidic Devices with 3D Sidewall Electrodes,” *Ind. Eng. Chem. Res.*, vol. 55, no. 51, pp. 13085–13093, 2016.

Dielectrophoresis Modeling

3.1 General Introduction

The research in the field of developing an integrated biological analysis system that can perform general biological analysis, cell manipulation, cell trapping and focusing etc is slowly inching towards a transformative and well established stage. In this chapter, we introduce a design for continuous separation structure based on DEP forces. The distribution of electric field in the DEP device was simulated using COMSOL Multiphysics software. A comparative simulation study of various electrode geometries present in literature is reported. We first conceived an idea of fabricating circular microchannel, but because of certain fabrication issues (detailed in Appendix-II) the structure was modified to C-serpentine. Simulation results for electric field gradient distribution is carried out both in a circular channel as well as in C-serpentine channel driven by AC fields. Compared with the previously reported DEP separation devices, the C-serpentine structure achieves continuous separation and also minimizes dead volumes. In addition, the proposed C-serpentine microchannel is more flexible in terms of structure design, for example the large/small radius of curvature, length etc can be optimized as well as, the channel can even be folded to reduce the device footprint.

The modeling and simulation carried out provides understanding of the particle behavior in the proposed channel. The ability to accurately control and manipulate micro and nano scale particles in liquid is fundamental for many applications including biological and medical studies, environmental protections, the development and fabrication of micro/nano electronic and optical devices. Most of such applications involve processes such as placing and patterning the particles into desired locations, as well as detecting and sorting them according to their properties. The demonstrated simulation results indicate its promising utilization for particle separation. With the promising simulation results obtained from the models, we have also fabricated a device using conventional photolithography techniques and screen printing technique which will be discussed in detail in Chapter 4 and Chapter 5.

3.2 Various Electrode Geometries and their Electric Field Simulations

The gradient of electric field is an important factor that affects cellular DEP. The non-uniform electric field on the microfluidic chip is mainly produced by electrodes, so the shape and the distribution of the electrode are vital to DEP force (F_{DEP}). Therefore the heart of any DEP device is a set of electrodes producing a high gradient electric field that drives particles by DEP. From equation (1.1) which has already been described in Chapter 1, we can see that F_{DEP} is proportional to the electric field gradient squared. Therefore the implementation of a strong spatial gradient throughout the microchannel is critical for efficient cell sorting and separation. Since E (electric field) is determined mostly by the electrodes, the geometry of the electrodes has the significant effect on DEP.

Different electrode geometries have been proposed in literature and is discussed in detail in Chapter 2 (Green et al. 1997) [1], (Jen and Chan 2011) [2], (Iliescu et al. 2010) [3], (Lin and Yeow 2007) [4], (Abidin et al. 2007) [5], we have listed some of the commonly used DEP electrode geometries below in Figure 3.1(a-f).

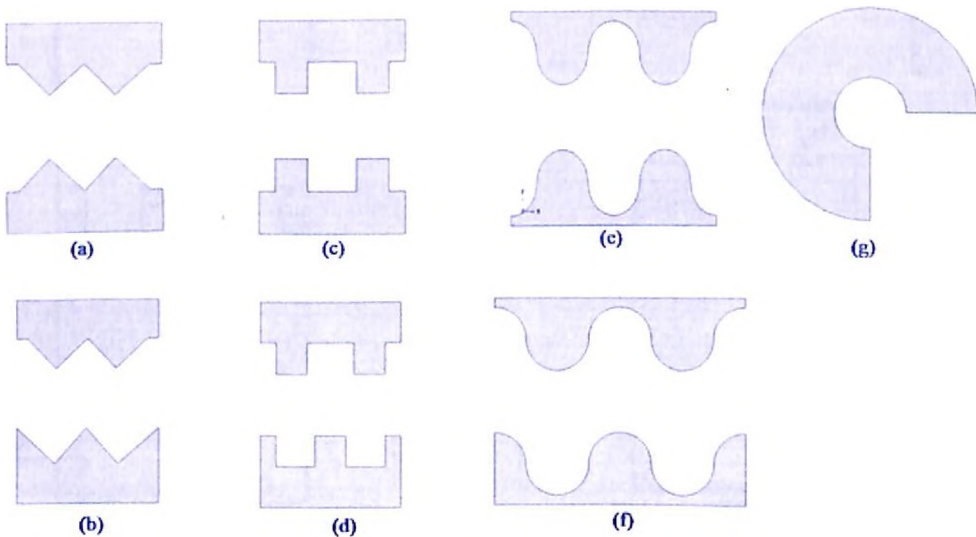


Figure 3.1: (a) Saw tooth electrodes (Set), (b) Saw tooth electrodes (Offset), (c) Castellated electrodes (Set), (d) Castellated electrodes (Offset), (e) Bell shaped electrodes (Set), (f) Bell shaped electrodes (Offset), (g) Circular electrode

Circular geometry as shown in Figure 3.1(g) is used in our study and is the least investigated electrode configuration. Simulations of electric field distributions are an essential step in the design of appropriate electrode geometry. To determine the layout of

the electrodes, it is necessary to estimate the forces acting on the particles of interest, cells, at different locations within the device. Therefore, for the above given geometries we have simulated the electric field distribution and gradient of electric field using COMSOL 4.3a. The simulation steps are given in detail in Appendix-II, present at the back of the thesis. This helps us in determining the areas that corresponds to p-DEP and n-DEP regions and are shown in Figure 3.2. The areas in red colour are the regions of high electric field and the regions in blue are the area with lower electric field. The commercial finite element analysis software COMSOL multiphysics is used for the electric field simulation using AC/DC module [6].

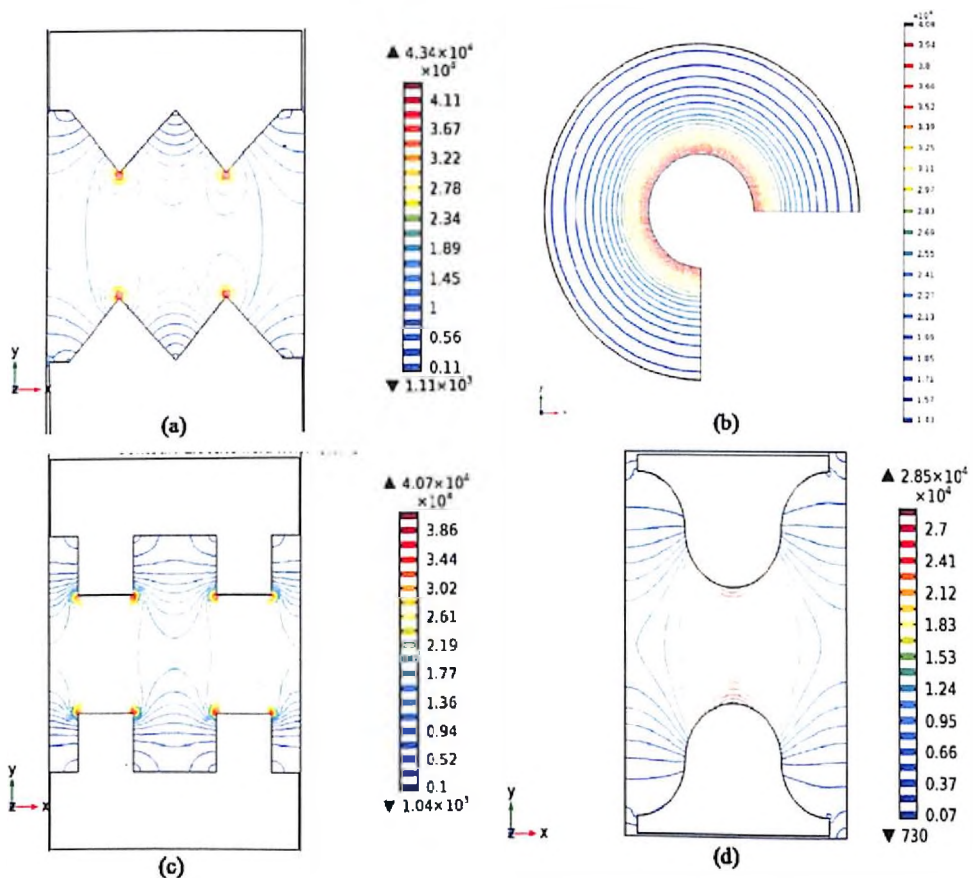


Figure 3.2: Electric gradient distribution in set type electrode geometry (5Vp-p, 200 μ m- electrode gap, 20 μ m- electrode height (a) Saw tooth, (b) Circular electrode, (c) Rectangular electrode (d) Bell shaped electrode

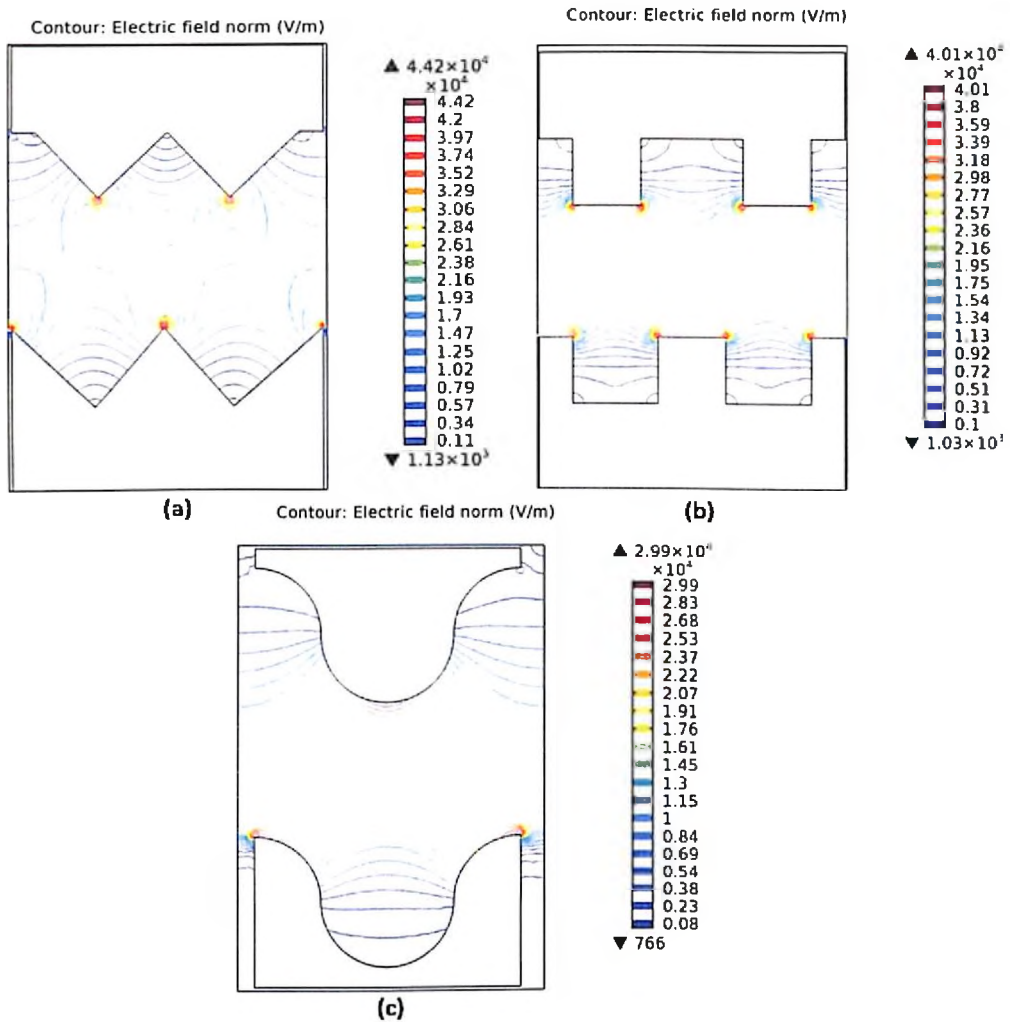


Figure 3.3: Electric gradient distribution in off-set electrode geometry (5Vp-p, 200 μ m- electrode gap, 20 μ m- electrode height (a) Saw tooth, (b) Circular electrode, (c) Rectangular electrode (d) Bell shaped electrode

Triangular, rectangular, bell shaped and circular electrodes were analyzed using COMSOL to estimate the electric field gradient generated. For drawing comparison between different electrode geometries, an actuation voltage of 5 Vp-p was applied between each electrode pair and the gap between the electrodes was kept as 200 μ m. Figure 3.2 and Figure 3.3 shows simulation results for electric field gradient distribution amongst different geometries in set and off-set arrangement. Also the field gradient distribution in set and off-set geometry is detailed in Table 3.1. It was observed from Figure 3.2 that the cell trapping regions varies among different electrode geometries. The results show that the saw tooth electrodes (off-set arrangement) in

comparison to other electrode designs had the highest value of electric field gradient, which is also in agreement with the reported literature [7]. However the shortcoming with this type of electrode configuration is that it is associated with stagnation regions due to sharp turns thereby making it more sensitive to contamination and particle adhesion. The castellated design with electrode fingers is one of the most common designs that have been reported, which also captures particles within tooth pockets. Using castellated electrodes, cells collected under p-DEP are held in deep and steep-sided potential energy wells at the electrode edges, whereas under the influence of n-DEP the cells are retained as triangular shaped aggregations in the shallow potential energy wells. Thus, cells attracted to the electrodes by p-DEP are not easily dislodged by flushing fluid over the electrodes, whereas those cells retained by n-DEP are readily and selectively removed by such action. Unlike sawtooth and castellated designs, the bell and circular geometries provides better protection against stagnation regions and particle adhesion because of elimination of sharp turns. In circular design the two extreme portions are wide apart making it easier to separate cells and more importantly the stagnation regions due to sharp turns are eliminated which provides better protection against particle adhesion. Also the value of electric field gradient as seen from the simulation is less than sawtooth configuration but is comparable to the castellated one which has been widely adopted in literature. In the bell shaped electrode design the value of electric field gradient is the lowest amongst all but is more flexible in the structural design as the curvature, width and length can be optimized.

In a quest to achieve efficient trapping of particles, few scientists have explored and reported the use circular geometry electrodes in literature. (Zhang et al. 2006) [8] reported continuous electrodeless particle separation in circular channel using DC voltage and electro-osmotic flow. Also (Jen and Chan 2011) [2] proposed concentric circular electrodes for pre-concentration of rare cells using stepping electric field at 16Vp-p and achieved an enrichment efficiency of 75%.

Therefore it was concluded that circular geometry has an edge over other geometries and is also not widely explored and so was found it appropriate for DEP based bio-particle separator in our study.

Table 3.1: Electric field gradient for different electrode configuration with $5 V_{p-p}$ actuation voltage (the distance between electrodes was $200 \mu\text{m}$)

Design	Type	Electric field gradient (V/m)
Saw Tooth	Set	4.34×10^4
	Off-Set	4.42×10^4
Circular		4.08×10^4
Rectangular (Castellated)	Set	4.07×10^4
	Off-Set	4.01×10^4
Bell Shaped	Set	2.85×10^4
	Off-Set	2.99×10^4

3.3 Simulation in Circular Geometry

The schematic geometry of proposed DEP based separation device used in our study is shown in Figure 3.4(a). The electrode structure is constructed by aligning two layers of microelectrodes face to face, one on the inner periphery and another on the outer periphery.

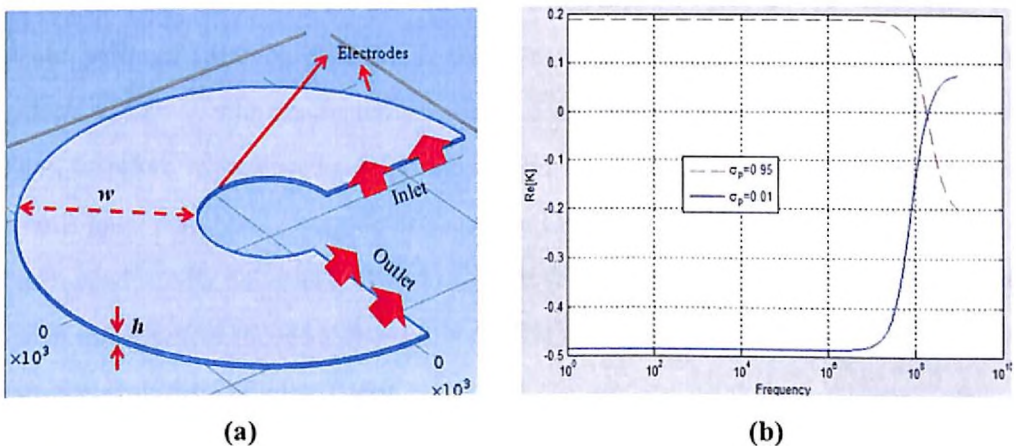


Figure 3.4: (a) Circular channel geometry, (b) $\text{Re}[K]$ as a function of frequency (SET-A) $\sigma_p = 0.95$, (SET-B) $\sigma_p = 0.01$

Further investigations on effect of variation in channel width (w) and channel height (h) has been carried out using COMSOL. Parameters that were taken into consideration are given in Table 3.2. These values of conductivity and permittivity were taken because bio-particles possess wide range of conductivities and permittivity.

Table 3.2 Simulation parameters

Electrical conductivity of fluid	0.56 S/m
Relative permittivity of fluid	78
Relative permittivity of two particles	36,97
Particle density	1050 Kg/m ³
Electrical conductivity of particles	0.95, 0.01 S/m
Voltage applied	5 V

Before doing simulations, a graph of CM factor versus frequency was plotted as shown in Figure 3.4(b) using MATLAB coding for two sets of particles with particle conductivity value of (SET A- 0.95, SET B- 0.01) respectively. The graph illustrates that the particles with dotted line (i.e SET A) will have positive value of mossotti factor over the frequency range 1 Hz-100 MHz while on the contrary, particles with continuous line (i.e. SET B) shows negative value of mossotti factor over the same frequency range. This was successfully verified by particle tracing simulation in COMSOL. We simulated two sets of particles (SET-A, SET-B). It was observed from the simulation results that particles in SET-A with conductivity value as 0.95 which had positive value of mossotti factor, therefore experienced p-DEP and moved towards high electric field regions i.e. towards inner peripheral electrode as shown in Figure 3.5(a). Whereas particles in SET-B with conductivity value as 0.01 had negative value of mossotti factor and experienced n-DEP and therefore moved towards low electric field region i.e towards outer periphery electrode as shown in Figure 3.5(b).

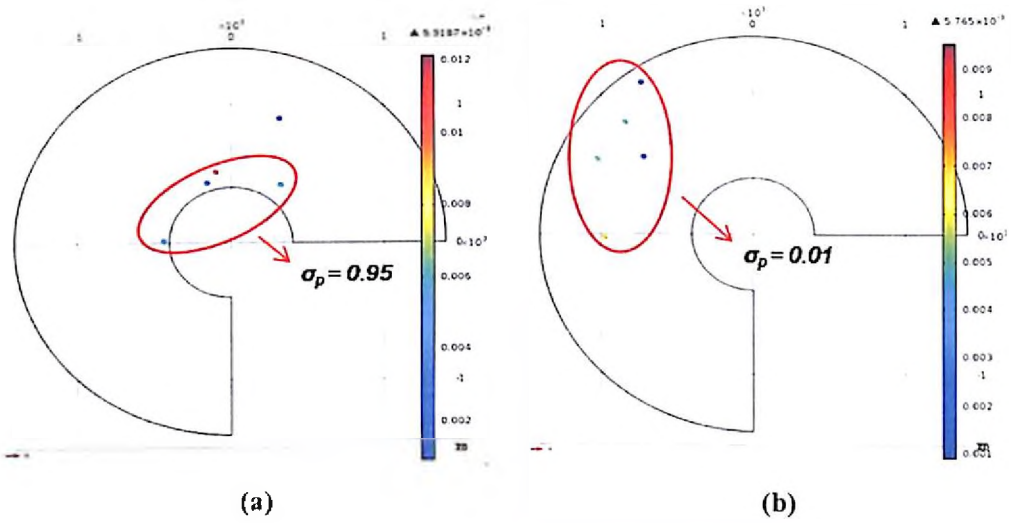


Figure 3.5: Particles with (a) p-DEP and (b) n-DEP behavior

In the Figure 3.5 the particles did not stick to the channel walls because bounce condition has been applied in order to see their deflection. For further confirmation of results so obtained, mixture of these two sets of particles was also simulated and the path followed by them was traced as shown in Figure 3.6.

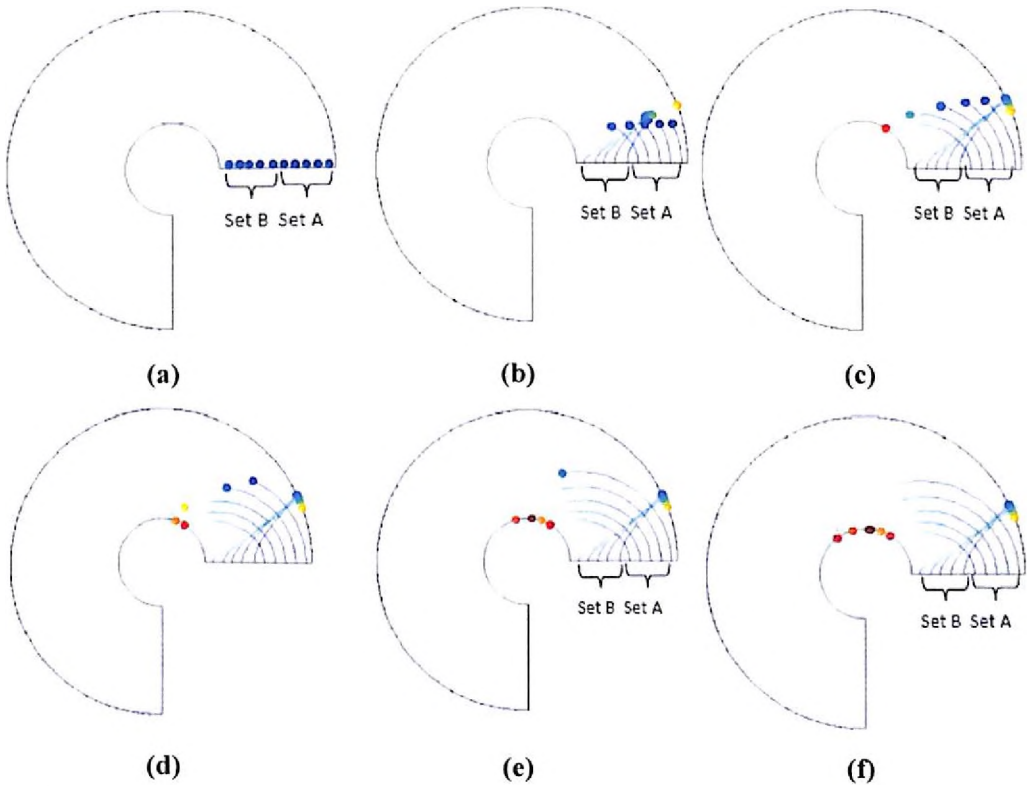


Figure 3.6: Step wise representation of particle separation of two sets of particles

3.3.1 Effect of variation in channel width

This section includes the simulation results to study the effect of different circular microchannel width on particle trajectory. The width of the microchannel varying from 1 mm, 500 μm to 200 μm is used in this study. The height of the microchannel is 20 μm , flow rate is $1.76 \text{ e}^{-11} \text{ m}^3/\text{sec}$ and an applied voltage of 5 Vp-p is used for this study. The results obtained by varying the channel width are shown in Figure 3.7. Figure 3.7(a) shows particle trajectory in 1mm wide microchannel, Figure 3.7(b) shows particle trajectory in 500 μm wide microchannel and Figure 3.7(c) shows particle trajectory in 200 μm wide microchannel.

It is inferred from the simulation results, that as the width of the channel is reduced from 1 mm to 500 μm and 200 μm , the particles tends to separate early and get deposited on the electrodes close to the inlet or as soon as they enter the channel. This trend can be explained from Equation 3.1

$$E = \frac{V}{d} \quad (3.1)$$

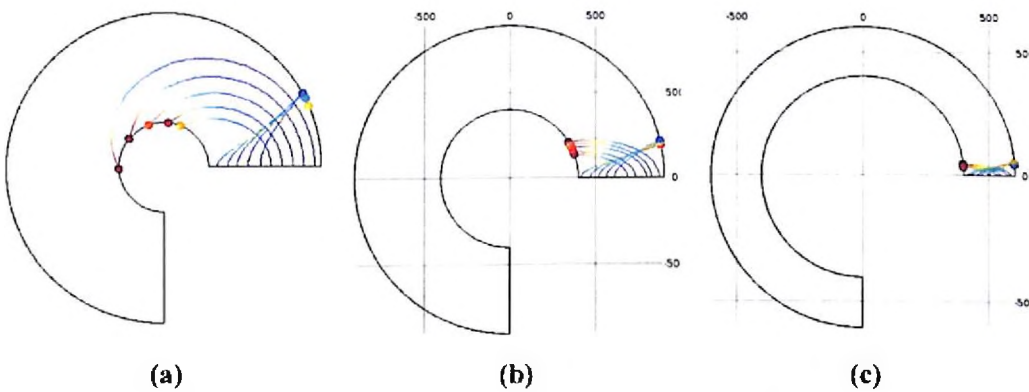


**Figure 3.7: Particle separation in circular channel of different widths
(a) 1mm, (b) 500 μm and (c) 200 μm**

where E is electric field intensity, V is voltage applied and d is distance between two electrodes. From Equation 3.1, it is evident that the electric field is inversely proportional to the distance between the two electrodes. So, when the electrode distance was reduced from 1 mm to 500 μm and 200 μm there is an increase in the electric field intensity. This increased electric field intensity lead to the increase in the attraction and repulsive forces experienced by the particles or in other words increased the F_{DEP} force, leading to their early separation and deposition as soon as they enter the channel.

3.3.2 Effect of variation in channel height

This section includes the simulation results to study the effect of different microchannel height on particle trajectory. The height of the microchannel varying from 20 μm , 15 μm to 10 μm is used in this study. The width of the microchannel is 1 mm, an applied voltage of 5Vp-p and flow rate of $1.76 \times 10^{-11} \text{ m}^3/\text{sec}$ is used for this study. The results obtained by varying the channel height are shown in Figure 3.8. Figure 3.8(a) shows particle trajectory in 20 μm high microchannel, Figure 3.8(b) shows particle trajectory in 15 μm high microchannel and Figure 3.8(c) shows particle trajectory in 10 μm high microchannel.

It is inferred from the simulation results, that as the channel height was reduced from 20 to 15 and 10 μm the particle separation became inefficient or the particles did not get separated. The reason for this particle behavior can be explained from the Equation 3.2.

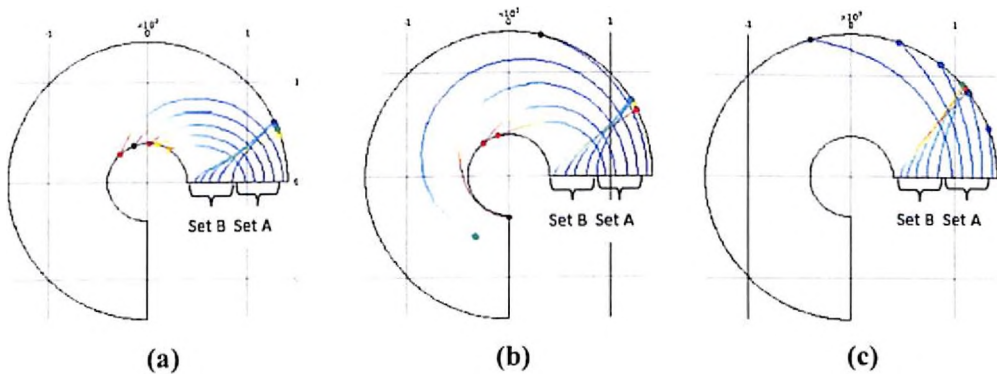


Figure 3.8: Particle separation in circular channel of different heights (a) 20 μm , (b) 15 μm and (c) 10 μm

$$Q = V * A \quad (3.2)$$

where Q is flow rate, V is flow velocity and A is channel area. From the above equation it is evident that there is an inverse relationship between the channel area and fluid velocity. So, as the channel height was reduced from 20 to 15 and 10 μm there was decrease in channel area. This decrease in channel area led to increase in the fluid velocity in smaller channel. Therefore the increased fluid velocity caused inefficient particle separation thereby dragging the particles along with the fluid due to increased electrokinetic flow velocity.

From the simulation results we decided to fabricate a wider channel of 1 mm width and 20 μm height. The prime reason for choosing wider microchannel is because it was observed that the channel length is very small for allowing high throughput separation. Therefore one alternative to increase the device throughput is to increase the channel cross-section. However the gap between the electrodes is the direct determinant of DEP force as increasing the intra electrode gap decreases the field gradient. So, the other possible alternative is to increase the number of electrode pairs, thereby the effective separation region will also become longer. In order to enhance the device throughput, we decided to fabricate a wider microchannel and also increased the channel length by adding more number of C shape structures to circular shape design. Therefore we decided to fabricate a C-serpentine channel, the details of which are discussed in the Section 3.4 below.

3.4 C-Serpentine Geometry

The schematic diagram of C-serpentine geometry used for trapping of cells is shown in Figure 3.9 below. The geometry is constructed by extending circular electrode by adding six S-shaped structures on either ends of the channel making it a C-serpentine channel. These S-shapes resembles bell shaped electrodes shown and discussed in Section 3.2 in Figure 3.1.

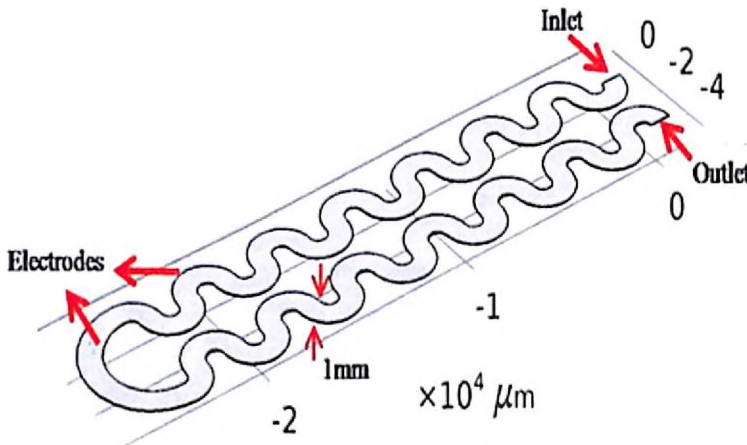


Figure 3.9: C-serpentine device schematic diagram

We choose off-set bell shaped structures as its gradient is more than the set type bell geometry. More importantly this design is free from the issue of stagnation regions as

there are no sharp edges in the structure. The electrodes form the inner and the outer periphery of the microchannel. The wavy electrodes serve as a signal input unit as well as channel wall.

3.4.1 Electric Field Distribution

Electric field distribution was studied in C-Serpentine channel to understand the high and low field gradient regions in the channel using COMSOL. Figure 3.10 (a) shows field gradient distribution inside the C-serpentine microchannel. On applying 5 Vp-p an electric field gradient of 8.03×10^3 V/m was obtained in 1 mm wide channel. It was observed in the simulation that the n-DEP and p-DEP regions alternate at each clockwise and anticlockwise turn. The regions in red are the regions with max field gradient and the regions in blue are the regions with minimum value of field gradient. Maximum field gradient was at the arch part of the channel (the regions in red) and the gradient minima were at the intermediate region of the microchannel (the regions in blue). Therefore it is inferred from the field gradient simulation that the p-DEP regions lies towards the small periphery and n-DEP regions occur towards the larger periphery. In a nutshell, particle with n-DEP will move towards low field gradient regions i.e. towards outer channel periphery, whereas the particles with p-DEP regions will be seen towards high field gradient regions i.e towards inner channel periphery as shown in Figure 3.10(b).

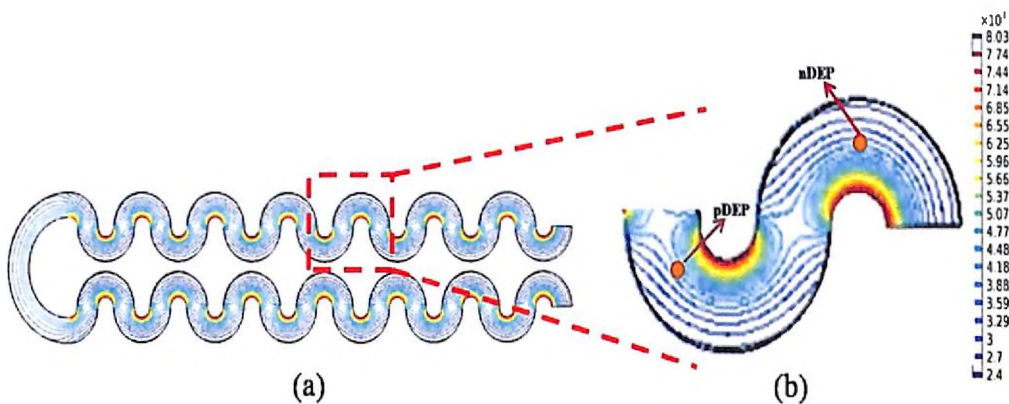
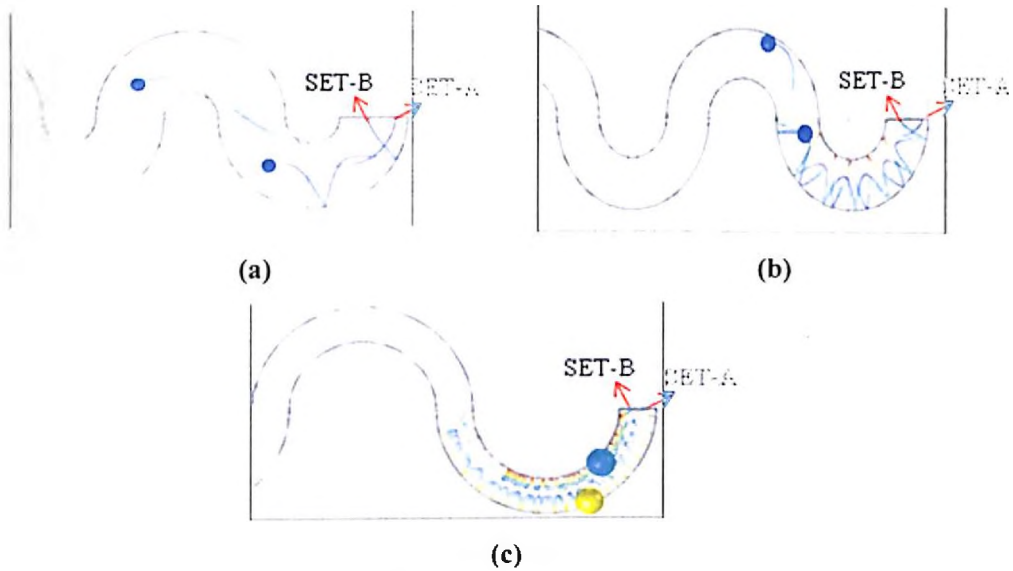


Figure 3.10: (a) Electric field gradient distribution (b) Expanded view

3.4.2 Effect of Variation in Channel Width

This section includes the simulation results to study the effect of different C-serpentine microchannel width on particle trajectory. The width of the microchannel varying from 1 mm, 500 μm to 200 μm is used in this study. The height of the microchannel is 20 μm with a flow rate of $1.76 \text{ e}^{-11} \text{ m}^3/\text{sec}$ and an applied voltage of 5 Vp-p is used for this study. The results obtained by varying the channel width are shown in Figure 3.11. Figure 3.11(a) shows particle trajectory in 1 mm wide microchannel, Figure 3.11(b) shows particle trajectory in 500 μm wide microchannel and Figure 3.11(c) shows particle trajectory in 200 μm wide microchannel.



**Figure 3.11: Particle separation in C-serpentine channel of different widths
(a) 1 mm, (b) 500 μm and (c) 200 μm**

It is observed from the simulation results that the two particles Set-A and Set B show the same particle trajectory as in the circular microchannel. Set-A particles experience p-DEP and move towards smaller periphery whereas Set-B particles experience n-DEP and move towards larger periphery. For better clarity of images particle trajectory is only shown in the initial part of the microchannel i.e. near the inlet. It is inferred from the simulation results, that as the width of the channel is reduced from 1 mm to 500 μm and 200 μm , the particles travel a very short distance inside the microchannel and tends to separate early. This trend can be explained from Equation 3.1 which indicates that, the electric field is inversely proportional to the distance between the two electrodes. So,

when the electrode distance was reduced from 1 mm to 500 μm and 200 μm there is an increase in the electric field intensity. This increased electric field intensity lead to the increase in the attraction and repulsive forces experienced by the particles or in other words increased the F_{DEP} force, leading to their early separation and deposition as soon as they enter the channel.

3.4.3 Effect of Variation in Channel Height

This section includes the simulation results to study the effect of different height of C-serpentine microchannel on particle trajectory. The height of the microchannel varying from 20 μm , 15 μm to 10 μm is used in this study. The width of the microchannel is 1mm, an applied voltage of 5Vp-p and flow rate of $1.76e^{-11}$ m^3/sec is used for this study. Figure 3.12 shows the results obtained by varying the channel height. Figure 3.12(a) shows particle trajectory in 20 μm high microchannel, Figure 3.12(b) shows particle trajectory in 15 μm high microchannel and Figure 3.12(c) shows particle trajectory in 10 μm high microchannel.

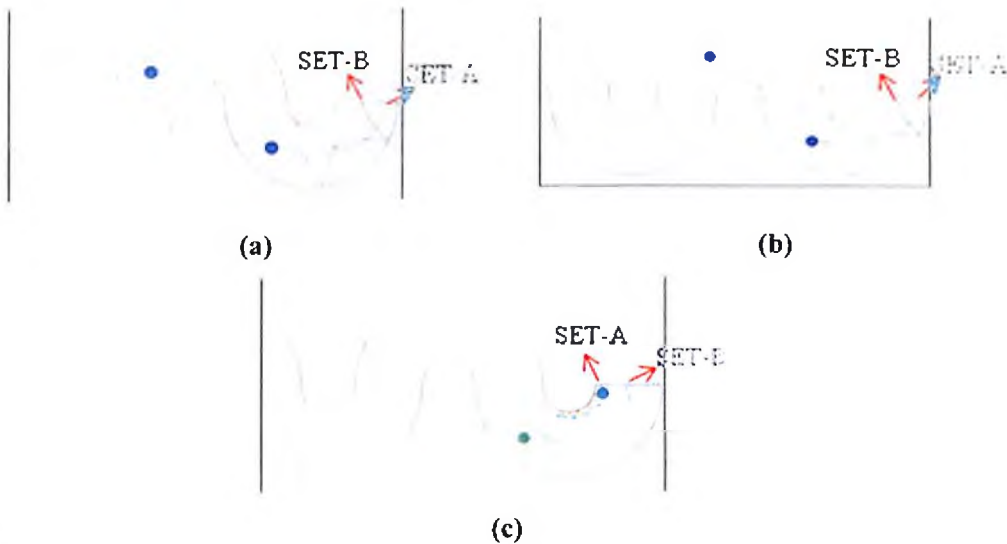


Figure 3.12: Particle separation in C-serpentine channel of different height (a) 20 μm , (b) 15 μm and (c) 10 μm

It was observed from the simulation results, that as the channel height was reduced from 20 to 15 and 10 μm there was not much change in the particle trajectories unlike as seen in circular microchannel. The only difference observed was in the distance travelled by each set of particles. The reason for this particle behavior can be explained from the

Equation 3.2 which states that channel area is inversely related to flow velocity. Therefore when the microchannel height was reduced from 20 to 10 μm , there was an increase in the flow velocity but not enough to drag the particles along the flow direction and cause inefficient particle separation.

3.5 MATLAB Modeling

Determination of the type of DEP moment a particle will experience can be accomplished by calculating $\text{Re}[K(\omega)]$ using Equation 1.2. As previously stated, the real portion of the CM factor will dictate whether the DEP force on a particle will be positive or negative. The CM factor is frequency dependent because it is determined from the frequency dependent complex permittivities of the particle and the medium [9], [10]. As such, by constructing a plot of the real component of the CM factor as a function of frequency it is possible to estimate the frequency ranges in which a particle will exhibit p-DEP and n-DEP.

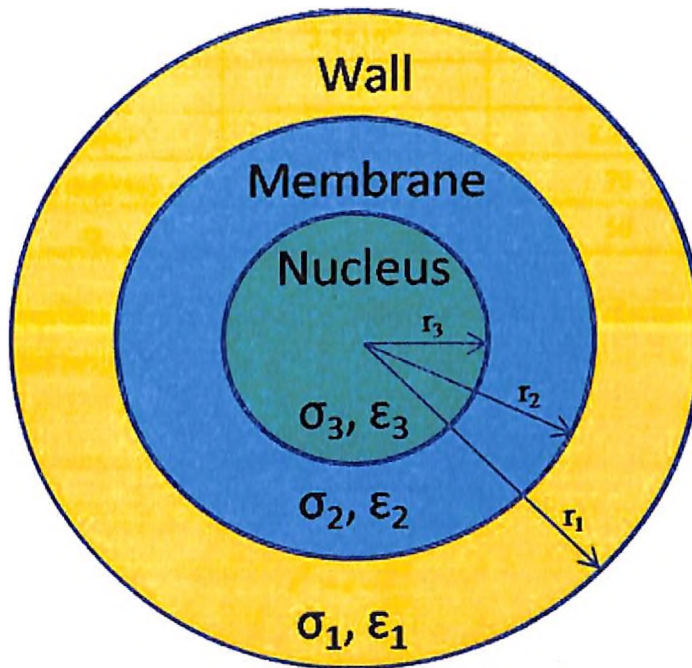


Figure 3.13: Two-shell model of a yeast cell

For testing of the device we have used yeast cells as model cells in our study. The parameters considered for live and dead yeast cells are detailed in Table 3.3. First, to determine the behavior of live and dead yeast cells over a frequency range, CM factor

has to be calculated. The common approach to calculate the massotti factor is to apply the double-shell spherical model [11]. As shown schematically in Figure 3.13, a cell in this model is treated as a dielectric sphere covered by two concentric layers (i.e cytoplasmic membrane and cell wall).

Each layer of the cell possesses different value of conductivity and permittivity, the values of which are given in table below.

Table 3.3: The values of the radius (r), electric conductivity (σ), and permittivity (ϵ) for each layer of live and dead yeast cells [11]

Symbol	Values	
	Live cells	Dead cells
$r_1(\mu\text{m})$	3	2.5
$\sigma_1 (\mu\text{S/cm})$	140	15
ϵ_1	60	60
$r_2(\mu\text{m})$	2.78	2.25
$\sigma_2 (\mu\text{S/cm})$	2.5×10^{-3}	1.6
ϵ_2	6	6
$r_3(\mu\text{m})$	2.772	2.242
$\sigma_3 (\mu\text{S/cm})$	2000	70
ϵ_3	50	50

The common approach to CM factor is by using Equation 1.1 as discussed in Chapter 1 and is also briefed below:

$$f_{CM} = \frac{\epsilon_{\text{cell}}^* - \epsilon_{\text{medium}}^*}{\epsilon_{\text{cell}}^* + 2\epsilon_{\text{medium}}^*} \quad (3.3)$$

$$\epsilon^* = \epsilon - \frac{i\sigma}{\omega} \quad (3.4)$$

where, ϵ^* is the complex permittivity, ϵ is the permittivity, σ is the electrical conductivity and ω is the angular frequency of the AC signal.

Since, yeast cells are double layered structures, the complex permittivity of such a cell is computed from Equation 3.5 and Equation 3.6:

$$\epsilon_{\text{cell}}^* = \epsilon_1^* \frac{\left(\frac{r_1}{r_2}\right)^3 + 2\left(\frac{\epsilon_{23}^* - \epsilon_1^*}{\epsilon_{23}^* + 2\epsilon_1^*}\right)}{\left(\frac{r_1}{r_2}\right)^3 - \left(\frac{\epsilon_{23}^* - \epsilon_1^*}{\epsilon_{23}^* + 2\epsilon_1^*}\right)} \quad (3.5)$$

$$\epsilon_{23}^* = \epsilon_2^* \frac{\left(\frac{r_2}{r_3}\right)^3 + 2\left(\frac{\epsilon_3^* - \epsilon_2^*}{\epsilon_3^* + 2\epsilon_2^*}\right)}{\left(\frac{r_2}{r_3}\right)^3 - \left(\frac{\epsilon_3^* - \epsilon_2^*}{\epsilon_3^* + 2\epsilon_2^*}\right)} \quad (3.6)$$

In the above equations, ϵ_1^* , ϵ_2^* and ϵ_3^* are respectively the complex permittivities of the cell wall, membrane and the nucleus. Also r_1 , r_2 and r_3 are the radius of cell wall, membrane and nucleus respectively.

The permittivity of cell was calculated using Equation 3.5 and Equation 3.6 and then substituted in Equation 3.3 to calculate mossotti value. Values of CM factor were calculated using MATLAB (MATLAB code is detailed in Appendix-II, present at the back of the thesis) and is presented in Figure 3.14 and 3.15 for live and dead yeast cell respectively. The MATLAB plot predicts the CM factor of the two types of cells suspended in 280 mM mannitol buffer as a function of frequency. The conductivity of the solution with live and dead cells was measured (EUTECH Instruments PC 5:10, ph/conductivity/TDS/temp measurement) to be 70 $\mu\text{S}/\text{cm}$ and 110 $\mu\text{S}/\text{cm}$ respectively at 25°C temp. The permittivity of the medium is taken as 6.9×10^{-10} C/(v.m), which is for pure water at 20°C. Mainly because of the discrepancies in the value of electrical conductivities of the cell membrane for the two types of cells, both cells respond dissimilarly to ac electric field.

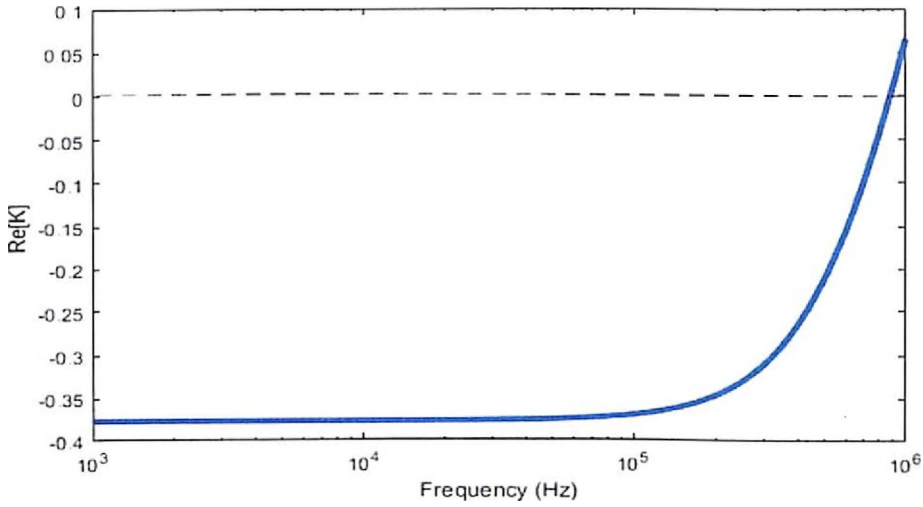


Figure 3.14: Plot of $\text{Re}[K(\omega)]$ vs. frequency for live yeast cells

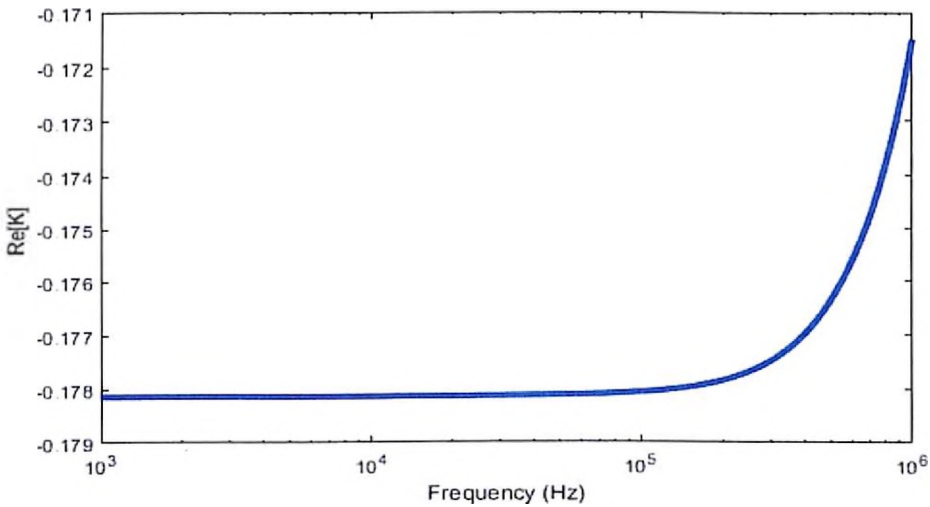


Figure 3.15: Plot of $\text{Re}[K(\omega)]$ vs. frequency for dead yeast cells

Figure 3.14 shows the MATLAB plot for live cells with $\text{Re}[K]$ value as -0.37 and Figure 3.15 shows MATLAB plot for dead cells with $\text{Re}[K]$ value of -0.17, the two types of cells suspended in 280 mM mannitol buffer as a function of the ac field frequency (from 1 kHz to 1 MHz). Due mainly to their discrepancies in the electric conductivities of cell membrane and cytoplasm, live and dead yeast cells respond dissimilarly to ac electric field. In the range from 1 kHz to 1 MHz AC field, dead cells possess a negative CM factor throughout and hence experience n-DEP. Whereas, live cells possess

negative CM factor till 1 MHz. at 1MHz crossover frequency occurs and CM factor becomes positive.

3.6 Conclusions

In the present chapter, we have discussed about the few commonly reported geometries in literature and proposed a new C-serpentine design. For various geometries we have simulated the electric field distribution and gradient of electric field to have a better understanding of high and low field gradient regions in the channel. This aids in estimating the p-DEP and n-DEP areas. In literature, few authors have introduced a serpentine channel with 90° turns to focus and separate polystyrene particles, however, the area where electric gradient can be generated is limited, that is, only within the corner of the channel turns, while the electric field is uniform in the straight section of the microchannel [12]–[16]. Additionally, serpentine design with 90° turns is more sensitive to contaminations or particle adhesion on the channel wall, as particles are deflected towards the outer sidewall of the microchannel. Also, a waved microchannel for the focusing of microparticles and cells using electrokinetic and negative DC DEP in a continuous flow have also been proposed [17]. Compared to the serpentine channel with 90° turns, the suggested design extends the regions creating the DEP effect to the full width of the microchannel, thereby allowing greater control over particle motion. Most importantly, the stagnation regions and locally amplified electric field due to sharp turns are eliminated, which provides better protection against particle adhesion to sidewalls. However the above research work exploited the waved geometry for focusing particles using insulator based DEP approach, where very high DC or AC biased DC fields are used say for example an electric field of 100-500V/cm are employed. This high electric field can greatly affect the cell viability. This drawback can be overcome by using AC fields, because of its ability to precisely control the forces applied on the particles by the electric field. In this thesis, we propose a C-serpentine microchannel for trapping of yeast cells using negative AC DEP. In addition, the proposed C-serpentine microchannel is more flexible in terms of structure design, for example the large/small radius of curvature, length etc can be optimized depending upon the need. As proposed by us, the channel can even be folded to reduce the device footprint.

We have also discussed MATLAB modeling of mossotti factor using two shell model of yeast cells. This helps in determining the p-DEP, n-DEP frequency ranges and cross-over

frequency for the cell type and medium. Also, the significance of performing the sorting of live and dead cells is that, it allows differential cell counting for point of care diagnosis. The existence of non-viable cells in cell suspension causes ubiquitous problem in the biomedical field. Enrichment of viable cells can increase the accuracy of biomedical assays as the presence of non-viable cells in the sample can lead to improper conclusions in monitoring the effects of experimental conditions.

References

- [1] N. G. Green, H. Morgan, and J. J. Milner, "Manipulation and trapping of sub-micron bioparticles using dielectrophoresis," *J. Biochem. Biophys. Methods*, vol. 35, pp. 89–102, 1997.
- [2] C.-P. Jen and H.-H. Chang, "A Dielectrophoretic Preconcentrator with Circular Microelectrodes for Biological Cells in Stepping Electric Fields," *Des. Test. Integr. Packag. MEMS/MOEMS (DTIP), Symp. IEEE*, pp. 352–355, 2011.
- [3] C. Iliescu, G. Tresset, L. Yu, and G. Xu, "3D Dielectrophoretic Chips : Trapping and Separation of Cell Populations," *Rom. J. Inf. Sci. Technol.*, vol. 13, no. 1, pp. 49–64, 2010.
- [4] J. T. Y. Lin and J. T. W. Yeow, "Enhancing dielectrophoresis effect through novel electrode geometry.," *Biomed. Microdevices*, vol. 9, no. 6, pp. 823–31, Dec. 2007.
- [5] Z. Z. Abidin, A. G. L. Abdullah, Z. Yunus, G. H. Markx, and A. Science, "Wire cloth electrodes: A study of electric field for dielectrophoretic separation of cells," *IJ Eng. Tech*, vol. 4, no. 2, pp. 205–212, 2007.
- [6] P. Puri, V. Kumar, M. Ananthasubramanian, and N. N. Sharma, "Design, simulation and fabrication of MEMS based dielectrophoretic separator for bioparticles," *Microsyst. Technol.*, vol. 23, no. 8, pp. 3371–3379, 2017.
- [7] M. R. Malik, T. Shi, and Z. Tang, "Trapping and Manipulation of Bioparticles by a 3-D Optimal Multiple-Designed Offset Carbon-Microelectrode Array in C-MEMS Fabrication," *J. Biomim. Biomater. Tissue Eng.*, vol. 10, pp. 25–42, 2011.
- [8] L. Zhang *et al.*, "Continuous electrodeless dielectrophoretic separation in a circular channel," *J. Phys. Conf. Ser.*, vol. 34, no. 1, pp. 527–532, 2006.
- [9] L. Benguigui and I. . Lin, "More about the dielectrophoretic force," *J. Appl. Phys.*, vol. 53, no. 2, pp. 1141–1143, 1982.
- [10] M. P. Hughes, "Strategies for dielectrophoretic separation in laboratory-on-a-chip systems," *Electrophoresis*, vol. 23, no. 16, pp. 2569–2582, 2002.
- [11] S. Patel, D. Showers, P. Vedantam, T. Tzeng, S. Qian, and X. Xuan, "Microfluidic separation of live and dead yeast cells using reservoir-based dielectrophoresis.," *Biomicrofluidics*, vol. 6, no. 3, p. 034102, 2012.
- [12] J. Zhu, T. R. J. Tzeng, G. Hu, and X. Xuan, "DC dielectrophoretic focusing of particles in a serpentine microchannel," *Microfluid. Nanofluidics*, vol. 7, no. 6, pp. 751–756, 2009.
- [13] J. Zhang, W. Li, M. Li, G. Alici, and N. T. Nguyen, "Particle inertial focusing and its mechanism in a serpentine microchannel," *Microfluid. Nanofluidics*, vol. 17, no. 2, pp. 305–316, 2014.
- [14] C. Church, J. Zhu, J. Nieto, G. Keten, E. Ibarra, and X. Xuan, "Continuous particle separation in a serpentine microchannel via negative and positive dielectrophoretic focusing," *J. Micromechanics Microengineering*, vol. 20, no. 6, pp. 065011–065016, 2010.
- [15] C. Church, J. Zhu, and X. Xuan, "Negative dielectrophoresis-based particle separation by size in a serpentine microchannel," *Electrophoresis*, vol. 32, no. 5, pp. 527–531, 2011.

- [16] J. Zhu, R. C. Canter, G. Keten, P. Vedantam, T. R. J. Tzeng, and X. Xuan, "Continuous-flow particle and cell separations in a serpentine microchannel via curvature-induced dielectrophoresis," *Microfluid. Nanofluidics*, vol. 11, no. 6, pp. 743–752, 2011.
- [17] M. Li, S. Li, W. Cao, W. Li, W. Wen, and G. Alici, "Continuous particle focusing in a waved microchannel using negative dc dielectrophoresis," *J. Micromechanics Microengineering*, vol. 22, no. 9, pp. 095001–095008, 2012.

Dielectrophoretic Trapping with Microfabricated Gold Electrodes

4.1 General Introduction

Electrode geometry has a very crucial role to play in DEP, as they generate a non-uniform electric field that gives rise to DEP effects. Previous electrode structures for early DEP studies were constructed from thin metal wires, needles or plates [1][2]. However, current DEP platforms utilize advanced microfabrication technologies to produce microelectrode arrays that are capable of generating strong DEP force with small applied voltages [3]–[5]. Because of the availability of advanced microfabrication techniques the electrode geometries and configurations are no longer restricted to wires, pins and plates, infact arbitrary shapes of planar electrodes with submicron dimensions could be fabricated.

Over the past many years, DEP devices with planar metal electrodes have dominated the subject. Wide range of materials used for the fabrication of electrodes in various DEP devices includes platinum, gold, silver and copper. However from literature survey we observed that the use gold electrode in DEP devices is widely reported. This is because the gold patterning technology is fully developed and matured in the area of MEMS. Wang et al [6], reported the enrichment and detection of E.coli bacteria using gold interdigitated electrodes. Gold interdigitated oblique electrodes fabricated on pyrex glass with PDMS channel has been used for sorting of stem cells and osteoblast cells [7]. Yafouz et al,[8] described the micro dot array with gold-coated glass microelectrode, as a promising electrode geometry to characterize and manipulate cells via DEP. Rajaraman et al [9] reported four fabrication technologies to make low cost DEP devices. In all the techniques gold interdigitated array were used as an electrode to manipulate polymer beads and tin oxide nanowires. Few authors have also reported the use of hydrogel coated metal electrodes to bring a significant improvement in the electric field generated [10][11].

In this chapter, we are investigating the DEP effect generated using circular and C-serpentine microelectrodes fabricated using gold. To the best of our knowledge, circular

and C-serpentine design has not been addressed in literature for electrode DEP. Fabrication details for both the electrode design are discussed in this chapter. The electrodes so fabricated are 2D electrodes with 200nm in height, and with 1mm wide and 30 μ m high channel. Further, the DEP performance of the device was verified using live and dead yeast cells [12]. Also, the efficiency of the fabricated device for trapping live and dead yeast cells is calculated by measuring the untrapped cells that have flown to the outlet.

4.2 Experimental Details

This chapter includes the detailed fabrication of the gold electrode based DEP device. The circular and C-serpentine design (as discussed in Chapter 3) is used for fabrication of gold electrode based DEP device. We successfully fabricated both the electrode designs on Si substrate. However, the circular microelectrodes could not be packaged because of some fabrication issues. The details of fabrication steps, mask design and sealing issues that surfaced during device packaging of circular electrodes are discussed in detail in Appendix-II. So, the device packaging and testing could only be performed in C-serpentine structure. Therefore, the fabrication process of only C-serpentine structure will be discussed in this chapter under sub-section 4.2.2. The details of sample preparation are also discussed in the sub-section 4.2.3.2

4.2.1 Mask Design

Gold electrode based DEP device includes a two mask process which is illustrated in Figure 4.1. Mask#1 is gold electrode mask which is shown in Figure 4.1(a) whereas Mask#2 is the mask for microchannel which is shown in Figure 4.1(b). L-Edit Layout Editor tool is used for designing of the mask layout. In the mask layout the width of the electrode and microchannel is 150 nm and 1mm respectively.

4.2.2 Fabrication Details

The C-Serpentine design based DEP device with gold as electrode material has been fabricated in this chapter. The fabrication includes two substrates namely silicon as bottom substrate and glass which is the top substrate. The silicon substrate includes the gold electrode and SU-8 microchannel, whereas the glass substrate includes the inlet/outlet for the microchannel. SU-8 polymer is used as structural layer as well as an adhesive layer for the DEP device. The schematic view of fabrication flow for DEP

device is shown in Figure 4.2. The detailed fabrication process is discussed in the following section:

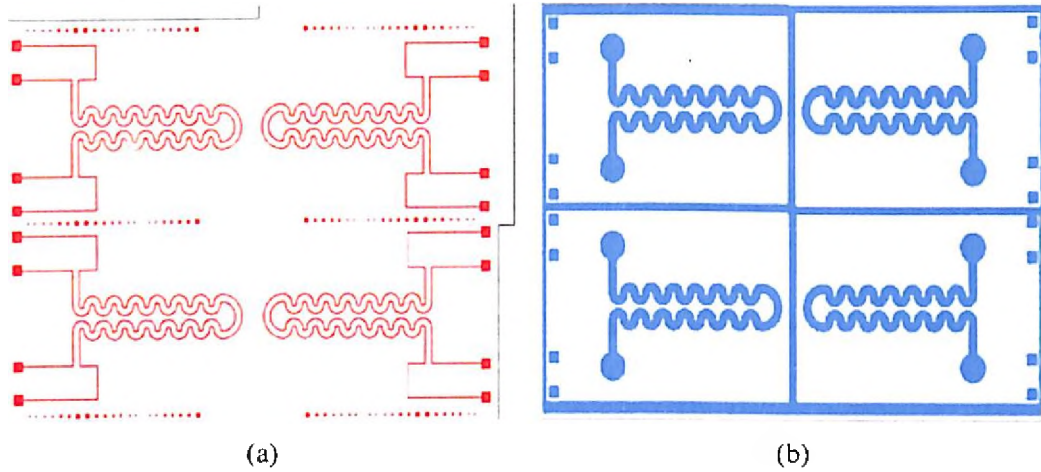


**Figure 4.1: Mask layout of DEP device (a) Mask#1 electrode mask
(b) Mask#2 microchannel mask**

4.2.2.1 Cleaning and substrate preparation

First we have taken single side polished P-type silicon (100mm or 4inch) wafers with a resistivity of (3-10) ohms-cm, and orientation, <100> in all experiments for fabrication of gold electrode based DEP device. In addition, another set of glass wafers has been used for closing of the microchannel. Though the wafer is fresh, they still are not clean, so before starting fabrication process we have cleaned the wafer properly. A two-step process for cleaning is carried out which includes (a) DI water rinsing and followed by (b) Piranha cleaning.

DI Water rinsing: Wafer is rinsed with DI water for 10 min. A large fraction of ionic impurities present on the wafer surface is removed and wafer becomes free from all ionic impurities except HO^+ and OH^- .

Piranha cleaning: After DI water rinsing; the wafers are cleaned using piranha solution. Piranha solution contains $\text{H}_2\text{SO}_4:\text{H}_2\text{O}_2$ in the ratio of 3:1 by volume. The wafers are dipped in the solution for 15 min. Organic impurities and alkali ions are removed due to strong oxidizing property of the solution. The surface of silicon is passivated with (OH) groups making it hydrophilic. After piranha cleaning the wafers are dipped in dilute HF (HF: DI water: 1:50) at room temperature to remove the native oxide. This is followed by N_2 blow drying. The completion of etching of the native oxide layer is confirmed by

4.2.2.2 Thermal oxidation

The very first step for fabrication of any MEMS device is thermal oxide growth. About 1 μm thick oxide is grown on silicon substrate. After the HF dip, the sample were loaded in the oxidation furnace for oxidation at 1000°C with flow of nitrogen. Initial dry oxidation was performed for 15 min in order to realize the better contact on the interface. Next, wet thermal oxidation was performed at same temperature for 3 hrs. Finally, dry oxidation was performed for 15 min and the wafers were unloaded at 500°C in nitrogen flow. The grown oxide thickness of the samples was measured using the surface Profilometer and was found to be of $\approx 1.01 \mu\text{m}$ thickness as schematically shown in Figure 4.2(a1).

4.2.2.3 Gold deposition

After thermal oxidation, the wafers were loaded for gold deposition. Thermal evaporation technique is used for deposition. The deposition was carried out with deposition rate of 0.2 nm/s. The layer thickness was controlled by the deposition time and by calibrated quartz crystal detector. In order to improve, the adhesion of the gold layer a thin layer of 20 nm chrome is deposited on the silicon substrate first. Followed by chrome deposition, a 200 nm gold layer was deposited as shown in Figure 4.2(a2).

4.2.2.4 Lithography

After gold deposition, the patterning of the gold layer is carried out. The wafer is coated with photoresist by spin coating technique. Before coating, the wafer is dehydrated and primed using hexamethyldisilazane (HMDS) primer at 150°C to remove the moisture and for good adhesion of resist for 30 min. After priming, the wafer is spin coated with positive photoresist AZ5214E at 4000 rpm for 40 sec to achieve the desired thickness of 1.2 μm . After coating, the wafers are heated using hotplate at 110°C for 1min. This process is known as prebake. After prebake, the wafer is exposed using mask aligner (EVG) at 110 mJ/cm^2 with UV light to get the desired pattern. The electrode pattern is transferred onto the substrate using an opaque mask#1, whose layout is shown in Figure 4.1(a) Immediately, after the exposure the wafer is developed for 60 sec using standards developer (AZ726MIF) and rinsed with DI water.

Further, the wafer is heated at 120°C for 4 min on the hotplate to remove the moisture. This process is known as hard bake. The parameters used for patterning are given below:

Spin speed:	4000 rpm
Prebake:	110°C for 1min
Exposure:	110 mJ/cm ²
Development:	30 sec+30 sec
Hard bake:	120°C for 4 min

The schematic view of gold patterning is shown in Figure 4.2 (a2) whereas a microscopic view of patterned gold structure after developing is illustrated in Figure 4.3(a).

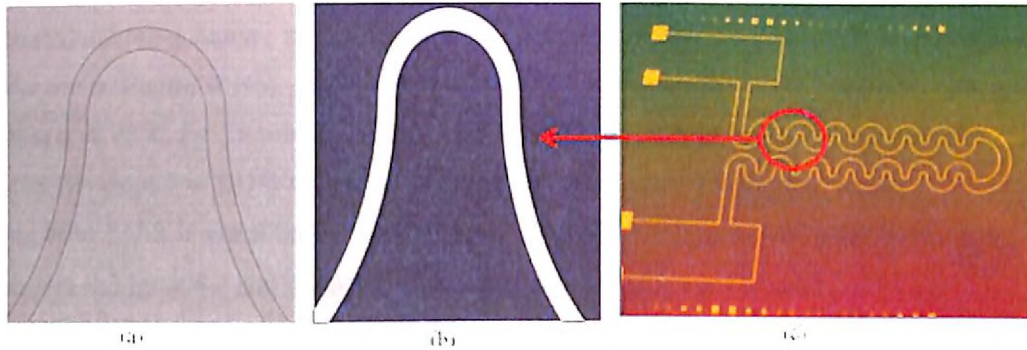


Figure 4.3: Gold Electrode (a) Pattern after developing, (b) Pattern after gold etching, (c) Complete fabricated gold electrode

4.2.2.5 Cr/Au etching

After patterning the Cr/Au, etching is carried out using wet etch process. The aqua regia solution is prepared for gold etching. The solution in ratio of HNO₃:HCl in 1:3 ratio is prepared. Then the wafer is dipped in prepared solution for 40 sec to etch the unpatterned gold layer.

Further, the chrome etchant is prepared to etch the unpatterned chrome. Typically chrome etchant are mixtures of perchloric acid (HClO₄), and ceric ammonium nitrate (CAN) powder. Approx 10 ml perchloric acid and 50 gm CAN powder is mixed with 150 ml DI water. The pattern glass sample is dipped into chrome etchant for 10 sec to etch the 20 nm layer thickness. After the etching, the sample is rinsed with DI water and dried with nitrogen as illustrated in schematic view in Figure 4.2(a3). The microscopic view of wafer after Cr/Au etching is illustrated in Figure 4.3(b). Device with complete electrode structure after the completion of developing and Cr/Au etching is shown in Figure 4.3(c)

4.2.2.6 SU-8 Coating and microchannel patterning

After gold electrode, the SU-8 polymer is used for fabrication of the micro channel for DEP device. SU-8 is the material of choice for Bio-MEMS and microfluidics devices and requires simple processing, less fabrication time. SU-8 (Microchem, 2035) is used for the experimental work. The SU-8 photoresist was spin coated at 500 rpm for 5 sec followed by 4000 rpm for 30 sec to achieve a thickness ($\sim 30\text{-}32\ \mu\text{m}$). The coated substrate was then soft baked on a hotplate at 70°C for 15 min and then ramped up to 90°C for 20 min. The substrate was then allowed to cool down to 25°C temperature. After baking, the SU-8 coated silicon substrate was exposed to UV light for 40 sec using an opaque mask#2, as shown is Figure 4.1(b). Immediately after UV exposure, the SU-8 substrate was post baked at 70°C for 15 min and ramped up to 90°C for 20 min. Finally, exposed substrate was developed in SU-8 developer (Microchem developer) for 60 sec to make sure that exposed SU-8 is cross linked appropriately. The SU-8 microchannel after developing is shown in Figure 4.4 and discussed in schematic view in Figure 4.2 (a4).

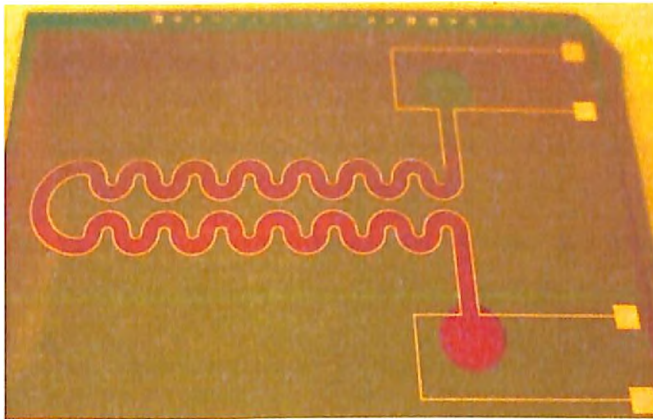


Figure 4.4: SU-8 pattern DEP device

4.2.2.7 Channel closing with glass substrate

A pyrex glass substrate of thickness $500\mu\text{m}\pm 25\mu\text{m}$ is used for closing of the microchannel. The glass substrate is patterned to make an inlet/outlet for the fluidic flow. A chrome layer of 200 nm thickness is deposited using the E-beam evaporation technique as shown in schematic view of Figure 4.2 (b2).

After chrome deposition, the wafer is dehydrated and primed using HMDS primer at 150°C to remove the moisture and for good adhesion of resist for 30 min. After priming,

the wafer is spin coated with positive photoresist AZ 5214E at 4000 rpm for 40 sec to achieve the desired thickness of 1.2 μm . After coating, the wafers are prebaked on hotplate at 110 °C for 1min. After prebake, the wafer is exposed using mask aligner (EVG) at 110mJ/cm² with UV light to get the desired pattern. Immediately, after the exposure the wafer is developed for 60 sec using standards developer (AZ726MIF) and then rinsed with DI water.

Further, the wafer is hard baked at 120 °C for 4 min on hotplate to remove the moisture. The parameters used for patterning are given below:

Spin speed:	4000 rpm
Prebake:	110°C for 1min
Exposure:	110mJ/cm ²
Development:	30 sec+30sec
Hard bake:	120°C for 4 min

4.2.2.8 Chrome patterning

After patterning of the glass with desired pattern, the chrome etchant is prepared to etch the unpattern chrome. Typically chrome etchant are mixtures of perchloric acid (HClO₄), and ceric ammonium nitrate (CAN) powder is used for etching (as discussed in Section 4.2.2.5). The pattern glass sample is dipped into chrome etchant for 100 sec to etch the 200 nm layer thickness. After the etching, the sample is rinsed with DI water and dried with nitrogen as illustrated in schematic view in Figure 4.2(b3). The glass substrate after chrome patterning is illustrated in Figure 4.5.

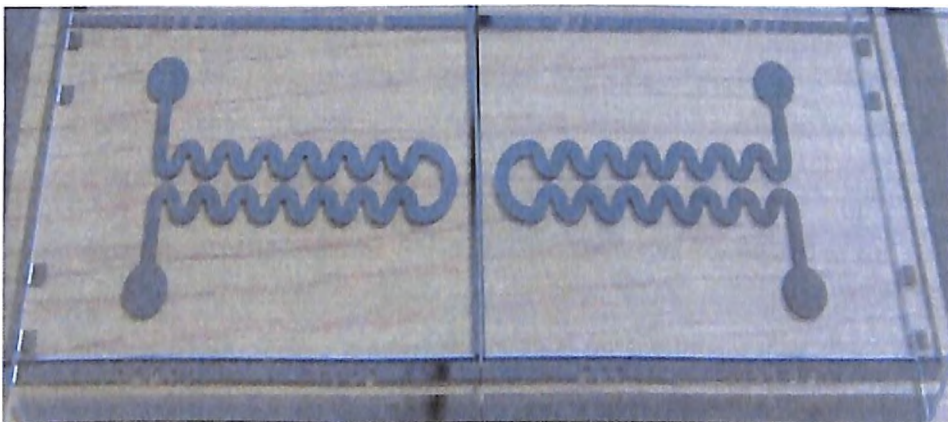


Figure 4.5: Chrome pattern on glass substrate

4.2.2.9 Glass dicing and drilling

After patterning of the chrome layer, the glass substrate is diced and drilled. From the chrome pattern on the glass substrate, the drilling of inlet and outlet holes can be done at precise location. An ultrasonic drilling is used for making inlet/outlet of the microchannel. The drilling of full glass wafer is really challenging because it is done by manually holding the substrate against the drill bit. And, it is observed during the drilling process, that the full glass wafer got damaged as the drilling caused cracks followed by the breakage of glass substrate. So, next we first diced the glass wafer along given scribe line and then used it for ultrasonic drilling. A 38×28 mm die size was diced and used for ultrasonic drilling, as holding and drilling a small glass wafer against the drill might result in a crack free drilling. After many trials, we managed to drill holes on the glass substrate safely.

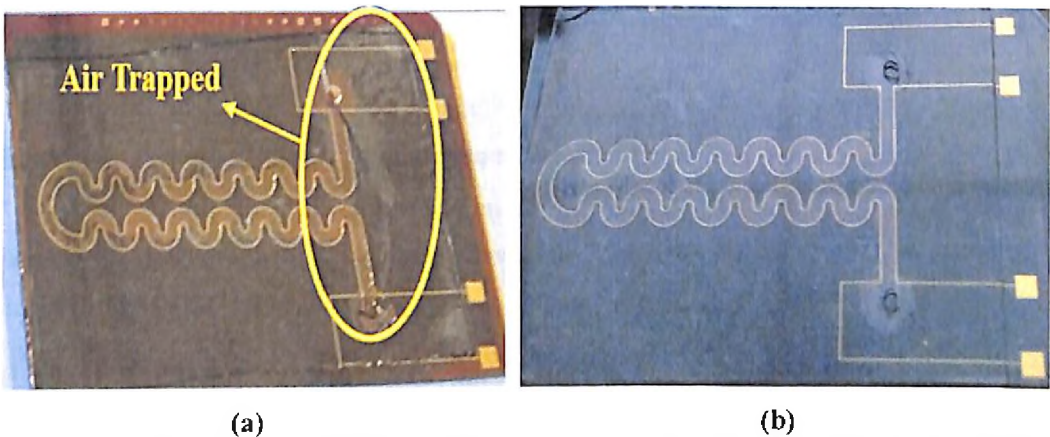
An ultrasonic drilling is a subtraction manufacturing process that removes material from the surface of a part through high frequency (≈ 20 kHz) of a tool against the material surface in the presence of fine abrasive particles. The fine abrasive grains of carborundum powder are mixed with water to form slurry that is distributed across the part and tip of the tool. A 1mm diameter tip is used for making the hole in the glass substrate. After, drilling, the glass substrate is cleaned using the piranha solution for further use.

4.2.2.10 Bonding of both substrates

The silicon substrate with SU-8 microchannel and glass substrate with drilled input and output ports are now ready for bonding. Adhesive bonding technique is used to make a perfect bond between glass and silicon substrate. A thin layer of SU-8 2002 is used as an adhesive for the bonding the two substrates. SU-8 plays the role of an adhesive layer as well as structural layer. The bonding with SU-8 could be conducted without any pressurizing equipment.

The drilled glass is spin coated with SU-8 2002 at 4000 rpm for 40 sec to form a thin adhesive layer of 2 μm thickness. Initial trials were done by coating the SU-8 first on the glass substrate, followed by its prebake at 70°C for 2 min and 90°C for 2 min and then cooled down to room temperature. Then the SU-8 coated glass substrate was brought in contact with silicon substrate to make a perfect bond. But, after the contact

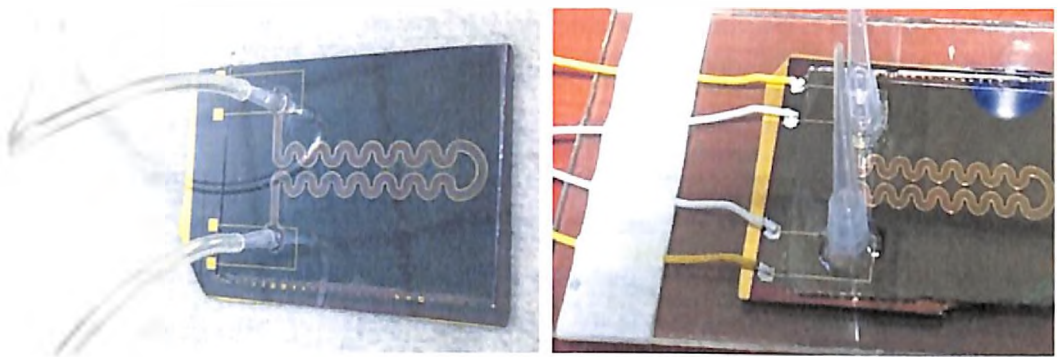
and manually pressing, the air-bubble has been observed in the bonded interface which is shown in Figure 4.6(a). To reduce the void formation and air bubble trapping between the bonded substrate, both the substrates were aligned and pressed manually from one side to another side. In addition to this, the prebake step was done after bonding both the substrates. This helped in achieving a bubble free bonding between the two substrates. So, the samples were heated at 70°C for 30 min on hotplate and followed by the exposure through glass in order to cure SU-8 and reduce its reflow. After exposure, the samples were post bake at 90°C is carried out for 30 min. A number of experiments were carried out to get the leakage proof i.e. void free bonding as shown in Figure 4.6(b) and the optimized best parameter is used for fabrication of the DEP devices.



(a) (b)
Figure 4.6: Glass bond DEP device (a) Air trapping in the channel (b) Glass bonded sample with no air traps

4.2.2.11 Wire bonding

After fabrication of the DEP microchannel, the devices were wire bonded. Manual wire bonding is carried out using the silver epoxy paste. The silver epoxy paste is mixed with curing agent in ratio of 1:1 and wire is bonded with this silver paste. After the wire bonding the sample is kept for the heating at 100°C in oven for 40 min to make perfect contact between the contact pad and wire as shown in Figure 4.7. Device with inlet and outlet tubes is shown in Figure 4.7 (a) and a wire bonded device is shown in Figure 4.7(b).



(a) With inlet/outlet fabrication
 (b) Wire bonded fabricated device

**Figure 4.7: Fabricated DEP device (a) With inlet/outlet fabrication
 (b) Wire bonded fabricated device**

4.2.3 Yeast Cells

4.2.3.1 The science of yeast cells

Yeasts are single celled eukaryotic organisms that are classified as members of fungus kingdom. The word “yeast” comes from the Indo-European roots meaning “boil”, “foam” or “bubble”. In 1680, Antony Van Leeuwenhoek first microscopically observed yeast cells, however in 1837 Theodor Schwann recognized them as fungi. The scientific name for the yeast is *Saccharomyces Cerevisiae* or “sugar eating fungus”.

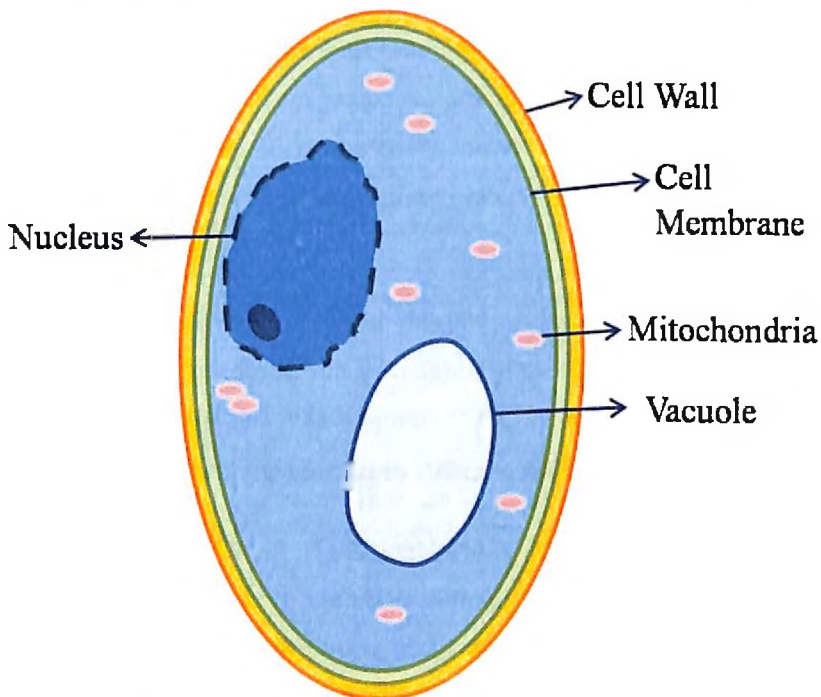


Figure 4.8: Diagrammatic representation of *Saccharomyces Cerevisiae*

The size of yeast cells may vary significantly, depending on species and environment, typically measuring 3-4 μ m in diameter, although some yeast can grow to 40 μ m in size. Yeast cells appear to be glassy or translucent in appearance but in colonies they appear white or cream colored. Diagrammatic representation of yeast cell is shown in Figure 4.8. A yeast cell consists of an outer cell wall followed by cell membrane or plasma membrane and nucleus. The nucleus contains the genetic code while the cell membrane allows gases and water to pass in and out of cell while controlling the passage of other chemicals, and the cell wall provides rigidity to the cell to maintain cell shape.

The shapes of the yeast cells may vary from circular, spherical, oval, elliptical, rectangular, elongated to dumb bell shaped. An important feature of these yeasts that makes them such useful organisms for studying biological processes in humans, is that their cells, like ours, have a nucleus containing DNA packaged into chromosomes. Most metabolic and cellular pathways thought to occur in humans, can be studied in yeast. Moreover, yeast chromosomes share a number of important features with human chromosomes.

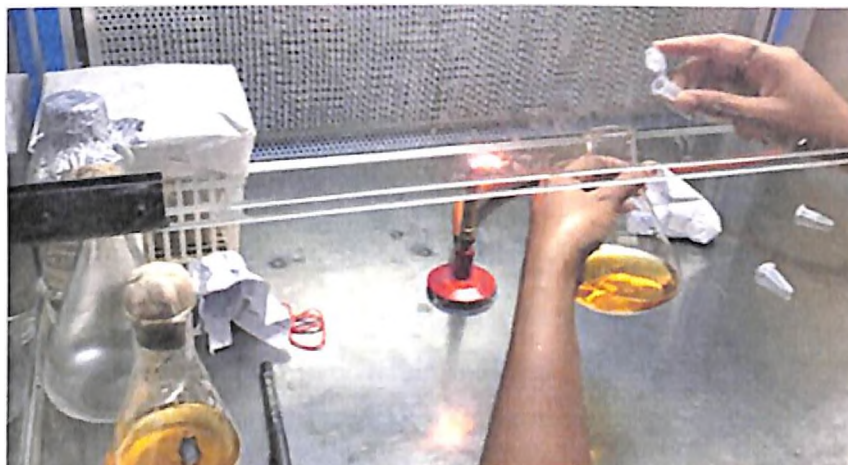
4.2.3.2 Sample preparation

The testing of fabricated DEP device is carried out using yeast cells. Two type of yeast cells (*Saccharomyces cerevisiae*) viable (live) and non-viable (dead) were prepared for the experimental work. Dry active yeast was procured from a local bakery shop. Yeast cells were chosen because it is easily available and also not very sensitive to contamination as other eukaryotic cell culture systems, as yeast in their own media will outgrow most other things.

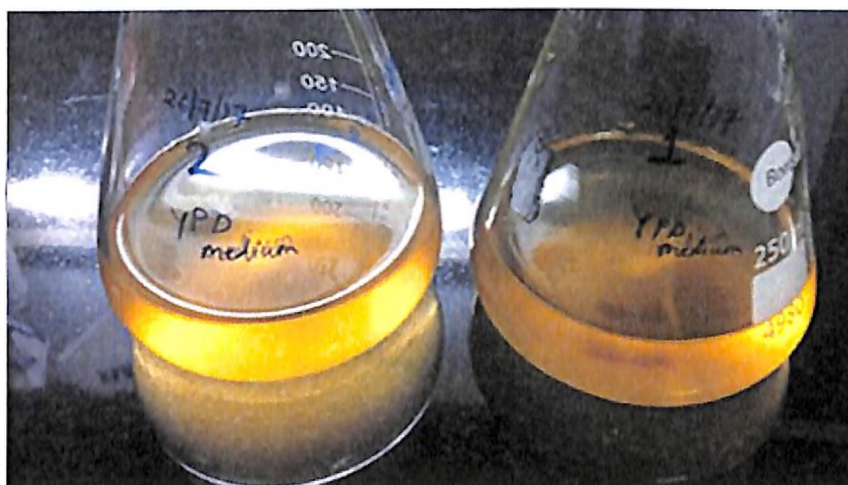
For making the yeast cells grow, first the nutrient media was prepared. An YPD (Yeast extract, Peptone and Dextrose) media is commonly used media for growth of the yeast cells. The YPD media contains Yeast Extract 0.3%, Peptone 1% and Dextrose 2%. All the reagents are weighed and then mixed in 100 ml autoclaved distilled (DI) water.

Therefore for preparing 200 ml of nutrient media, 0.6 : 2 : 4gm each of the nutrient ingredients were measured and added to 200 ml of autoclaved distilled water and were mixed thoroughly. The nutrient media was then autoclaved at 120°C for 15-20 min, this helps in obtaining a completely sterile media as autoclaving kills all forms of micro-organisms including spores. Now, 200 ml of this nutrient medium was then

divided into two equal parts of 100 ml each and to this 1 gm of dry active yeast granules were added in sterile atmosphere (in laminar air flow) as shown in Figure 4.9(a) and were again mixed thoroughly until a clear solution is obtained as shown in Figure 4.9(b). Followed by thorough mixing of all the ingredients, yeast was allowed to grow overnight in an incubator at 30°C with continuous stirring at 150 rpm as shown in Figure 4.10.



(a)



(b)

**Figure 4.9: Cell preparation (a) Adding 1 gm Yeast in to YPD nutrient media
(b) Media after addition of yeast**

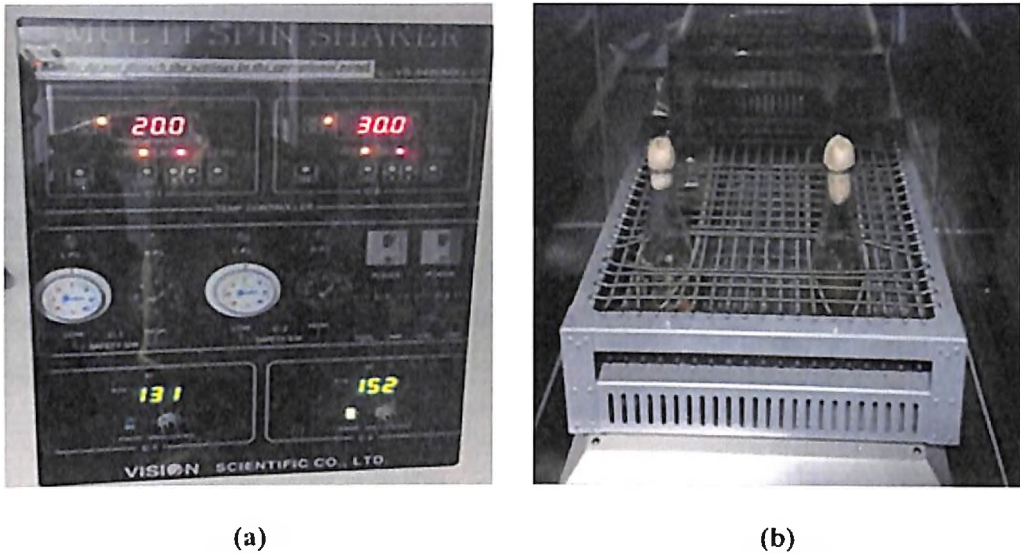


Figure 4.10: Incubation of yeast cells at 30°C for overnight

The culture was taken out from the incubator after 14 hrs, and it was observed that the media which was clear initially got turbid indicating that the growth of yeast has occurred in the media and the cells were seen settled at the bottom of the flask. Now the culture with grown yeast cell was poured into falcon tubes and centrifuged (REMI. Compufuge) at 10,000 rpm at 4°C for 15 min so as to pallet down the yeast cells as shown in Figure 4.11(b). After palleting down the yeast cells the supernatant was discarded and the cells were washed in 280 mM Mannitol.

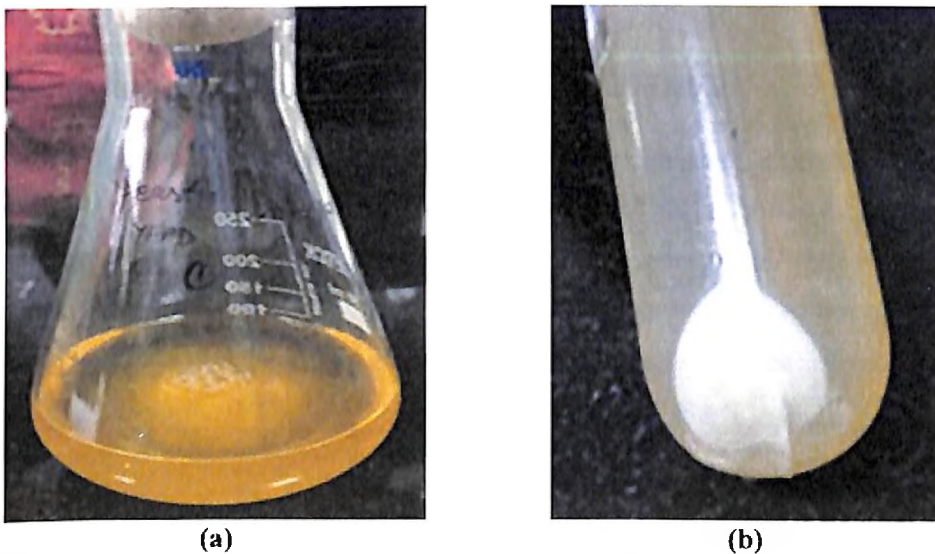


Figure 4.11: (a) Turbid media, with yeast cells at bottom, (b) Pallet of yeast cells in 280 mM mannitol

Non viable yeast cells were prepared by heat treating the yeast cells in water-bath at 80°C for 30 min shown in Figure 4.12(a). The dead cells were then stained using methylene blue dye (0.1%). Methylene blue gets oxidized in live cells but remains unchanged in dead cells therefore dead cells tends to take up blue stain. After adding dye, for 2 min the dye was allowed to react with the cells. This was followed by washing the cells four times with mannitol to remove any excess of stain. After palleting down both viable and non viable cells, they were suspended in 25 ml of 280 mM mannitol as shown in Figure 4.12(b).

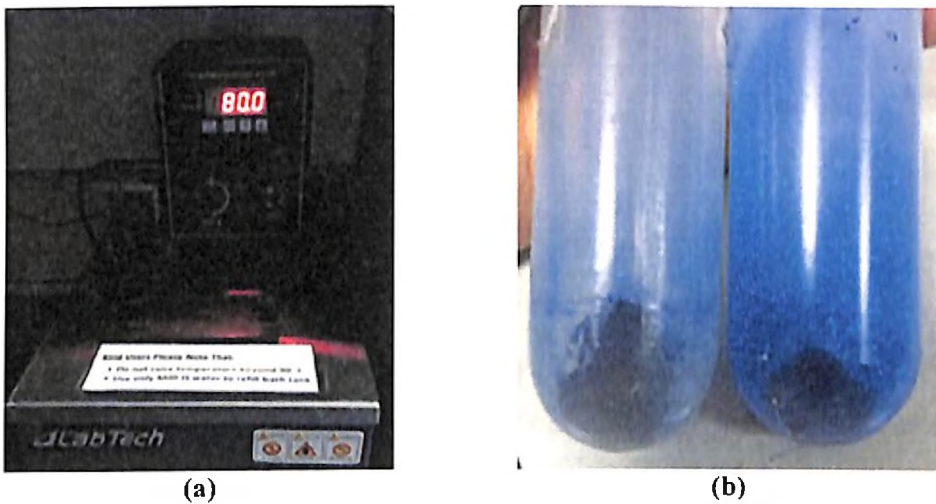


Figure 4.12: (a) Heat treatment to yeast cells and (b) Dead cells stained with methylene blue

4.3 Testing and Characterization of the DEP Device

The DEP device testing was carried out using a customized setup as shown in Figure 4.13. The setup includes a microscope (Motic SMZ168 series, stereomicroscope), syringe pump (Hygeia Medical Devices) and a signal generator (Aplab Sine/Square wave generator 1MHz, 2014D). The testing of the devices was carried out at different frequency ranges. Syringe pump was used to ensure continuous flow of cell solution which also prevents cells from settling at the bottom of the channel.

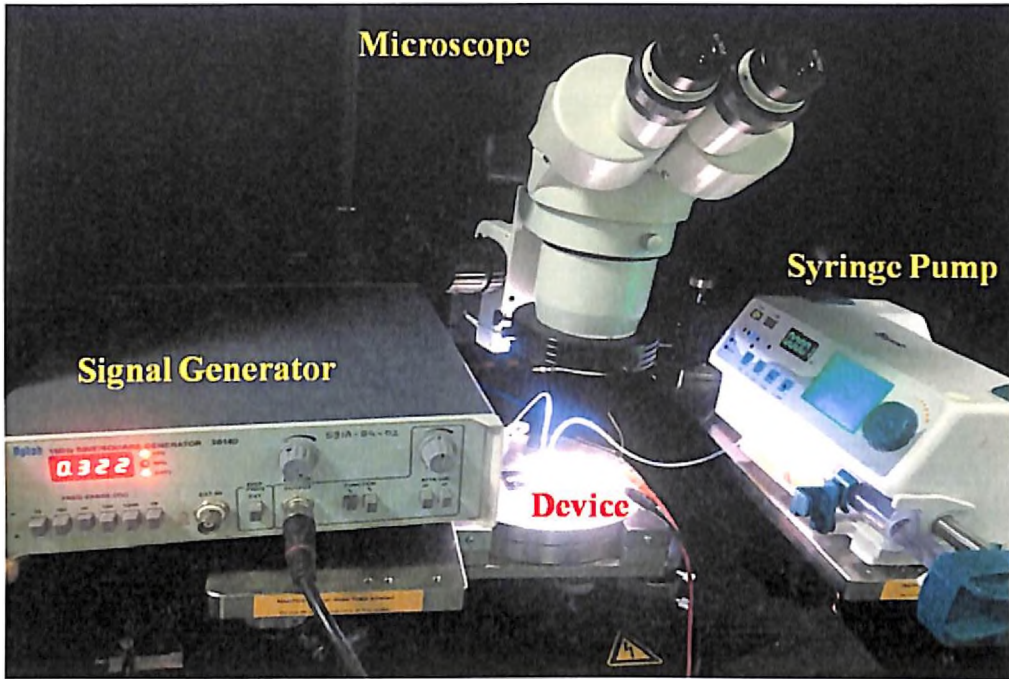


Figure 4.13: Experimental set-up

In addition to device testing, the efficiency of the device was also calculated. For calculating the device efficiency, number of cells per ml was counted using Naubauer improved hemocytometer. The hemocytometer was originally invented by Louis-Charles Malassez to count blood cells. But later on, biologists and experimental doctors discovered that it could be applied to other areas, to count yeast, sperm, and other types of human and animal cells.

The current hemocytometer is composed of nine equally sized bigger squares of 1mm^2 each. The central one is different from the other ones because it is divided into 25 smaller squares, while the ones in the corners are divided into 16 smaller squares. The rest of the squares are not used. In addition, the small 25 squares inside the central square are subdivided into 16 even smaller squares each as shown in Figure 4.14 (b) and Figure 4.14 (c). This allows counting very tiny cells with the same precision level as larger ones (but with a higher magnification).

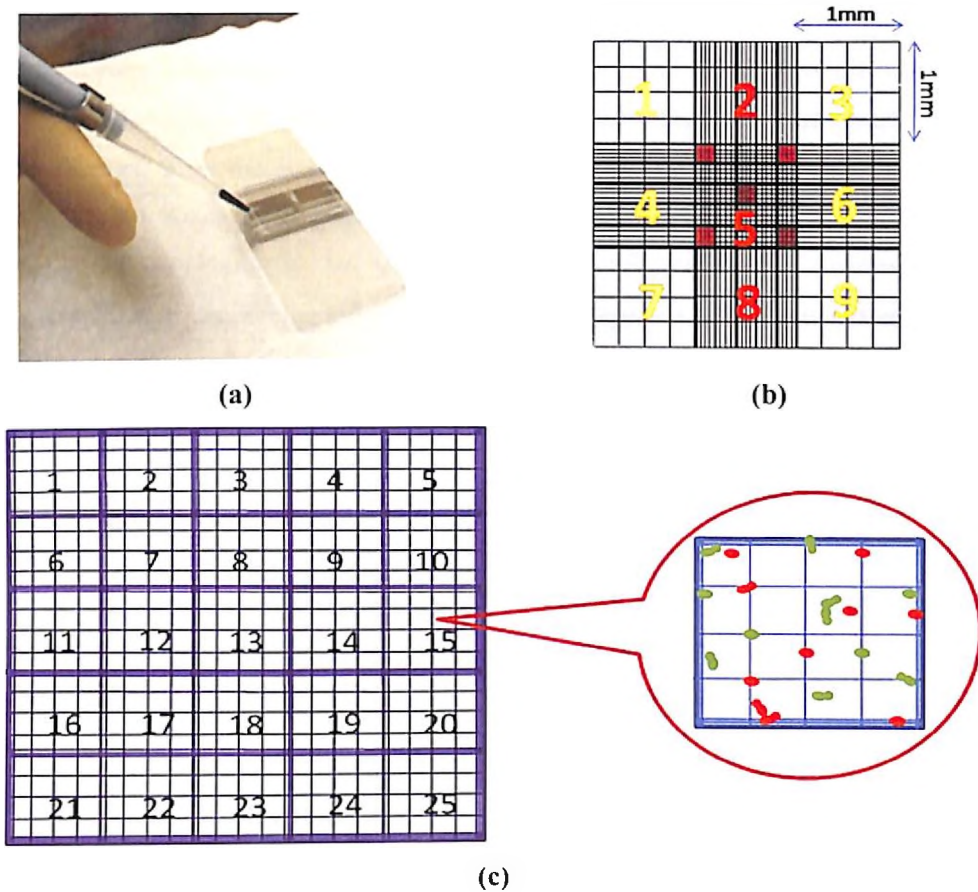


Figure 4.14: Hemocytometer (a) Sample loading (b) Counting chambers (c) Zoomed view of centre square

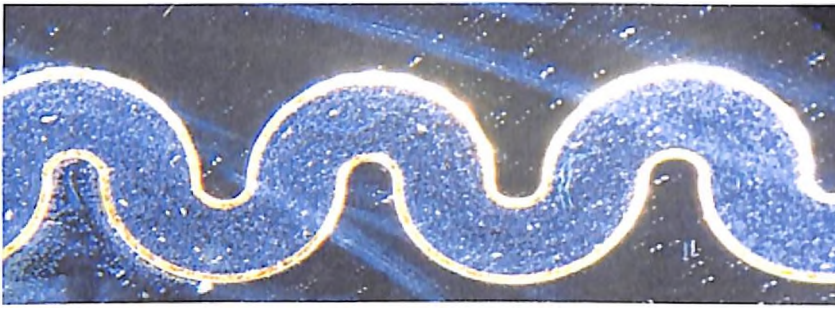
4.4 Results and Discussion

The gold electrodes based DEP device using C-Serpentine design has been tested for trapping of dead and live cells. The trapping was carried out using an AC signal of 10Vp-p and the frequency was varied from 100 kHz to 1 MHz. After sample preparation, conductivity of each of the solution was measured by carefully maintaining them at room temperature (25°C). The conductivity was measured using (EUTECH Instruments, ph/conductivity/TDS/temp measurement). The conductivity of live and dead cells was found to be 70 $\mu\text{S}/\text{cm}$ and 110 $\mu\text{S}/\text{cm}$ respectively. The conductivity was then used to calculate the massotti factor. The massotti factor was observed from the graph (discussed in Section 3.5) is -0.17 for dead cells with conductivity 70 $\mu\text{S}/\text{cm}$ and -0.37 for live cells with conductivity 110 $\mu\text{S}/\text{cm}$ respectively. Massotti factor graph shows the frequency range over which the two cell types will experience n-DEP and p-DEP.

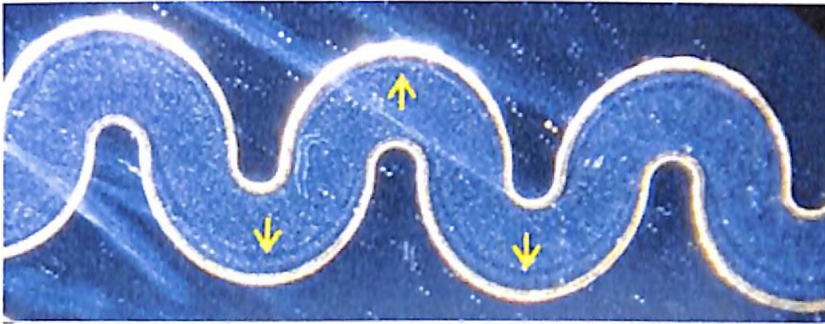
Three sets of experiments were carried out for separation of the cells. In the first set, dead cells were injected into the microchannel, in the second set of experiment live cells were injected, while in the third set, a mixture of both live and dead cells were injected in the channel. This was done in order to observe the trapping frequency of both the individual cells. Once the trapping frequency of each of the cells is known, the third set of experiment was performed by mixing of both dead and live cells. In addition to these three experiments, the device efficiency was also carried out using hemocytometer. For each set of experiments, four set of trials (R1-R4) were performed.

4.4.1 Dead Cells

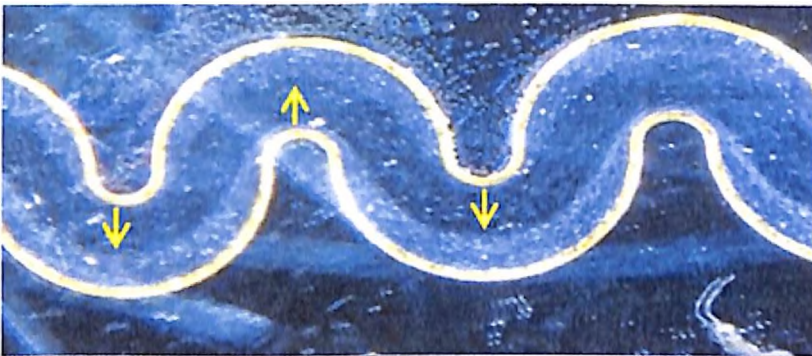
Freshly prepared dead cell solution with cell concentration of 2×10^7 cells/ml was taken and from it 5 ml solution was drawn for performing the experiments. The solution was loaded in syringe pump and injected into the channel with a constant flow rate of 0.5 ml/hr. From Figure 4.15 (a) it can be observed that the cells filled the entire channel. Now, an AC signal of 10 Vp-p was used and frequency was ramped up from 100 kHz with the step size of 50 kHz. It was observed that at 300 kHz the cells started to stream itself along the channel periphery as shown in Figure 4.15(b). This indicates that the dead cells started experiencing some DEP force and therefore got attracted towards the electrodes. The Figure 4.15 (b) below shows that the cell stream divides and the stream of cells is seen flowing along the two electrode peripheries. The cell streaming continued, but there was no registration of cells seen at the periphery even after 5 min. Further, we have increased the frequency upto 1 MHz but there no trapping was observed. The possible reason of this cell not getting trapped could be that the concentration of cells taken was high for the device to trap the cells. Therefore in this case, either of the two remedies can be employed. Either the voltage of the AC signal can be increased or the cell concentration can be reduced or diluted. We first increased the voltage to 15 and then to 20 V and varied the frequency from 1 kHz to 1 MHz, but no cell trapping was observed, instead now a wider stream of dead cells could be seen flowing along the periphery as shown in Figure 4.15 (c). Therefore, now the cell solution was diluted to 91×10^6 cells/ml by adding more mannitol solution to it.



(a) Channel filled with cells



(b) Streaming of cells



(c) Wider stream of cells



(d) Cell registration at electrode

Figure 4.15: Streaming and trapping of the dead cells in micro-channel

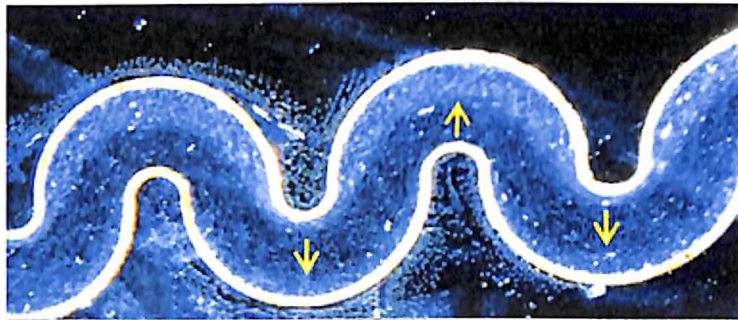
After adding mannitol the cells were again injected in the channel, with a flow rate of 0.5 ml/hr and with voltage of 10V. It was observed that now the clusters of cells were seen to be trapped along the larger periphery as shown in Figure 4.15(d).

4.4.2 Live Cell

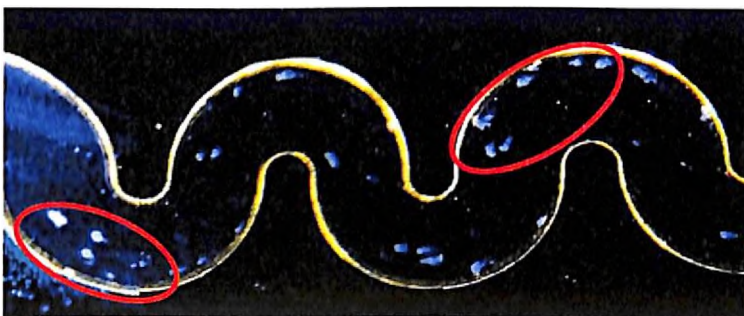
After performing the test with dead cells, the fluidic channel was cleaned thoroughly by flushing it with DI water for 20 min to ensure that no dead cell residue is left in the channel. Freshly prepared live cell solution with cell concentration of 32.3×10^6 cells/ml was prepared and from it 5 ml solution was drawn for performing the experiments.



(a) Channel filled with live cells



(b) Streaming of cells



(c) Cell registration at Electrode

Figure 4.16: Live cells trapping in microchannel

The solution was loaded in syringe pump and injected into channel with a constant flow rate of 0.5 ml/hr. From Figure 4.16 (a) it can be observed that the cells filled the entire channel. Now, the frequency of an AC signal was slowly ramped from 100 kHz onwards with step size of 50 kHz, with voltage 10 Vp-p and flow rate of 0.5 ml/hr. It was observed that at around 700 kHz the cells started to stream itself along the channel periphery as shown in Figure 4.16 (b) and then after few seconds, the cells started to get trap along the larger periphery and formed cell clusters as shown in Figure 4.16 (c). This indicates that the live cells experienced negative dielectrophoretic force and were thus attracted towards the larger periphery.

4.4.3 Mixture of Live and Dead Cell

The third set of experiment was carried out using mixture of dead and live cells solution. To prepare cell mixture, 10 ml each of dead and live cells were thoroughly mixed together using vortex. The conductivity of the solution was set at 100 $\mu\text{S}/\text{cm}$ at 25°C. Figure 4.17 compares the predicted massotti factors of the two types of cells as a function of AC field frequency (from 1 kHz to 1 MHz). Before performing trapping experiments, the microchannel was cleaned by flushing DI water for 10 min using syringe pump. After flushing, the homogeneous solution of dead and live cells was injected into the microchannel.

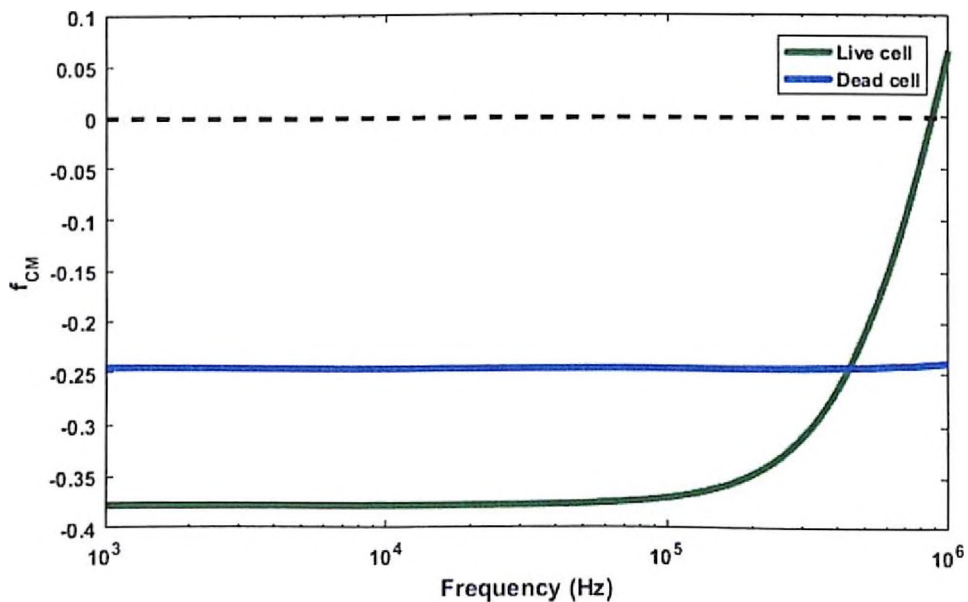


Figure 4.17: Clausius-Mossotti plot of live (green) and dead (blue line) yeast cells

In order to verify the response of each cell, we applied an AC field and increased the frequency starting from 100 kHz. at around 350 kHz we observed that cells started to get trap at the periphery. At 350 kHz we collected 1ml of output solution to perform the quantitative analysis of both dead and live cells. Later, the applied frequency was increased and cell trapping was again observed at 700 kHz. At 700 kHz, we again collected 1ml of the output solution to observe the dead and live cells present in per ml of solution. For comparing the results, the image shots were taken at the same portion of channel for both dead and live cells. In Figure 4.18 (a) when 350 kHz signal was applied, dead cells can be seen trapped at the bottom boundary of the channel while the upper channel boundary has very less number of cells. While in Figure 4.18 (b), when the signal was switched to 700 kHz, live cells were seen getting trapped on almost all the larger periphery of the channel. This clearly shows the response of each cell is specific to the frequency applied.

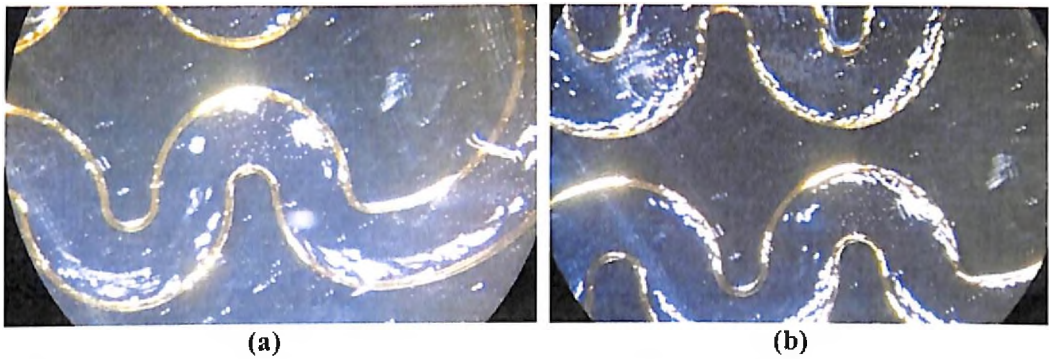


Figure 4.18: (a) Trapping of dead cells at 350 kHz, (b) Trapping of live cells at 700 kHz

4.5 Device Efficiency

To calculate the efficiency of the device, number of cells injected in the channel and the number of cells that came out from the channel were counted using hemocytometer. The design of hemocytometer and the counting chambers has been discussed in Section 4.3. Yeast cells have an average size of 5-10 μ m. In comparison to the size of a hemocytometer square (1mm), they are 100-200 times smaller. So, in this case we count the smaller squares (i.e., the ones in the central square, which measure 25 \times 0.2 mm), the squares that are marked red in Figure 4.14 (b). They also have helper lines that divide each of them into 16 even smaller squares. Cell culture with dead and live yeast cells respectively was taken and mixed thoroughly in a vortex to ensure that the cells are distributed homogeneously in the solution. The procedure for counting of the cells is detailed below:

4.5.1 Adding Methylene Blue Dye (MB dye)

Since the dead cells were already stained with methylene blue 0.1%, therefore they can be pipetted in the hemocytometer without any further treatment. Whereas the live cells are required to be mixed with MB dye first and then can be used for cell counting. A dye (i.e MB dye) will penetrate cells that are dead but will be excluded from live ones so both populations can be counted separately.

4.5.2 Dilution of Sample

The idea behind sample dilution is that we don't want to have too many cells in the small space where we are going to count (as the cells would overlap, and it will get difficult to count them), therefore we need to have enough (at least 100) for the count to be significant.

In case of dead cells, 10 μ l of cell suspension (from the cell stock) was diluted with 10 μ l of DI water and was mixed thoroughly. From this mixture 10 μ l solution was pipette onto the hemocytometer and we observed that there were many cell clusters seen under the microscope, which made counting difficult. So, further 10 μ l of DI water was again added, mixed and pipette onto the hemocytometer.

While in the case of live cells (from the cell stock), 10 μ l of live cell suspension was diluted with 0.2 μ l of 0.1% methylene blue and 10 μ l of DI water and mixed well. From this mixture 10 μ l of sample was pipette onto the hemocytometer and viewed under microscope, to find just enough countable cells.

4.5.3 Preparing the Hemocytometer

Before loading the sample in hemocytometer, the counting chambers and the cover slip was thoroughly cleaned with ethanol and soft tissue wipe. Now the cover slip was placed on the cytometer and 10 μ l sample solution was slowly pipetted along one edge of the cover slip.

4.5.4 Counting Yeast Cells in the Centre Square of Cytometer

Yeast cells were counted in the centre square of hemocytometer. Out of the 25 squares, 4 squares at the corners and 1 square in the centre are counted. Also, only the cells that are present on the side lines that are marked in red as shown in Figure 4.19 are counted while if the cells are present on the other two side lines they are neglected. The number

of cells/ml is calculated using Equation 4.1. The volume of small square is $4 \times 10^{-6} \text{ mm}^3$ which is used for calculations.

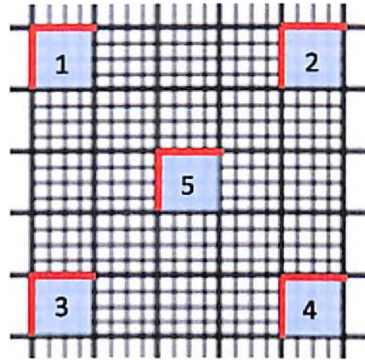


Figure 4.19: Hemocytometer: centre square

$$\text{No. of } \frac{\text{Cells}}{\text{ml}} = \frac{A_{SS} \times DF}{V_{SS}} \quad (4.1)$$

where, A_{SS} is average number of cells in small squares.

DF is dilution factor

V_{SS} is volume of small square.

4.5.4.1 Counting dead and live cells (input)

The number of dead and live cells in the stock solution per ml was calculated. The cell count in five squares of hemocytometer as shown in Figure 4.19 is used for calculation. The dead and live cell count is detailed in Table 4.1. The dilution factor of 4 and 2.02 is calculated for dead and live cells respectively. It was calculated from the Table 4.1 that the dead cell count is 91×10^6 cells/ml and the cell count for live cells is 32.3×10^6 cells/ml respectively. Also, the cells observed in 5 different squares in hemocytometer under microscope are shown in Figure 4.20.

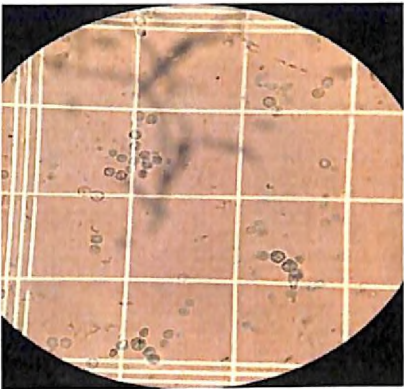
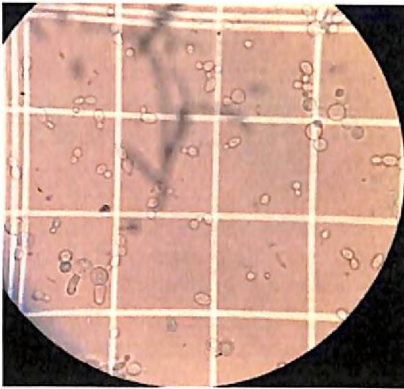
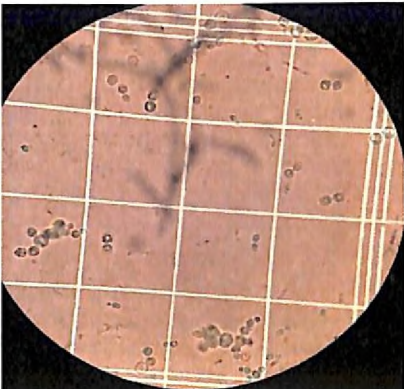
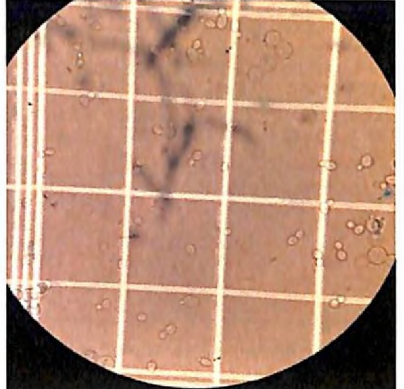
Table 4.1: Dead and live cells count (input)

Position (hemocytometer)	Dead cells	Live Cells
1	82	72
2	75	62
3	82	67

4	114	58
5	102	61
Total	455	320
Dilution factor	4.0	2.02
Average	91	64
No. of cells/ml	91×10^6	32.3×10^6

Dead cells/ml = $91 \times 4 / 4 \times 10^{-6} = 91 \times 10^6$ cells/ml

Live cells/ml = $64 \times 2.02 / 4 \times 10^{-6} = 32.3 \times 10^6$ cells/ml

Position (hemocytometer)	DEAD CELLS	LIVE CELLS
1		
Cell count	82	72
		
Cell count	75	62

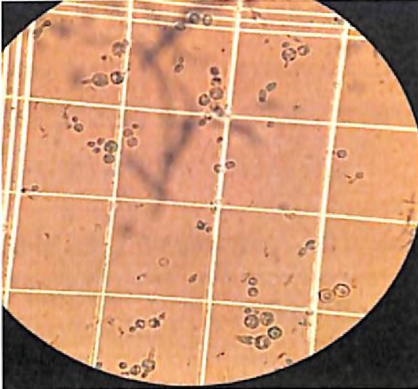
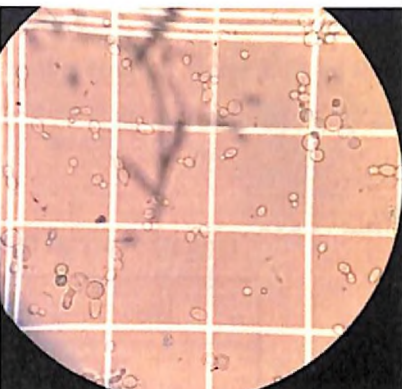
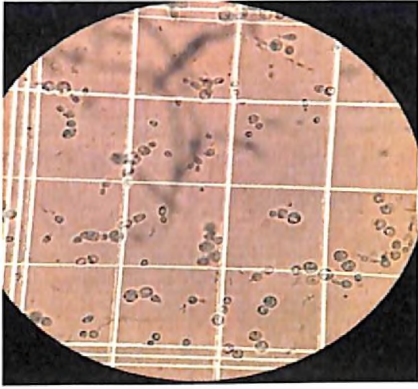
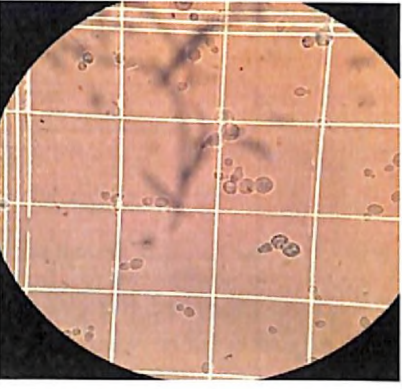
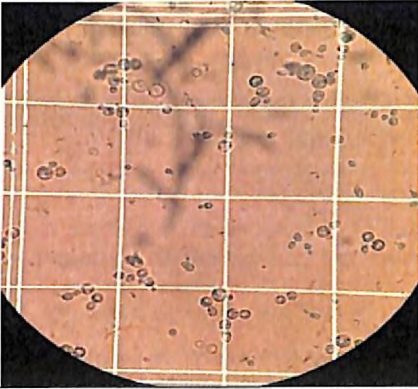
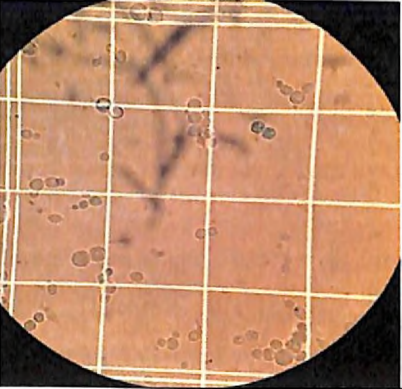
Position (hemocytometer)	DEAD CELLS	LIVE CELLS
3		
Cell count	82	67
4		
Cell count	114	58
5		
Cell count	102	61

Figure 4.20: Microscopic view of dead and live yeast cells at five different chambers in hemocytometer

4.5.4.2 Counting input cell density in cell mixture

From the 20 ml solution of prepared cell mixture, 10 μ l solution was pipette out and mixed twice with 10 μ l of DI water. This dilution helps in obtaining just enough cells that can be counted easily in hemocytometer. Therefore the dilution factor DF for this case is 4. Number of dead and live cells observed in five squares (position: 1-5) of hemocytometer is given in Table 4.2:

Table 4.2: Live and dead cell count in cell mixture (input)

Position (hemocytometer)	Live cells	Dead cells
1	52	46
2	43	21
3	32	35
4	39	41
5	28	42
Sum	194	185
Total	379	
Avg. no. of cells	75.8	
D.F	4	
Cell density	7.58×10^7 cells/ml	

4.5.4.3 Counting dead and live cells (output)

The efficiency of the device is calculated using Equation 4.2. The efficiency for both dead and live cell is calculated and discussed in this section.

$$\text{Efficiency} = \frac{\text{Input(cells/ml)} - \text{Output(cells/ml)}}{\text{Input(cells/ml)}} \times 100 \quad (4.2)$$

4.5.4.3.1 Dead cells

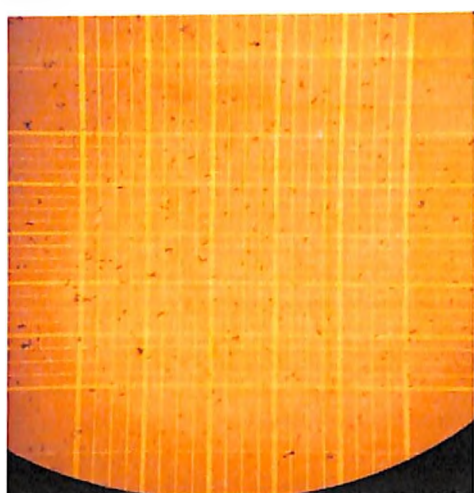
To ensure the repeatability of the device, the experiment was repeated four times. No dilution of output solution in case of dead cells is done. Therefore in this case, the dilution factor is taken to be 1. With the objective of determining the number of cells that came out untrapped, 1 ml of output solution was collected and counted for number of cells present. For each run, the no. of cells counted in five small squares in centre of

hemocytometer is detailed in Table 4.3. From Table 4.3, it is observed that the total cell out in each run is 32, 28, 43 and 40.

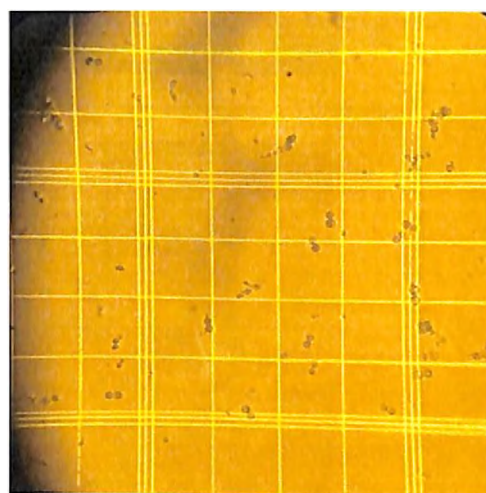
Table 4.3: Dead cells count (output)

Position	No. of cells counted			
	Run 1	Run 2	Run 3	Run 4
1	8	9	14	9
2	6	4	8	3
3	4	5	5	12
4	3	3	8	10
5	11	7	6	6
Total	32	28	43	40

Cells position for Run 1 is shown in Figure 4.22 in all the five squares. Figure 4.21 shows the 10X and 40X Microscopic view of the centre square of hemocytometer. Initially the hemocytometer is viewed first under 10X so as to focus the centre square, then after it is viewed under 40X. It was seen that under 40X the cells were visible but for accurately measuring the cell count higher magnification of 100X was used.

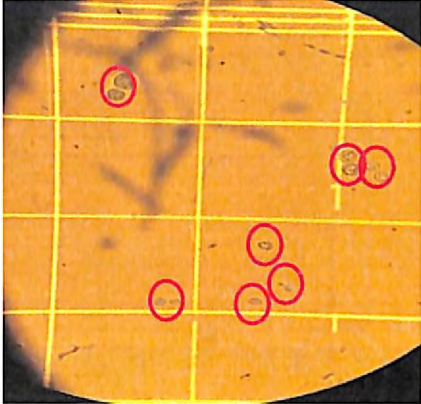
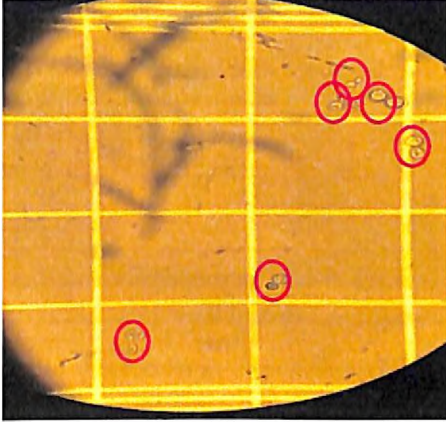
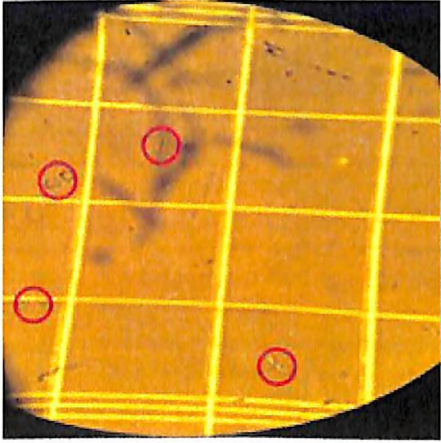


10X View



40X View

Figure 4.21: Cells under microscope at 10X and 40X view

POSITION (hemocytometer)	RUN 1 (100X view)
1 Cell count	 <p>8</p>
2 Cell count	 <p>6</p>
3 Cell count	 <p>4</p>

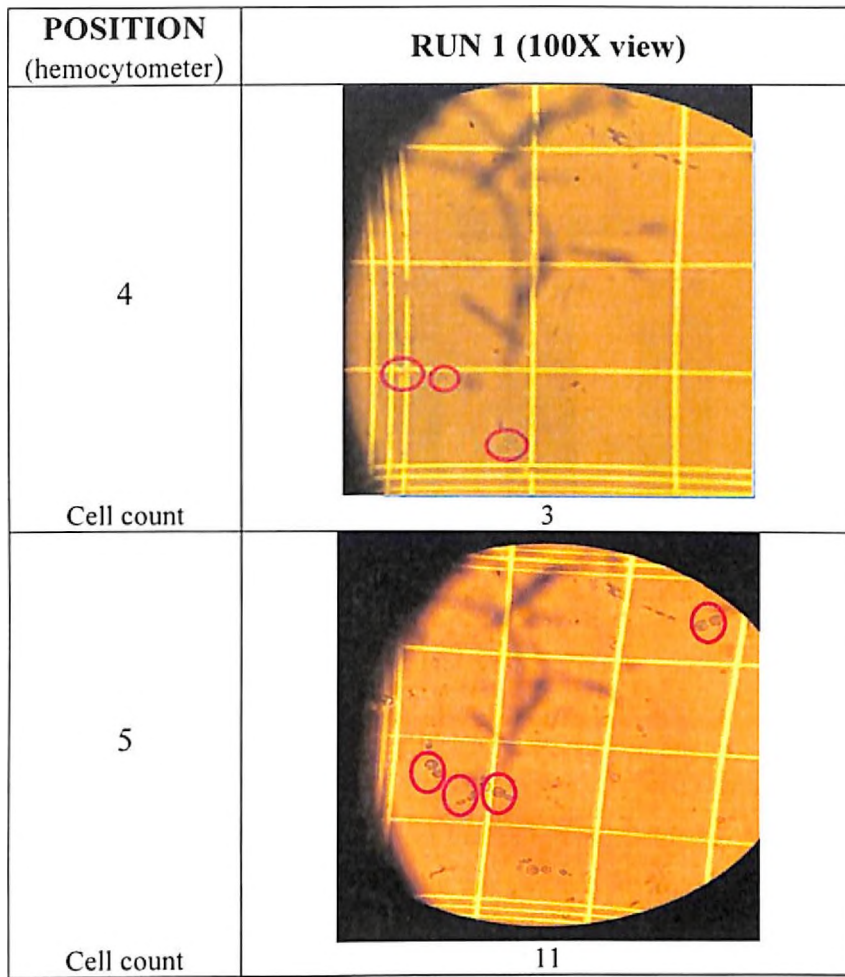


Figure 4.23: Microscopic view of dead cells in five different chambers of hemocytometer

For each run, the cell density and efficiency was calculated which is given in Table 4.4. The efficiency was calculated using Equation 4.2. The efficiency of all the four runs were comparable but maximum efficiency of 98.4% was observed in Run2.

Table 4.4: Device efficiency using dead cells

Run	Avg. No. of cells	Density (No. cells/ml)	Efficiency
1	6.4	1.6×10^6	98.1%
2	5.6	1.4×10^6	98.4%
3	8.6	2.1×10^6	97.6%
4	8.0	2.0×10^6	97.9%

The efficiency in all the four runs is shown in graph and presented in Figure 4.23 below. Now, the average of the efficiency from all the four runs was calculated to be 97.9%

Efficiency of gold device for trapping Dead cells = $(98.1 + 98.4 + 97.6 + 97.8)/4 = 97.9\%$

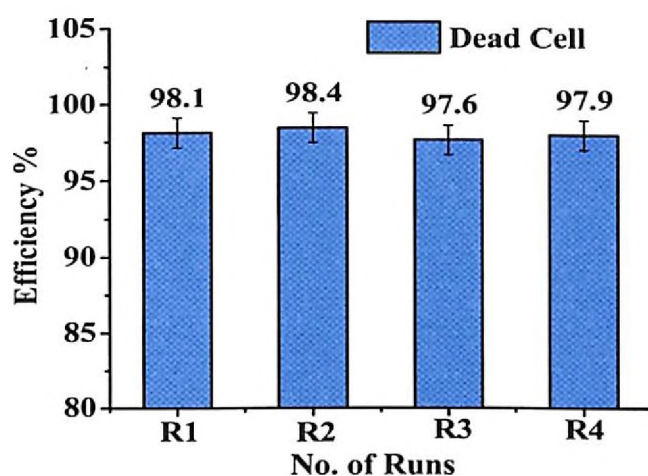


Figure 4.23: Dead cells- efficiency per run

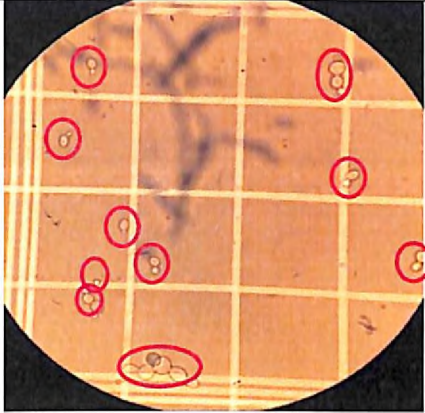
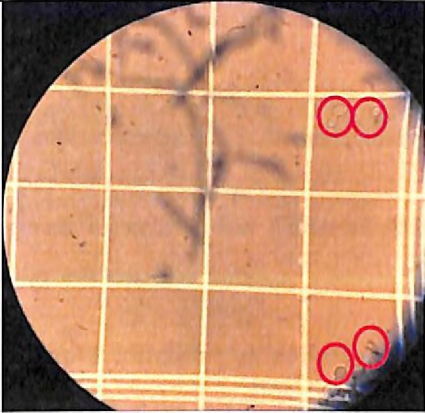
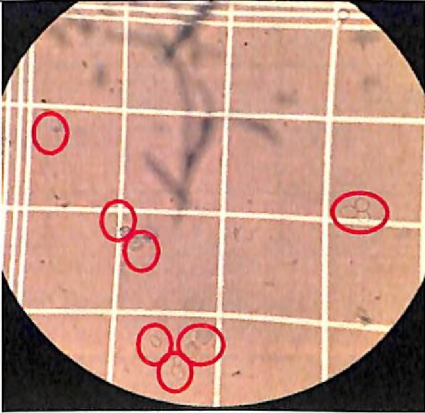
4.5.4.3.2 Live cells

In similar manner, the trapping efficiency for live cells was calculated. Again four sets of runs were performed and the cells that did not get trapped and flowed to the output were counted. In case of live cells, 0.2 μ l of MB dye was mixed with the output cell solution. Therefore in this case the dilution factor is 1.02. The cell counts obtained from the four experiments are listed in Table 4.5 below. Total number of cells observed in each run are 36, 36, 45 and 49.

Table 4.5: Live cells count (output)

Position	No. of cells counted			
	Run 1	Run 2	Run 3	Run 4
1	10	8	19	9
2	6	7	10	12
3	9	6	10	17
4	5	6	3	6
5	16	9	3	5
Total	36	36	45	49

No. of cells that were observed in Run1 for all five locations is shown in Figure 4.24. For each run, the cell density and efficiency was calculated which is given in Table 4.6. The efficiency was calculated using Equation 4.2. The efficiency of all the four runs were comparable but maximum efficiency of 94.3% was observed in Run1 and Run2.

POSITION (hemocytometer)	RUN 1 (100X view)
1 Cell count	 <p style="text-align: center;">10</p>
2 Cell count	 <p style="text-align: center;">6</p>
3 Cell count	 <p style="text-align: center;">9</p>

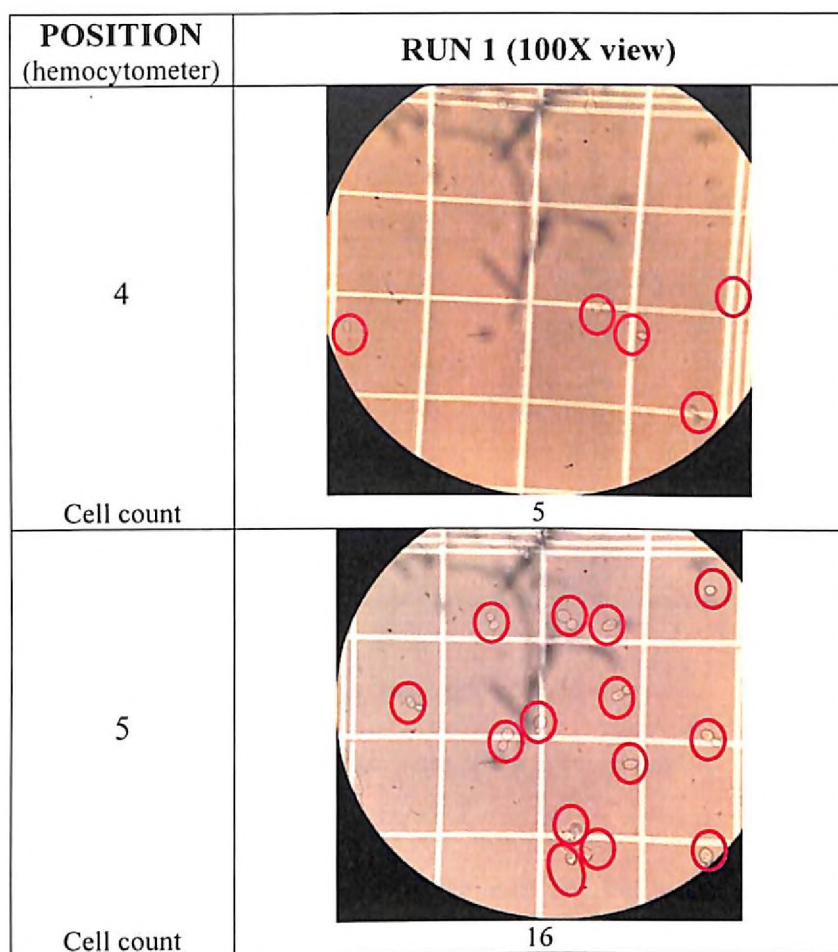


Figure 4.24: Microscopic view of live cells in five different chambers of hemocytometer

Table 4.6: Device efficiency for each run with live cells

Run	Avg. no. of cells	No. cells/ml	Efficiency
1	7.2	1.8×10^6	94.3%
2	7.2	1.8×10^6	94.3%
3	9.0	2.2×10^6	92.8%
4	9.8	2.4×10^6	92.2%

The efficiency of each of the runs is shown in graph below Figure 4.25. Now, the average of the efficiency from all the four runs was calculated

Efficiency of gold device for trapping live cells = $(94.3+94.3+92.8+92.2)/4 = 93.4\%$

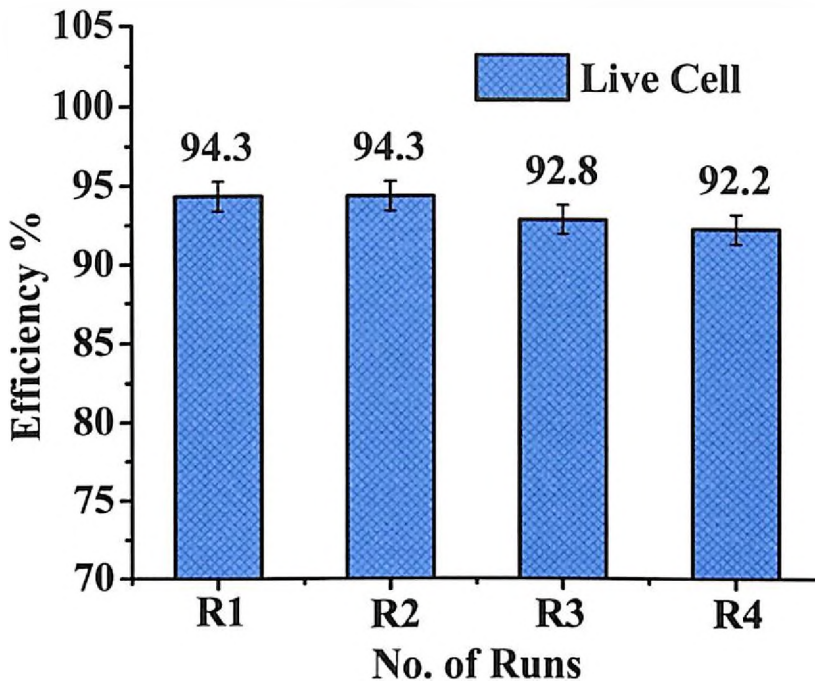


Figure 4.25: Live cells-efficiency per run

4.5.4.4 Estimation of cell viability

Electric fields are often used for cell manipulation, but unfortunately they are associated with an inevitable phenomenon of joule heating. Excess temperature elevations inside channel may cause bubble formation, denaturation of proteins, nucleic acids, and live biological samples and break down of the chip system. Therefore, this sets an upper limit for the use of high electrical voltages for many applications. For this reason, determining the viability of the trapped cells becomes an essential step.

Cell viability test was performed by releasing the trapped cells from the microchannel by withdrawal of the input signal and flushing the channel with mannitol. The flushed cell suspension was now collected from the outlet reservoir and then stained with MB dye. On staining, viable cells will reject the dye and will remain translucent while the non-viable cells will acquire blue colour. The impact of electric field on cell viability can be determined by comparing the percentage of live cells at the input and output.

Since the live cells count at the inlet has already been performed and discussed in Section 4.5.5.1, therefore now the live cell count at the outlet in the flushed cell suspension from the four runs is now determined and is given in Table 4.7.

Table 4.7: Trapped cell count

Position (hemocytometer)	No. of cells counted			
	Run 1	Run 2	Run 3	Run 4
1	65	55	50	53
2	60	62	56	60
3	70	60	53	65
4	72	63	69	70
5	50	63	71	61
Total	317	303	299	309

For determination of cell density, 10 μ l of cell suspension was pipetted from the solution collected in the four runs respectively and to it 0.2 μ l of dye and 10ul of DI water was added and mixed thoroughly, giving Dilution factor of 2.02. The cell density at the outlet was then divided with inlet cell density (32.3×10^6 cells/ml) to give % of viable cells at the outlet as described in Table 4.8

Table 4.8: Percentage of viable cells

Run	Avg. no. of cells	Outlet cell density (No. cells/ml)	% Viability
1	63.4	32.0×10^6	99.07%
2	60.6	30.6×10^6	94.73%
3	59.8	30.1×10^6	93.46%
4	61.8	31.2×10^6	96.59%

From the above calculations, an average percentage of viable cells was calculated to be 96%.

4.5.4.5 Cell mixture

Cell mixture analysis was carried out by performing the trapping experiment twice. The cell count for both the runs is given in Table 4.9 when 350 kHz frequency was applied.

Table 4.9: Cell count at 350 kHz

Position (hemocytometer)	Run 1		Run 2	
	Live cells	Dead cells	Live cells	Dead cells
1	41	6	28	12
2	48	6	38	5
3	22	2	40	4
4	25	4	45	6
5	30	10	50	10
Total	194		232	
D.F	1		1	

Table 4.10: Device efficiency for each run

Run	Avg. no. of cells	Density (No. cells/ml)	Efficiency
1	38.8	9.70×10^6	87.2%
2	46.4	1.16×10^7	84.6%

Device efficiency was obtained by calculating the average cell number and cell density in the two runs as given in Table 4.10.

Average device efficiency is 85.9% ~ 86.0%

After, performing trapping experiment at 350 kHz and collecting 1ml of output solution, the signal was increased to 700 kHz keeping other conditions constant. After switching the signal first 1ml of the solution was collected and discarded to make sure that the live cells that were there in the output tubing is removed from the previous run. Now, another ml of the output solution was collected in a fresh eppendorf and analyzed for cell density. The cell count of both live and dead cells in detailed in Table 4.11.

Table 4.11: Cell count at 700 kHz

Position	Run 1		Run 2	
	Live cells	Dead cells	Live cells	Dead cells
1	5	40	8	36
2	10	38	11	41
3	10	36	16	26
4	7	42	10	35
5	4	45	13	32
Total	250		228	
D.F	1		1	

Device efficiency was obtained by calculating the average cell number and cell density in the two runs as given in Table 4.12:

Table 4.12: Device efficiency for each run at 700 kHz

Run	Avg. no. of cells	Density (No. cells/ml)	Efficiency
1	50.0	1.25×10^7	83.5%
2	45.6	1.14×10^7	84.9%

Average device efficiency is 84.2%

4.6 Conclusions

1. The gold electrode based DEP device using C-Serpentine design is successfully fabricated and tested. Gold electrodes of height 200 nm were deposited using thermal evaporation technique. And SU-8 based microchannel is patterned over the 200 nm thick gold electrode. Further, drilling of inlet/outlet ports was carried out using ultrasonic drilling. An adhesive bonding technique is used to make perfect sealing between the glass and silicon substrate, for which the bonding parameters were optimized. The fabricated device was initially tested for leakage by flowing DI water through the channel and no leakage was observed. No leakage indicates that both silicon and glass substrate has bonded well with each other.

2. For studying the device performance, yeast cells were used as model cells. The yeast cells were grown using YPD media. The procedure for cell growth and culturing was carried out in a sterile environment and are presented in detail in Section 4.2.3.2. Dead yeast cells were prepared by heat killing live yeast cells. The conductivity of both live and dead yeast cell suspension was measured using conductivity meter. The value of suspension conductivity was further used to predict the value of CM factor. This in turn helped in determining the frequency range over which each cell will experience p-DEP and n-DEP.
3. The experiments were done with an objective to dielectrophoretically trap live and dead yeast cells in microchannel using AC driven electric field. With both cell types 4 sets of experiments were performed. The details of experiment are given in Section 4.4. Dead cells were observed to get trap at 300 kHz whereas, live cells showed trapping at 700 kHz. The reason behind this frequency specific response is that in case of dead cells their cell wall is damaged therefore electric lines can easily pass through the cells and cause it to trap at lower frequency. Whereas, in case of live cells that have their cell wall intact, do not allow the electric lines to pass through them so easily. therefore when higher frequency is applied then only cell trapping was observed.
4. The efficiency of the gold electrode DEP device is also investigated for both live and dead cells. For each of the cells, four runs were performed. In case of dead cells, the calculated device efficiency is 97.9% and in the case of live cells the device efficiency is calculated to be 94.3%. However the efficiency of the device can further be increased if 3D electrodes were employed, as in case of 3D electrodes the electric field is distributed across whole of the channel unlike 2D electrodes where the electric lines remained confined at the micro-channel base.
5. Trapping of the cells was also tested for cell mixture. Dead cells were observed to get trap at 350 kHz whereas, live cells showed trapping at 700 kHz. In case of dead cells, the calculated device efficiency is 86% and in the case of live cells the device efficiency is calculated to be 84.2%.
6. It was observed from the experimental results that the cell trapping efficiency value is high when trapping of individual cells is performed, however the efficiency value drops when mixed cell suspension is taken. The reason for this discrepancy in

trapping efficiency is because the cell density in case of mixed cells is more i.e 7.58×10^7 cells per ml when compared to live and dead cell density i.e 32.6×10^6 and 91×10^6 cells per ml respectively. Therefore, it is possible that in the case of mixed cells, the DEP force generated was not sufficient enough to effectively capture cells and thus more number of cells went untrapped. However, the trapping efficiency can be further improved by diluting the mixed cell suspension or by increasing the applied voltage.

7. As proven by Ramos et al [13], the joule heating effect can be ignored for solutions with low conductivity. The variation of temperature calculated and measured for a solution with a conductivity of $100 \mu\text{S}/\text{cm}$ was in the range of $1\text{-}6^\circ\text{C}$ for an applied voltage of 20 Vp-p . Since the input voltage in our study is only 10V and the medium conductivity is in the same order of magnitude, the % viability obtained in our study is 96% .

References

- [1] H. Pohl and R. Pethhig, "Dielectric measurements using non-uniform electric field (dielectrophoretic) effects," *J. Phys. E.*, vol. 10, no. 2, p. 190, 1977.
- [2] T. . Jones and J. . Kraybill, "Active feedback controlled dielectrophoretic levitation," *J. Appl. Phys.*, vol. 60, no. 4, pp. 1247–1252, 1986.
- [3] S. Shim, K. Stemke-Hale, J. Noshari, F. F. Becker, and P. R. C. Gascoyne, "Dielectrophoresis has broad applicability to marker-free isolation of tumor cells from blood by microfluidic systems," *Biomicrofluidics*, vol. 7, no. 1, p. 011808, 2013.
- [4] R. Martinez-Duarte, F. Camacho-Alanis, P. Renaud, and A. Ros, "Dielectrophoresis of lambda-DNA using 3D carbon electrodes," *Electrophoresis*, vol. 34, no. 7, pp. 1113–1122, 2013.
- [5] R. Hamada, H. Takayama, Y. Shonishi, L. Mao, M. Nakano, and J. Suehiro, "A rapid bacteria detection technique utilizing impedance measurement combined with positive and negative dielectrophoresis," *Sensors Actuators, B Chem.*, vol. 181, pp. 439–445, 2013.
- [6] R. Wang, Y. Xu, H. Liu, J. Peng, J. Irudayaraj, and F. Cui, "An integrated microsystem with dielectrophoresis enrichment and impedance detection for detection of Escherichia coli," *Biomed. Microdevices*, vol. 19, no. 2, p. 34, 2017.
- [7] H. Song, J. M. Rosano, Y. Wang, C. J. Garson, B. Prabhakarandian, and K. Pant, "Continuous-Flow Sorting of Stem Cells and Differentiation Products based on Dielectrophoresis," *Lab Chip*, vol. 15, no. 5, pp. 1320–1328, 2015.
- [8] B. Yafouz, N. A. Kadri, and F. Ibrahim, "Microarray dot electrodes utilizing dielectrophoresis for cell characterization.," *Sensors*, vol. 13, no. 7, pp. 9029–9046, 2013.
- [9] S. Rajaraman, H. (Moses) Noh, P. J. Hesketh, and D. S. Gottfried, "Rapid, low cost microfabrication technologies toward realization of devices for dielectrophoretic manipulation of particles and nanowires," *Sensors Actuators B Chem.*, vol. 114, no. 1, pp. 392–401, Mar. 2006.
- [10] R. Krishnan, B. D. Sullivan, R. L. Mifflin, S. C. Esener, and M. J. Heller, "Alternating current electrokinetic separation and detection of DNA nanoparticles in high-conductance solutions.," *Electrophoresis*, vol. 29, no. 9, pp. 1765–74, May 2008.
- [11] A. Sonnenberg, J. Y. Marciniak, R. Krishnan, and M. J. Heller, "Dielectrophoretic isolation of DNA and nanoparticles from blood.," *Electrophoresis*, vol. 33, no. 16, pp. 2482–90, Aug. 2012.
- [12] P. Puri, V. Kumar, S. U. Belgamwar, M. Ananthasubramanian, and N. N. Sharma, "Microfluidic platform for dielectrophoretic separation of bio-particles using serpentine microelectrodes," *Microsyst. Technol.*, pp. 1–8, 2018.
- [13] A. Ramos, H. Morgan, N. G. Green, and A. Castellanos, "Ac electrokinetics: A review of forces in microelectrode structures," *J. Phys. D. Appl. Phys.*, vol. 31, no. 18, pp. 2338–2353, 1998.

Dielectrophoretic Trapping with Printed Carbon Electrodes

5.1 General Introduction

Much advancement has been made in the area of DEP, and most of the work has been reported using metal electrodes [1]–[4]. However, there are still some challenges that need to be addressed before AC-DEP devices can come across the end users. The fabrication of these metal electrodes requires a complicated and an expensive fabrication technique (metal evaporators or metal sputters) that often restricts the yield and results in more expensive devices. The high-cost yet low-yield device manufacturing induced by traditional microelectromechanical systems (MEMS), tends to become worse in the case of disposable DEP devices for some applications, especially in health care, to avoid sample contamination.

Although other low-cost and easy-going methods such as hot embossing, injection molding, and laser photo-ablation can be used to fabricate microfluidic devices, they show poor capability to integrate electronic elements (for example, electrode arrays) that are necessary for DEP manipulation. Starting in the 2000s, alternative techniques have been explored to overcome common problems (e.g. electrode fouling) in metal-electrode DEP. Insulator-based DEP and light induced DEP are the most significant examples in this period. More recently, new 3D techniques like carbon-electrode DEP [5][6], contactless DEP [7][8], and the use of either C-MEMS or doped PDMS [9][10] have further simplified the fabrication process. However, the state-of-the-art of fabrication methods still cannot meet all the requirements for practical DEP chips such as low cost, simple process and high throughput.

The previous chapter detailed the fabrication steps involved in the fabrication of gold electrode based DEP device. The fabrication of these metal electrodes was performed using thermal evaporation technique that often restricts the yield and results in more expensive devices. Therefore, we conceived an idea of replacing metal electrodes with carbon electrodes using an inexpensive screen printing technology.

The present chapter elaborates the fabrication of carbon electrodes along with its testing for trapping live and dead yeast cells [11]. The beauty of our work is the extreme simplicity of the device fabrication procedure, i.e., the principal component: the microelectrodes, were constructed via screen printing process, which made it possible for the inexpensive yet high-throughput mass production, especially considering the widespread presence of such a technology in industry [12]. The details of screen-printing technology has already been discussed in Chapter 2 along with few contributions of this technology to DEP [13], [14]. Zhu et al in 2015 [14] was the first to report the use of screen printed dielectric paste electrodes with castellated geometry for separation of yeast and polystyrene particles. The electrodes created alternate regions of low and high sharp electric field regions, therefore the cells trapped at electrode edges by p-DEP became dead and low viability percentage was obtained. This viability problem was further addressed by Lin et al in 2016 [13], where they proposed the use of 3D wavy sidewall electrode along with offset castellated electrodes to continuously separate particles in three different outlets.

In our study, we propose the use of only 3D serpentine sidewall electrodes. With serpentine structure stronger and long range electric field gradient can be generated in the entire microchannel, which leads to better device performance. In our work, instead of metal electrodes, conductive carbon paste (SIL 060 by SILTECH CORPORATION) was used to screen-print C-Serpentine electrodes with 3D structures which not only reduces the cost dramatically but also increases the trapping efficiency when compared to the previous studies. Unlike pyrolysis, which is one of the widely adopted method for fabricating carbon electrodes, screen printing technology consumes less efforts and time. Also pyrolysis method is associated with stress-induced peeling off and delamination of carbon structures from the substrate, shrinkage of photoresist structures and self organization of electrodes. Unfortunately, the fact that SU-8 structures shrink during carbonization, the gap between the adjacent electrodes also increases which in turn affects the DEP force and device throughput.

The use of 3D electrode structures over more traditional planar structures is emphasized here as a way to increase the throughput of DEP devices. Also, it is a very common practice to pack microfluidic devices with Poly-Di-Methyl-Siloxane (PDMS), because it is an inexpensive, biocompatible, an easy to mold and can be coated with a controlled

thickness. But there are few demerits associated with PDMS based microchannels, say for example, PDMS experience elastic deformations under imposed flow rates and also studies have shown that PDMS tends to absorb small molecules which significantly alters the composition of the solution [15], [16]. These deformations affect the flow rate and pressure distribution in the channel. Another well known issue with PDMS is that it does not provide a leak proof bond with the substrate even if the substrate is treated with oxygen plasma, which is again a time consuming process. In order to avoid these kinds of issues we propose the use of pyrex glass to cover the channel using SU-8 as an adhesive layer in our fabrication work. Pyrex glass on the top provides good adhesion with the substrate therefore a leak proof device can be fabricated and also it does not undergo any elastic deformation.

In this chapter, we will discuss the fabrication of carbon based DEP device using screen printing technology and the use of SU-8 as structural as well as an adhesive layer. The main challenge in the fabrication of carbon based device involves the fabrication of SU-8 micro channel over carbon electrodes. This is because, the SU-8 possess poor adhesion to glass substrate and tend to peel off very easily during the SU-8 development process. In addition to this, the conductive carbon paste shows incompatibility with (Methyl Ethyl Ketone) MEK, alcohol or any such similar solvents. Therefore we have optimized our process of SU-8 adhesion by doing a number of trials on glass substrate. It is well known that the adhesion of SU-8 can be improved either by using the piranha cleaning or exposing the substrate to oxygen plasma. We have used piranha cleaning in order to improve the adhesion to the substrate. Further the process parameters such as exposure time, prebake and post bake and development time is also optimized for glass substrate. To the best of our knowledge, the present work on carbon electrode based DEP device using SU-8 microchannel and glass sealing is so far the first reporting in available literature.

5.2 Conductive Carbon Inks

Conductive inks and pastes are becoming increasingly popular, both in research community and also with makers and educators. The use of conductive carbon inks constitutes a low cost method of applying conductors to various types of substrates like plastics, polyester films, polyimide films, ceramics and other materials by means of screen printing technique. Conductive carbon inks consist of three main components

namely: a polymer binder (paint binding agents), a conductive material, and a solvent as shown in Figure 5.1. After printing of the ink, the solvent evaporates following a curing mechanism, which varies for every paint system, leaving a conductive pattern on the substrate. Generally, first-grade conductors such as precious metal powder and carbon powder can only be used as conductive materials.

Conductive carbon inks are usually highly thixotropic in nature i.e they possess time dependent shear thinning property. Therefore to achieve the viscosity necessary for processing these inks must be carefully mixed prior to their application. Proper mixing results in the significant reduction in viscosity which ensures easy printing. An interesting aspect of these carbon inks is that they can be used to substitute expensive precious metals coatings. The substitution of gold by carbon conductive inks not only eliminates the necessity of using the extremely expensive raw material but also labour intensive processes.

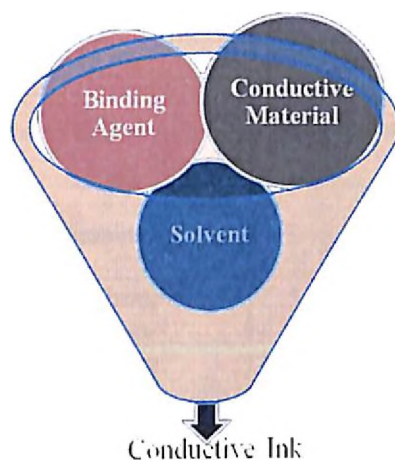


Figure 5.1: Composition of conductive inks

Conductive carbon inks and pastes provide superb performance and adaptability for a variety of applications including biomedical sensors, automotive, electrodes, energy storage, aerospace, etch resists, printed heaters and thin film photovoltaic.

5.3 Experimental Details

This chapter includes the detailed fabrication of the carbon electrode based DEP device. C-serpentine structure is made using conductive carbon paste (SIL 060 by SILTECH

CORPORATION), instead of metal electrodes, using screen-printing technology. C-Serpentine geometry with 3D electrode structures, not only reduces the cost dramatically but also increases the trapping efficiency. The fabrication process is discussed step by step in Section 5.3.2. In addition, the testing of the devices using dead and live yeast cell are also investigated. We also report a comparative analysis of trapping efficiency achieved by gold and carbon electrode DEP device, at the end of this chapter.

5.3.1 Mask Design

Carbon electrode based DEP device includes two mask process as shown in Figure 5.2. MASK#1 is carbon electrode mask which is shown in Figure 5.2(a) whereas MASK#2 is the mask for fabricating the microchannel as shown in Figure 5.2(b). L-Edit layout editor tool is used for designing of the mask layout. In addition to electrode and micro-channel mask, some test structures like U shaped, straight lines and spiral shape of different dimensions were also designed to characterize the carbon structures. Test structures were printed in order to see the repeatability of printing process. The dimension details of each mask design are given in Table 5.1:

Table 5.1: Dimensions of different screen printed carbon test structures

S.No.	Structure Name	Dimensions	
1	Spiral Shape	$S_L: 7400\mu\text{m}$, $S_W: 200\mu\text{m}$	
2	U Shape I (U_L , U_W)	$U_L: 3750\mu\text{m}$, $U_W: 200\mu\text{m}$	
3	U Shape II (U_L , U_W)	$U_L: 3750\mu\text{m}$, $U_W: 300\mu\text{m}$	
4	U Shape III (U_L , U_W)	$U_L: 3750\mu\text{m}$, $U_W: 150\mu\text{m}$	
5	Line-I (L_L , L_W)	$L_L: 8000\mu\text{m}$, $L_W: 200\mu\text{m}$	
6	Line-II (L_L , L_W)	$L_L: 8000\mu\text{m}$, $L_W: 300\mu\text{m}$	

(U shape length- U_L , U shape width- U_W , Line length- L_L , Line width- L_W , Spiral width- S_W , Spiral length- S_L)

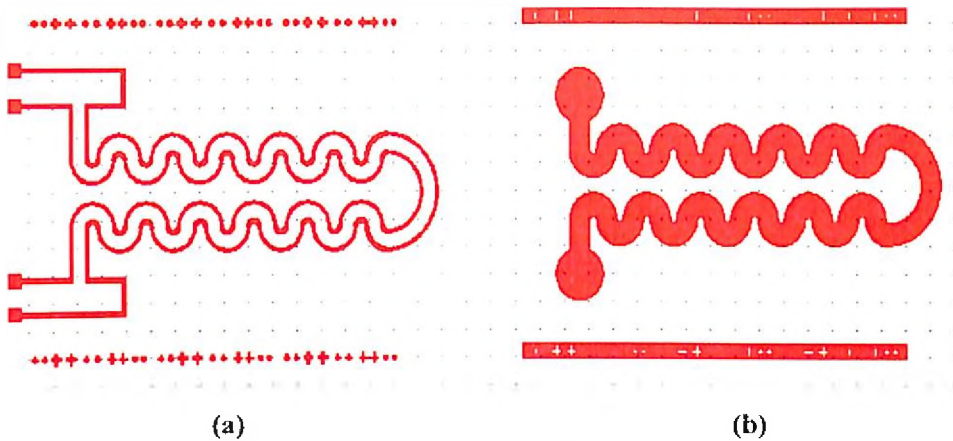


**Figure 5.2: Mask layout of DEP device (a) Mask#1 electrode mask
(b) Mask#2 microchannel mask**

In order to optimize the carbon patterning of minimum feature size a few test structures with different width, length has been designed. The test structure from 150 μm width to 300 μm width is designed and fabricated. In the mask layout the width of the electrode and microchannel is 150 μm and 1mm respectively. In addition to feature sizes, the process parameter such as curing and dry conditions, thickness, adhesion properties with Si/glass substrate, resistance values of screen printing electrodes is optimized using these test structure.-

5.3.2 Fabrication Details

Carbon electrode DEP device is fabricated entirely on glass. The fabrication includes two glass substrates. The bottom glass substrate comprises of the carbon electrodes and SU-8 microchannel whereas, top glass substrate includes the inlet/outlet ports for the microchannel. SU-8 polymer is used as structural layer as well as an adhesive layer for the DEP device. The schematic view of fabrication flow for DEP device is shown in Figure 5.3. The detailed fabrication process is discussed in the following section:

5.3.2.1 Cleaning and substrate preparation

All the glass wafers which were to be used as substrates for electrodes as well as for closing channel were taken and subjected to cleaning. Though the wafers are fresh, they still are not clean, so before starting fabrication process we have to clean the wafers properly. A two-step process for cleaning is considered with DI water rinse, followed by piranha cleaning.

DI Water rinse: Wafer is rinsed with DI water for 10 min. A large fraction of ionic impurities present on the wafer surface is removed and wafer becomes free from all ionic impurities except HO^+ and OH^- .

Piranha cleaning: After DI water rinsing; the substrates were cleaned using piranha solution. Piranha solution contains $\text{H}_2\text{SO}_4:\text{H}_2\text{O}_2$ in the ratio of 3:1 by volume. The wafers were dipped in the solution for 15 min. Organic impurities and alkali ions are removed due to strong oxidizing property of the solution. The surface of glass is passivated with (OH) groups making it hydrophilic. After piranha cleaning the wafers are dipped in dilute HF (HF: DI water: 1:50) at room temperature to remove the native oxide. This is followed by N_2 blow drying. A set of eight samples were prepared for the experimental work.

5.3.2.2 Carbon electrode printing

After cleaning, the glass substrates were loaded for carbon electrode patterning using Screen Printing Technique, in which the carbon ink is forced through the open regions of a mesh screen to form a pattern on the surface. Here, we have used a low resource and thus highly available scheme for electrode fabrication based on simple, stencil method. Carbon electrodes from conductive carbon ink can readily be deposited using screen or stencil printing methods. A VTT-DC machine is used for printing of carbon electrodes. The screen printing machine is illustrated in Figure 5.4(a) which is available at Center for Nanoscience and Engineering (CeNSE), IISc-India. A desired pattern on nylon mesh stencil which is shown in Figure 5.4(b) and glass substrate is loaded in screen printing machine. Afterwards, carbon ink shown in Figure 5.4(c) is poured onto the stencil and spread with a squeegee. After printing, the stencil was removed from the substrate and the substrate with printed carbon electrodes was placed in the oven at 100°C for 1 hr, this removes the solvent from the paste. Thus this process creates a stencil pattern on the substrate. After printing and baking the substrate for 1 hr, the height of carbon electrodes on four glass samples were measured using Profilometer (Veeco, DEKTAK 6M, Stylus Profiler), and the average height was found to be $18\ \mu\text{m}$.

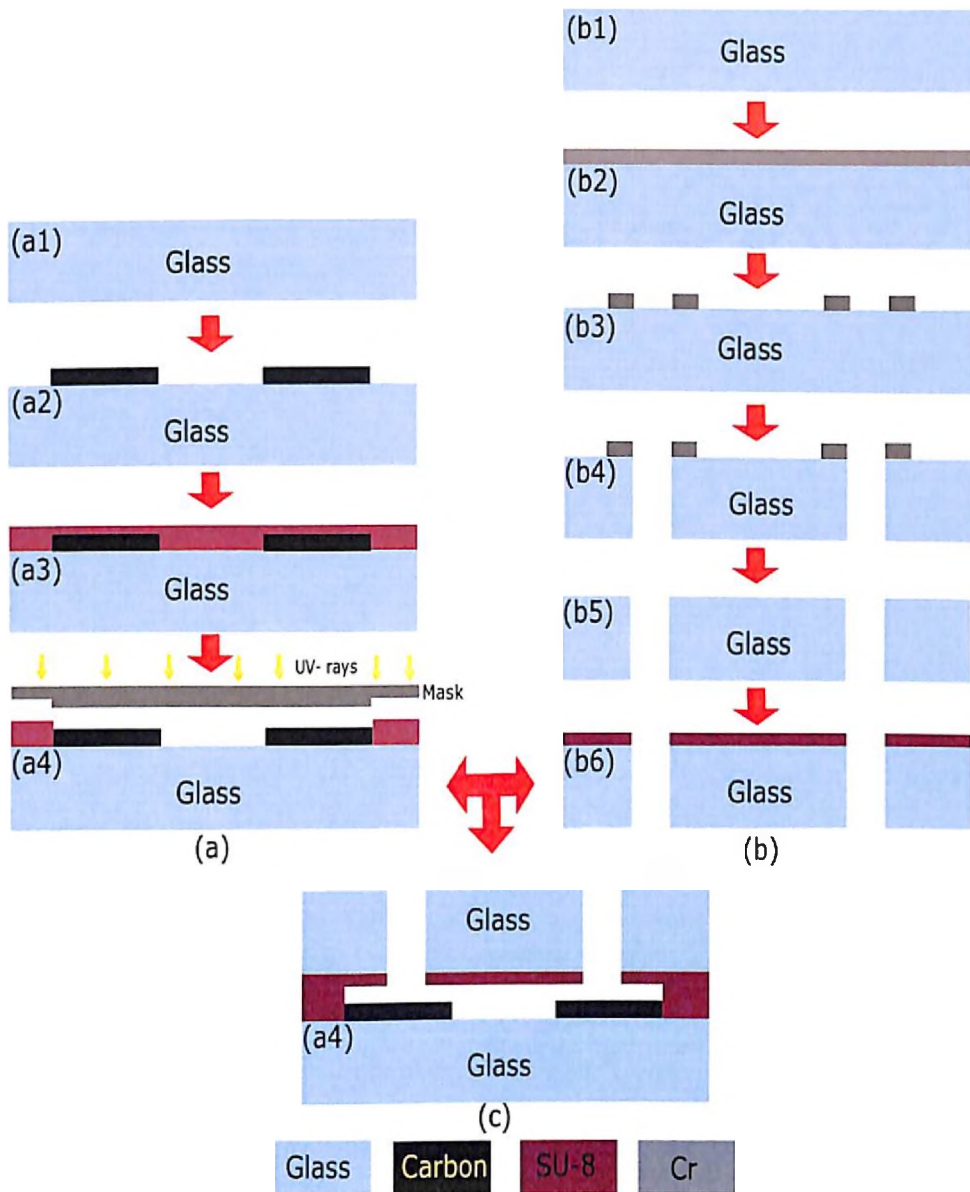


Figure 5.3: Schematic cross section view of the fabrication flow of carbon electrode based DEP device (a) Glass substrate bottom wafer (b) Glass substrate top wafer (c) Top and bottom bonded wafer. Exploded view of bottom wafer (a1) Clean glass wafer (a2) Printed carbon electrodes (a3) SU-8 coating (a4) SU-8 channel. Exploded view of top wafer (b1) Clean glass wafer (b2) Cr deposition (b3) Cr patterning (b4) Glass drilling (b5) Cr etching (b6) SU-8 Coating for adhesive bonding

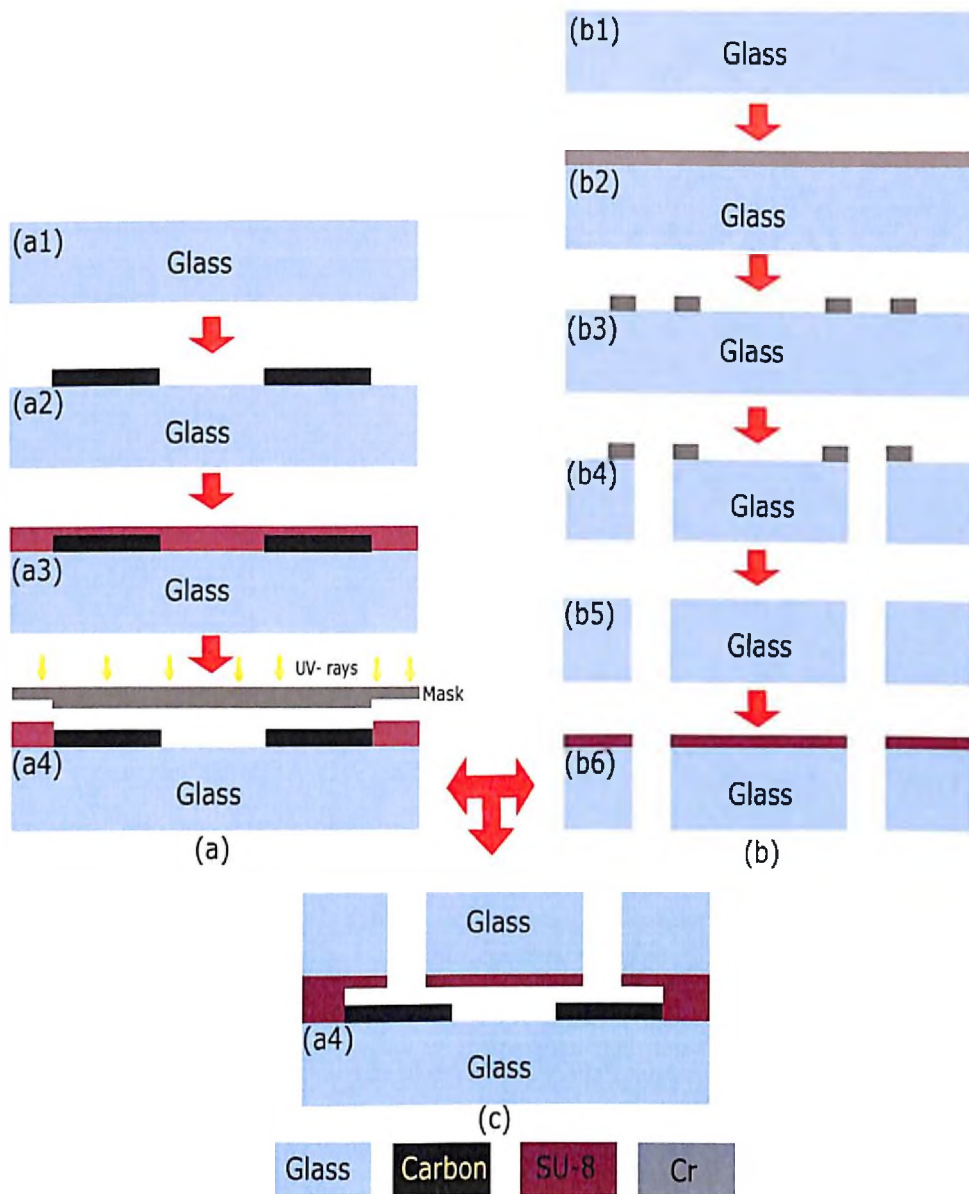


Figure 5.3: Schematic cross section view of the fabrication flow of carbon electrode based DEP device (a) Glass substrate bottom wafer (b) Glass substrate top wafer (c) Top and bottom bonded wafer. Exploded view of bottom wafer (a1) Clean glass wafer (a2) Printed carbon electrodes (a3) SU-8 coating (a4) SU-8 channel. Exploded view of top wafer (b1) Clean glass wafer (b2) Cr deposition (b3) Cr patterning (b4) Glass drilling (b5) Cr etching (b6) SU-8 Coating for adhesive bonding

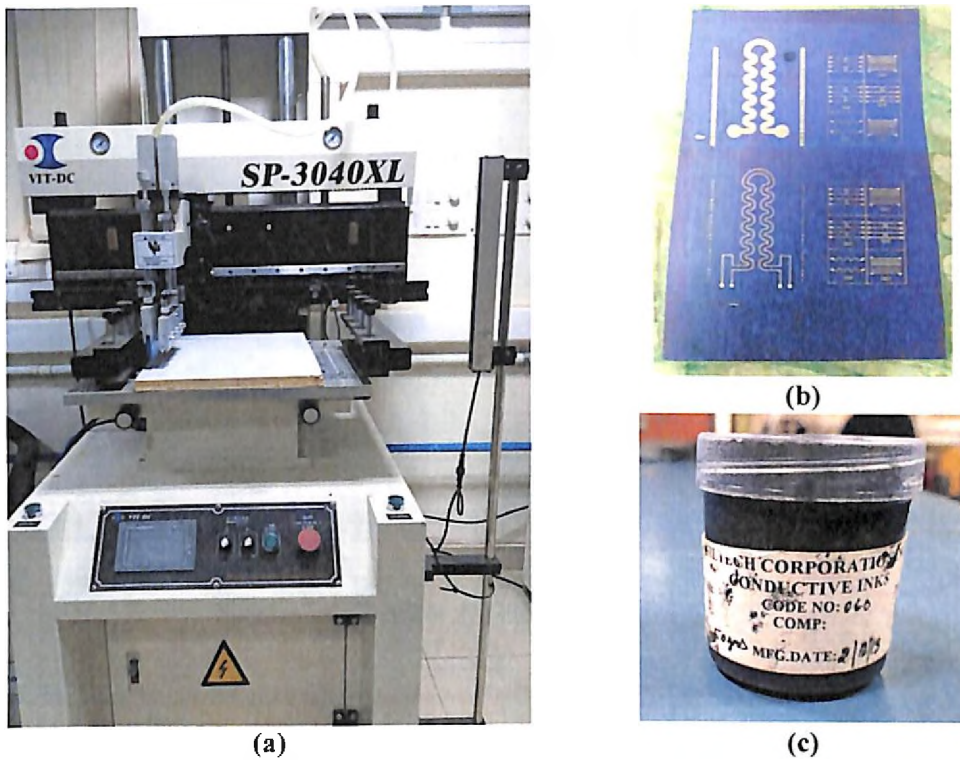


Figure 5.4: (a) Screen printing machine (b) Stencil mask pattern
(c) Conductive carbon Ink

5.3.2.3 SU-8 Coating and patterning

After carbon electrode patterning, SU-8 polymer is used for fabrication of the micro channel for DEP device. SU-8 is the material of choice for Bio-MEMS and microfluidics devices and requires simple processing and less fabrication time. SU-8 (Microchem, 2035) is used for the experimental work. The SU-8 photoresist was spin coated at 500 rpm for 5 sec followed by 4000 rpm for 30sec. The coated substrate was then soft baked on a hotplate at 70°C for 20 min and then the temperature was ramped to 90°C for 20 min. After 20 min at 90°C, the substrate was then allowed to slowly cool down to 25°C temperature. After baking, the SU-8 coated glass substrate was patterned by exposing to UV light for 50sec using an opaque mask#2 as shown in Figure 5.2(b). Immediately after UV exposure, the substrate was post baked at 70°C for 20 min and ramped up to 90°C for 20 min. Finally, exposed substrate was developed in SU-8 developer (Microchem developer) for 60 sec to make sure that exposed SU-8 is cross linked appropriately. The SU-8 microchannel after developing is shown in Figure 5.5 and discussed in schematic view of Figure 5.3 (a4). The height of the SU-8 was measured using DEKTAK Profiler and was found to be ~30µm.

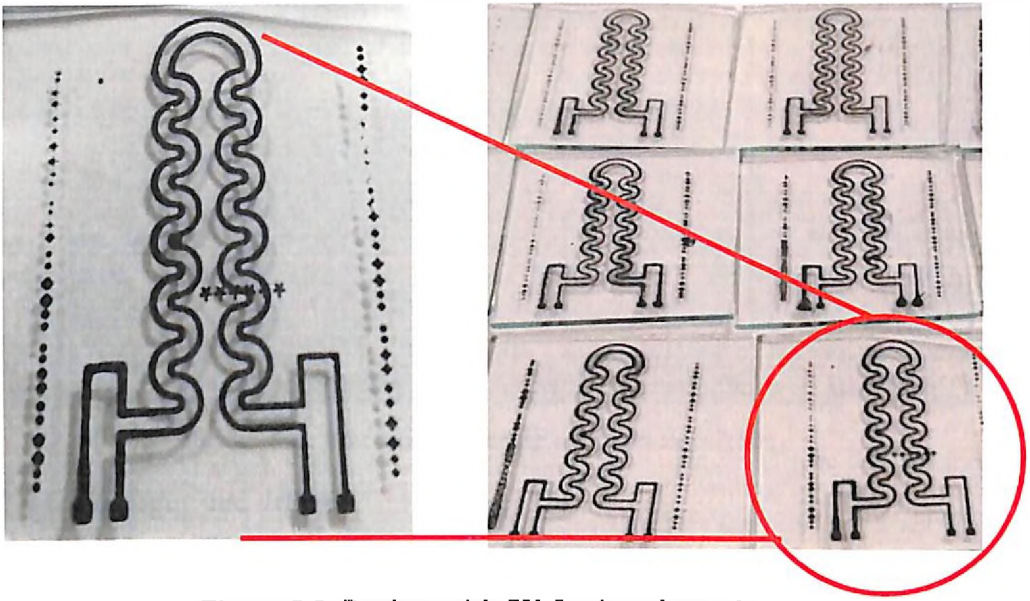


Figure 5.5: Devices with SU-8 microchannels

5.3.2.4 Chrome patterning on top glass substrate

The steps for patterning the top glass substrate with chrome are similar to the ones that have been discussed in Chapter 4 under section 4.2.2.7. In a nut shell, the glass substrate is patterned to make an inlet/outlet for the fluidic flow. For which, a chrome layer of 200 nm thickness is deposited using the e-beam evaporation technique as shown in schematic view of Figure 5.3(b2).

The parameters used for patterning are given below:

Spin speed:	4000 rpm
Prebake:	110°C for 1min
Exposure:	110mJ/cm ²
Development:	30 sec+30sec
Hard bake:	120°C for 4 min

5.3.2.5 Chrome patterning and etching

After patterning of the glass with desired pattern, a chrome etchant is prepared to etch the unpattern chrome. The process apoted for chrome etching has been discussed in detail in Chapter 4 under section 4.2.2.8. After etching, the schematic view of glass substrate is shown in Figure 5.3(b3). The glass substrate after chrome patterning is illustrated in Figure 5.6.

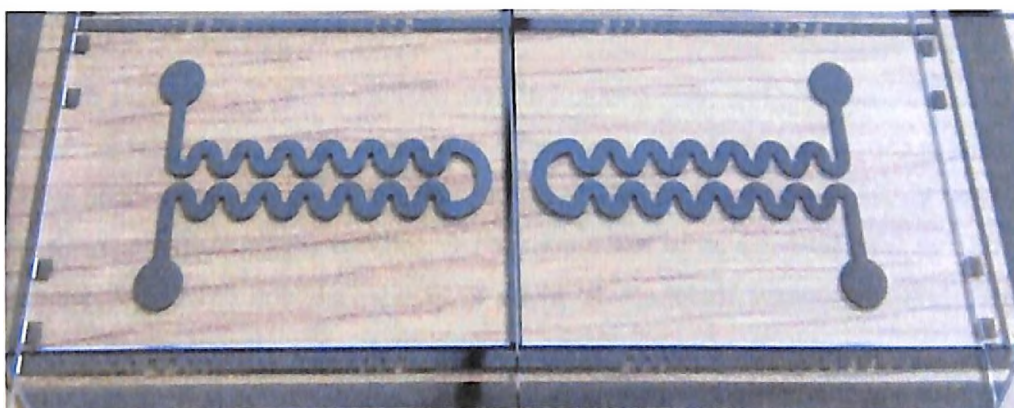


Figure 5.6: Chrome patterning on glass substrate

5.3.2.6 Glass dicing and drilling

After patterning of the chrome layer with desired pattern and etching away the unpatterned chrome, the glass substrate is diced and drilled. The glass substrate with drilled holes is shown Figure 5.7. From the chrome pattern on the glass substrate, the drilling of inlet and outlet holes can be done at precise location. An ultrasonic drilling is used for making inlet/outlet holes for the microchannel the details of which has been discussed in detail in Chapter 4 under section 4.2.2.9. The schematic of the wafer with holes drilled is shown in Figure 5.3(b4).

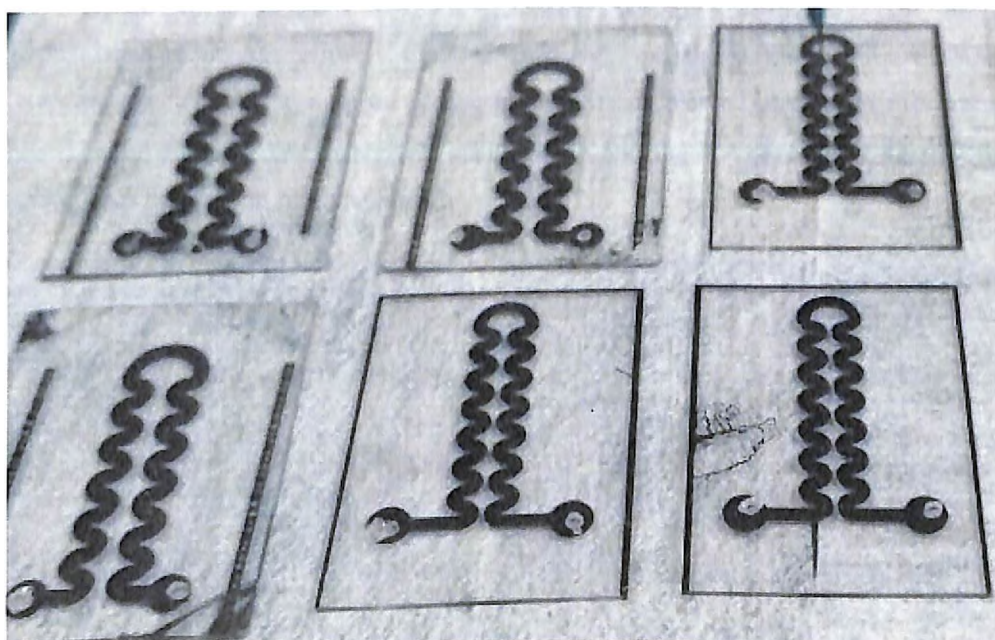


Figure 5.7: Drilled glass substrates

5.3.2.7 Bonding of both substrates

The glass substrate with SU-8 microchannel in Figure 5.3(a4) and glass drilled substrate in Figure 5.3(b5) is ready for the bonding. Adhesive bonding technique is used to make a perfect bond between the two glass substrates. A thin layer of SU-8 2002 is used as adhesive for performing the bonding. SU-8 plays a role of an adhesive layer as well as structural layer. The bonding with SU-8 could be conducted without the use of any pressurizing equipment.

The drilled glass is spin coated with SU-8 2002 at 4000 rpm for 40 sec to form a thin adhesive layer of 2 μm thickness. Initial trials were done by coating the SU-8 first on the glass substrate, followed by its prebake at 70°C for 2 min and 90°C for 2 min and then cooled down to room temperature. Then the SU-8 coated glass substrate was brought in contact with the bottom glass substrate to make a perfect bond. But, after the contact and manually pressing, the air-bubble has been observed in the bonded interface. To reduce the void formation and air bubble trapping between the bonded substrate, both the substrates were aligned and pressed manually from one side to another side. In addition to this, the prebake step was done after bonding both the substrates. This helped in achieving a bubble free bonding between the two substrates. So, the samples were heated at 70°C for 30 min on hotplate and followed by the exposure through glass in order to cure SU-8 and reduce its reflow. After exposure, the samples were post bake at 90°C is carried out for 30 min. A number of experiments were carried out to get the leakage proof i.e. void free bonding as shown in Figure 5.8 and the optimized best parameter is used for fabrication of the DEP devices.

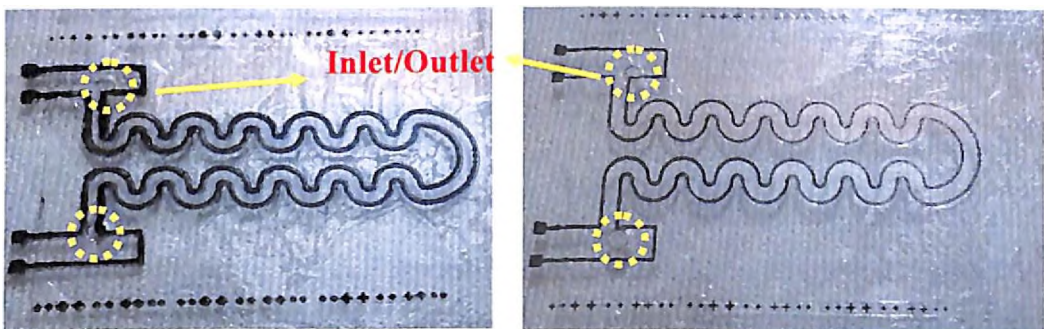


Figure 5.8: Glass bonded DEP device with inlet/outlet holes

5.3.2.8 Wire bonding

After fabrication of the DEP microchannel followed by its sealing with glass, the devices were wire bonded in order to interface it with other electronic devices. Manual wire bonding is carried out using silver epoxy paste. The silver epoxy paste is mixed with curing agent in ratio of 1:1 and wire is bonded with silver conductive paste. After wire bonding the sample were kept for heating at 100°C in oven for 40 min to make perfect contact between the electrode pad and wire as shown in Figure 5.9.

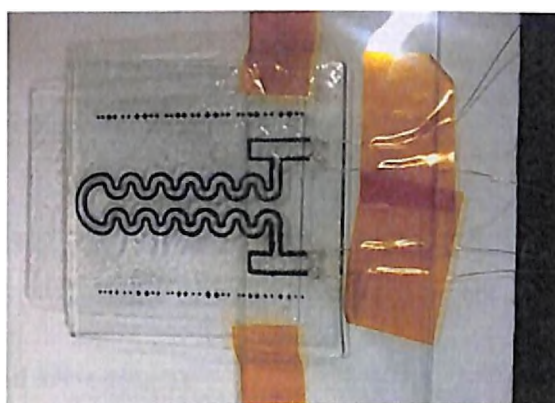


Figure 5.9: Wire Bonded Carbon DEP device

5.3.2.9 Cell preparations

The testing of fabricated carbon DEP device is carried out using yeast cells. Two type of yeast cells (*Saccharomyces cerevisiae*) viable (live) and non-viable (dead) are prepared for the experimental work. Dry active yeast was procured from a local bakery shop. Yeast cells were chosen because it is easily available and also are not very sensitive to contamination as other eukaryotic cell culture systems as yeast in their own media will outgrow most other things. The cell preparation method and its recipe have already been explained in detail in Chapter 4 under Section 4.2.3.2.

5.4 Testing and Characterization of the DEP Device

The DEP device testing was carried out using the customized setup as shown in Figure 5.10. The setup includes a Microscope, Syringe pump (Hygeia Medical Devices) and a Signal generator (Aplab Sine/Square wave generator 1MHz). The testing of the devices was carried out at different frequency ranges. Syringe pump was used to ensure continuous flow of cell solution which also prevents cells from settling at the bottom of the channel.

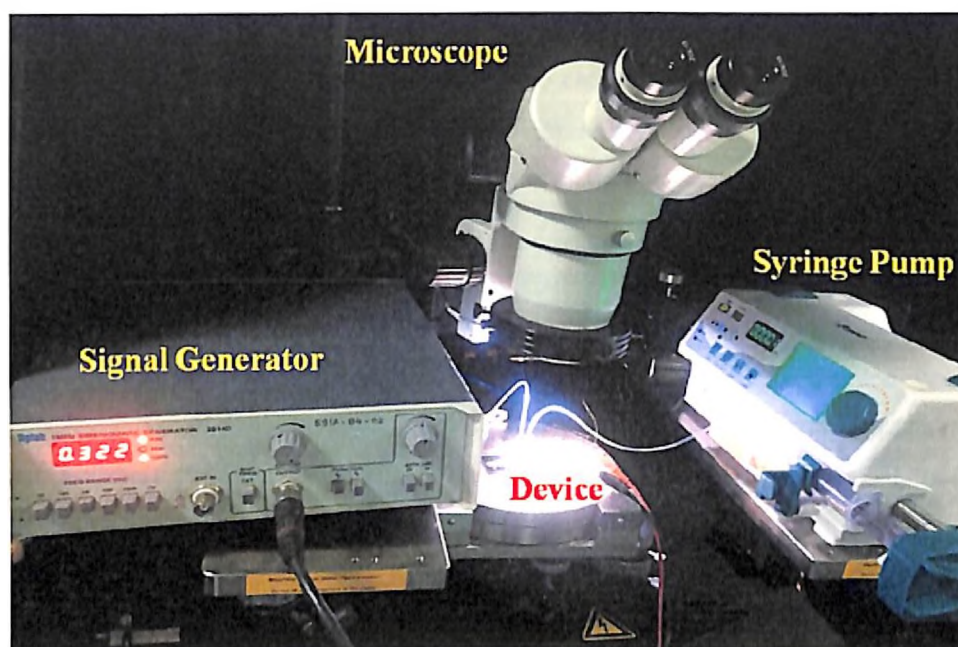


Figure 5.10: Experimental set-up

5.5 Results and Discussion

The carbon electrodes based DEP device has been tested for trapping of dead, live and mixture of dead and live yeast cells. The trapping was carried out using an ac signal of 10 V_{p-p} with varying frequency from 100 kHz to 1MHz range. After cell growth and solution preparation, conductivity of each of the solution was measured by carefully maintaining them at room temperature. The conductivity was measured using EUTECH Instruments, ph/conductivity/TDS/temp measurement. The conductivity of live and dead cells was measured to be 70 $\mu\text{S}/\text{cm}$ and 110 $\mu\text{S}/\text{cm}$ respectively. Massotti factor was calculated from the MATLAB plot using the measured value of conductivity. The massotti factor was observed from the graph (discussed in section 3.5) is -0.17 for dead cells with conductivity 70 $\mu\text{S}/\text{cm}$ and -0.37 for live cells with conductivity 110 $\mu\text{S}/\text{cm}$ respectively. Massotti factor graph shows the frequency range over which the two cell types will experience n-DEP and p-DEP.

Three sets of experiments were carried out for separation of the cells. In the first set, dead cells were injected into the microchannel, in the second set of experiment live cells were injected, while in the third set, a mixture of both live and dead cells were injected in the channel. This was done in order to observe the trapping frequency of both the individual cells. Once the trapping frequency of each of the cells is known, the third set

of experiment was performed by mixing of both dead and live cells. In addition to these three experiments, the device efficiency was also carried out using hemocytometer. For each set of experiments, four set of runs (R1-R4) were performed.

5.5.1 Electrical Characterization

Carbon test structures as well as C-serpentine structures that were printed on glass substrate were checked for continuity using digital multimeter. After checking structure continuity, electrical resistance was also measured for the screen printed designs. Electrical resistance measurements were carried out using a four probe measurement system available at CEERI, Pilani as shown in Figure 5.11, and the values obtained are listed in Table 5.2 below.

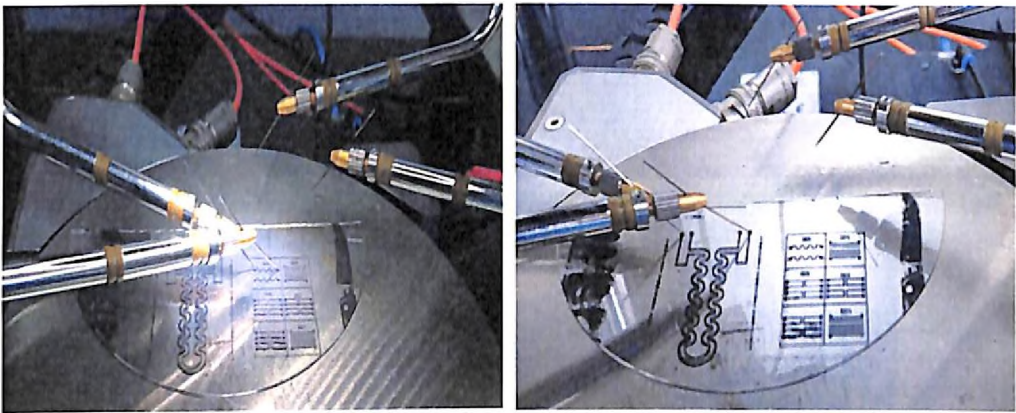


Figure 5.11: Resistance measurement using four probe IV-CV system

Table 5.2: Test structures and their resistance value

S.No.	Test Structure	Resistance Value (k-ohms)
1	Spiral Shape	9.00-9.40
2	U Shape-I (200 μ m thickness)	9.12-12.68
3	U Shape-II (300 μ m thickness)	7.16-13.98
4	U Shape-II (150 μ m thickness)	4.55-6.28
5	Lines-I (200 μ m width)	12.00-14.00
6	Line-II (300 μ m width)	5.20-7.16
7	C-Serpentine	240-290

5.5.2 Dead Cells

Freshly prepared dead cell solution as illustrated in Chapter 4 under Section 4.2.3.2, with cell concentration 91×10^6 cells/ml was taken and from it 5ml solution was drawn for performing the experiments. The solution was loaded in syringe pump and injected into the channel with a constant flow rate of 0.5 ml/hr. From Figure 5.12(a) it can be observed that the cells filled the entire channel. Now, an ac signal of 10 V_{p-p} was applied and the frequency was ramped up from 100 kHz with the step size of 50 kHz.



(a) Channel filled with cells



(b) Cell trapping at electrode

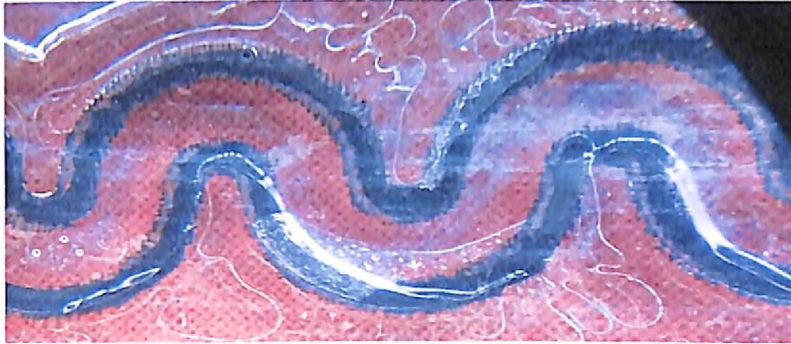
Figure 5.12: Dead cell trapping in carbon DEP device

As the frequency was gradually increased from 100 kHz, it was observed that at 300 kHz, cell clusters were seen getting trapped at the larger periphery of the channel indicating n-DEP trapping of dead yeast cells as shown in Figure 5.12 (b).

5.5.3 Live Cells

After performing the test with dead cells, the fluidic channel was cleaned thoroughly by flushing it with DI water for 20 min to ensure that no dead cell residue is left in the channel. Freshly prepared live cell solution with cell concentration of 32.3×10^6 cells/ml

was prepared and from it 5 ml solution was drawn for performing the experiments. The solution was loaded in syringe pump and injected into the channel with a constant flow rate of 0.5 ml/hr. From Figure 5.13(a) it can be observed that the live cells filled the entire channel. After a continuous flow was established inside the microchannel, the AC signal was switched on.



(a) Channel filled with live cells



(b) Cells trapped inside channel

Figure 5.13: Live cell trapping in carbon DEP device

Now, the frequency of an ac signal was slowly ramped from 100 kHz onwards with step size of 50 kHz, with voltage 10 V_{p-p} and flow rate of 0.5 ml/hr. It was observed that at around 800 kHz the cells started to experience n-DEP and cell aggregates started to form at channel periphery within few seconds as shown in Figure 5.13(b). This indicates that the live cells experienced n-DEP force and were thus attracted towards the larger periphery.

5.5.4 Mixture of Live and Dead Cell

The third set of experiment was carried out using mixture of dead and live cells solution. To prepare cell mixture, 10ml each of dead and live cells were thoroughly mixed together using vortex. The conductivity of the solution was set at 100 μ S/cm at 25°C.

Figure 4.18 in chapter 4 compares the predicted massotti factors of the two types of cells as a function of AC field frequency (from 1 kHz to 1 MHz) plotted using MATLAB. From the MATLAB plot it is inferred that the dead cells continue to have negative value of massotti factor throughout the frequency range, however for live cells a cross-over frequency exists at around 1 MHz. Since our signal generator had max frequency range upto 1 MHz, therefore the response of the cells at higher frequency could not be performed. Before performing trapping experiments, the microchannel was cleaned by flushing DI water for 10 min using syringe pump. After flushing, the homogeneous solution of dead and live cells was injected into the microchannel.



(a) Trapped dead cells at 300 kHz



(b) Trapped live cells at 700 kHz

Figure 5.14: Trapping of cells in mixture

In order to verify the response of each cell, we applied an AC field and increased the frequency starting from 100 kHz, at 300 kHz we observed that cells started to get trap at the periphery. At 300 kHz we collected 1 ml of output solution of eluted cells to perform the quantitative analysis of both dead and live cells. Later, the applied frequency was increased and cell trapping was again observed at 700 kHz. At 700 kHz, we again collected 1 ml of the output solution to observe the dead and live cells present in per ml of solution. For comparing the results, the image shots were taken at the same portion of

channel for both dead and live cells. In Figure 5.14(a) when 300 kHz signal was applied, dead cells can be seen trapped at the bottom boundary of the channel while the upper channel boundary has very less number of cells. While in Figure 5.14(b), when the signal was switched to 700 kHz, live cells were seen getting trapped on almost all the larger periphery of the channel. This clearly shows the response of each cell is specific to the frequency applied.

5.6 Device Efficiency

In case of carbon device too, the procedure used to calculate the device efficiency is same as the one used for gold device as discussed in Chapter 4 under Section 4.5. The input cell density that has been calculated for live cells is 32.6×10^6 cells/ml and 91×10^6 cells/ml in case of dead cells, as already discussed in Chapter 4.

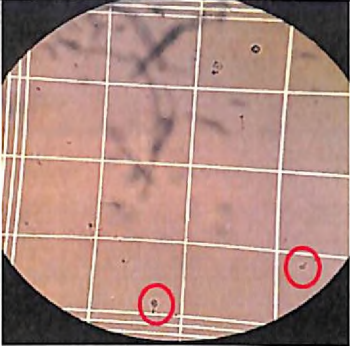
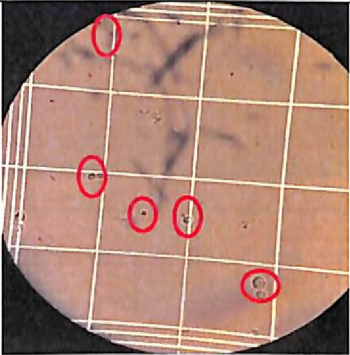
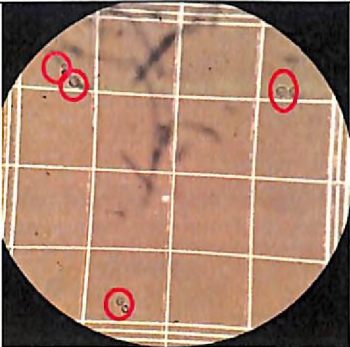
5.6.1 Counting Dead Cells (Output)

To ensure the repeatability of the device, the experiments were repeated four times. No dilution of output solution in case of dead cells is done. Therefore in this case dilution factor is taken to be 1. With the objective of determining the number of cells that came out untrapped, 1 ml of output solution was collected and counted for number of cells present. For each run, the no. of cells counted in five small chambers in centre square of hemocytometer (described in detail in Chapter 4 under Section 4.3) is detailed in Table 5.3. From Table 5.3, it was observed that the total cell out in each run is 24, 23, 26 and 24.

Table 5.3: Dead cell count in different runs

Position (hemocytometer)	No. of cells counted			
	Run 1	Run 2	Run 3	Run 4
1	2	7	10	2
2	5	7	5	8
3	4	2	2	3
4	10	4	8	9
5	3	3	1	2
Total	24	23	26	24

Microscopic view of the cells counted inside five different chambers on hemocytometer during RUN 1 is shown in Figure 5.15 below.

POSITION (hemocytometer)	RUN 1 (100X view)
1 Cell count	 <p style="text-align: center;">2</p>
2 Cell count	 <p style="text-align: center;">5</p>
3 Cell count	 <p style="text-align: center;">4</p>

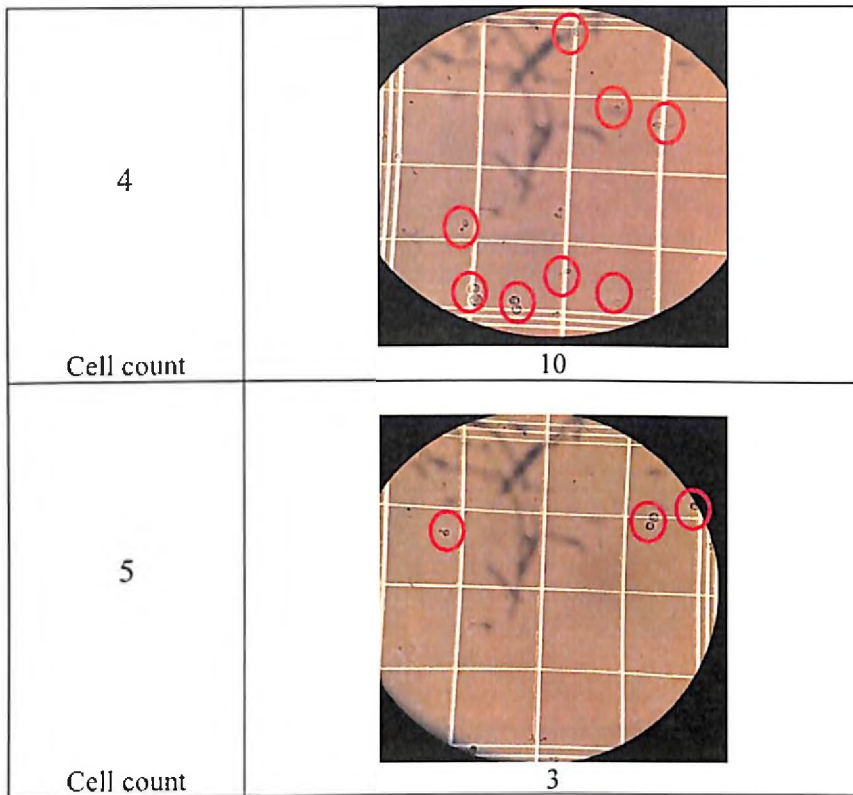


Figure 5.15: Microscopic view of dead cells in five different chambers of hemocytometer

For each run cell density and efficiency was calculated which is given in Table 5.4. The efficiency was calculated using Equation 4.1 given in Chapter 4 and is detailed in Table 5.4. The efficiency of all the four runs were comparable but maximum efficiency of 98.7% was observed in Run2.

Table 5.4: Cell density and device efficiency in different runs

Run	Avg. No. of cells	Density (No. cells/ml)	Efficiency
1	4.8	12.0×10^5	98.6%
2	4.6	11.5×10^5	98.7%
3	5.2	13.0×10^5	98.5%
4	4.8	12.0×10^5	98.6%

The efficiency in all the four runs is shown in graph Figure 5.16 below. Now, the average of the efficiency from all the four runs was calculated to be 98.6%

Efficiency of carbon device for trapping Dead cells = $98.6 + 98.7 + 98.5 + 98.6/4 = 98.6\%$

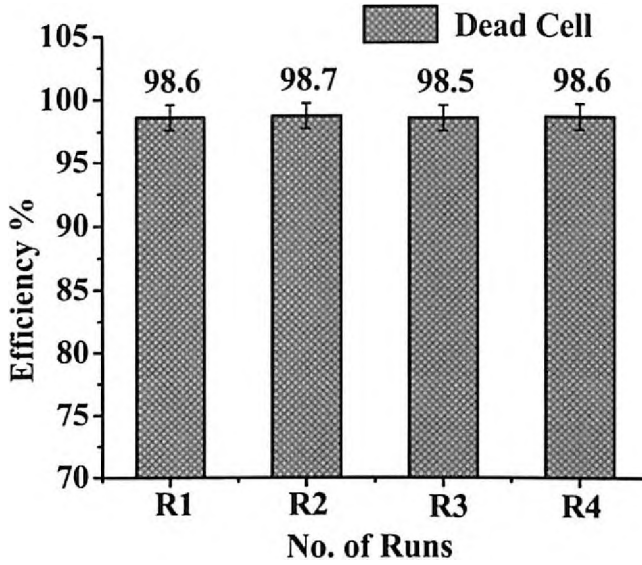


Figure 5.16: Dead cells: efficiency per run

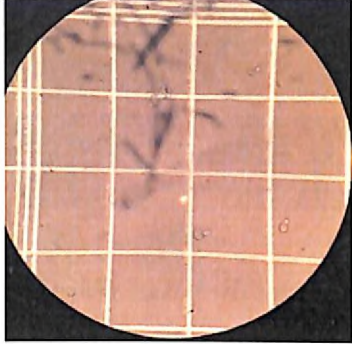
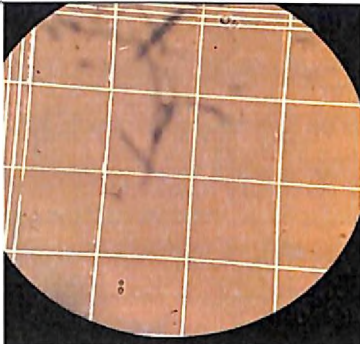
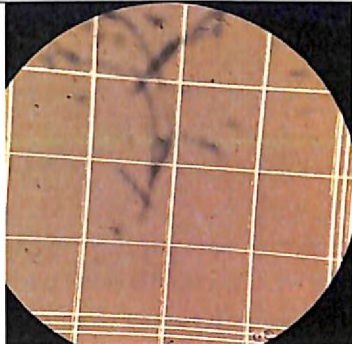
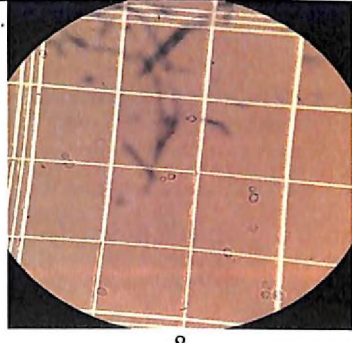
5.6.2 Counting Live Cells (Output)

In similar manner, the trapping efficiency for live cells was calculated. Again four sets of runs were performed and the cells that did not get trapped and flowed to the output were counted. In case of live cells, 0.2 μl of MB dye was mixed with the output cell solution. Therefore in this case the dilution factor calculated is 1.02. The cell count obtained from the four experiments is listed in Table 5.5 below. Total no. of cells observed in each run is 23, 20, 26 and 37.

Table 5.5: Live cell count in different runs

Position (hemocytometer)	No. of cells counted			
	Run 1	Run 2	Run 3	Run 4
1	5	3	14	10
2	2	12	2	7
3	0	0	2	8
4	8	0	3	6
5	10	5	7	6
Total	23	20	26	37

Microscopic view of the cells counted in RUN 1 is shown in Figure 5.17 below.

POSITION (hemocytometer)	RUN 1 (100X view)
1 Cell count	 5
2 Cell count	 2
3 Cell count	 0
4 Cell count	 8

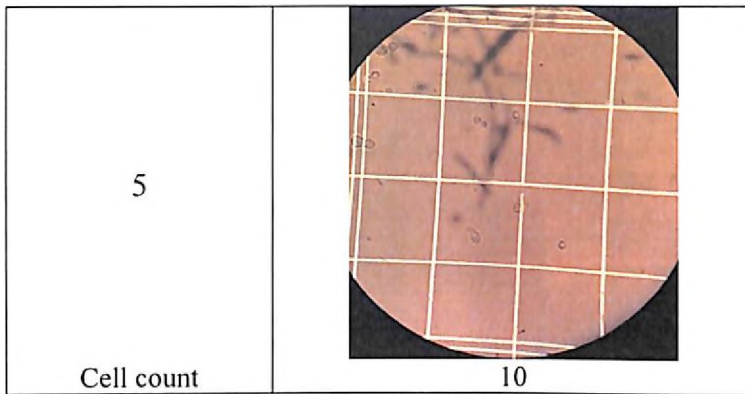


Figure 5.17: Microscopic view of live cells in five different chambers of hemocytometer

No. of cells that were observed in Run1 for all five locations is shown in Figure 5.17. For each run, the cell density and efficiency was calculated which is given in Table 5.6. The efficiency was calculated using Equation 4.1 given in chapter 4. The efficiency of all the four runs were comparable but maximum efficiency of 96.8% was observed in Run2.

Table 5.6: Cell density and device efficiency in different runs

Run	Avg. No. of cells	Density (No. cells/ml)	Efficiency
1	5.0	12.7×10^5	96.0%
2	4.0	10.2×10^5	96.8%
3	5.6	14.2×10^5	95.5%
4	7.4	18.8×10^5	94.1%

The efficiency of each of the runs is shown in graph below Figure 5.18. Now, the average of the efficiency from all the four runs was calculated

Efficiency of carbon device for trapping live cells = $96+96.8+95.5+94.1/4 = 95.6\%$

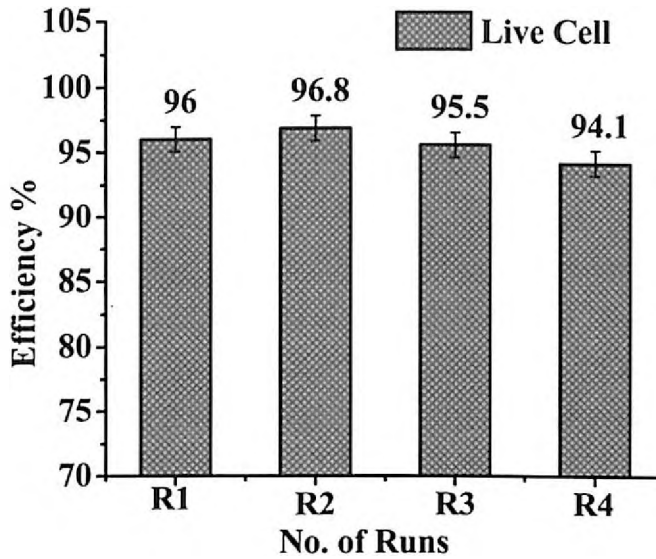


Figure 5.18: Live cells: efficiency per run

5.6.3 Viability Test

Cell viability test was performed by releasing the trapped cells from the microchannel by withdrawal of the input signal and flushing the channel with mannitol. The flushed cell suspension was now collected from the outlet reservoir and then stained with methylene blue. On staining, viable cells will reject the dye and will remain translucent while the non-viable cells will acquire blue colour. The impact of electric field on cell viability can be determined by comparing the percentage of live cells at the input and output.

Since the live cells count at the inlet has already been performed and discussed in Chapter 4 under Section 4.5.4.1, therefore now the live cell count at the outlet in the flushed cell suspension from the four runs is now determined and is given in Table 5.7 below.

Table 5.7: Trapped cell count

Position (hemocytometer)	No. of cells counted			
	Run 1	Run 2	Run 3	Run 4
1	50	61	60	45
2	65	56	63	81

3	72	70	74	52
4	70	66	40	79
5	48	65	77	55
Total	305	318	314	312

For determination of cell density, 10 μl of cell suspension was pipetted from the solution collected in the four runs respectively and to it 0.2 μl of dye and 10 μl of DI water was added and mixed thoroughly, giving dilution factor of 2.02. The cell density at the outlet was then divided with inlet cell density (32.3×10^6 cells/ml) to give % of viable cells at the outlet as described in Table 5.8.

Table 5.8: Percentage of viable cells

Run	Avg. No. of cells	Outlet cell density (No. cells/ml)	% Viability
1	61.0	30.8×10^6	95.35%
2	63.6	32.1×10^6	99.38%
3	62.8	31.7×10^6	98.14%
4	62.4	31.5×10^6	97.52%

From the above calculations, an average percentage of viable cells at the outlet was calculated to be 97.59~98%.

5.6.4 Counting Cells in Mixture

Cell mixture analysis was carried out by performing the trapping experiment twice. The cell count for both the runs is given in Table 5.9 when 300 kHz frequency was applied.

Table 5.9: Cell count in each run (300 kHz)

Position (hemocytometer)	Run 1		Run 2	
	Live cells	Dead cells	Live cells	Dead cells
1	28	7	35	6
2	30	2	26	4
3	38	5	20	5
4	40	5	42	3

5	35	4	40	5
Total	194		186	
D.F	1		1	

Table 5.10: Device efficiency for each run

Run	Avg. No. of cells	Density (No. cells/ml)	Efficiency
1	38.8	9.7×10^6	87.2%
2	37.2	9.3×10^6	87.7%

Device efficiency was obtained by calculating the average cell number and cell density in the two runs as given in Table 5.10.

Average device Efficiency is 87.45%

After, performing trapping experiment at 300 kHz and collecting 1 ml of output solution, the signal was increased to 700 kHz keeping other conditions constant. After switching the signal first 1ml of the solution was collected and discarded to make sure that the live cells that were there in the output tubing is removed from the previous run. Now, another ml of the output solution was collected in a fresh eppendorf and analyzed for cell density. The cell count of both live and dead cells in detailed in Table 5.11.

Table 5.11: Cell count in each run (700 kHz)

Position (hemocytometer)	Run 1		Run 2	
	Live Cells	Dead Cells	Live Cells	Dead Cells
1	5	28	10	41
2	2	40	4	35
3	8	32	6	26
4	4	30	7	37
5	6	35	5	20
Total	190		191	
D.F	1		1	

Device efficiency was obtained by calculating the average cell number and cell density in the two runs as given in Table 5.12:

Table 5.12: Device efficiency for each run (700 kHz)

Run	Avg. No. of cells	Density (No. cells/ml)	Efficiency
1	38	9.5×10^6	87.4%
2	38.2	9.55×10^6	87.3%

Average device Efficiency is 87.35%

5.7 Biocompatibility Test of Carbon Ink

To test the biocompatibility of carbon ink with yeast cells, a cell culture test was performed. For culturing of cells, a 50 ml of yeast extract, peptone and D-glucose media (Y- 0.25 gms, P- 0.5 gms, D – 1 gms) was prepared in a flask. From this 50 ml solution, a 5ml media was taken in a separate test tube. Now, to the rest of 45 ml media solution a 2% Agar i.e 0.9 gms was added and mixed gently. The flask and the tube were now autoclaved at 121°C for 30 min at 15 psi to kill all micro-organisms and spores. After autoclaving the media was allowed to cool to room temperature. After cooling, 45ml of media solution was poured into two petri dishes namely control and test and was allowed to solidify. While in the 5 ml of media, 10 mg of dry active yeast was added and mixed thoroughly. After solidification, in the control petri dish 100 µl of cell suspension was pipetted and spread thoroughly using a sterile spreader under laminar flow cabinet. While in the test petri dish, first 100 µl of carbon ink was pipette (that was dissolved in 1 ml of alcohol) and spread thoroughly followed by the spreading of 100 µl of cell suspension.

It is to be noted that all the above procedure was performed in laminar hood to prevent the cells and media from any contamination. The two petri dishes were covered and then placed in an incubator at 30°C for overnight. Figure 5.19 shows (a) control petri dish with just media and cells, and (b) shows test petri dish with encircled particles of carbon ink.

The two petri dishes were then observed after 14 hrs as shown in Figure 5.19 (c,d), 20 hrs as shown in Figure 5.19 (e,f) and 25 hrs as shown in Figure 5.19 (g,h). It was observed that the yeast cells growth occurred in both the petri dishes and with the time elapsed the growth also increased in the two petri dishes.

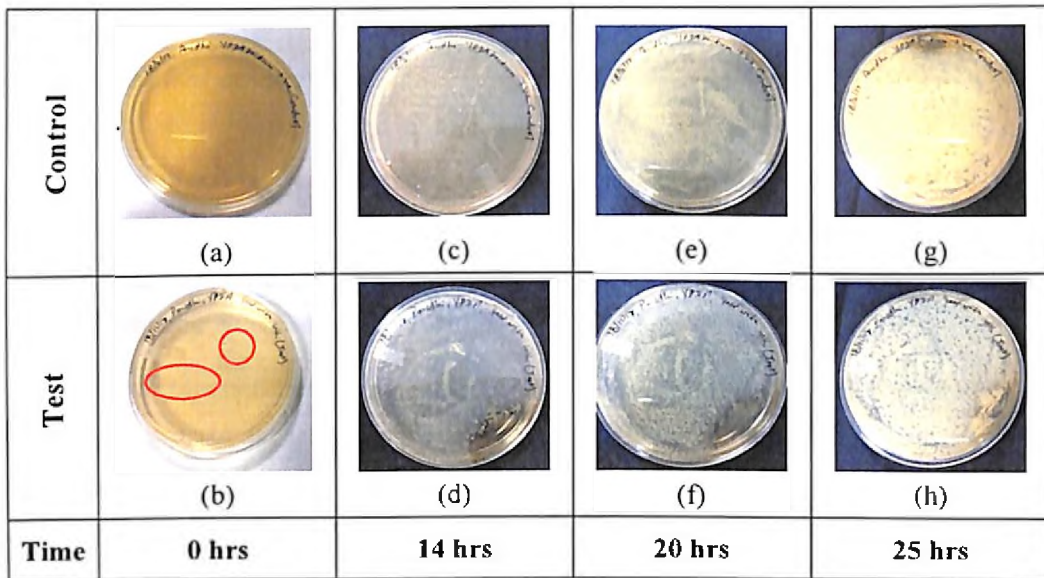


Figure 5.19: (a) Control petri dish, (b) Test petri dish, Cell growth in both control and test petri dishes after (c,d) 14 hrs, (e,f) 20 hrs, (g,h) 25 hrs

5.8 Conclusions

1. Carbon electrode based DEP device is successfully fabricated and tested. The SU-8 microchannel is fabricated over 18 μm thick screen printed carbon electrode. An adhesive bonding technique is used to make perfect sealing between the two glass substrates. The device leakage proof testing was carried out by flushing of the DI water after the bonding of the two glass substrates.
2. Screen printing proved to be an easy and cost effective process for fabricating carbon electrodes. It is less time consuming when compared to the commonly reported carbonisation or pyrolysis process. Pyrolysis requires high temperature $\sim 1100^\circ\text{C}$, which in turn makes the process costly because high temperature substrates are required for carbonisation and the shrinkage of the polymer presents another fabrication challenge. Also it has been reported that screen printed carbon electrodes possess porous and coarse surface therefore, the electric field is more non-uniform than the smooth metal electrodes that further improves the DEP force acting on any particle [17].
3. Screen printed carbon test structures with different widths were fabricated for analyzing the minimum feature size that can be printed. The resistance of these test structures was measured using IV-CV probe system. The value of resistance was

higher than that of fabricated gold electrodes, but it was still sufficient to create the required non uniform electric field and cause cell trapping. Keeping the channel height same as taken in case of gold electrode i.e $\sim 30\mu\text{m}$, the trapping efficiency of screen printed carbon device was calculated to be 98.6% for dead cells and 95.6% for live cells, which is higher than the trapping efficiency of gold device. Such good trapping efficiency clearly indicated that carbon electrodes can be used as a cost effective alternative to gold.

4. Also, we reported the packaging of the fabricated device using glass substrate. The glass substrate is a good alternative to commonly reported PDMS or pressure sensitive adhesive (PSA). Fabrication of PDMS replica requires master mold which is fabricated in clean room following a number of processes eg etching, lithography etc which add ones to the cost. On the other hand the microchannel cut out of PSA requires the use of rolling press to seal the device. This operation is challenging when using fragile substrates like Si or glass. Therefore closing the microchannel with glass was an easy alternative as it just required a thin SU-8 coating that acts as an adhesive. The fabricated device was tested to be leakage proof. In addition the mixture of the both type of cell was also studied and investigated. Our approach successfully trapped the yeast cells while preserving the viability of live cells as discussed in Section 5.6.3. Additionally, we have demonstrated n-DEP trapping of yeast cells with the purpose of inducing less stress on the cell. This is because the p-DEP force is twice as strong as a n-DEP force and induces stress on a particle during p-DEP capture thereby resulting in cell damage.
5. We also investigated the cellular response or biocompatibility of yeast cells with conductive paste of carbon. We observed that the cells growth occurred in both control as well as in test petri dishes. Also, the growth seems to increase with time in each of the dishes. The result indicates its usefulness in eventual studies involving carbon-MEMS devices.

References

- [1] P. R. C. Gascoyne and J. V. Vykoukal, "Dielectrophoresis-based sample handling in general purpose programmable diagnostic instruments," *Proc. IEEE*, vol. 92, no. 1, pp. 22–42, 2004.
- [2] N. Green and H. Morgan, "Dielectrophoretic separation of nanoparticles," *J. Phys. D. Appl. Phys.*, vol. 30, no. 11, p. L41, 1997.
- [3] R. Pethig, "Dielectrophoresis: Status of the theory, technology, and applications," *Biomicrofluidics*, vol. 4, no. 2, p. 022811, 2010.
- [4] N. G. Green and H. Morgan, "Dielectrophoretic investigations of sub-micrometre latex spheres," *J. Phys. D. Appl. Phys.*, vol. 30, no. 18, pp. 2626–2633, 1997.
- [5] R. Martinez-Duarte, P. Renaud, and M. J. Madou, "A novel approach to dielectrophoresis using carbon electrodes," *Electrophoresis*, vol. 32, no. 17, pp. 2385–2392, 2011.
- [6] M. del C. Jaramillo, E. Torrents, R. Marinez-Duarte, M. J. Madou, and A. Juarez, "On-line separation of bacterial cells by carbon-electrode dielectrophoresis," *Electrophoresis*, vol. 31, no. 17, pp. 2921–2928, 2010.
- [7] H. Shafiee, J. L. Caldwell, M. B. Sano, and R. V. Davalos, "Contactless dielectrophoresis: A new technique for cell manipulation," *Biomed. Microdevices*, vol. 11, no. 5, pp. 997–1006, 2009.
- [8] H. Shafiee, M. B. Sano, E. A. Henslee, J. L. Caldwell, and R. V. Davalos, "Selective isolation of live/dead cells using contactless dielectrophoresis (cDEP)," *Lab Chip*, vol. 10, no. 4, pp. 438–445, 2010.
- [9] X. Niu, S. Peng, L. Liu, W. Wen, and P. Sheng, "Characterizing and patterning of PDMS-based conducting composites," *Adv. Mater.*, vol. 19, no. 18, pp. 2682–2686, 2007.
- [10] X. Gong and W. Wen, "Polydimethylsiloxane-based conducting composites and their applications in microfluidic chip fabrication," *Biomicrofluidics*, vol. 3, no. 1, p. 012007, 2009.
- [11] P. Puri, V. Kumar, S. U. Belgamwar, and N. N. Sharma, "Microfluidic Device for Cell Trapping with Carbon Electrodes Using Dielectrophoresis," *Biomed. Microdevices*, vol. 20, no. 4, p. 102, 2018.
- [12] D. Christopher, L. Julian, and W. A. R., "Printed Microfluidics," *Adv. Funct. Mater.*, vol. 27, no. 11, pp. 1604824–1604835, 2017.
- [13] X. Lin, J. Yao, H. Dong, and X. Cao, "Effective Cell and Particle Sorting and Separation in Screen-Printed Continuous-Flow Microfluidic Devices with 3D Sidewall Electrodes," *Ind. Eng. Chem. Res.*, vol. 55, no. 51, pp. 13085–13093, 2016.
- [14] H. Zhu, X. Lin, Y. Su, H. Dong, and J. Wu, "Screen-printed microfluidic dielectrophoresis chip for cell separation," *Biosens. Bioelectron.*, vol. 63, pp. 371–378, 2015.
- [15] T. Gervais, J. El-Ali, A. Gunther, and K. F. Jensen, "Flow-induced deformation of shallow microfluidic channels," *Lab Chip*, vol. 6, no. 4, pp. 500–507, 2006.

- [16] M. W. Toepke and D. J. Beebe, "PDMS absorption of small molecules and consequences in microfluidic applications." *Lab Chip*, vol. 6, no. 12, pp. 1484–1486, 2006.
- [17] M. Tang, Y. Ma, and P. Yang, "The theory research and electric field simulation of the AHPC," in *Journal of Physics: Conference Series*, 2013. p. 012010.

Overall Conclusions and Future Scope

6.1 Overall Conclusions

Two goals comprised the research efforts of this dissertation. The first goal was to fabricate a microfluidic device with electrodes made out of carbon instead of very commonly used gold. The second aim was to test the fabricated device with carbon electrode for cell trapping and also compare its performance with that of fabricated gold electrode based DEP device. This chapter goes over the main points of the research on screen printed carbon based DEP device and provides future research directions and possible guidelines in the respective area. The important results of the present study are summarized in the following paragraphs.

1. From literature review we studied various 2D and 3D commonly used electrode geometries that are widely reported in literature (castellated, interdigitated, extruded, and 3D posts of pyrolysed carbon etc). Since carbon electrodes fabricated with printing technology for DEP cell trapping application is less perused in literature, the investigation on this aspect forms an interesting premises of research and investigations.
2. In chapter 4, gold electrode based 2D DEP device has been fabricated using the traditional photolithography method and sputtering. Gold electrodes of height 200nm were fabricated using sputtering in the microfluidic channel of height 30 μ m. SU-8 based microchannel is fabricated over the 200nm thick gold electrode. An adhesive bonding technique is used to make perfect sealing between the glass and silicon. The fabricated device was initially tested for leakage by flowing DI water through the channel and no leakage was observed. No leakage indicates that both silicon and glass substrate has bonded well with each other.
3. For testing of the fabricated device was performed using yeast cells. The yeast cells were grown using Yeast, Peptone and D-glucose (YPD) media. The

procedure for cell growth and culturing was carried out in a sterile environment i.e. under laminar flow to prevent any contamination.

4. We observed from the experiments, the dead cells are got trapped at 300 kHz frequency, and the live cell got trapped at 700 kHz frequency. The reason behind this frequency specific response is that in case of dead cells their cell wall is damaged therefore electric lines can easily pass through the cells and cause it to trap at lower frequency. However, when a cell is live, the cell membrane is intact and insulating and the electric field is not able to penetrate at lower frequency. To overcome this resistance offered by the cell membrane, higher frequency is required to trap the cell.
5. The efficiency of the gold electrode DEP device is also investigated for both live and dead cells. For each of the cells, four runs were performed. In case of dead cells, the calculated device efficiency is 97.9% and in the case of live cells the device efficiency is calculated to be 94.3%. The efficiency is comparable with the other dielectrophoretic devices that have been proposed and reported in literature. However the efficiency of the device can further be increased if 3D electrodes were employed, as in case of 3D electrodes the electric field is distributed across whole of the channel unlike 2D electrodes where the electric lines remained confined near the vicinity of the electrodes.
6. Trapping efficiency of the device was also calculated when a suspension containing both live and dead yeast cells was inserted in the channel. The efficiency of the device was calculated to be 84.2%. One of the primary motivations in performing this experiment is that when the subpopulation of same type of cells with the same radius are separated, the DEP force difference occurs only based on the real part of the CM factor, which might be a challenge for cell separation applications.
7. In chapter 5, carbon electrode based DEP device was fabricated and tested. For making carbon electrodes screen printing method was adopted. Screen printing has proven to be a good alternative to resist pyrolysis, which is one of the widely used method to fabricate carbon electrodes. Printing allows multiple components to be fabricated simultaneously, with relatively few processing steps and few sources of materials. Replacing subtractive processes such as photolithography

and etching with additive processes reduces process complexity as well as materials waste. This makes printing a low cost process with the production of fully disposable microfluidic devices. The SU-8 based microchannel is fabricated over 18 μm thick screen printed carbon electrodes, the channel height remained constant as in the case of gold electrodes. The device was covered with glass substrate, in order to allow easy visualization. An adhesive bonding technique was used to make perfect sealing between the two glass substrates. The device leakage proof testing was carried out by flushing of the DI water after the bonding of the channel.

8. It was observed that cell trapping in carbon electrodes occurred at 300 kHz for dead cells and 800 kHz for live cells, when 10Vp-p signal and flow rate of 0.5ml/hr was applied.
9. The resistivity of the screen printed carbon electrodes was measured using four probe system and was found out to be 300 K Ω . The value of resistivity was higher than that of fabricated gold electrodes, but it was still sufficient to create the required non uniform electric field and cause cell trapping. Keeping the channel height same as taken in case of gold electrode i.e $\sim 30\mu\text{m}$, the trapping efficiency of screen printed carbon device was calculated to be 98.6% for dead cells and 95.6% for live cells, which is higher than the trapping efficiency of gold device. It was observed that the % difference in the trapping efficiency of carbon electrodes is approximately 2% higher than that of gold electrodes. Therefore it is inferred from this study that carbon can prove to be a cheap and reliable alternative to gold in near future, and the excellent properties of carbon should be exploited complimentary to, alternative to and beyond noble metals material capabilities. More efficient devices not only needs to be constructed from a low cost material but also from inexpensive fabrication techniques.
10. Also, we reported the packaging of the fabricated device using glass substrate. The glass substrate is a good alternative to PDMS. The fabricated device was tested to be leakage proof. In addition the mixture of the both type of cell was also studied and investigated. It is observed that cell got trapped on investigated frequency of respective cell when the mixture solution is used. Our approach successfully trapped the dead cells while preserving the viability of live cells.

11. The cellular response of yeast cells with conductive paste of carbon was also investigated. It was observed that the cells growth occurred in both control as well as test petri dishes. Also, the growth seems to increase with time in each of the dishes. The result indicates its usefulness in eventual studies involving carbon-MEMS devices.

6.2 Future Scope of the Work

No research concludes with an absolute end. There is enough room for innovation in the fabrication of cost effective DEP devices. Several materials like conductive carbon inks, polymers with high carbon contents needs better understanding so that fabrication design strategies can be improved further. The research in this area will find a milestone when the carbon will be used in various microfluidic applications. From the perspective of present work, the following aspects can be studied and investigated further.

1. Screen printing while also capable of forming electrodes, suffers from reduced resolution, larger minimum feature size and require a mask for each design. But, screen printing is uniquely useful for forming microchannels and the throughput of this technique makes it attractive for high volume manufacturing. From various printing techniques we have chosen screen printing to fabricate innovative C-serpentine electrodes. Other printing technologies like inkjet jet printing or solid wax printing can be explored to fabricate cost effective DEP devices.
2. The fabricated device can be tested for various other cell types with different medium conductivities. Due to lack of facility, this study was not been able to be conducted during this thesis.
3. Study of different forces acting on a particle under the influence of DEP can be performed using numerical modeling technique. This will help in numerically predicting the cell trapping frequency of the respective cell.

Equipments used

Chemical Wet Bench:

The chemical wet bench is used for 2-6" silicon wafers prior to processing in diffusion furnaces, LPCVD furnaces or before metal depositions. The clean performed are high quality, final cleans which precede high temperature processing. The wet bench has different acids baths for Piranha, RCA1, RCA2 and HF dip as shown in Figure A-1. The bench includes the controller used to control the time and temperature of the bath during the cleaning. The same type of bench also used for chemical texturing of the silicon.

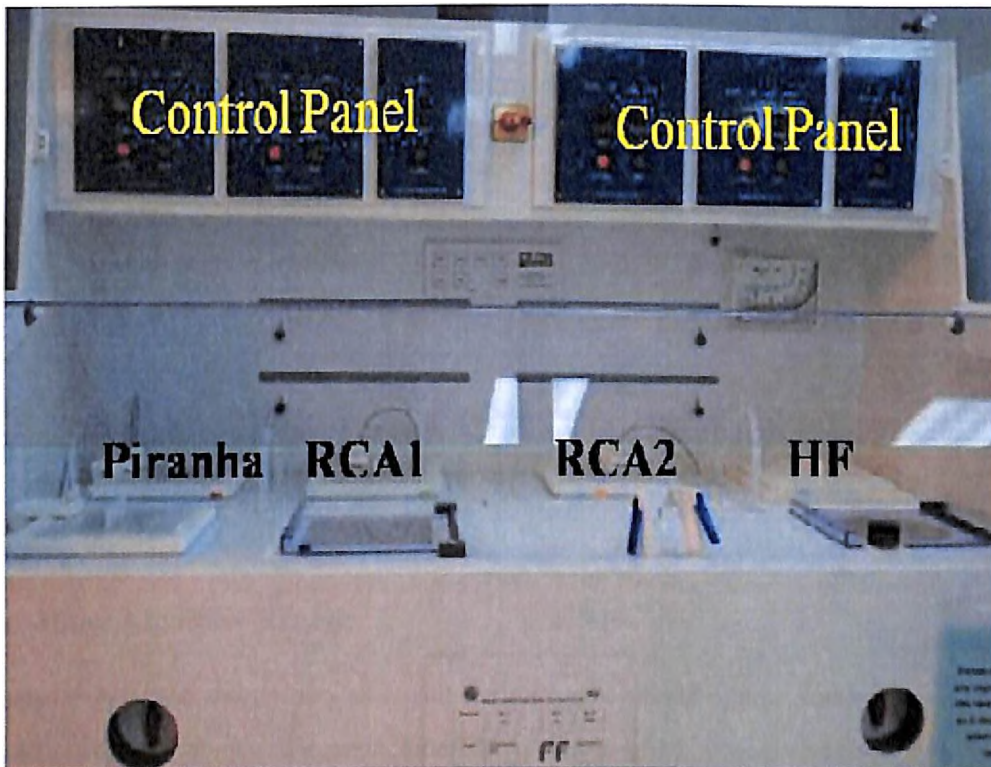


Figure A1: Chemical wet bench set up for cleaning and etching purpose

Screen Printing System:

Screen printing machine is used for pattern transferring onto a desired surface. It is an act of pushing variety of inks through a stencil as the squeegee is moved across it.

This causes the ink to get transferred onto the surface except in the areas that are made impermeable. The machine used for screen printing is shown in Figure A-2.



Figure A2: Screen printing system

Laminar Air Flow Bench:

Laminar Air Flow Bench is also called Tissue culture hood and is a type of enclosed bench, designed to prevent contamination of any particle sensitive material. In the cabinet, air is drawn through HEPA filters and blown in very smooth laminar flow towards the user. The cabinet is also equipped with a UV lamp that helps to sterilize the interior and the contents before usage in order to prevent any contamination during sample preparation. Laminar cabinet is shown in Figure A-3.

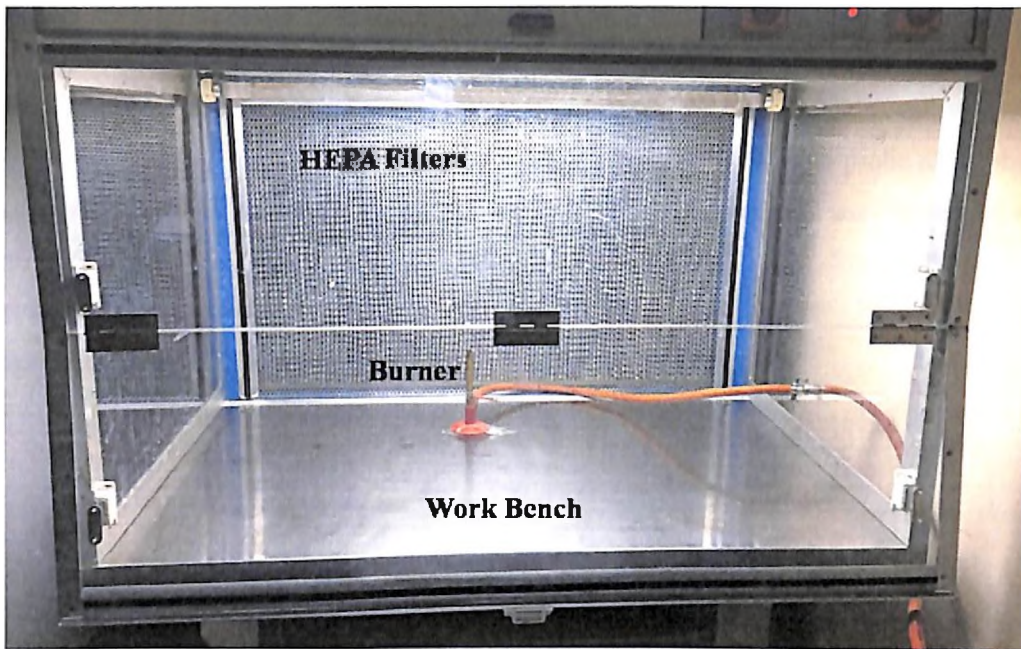


Figure A3: Laminar air flow system

Hemocytometer:

The hemocytometer is a device originally designed and usually used for counting blood cells. The hemocytometer was invented by Louis-Charles Malassez and consists of a thick glass microscope slide with a rectangular indentation that creates a chamber. This chamber is engraved with a laser-etched grid of perpendicular lines. The device is carefully crafted so that the area bounded by the lines is known, and the depth of the chamber is also known. By observing a defined area of the grid, it is therefore possible to count the number of cells or particles in a specific volume of fluid, and thereby calculate the concentration of cells in the fluid overall.

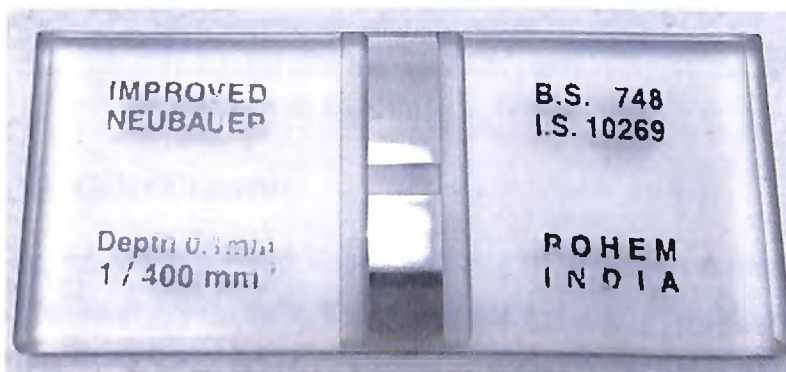


Figure A-4: Hemocytometer

Dektak Stylus Profiler System:

Stylus Profiler System is used to measure surface profile such as steps and curvature. A stylus profiler uses a probe to detect the surface, physically moving a probe along the surface in order to acquire the surface height. A feedback system is used to keep the arm with a specific amount of torque on it, known as set-point. The changes in the z-position of arm holder can then be used to reconstruct the surface. Stylus profiler system is shown in Figure A-5.



Figure A-5: DEKTAK, stylus profiler

Digital CCD Color Camera:

The QImaging MicroPublisher with real-time viewing (RTV) camera as shown in Figure A-6 is used for viewing yeast cells. The 30-bit color digitization produces high-quality images of brightfield, darkfield, and fluorescence work. The MicroPublisher 5.0 RTV has a pixel size of $3.4\mu\text{m}\times 3.4\mu\text{m}$ and resolution of 5 million real pixels. The camera is

equipped with an objective lens of 10X, 40X and 100X magnification that helps in better visualization.

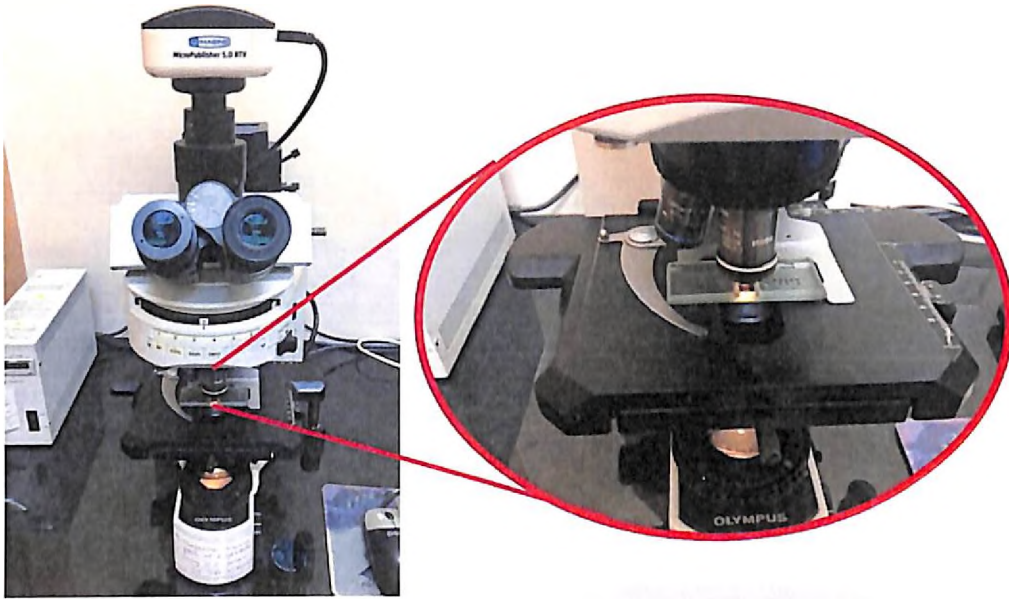


Figure A-6: Digital CCD color camera

MATLAB Code for Calculating Massotti Factor

DEAD CELLS

```

clear;
clc;

r1 = 2.5e-6; % m
r2 = 2.25e-6; % m
r3 = 2.242e-6; % m

sigma_1 = 15e-4; % S/m
sigma_2 = 1.6e-4; % S/m
sigma_3 = 7e-3; % S/m
sigma_f = 70e-4; % S/m

e_0 = 8.85e-12;
e_1 = 60*e_0;
e_2 = 6*e_0;
e_3 = 50*e_0;
e_f = 6.9e-10;

omega = (0:1:1000)*1e3;

e_com_1 = e_1 - (sigma_1./omega)*1j;
e_com_2 = e_2 - (sigma_2./omega)*1j;
e_com_3 = e_3 - (sigma_3./omega)*1j;

e_com_f = e_f - (sigma_f./omega)*1j;

C = (r2/r3)^3 + 2*((e_com_3-e_com_2)./(e_com_3 + 2*e_com_2));
D = (r2/r3)^3 - ((e_com_3-e_com_2)./(e_com_3 + 2*e_com_2));

e_com_23 = e_com_2 .* C./D;

A = (r1/r2)^3 + 2*((e_com_23-e_com_1)./(e_com_23 + 2*e_com_1));
B = (r1/r2)^3 - ((e_com_23-e_com_1)./(e_com_23 + 2*e_com_1));

e_com_p_1 = e_com_1 .* A./B;
%e_com_1 * A/B

fcm_1 = (e_com_p_1 - e_com_f)./(e_com_p_1+2*e_com_f); %

figure(1);
plot(omega,real(e_com_p_1));
xlabel('omega');
ylabel('e-com-p');

figure(2);
plot(omega,real(fcm_1));

```

```
xlabel('omega');
ylabel('E_c[M]');
```

LIVE CELLS

```
clear;
clc;

r1 = 3e-6; % m
r2 = 2.78e-6; % m
r3 = 2.772e-6; % m

sigma_1 = 14e-3; % S/m
sigma_2 = 25e-8; % S/m
sigma_3 = 0.2; % S/m
sigma_f = 110e-4; % S/m

e_0 = 8.85e-12;
e_1 = 60*e_0;
e_2 = 6*e_0;
e_3 = 50*e_0;
e_f = 6.9e-10;

omega = (0:1:1000)*1e3;

e_com_1 = e_1 - (sigma_1./omega)*1j;
e_com_2 = e_2 - (sigma_2./omega)*1j;
e_com_3 = e_3 - (sigma_3./omega)*1j;

e_com_f = e_f - (sigma_f./omega)*1j;

C = (r2/r3)^3 + 2*((e_com_3-e_com_2)./(e_com_3 + 2*e_com_2));
D = (r2/r3)^3 - ((e_com_3-e_com_2)./(e_com_3 + 2*e_com_2));

e_com_23 = e_com_2 .* C./D;

A = (r1/r2)^3 + 2*((e_com_23-e_com_1)./(e_com_23 + 2*e_com_1));
B = (r1/r2)^3 - ((e_com_23-e_com_1)./(e_com_23 + 2*e_com_1));

e_com_p_1 = e_com_1 .* A./B;
%e_com_1 * A/B

fcm_1 = (e_com_p_1 - e_com_f)./(e_com_p_1+2*e_com_f); %

figure(1);
plot(omega,real(e_com_p_1));
xlabel('omega');
ylabel('e-com-p');

figure(2);
plot(omega,real(fcm_1));
```

```
xlabel('omega');
ylabel('r_C_M');
```

CELL MIXTURE

```
clear;
clc;
```

```
r1 = 3e-6; % m
r2 = 2.78e-6; % m
r3 = 2.772e-6; % m
```

```
sigma_1 = 14e-3; % S/m
sigma_2 = 25e-8; % S/m
sigma_3 = 0.2; % S/m
sigma_f = 100e-4; % S/m
```

```
e_0 = 8.85e-12;
e_1 = 60*e_0;
e_2 = 6*e_0;
e_3 = 50*e_0;
e_f = 6.9e-10;
```

```
omega = (0:1:1000)*1e3;
```

```
e_com_1 = e_1 - (sigma_1./omega)*1j;
e_com_2 = e_2 - (sigma_2./omega)*1j;
e_com_3 = e_3 - (sigma_3./omega)*1j;
```

```
e_com_f = e_f - (sigma_f./omega)*1j;
```

```
C = (r2/r3)^3 + 2*((e_com_3-e_com_2)./(e_com_3 + 2*e_com_2));
D = (r2/r3)^3 - ((e_com_3-e_com_2)./(e_com_3 + 2*e_com_2));
```

```
e_com_23 = e_com_2 .* C./D;
```

```
A = (r1/r2)^3 + 2*((e_com_23-e_com_1)./(e_com_23 + 2*e_com_1));
B = (r1/r2)^3 - ((e_com_23-e_com_1)./(e_com_23 + 2*e_com_1));
```

```
e_com_p_1 = e_com_1 .* A./B;
%e_com_1 * A/B
```

```
fcm_1 = (e_com_p_1 - e_com_f)./(e_com_p_1+2*e_com_f); %
```

```
%%
```

```
r1 = 2.5e-6; % m
r2 = 2.25e-6; % m
r3 = 2.242e-6; % m
```

```
sigma_1 = 15e-4; % S/m
sigma_2 = 1.6e-4; % S/m
sigma_3 = 7e-3; % S/m
```



```

sigma_f = 100e-4; % S/m

e_0 = 8.85e-12;
e_1 = 60*e_0;
e_2 = 6*e_0;
e_3 = 50*e_0;

e_f = 6.9e-10;

omega = (0:1:1000)*1e3;

e_com_1 = e_1 - (sigma_1./omega)*1j;
e_com_2 = e_2 - (sigma_2./omega)*1j;
e_com_3 = e_3 - (sigma_3./omega)*1j;

e_com_f = e_f - (sigma_f./omega)*1j;

C = (r2/r3)^3 + 2*((e_com_3-e_com_2)./(e_com_3 + 2*e_com_2));
D = (r2/r3)^3 - ((e_com_3-e_com_2)./(e_com_3 + 2*e_com_2));

e_com_23 = e_com_2 .* C./D;

A = (r1/r2)^3 + 2*((e_com_23-e_com_1)./(e_com_23 + 2*e_com_1));
B = (r1/r2)^3 - ((e_com_23-e_com_1)./(e_com_23 + 2*e_com_1));

e_com_p_2 = e_com_1 .* A./B;
e_com_1 .* A/B

fcm_2 = (e_com_p_2 - e_com_f)./(e_com_p_2+2*e_com_f);

figure(1);
plot(omega,real(e_com_p_1),omega,real(e_com_p_2));
xlabel('omega');
ylabel('e-com-p');
legend('Live cell','Dead cell');
figure(2);
plot(omega,real(fcm_1),omega,real(fcm_2));
xlabel('omega');
ylabel('f_C_M');
legend('Live cell','Dead cell');

```

Simulation Steps for Determining Electric Field Gradient

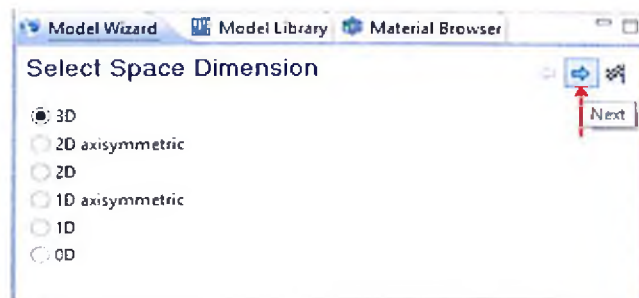
This section details the simulation steps taken to carry out a comparative analysis of electric field gradient generated by different geometries as discussed in Chapter 3 under Section 3.2. In the section below, the simulation steps involved in the study of only bell shaped electrodes are defined in detail. For other geometries, the simulation steps are the same as defined for bell shaped structure.

The simulation can be divided in following few steps:-

- Domain selection
- Physics and study selection
- Building geometry
- Defining material
- Applying boundary conditions
- Meshing
- Study

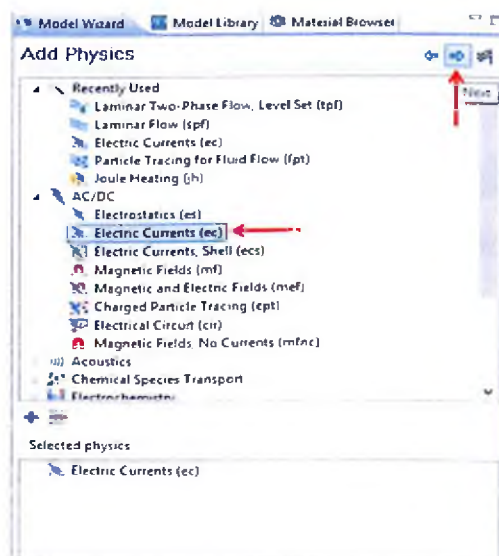
1. Domain selection

First step is to select space domain. This domain can either be 0, 1, 2 or 3D and can be selected under select space dimension head. In our study, 3D domain is selected.



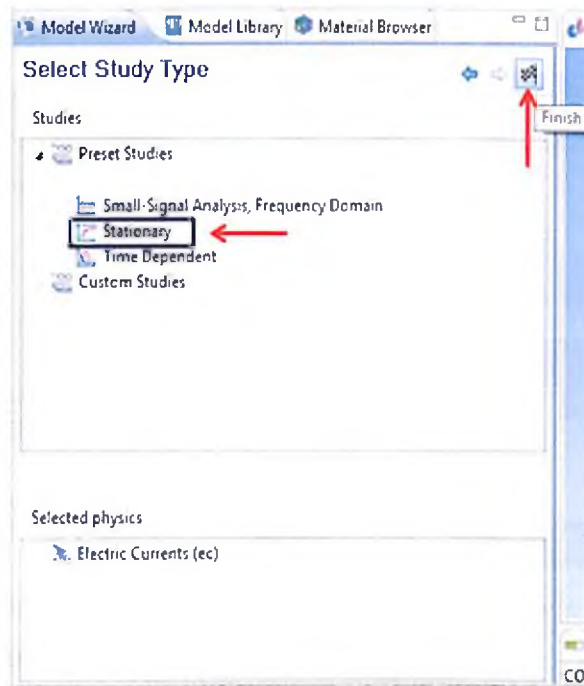
2. Physics selection

Under this step, the physics which is to be studied is selected followed by pressing next button. In our work, we selected electric current physics under AC/DC module.



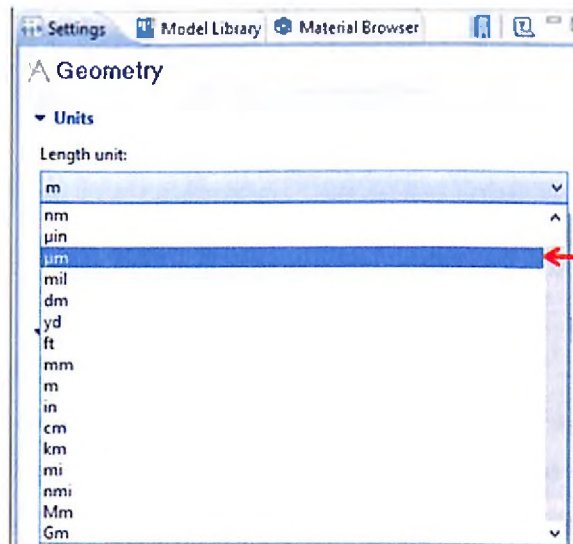
3. Study selection

Under this step, the study which is to be applied is selected followed by pressing finish button. In our work, we selected stationary study under select study type column.



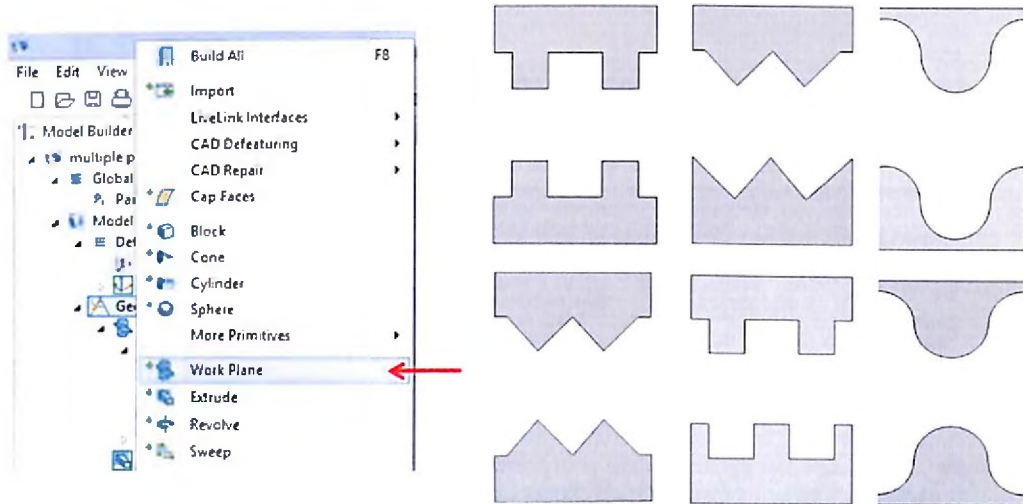
4. Unit selection

Under this step, the unit of the dimension which is to be constructed is selected under geometry head. Here μm dimension is selected.

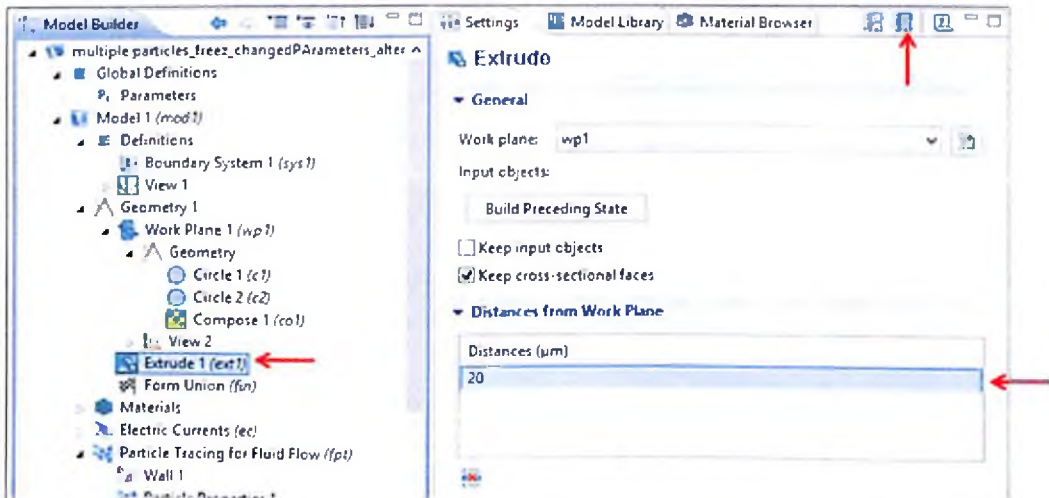


5. Building geometry

For building a 3D geometry, select work plane under geometry head. And under this work plane, click onto plain geometry and select the shape that is to be drawn. In this study, different set and off set electrode geometries were drawn and the gap between the electrode pair is $200\ \mu\text{m}$.



After drawing the geometries, the work plane is extruded to a height of $20\ \mu\text{m}$ so as to obtain 3D electrode structures.



6. Defining material

After drawing the geometry, material is defined to each of the domains. In this simulation study the electrodes (domain 2, 3) are defined as gold and the surrounding medium (domain 1) is defined as water. The material properties considered for gold and water respectively are tick marked in green.

Defining Gold

Settings

Label: Au - Gold

Geometric Entity Selection

Geometric entity level: Domain

Selection: Manual

Active: 2
3

Override

Material Properties

Material Contents

Property	Variable	Value	Unit	Property group
<input checked="" type="checkbox"/> Electrical conductivity	sigma...	45.6e6[S...	S/m	Basic
<input checked="" type="checkbox"/> Relative permittivity	epsilo...	1	1	Basic
Coefficient of thermal expans...	alpha...	14.2e-6[1/...	1/K	Basic
Heat capacity at constant pres...	Cp	1251[J/(k...	J/(kg K)	Basic
Density	rho	19320[kg/...	kg/m ³	Basic
Thermal conductivity	k_iso...	317[W/(m...	W/(m...)	Basic
Young's modulus	E	70e9[Pa]	Pa	Young's modulus and
Poisson's ratio	nu	0.43	1	Young's modulus and

Defining Water

Settings

Label: Water

Geometric Entity Selection

Geometric entity level: Domain

Selection: Manual

Active: 1

Override

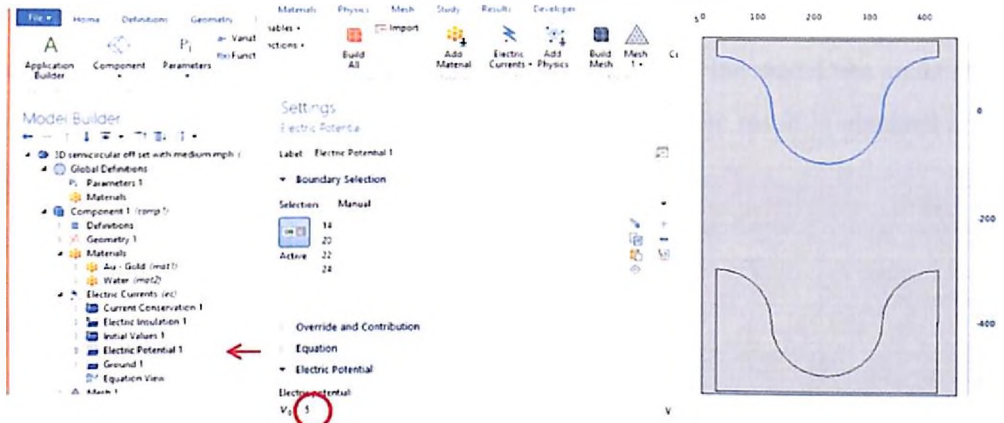
Material Properties

Material Contents

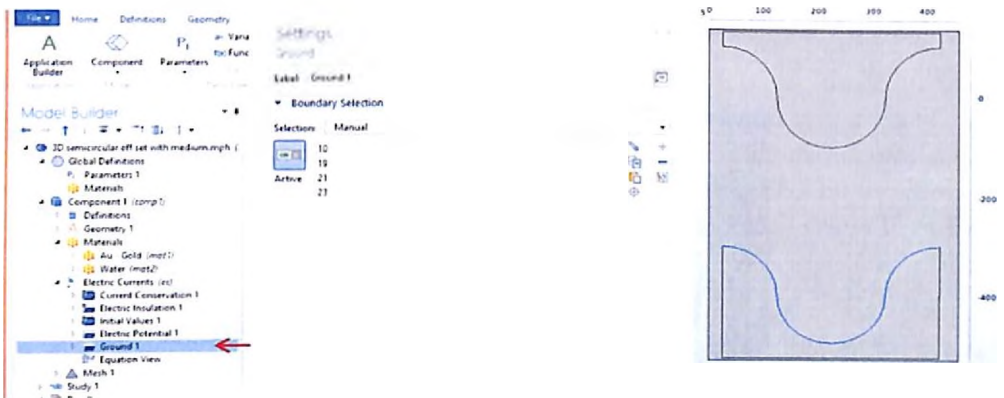
Property	Variable	Value	Unit	Property group
<input checked="" type="checkbox"/> Electrical conductivity	sigma...	5.5e-6[S...	S/m	Basic
<input checked="" type="checkbox"/> Relative permittivity	epsilo...	80	1	Basic
Dynamic viscosity	mu	0.01[1/...	Pa·s	Basic
Ratio of specific heats	gammas	1.0	1	Basic
Heat capacity at constant pres...	Cp	Cp(T[1/...	J/(kg K)	Basic
Density	rho	rho(T[1/...	kg/m ³	Basic
Thermal conductivity	k_iso...	k(T[1/K]...	W/(m...)	Basic
Speed of sound	c	cs(T[1/K]...	m/s	Basic

7. Applying boundary conditions

After defining the material to the geometry, the boundary conditions are applied. Under electric currents we selected electric potential 1 and selected the boundaries of one of the electrode at which a potential of 5V is applied.

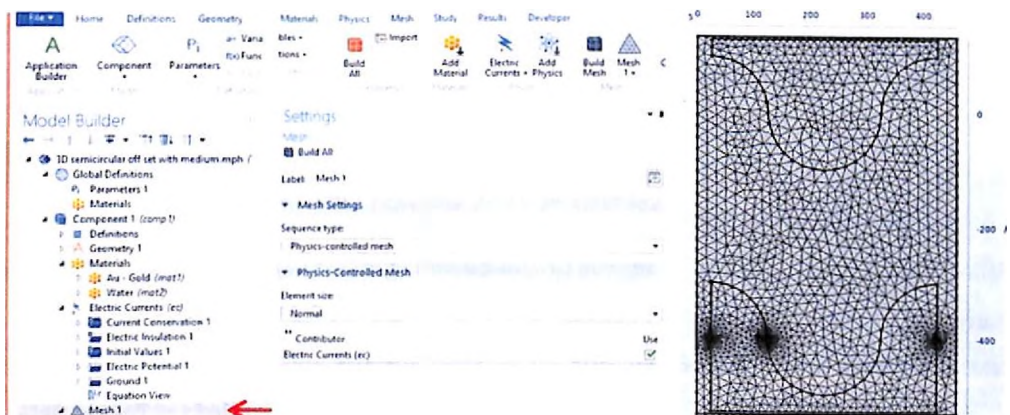


The boundary of other electrode is selected and is defined as ground 1.



8. Meshing

In this step, the geometry is divided into small geometric domains via mesh. The mesh used here is triangular mesh with normal mesh size.



9. Study

After carrying out the above steps, the last thing is to compute the model tree under study head. After the software finishes its computation, a plot of the result is obtained in the graphics window.

Fabrication of Circular Channel Electrode

Fabrication Details

1. Mask design

Gold electrode based DEP device includes a two mask process which is illustrated in Figure B1. Mask#1 is gold electrode mask which is shown in Figure B1(a) whereas Mask#2 is the mask for microchannel which is shown in Figure B1(b). L-Edit Layout Editor tool is used for designing of the mask layout. In the mask layout the width of the electrode and microchannel is 150 nm and 1mm respectively.

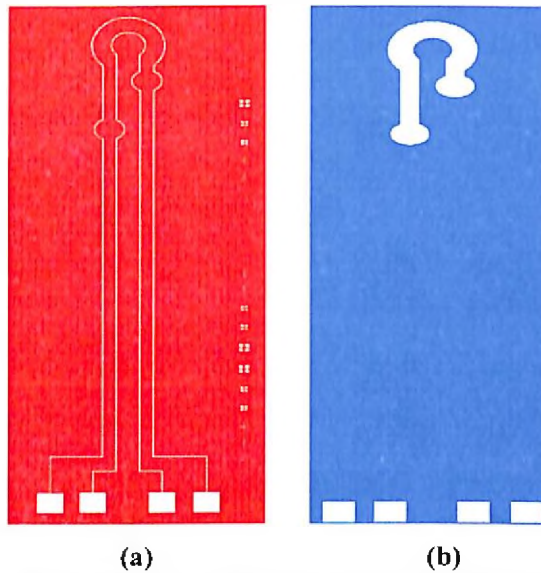


Figure B1: L-EDIT mask layout (a) Electrode mask (b) Microchannel mask

2. Cleaning and substrate preparation

First we have taken single side polished P-type silicon (100mm or 4inch) wafers with a resistivity of (3-10) ohms-cm, and orientation, <100> in all experiments for fabrication of gold electrode based DEP device. A two-step process for cleaning is carried out which includes (a) DI water rinsing and followed by (b) Piranha cleaning. Details of each steps are discussed in chapter 4 under Section 4.2.2.1.

3. Thermal oxidation

The very first step for fabrication of any MEMS device is thermal oxide growth. About $1\mu\text{m}$ thick oxide is grown on silicon substrate. Thermal oxidation process and parameters used are discussed in detail in Section 4.2.2.2. The grown oxide thickness of the samples was measured using the surface profilometer and was found to be of $\approx 1.01\mu\text{m}$ thickness as schematically shown in Figure B2(i).

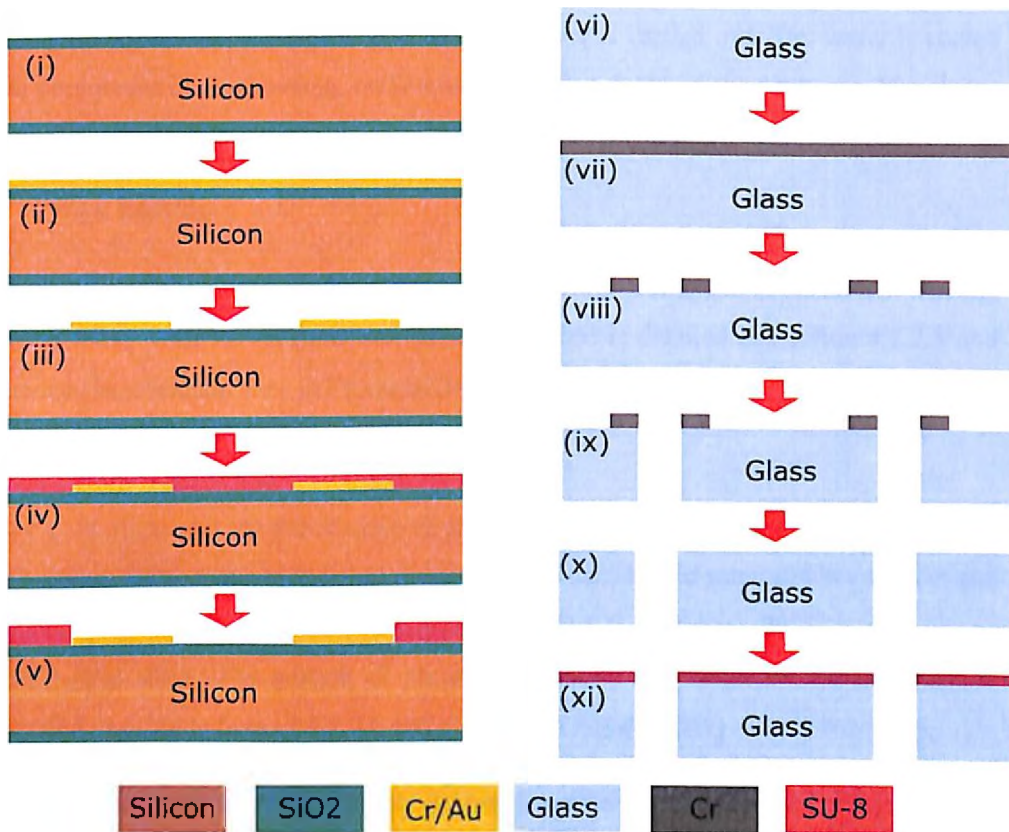


Figure B2: Schematic cross section view of the fabrication flow of circular gold electrode based DEP device (i) Oxide deposition on Si wafer (ii) Cr/Au deposition (iii) Au electrode patterning (iv) SU-8 coating (v) SU-8 microchannel after lithography, (vi) Clean glass wafer (vii) Cr deposition (viii) Cr patterning (ix) Glass drilling (x) Cr etching (xi) SU-8 coating for adhesive bonding.

4. Gold deposition

After thermal oxidation, the wafers were loaded for gold deposition. Thermal evaporation technique is used for deposition. The deposition was carried out with deposition rate of 0.2 nm/s. Followed by chrome deposition, a 200 nm gold layer was deposited as shown in Figure B2(ii) and discussed in Section 4.2.2.3.

5. Lithography

After gold deposition, the patterning of the gold layer is carried out. The wafer is coated with photoresist by spin coating technique. A detailed description of lithography process along with the parameters used is discussed in Section 4.2.2.4.

6. Cr/Au Etching

After patterning the Cr/Au, etching is carried out using wet bench process. The etching process along with the reagents and parameters used is detailed in Section 4.2.2.5 and illustrated in schematic view in Figure B2(iii).

7. SU-8 coating and microchannel patterning

After gold electrode, the SU-8 polymer is used for fabrication of the micro channel for DEP device. SU-8 is the material of choice for Bio-MEMS and microfluidics devices and requires simple processing, less fabrication time. SU-8 (Microchem, 2035) is used for the experimental work. The process of photoresist coating and microchannel patterning is discussed in detail in Section 4.2.2.6 and is shown in Figure B2(iv) and Figure B2(v).

8. Chrome coating and patterning onto glass substrate

A pyrex glass substrate of thickness $500\mu\text{m}\pm 25\mu\text{m}$ is used for closing of the microchannel as shown in schematic Figure B2(vi). The glass substrate is patterned to make an inlet/outlet for the fluidic flow. A chrome layer of 200 nm thickness is deposited using the E-beam evaporation technique as shown in schematic view of Figure B2 (vii). A schematic of the chrome pattern obtained after lithography is shown in Figure B2(viii) and is discussed in detail in Section 4.2.2.7.

9. Glass dicing and drilling

After patterning of the chrome layer, the glass substrate is diced and drilled. An ultrasonic drilling is used for making inlet/outlet of the microchannel. Schematic diagram of glass substrate with drilled inlet and outlet holes is shown in Figure B2(ix) and discussed in detail in Section 4.2.2.9.

10. Chrome etching

After drilling holes in the glass substrate at desired location, the chrome etchant is prepared to etch the chrome pattern. Typically chrome etchant are mixtures of perchloric acid (HClO_4), and ceric ammonium nitrate (CAN) powder is used for etching. Details of chrome etching is given in Section 4.2.2.8 and illustrated in schematic view in Figure B2(x).

Issues in Device Packaging

The last step after device fabrication is to package it. However, after fabrication of DEP device with circular electrodes, unfortunately we could not package the device with glass substrate. Therefore fabrication steps as shown in schematic diagram from Figure B2(ix) to B2(xi) could not be performed. Even after multiple trials for drilling inlet and outlet holes in the glass substrate with the help of ultrasonic drilling machine, the glass substrate got shattered each time. This was because the inlet and outlet ports were 1mm in diameter and was very near to each other and drilling holes in glass this close made it to crack again and again.

Although the other possible alternative to glass could be polydimethylsiloxane (PDMS). PDMS is one of the most widely used material for closing any microfluidic channel as it is cheap, transparent and can be cured into any shape with desired thickness. However closing the channel with PDMS requires prior treatment with O_2 plasma for reducing its hydrophobicity which is a time consuming process and also the plasma treated PDMS within 24hrs will become hydrophobic again if it is left in air. Hydrophobic regions can cause all sorts of problems with fluid flow like air bubble formation in the channel, protein adsorption etc. None the less, the channel sealed with PDMS often comes with an inevitable phenomenon of leakage and PDMS deformation. Because of the above mentioned issues, neither packaging the circular microelectrode DEP device with PDMS was desirable nor could the packaging with glass be achieved. Therefore we had to switch from circular electrode design to C-serpentine design.

CONDUCTIVE CARBON INK DATA SHEET

SILTECH CORPORATION INC

No-166, 5th Cross, 1st Main, South avenue layout
 Gottigere, B G Road, BANGALORE-83
 Tel/Fax 080- 65654565, 92430 81267, 98453 56726

PRODUCT DATA SHEET

CODE NO 060

DESCRIPTION : CONDUCTIVE CARBON PREPARATION NO. SIL.NO.060 is specially designed For screen printing application on flexible substrate like polyester, polycarbonate, Polyimide,etc It is a dispersion of fine carbon particles in a thermoplastics resin System

ADVANTAGES :
 Excellent flexibility
 Adheres well to both bare and ITO sputtered membrane touch key boards.
 Thixotropics nature provides good dispersion for excellent screen printing Characteristics

TYPICAL APPLICATION:

- 01 As a protective coating for silver and copper conductive lines.
 And pads on flexible and rigid circuit boards.
- 02 A low cost PTF- resistors in the additive circuits
- 03 In Bio-sensors
- 04 As a low cost heater

TYPICAL PROPERTIES (WET PRODUCT)

Pigment : Carbon
 Binder : thermoplastic
 Solvent : SILTECH THINNER
 Solid content : 70 %
 Viscosity (KCPS): 150-200 KCPS
 (at 25 °C, Brookfield Model RVT, Spindle No 7 spindle Speed 10 RPM.)

SELF LIFE: One years in unopened containers.

TYPICAL PROPERTIES AS CURED PRODUCT

SHEET RESISTIVITY : 250 ohm/sq. at one mil
 Coverage : 180-200 sq.cm/gm
 Film thickness : 12 microns

MIXING DILUTION This product is ready to use consistency. This product is applied by standard screen printing techniques. But should be mixed Thoroughly with a plastic spatual prior to each use. Mix smoothly from the Bottom of the container, being careful not to whip air into the product Using Plastic spatual will decrease the possibility of introducing plastic grinding From the container side walls into the product possibly clogging screens.

If necessary use SILTECH thinner for printable consistency.

APPLICATION

SCREEN : 150 - 325 Mesh Nylon/polyester Stainless steel
Squeejee Type : polyurethane
Emulsion thickness : 20-40 microns
Curing : 100^o C -30 minutes
Film thickness(325 mesh nylon after curing) : 10 microns
Storage : stored in a room temperature in a cool, dry place, and should not be Refrigerated

CLEAN UP

Screens may be cleaned up with MEK, acetone or other similar solvents

RESEARCH PUBLICATIONS

A. International Journals (Peer reviewed)

- 1 U Vidhya Devi, **Paridhi Puri**, NN Sharma, M Ananthsubramanian, "Electrokinetics of Cell in Dielectrophoretic Separation: A Biological Perspective", *J. BioNanoScience*, Springer, 4(3), Sept 2014, 276-287
- 2 **Paridhi Puri**, Vijay Kumar, M. Ananthasubramanian, N.N. Sharma "Design, simulation and fabrication of MEMS based dielectrophoretic separator for bio-particles". *Microsystem Technologies*, Springer, 23(8), Aug 2017, 3371-3379
- 3 **Paridhi Puri**, Vijay Kumar, Sachin U. Belganwar, M. Ananthasubramanian, N.N. Sharma "Microfluidic platform for dielectrophoretic separation of bio-particles using serpentine microelectrodes" *Microsystem Technologies*, Springer, Oct 2018, 1-8.
- 4 **Paridhi Puri**, Vijay Kumar, Sachin U. Belganwar, N.N. Sharma "Microfluidic device for cell trapping with carbon electrodes using dielectrophoresis" *Biomedical microdevices*, Springer, 20(4), Dec 2018, 102.

B. International Conferences

- 1 **Paridhi Puri**, U Vidhya Devi, M Ananthsubramanian, N.N. Sharma." Design and Simulation of Different Electrode Geometries for Cell Separation Using Dielectrophoresis". International conference on Emerging Technology.-Micro to Nano (ETMN-2013), at Goa, during Feb 23-24, 2013, pp.297-298.
- 2 U Vidhya Devi, **Paridhi Puri**, NN Sharma, M Ananthsubramanian, "Electrochemical Characterization of Biological Cells and its Dielectrophoretic Study for Selective Concentration and Separation", International conference on Emerging Technology. Micro to Nano (ETMN 2013), at Goa, during Feb 23-24, 2013, pp. 203-204
- 3 **Paridhi Puri**, Vijay Kumar, M. Ananthasubramanian, NN Sharma, "Study on MEMS Based Dielectrophoretic Separation of Bio-particles Using Circular Microelectrodes", Proc. of VIIth International Conf. on Smart Materials Structures and Systems, (ISSS 2014), IISc, Bangalore, 8-11 July, 2014, Bangalore.
- 4 **Paridhi Puri**, Vijay Kumar, M. Ananthasubramanian, NN Sharma, "Dielectrophoretic Separation of Bio-particles Using C-Serpentine Microelectrodes", International Conf. on Smart Materials Structures and Systems, (ISSS 2017), IISc, Bangalore, 5-7 July, 2017, Bangalore.

C. International Workshops

1. Participated in the 24th Hands on Training on PDMS Microfluidics and Micro and Nano Characterization Techniques conducted at the Centre for Nano Science and Engineering, Indian Institute of Science (CeNSc, IISc), Bangalore from 10th -18th March 2016.
2. Participated in 7th INUP Familiarization Workshop on Nanofabrication Technologies, conducted at IIT Bombay, from May 22-24, 2017.
3. Participated in international workshop on Nano/Micro 2D-3D Fabrication, Manufacturing of Electronic – Biomedical devices & Applications (IWNEBD-2018) 31st Oct. - 2nd Nov., 2018 at IIT. Mandi, presented poster “Registration of Cells using Dielectrophoresis in a C-Serpentine channel”.

Biography of Candidate

Paridhi Puri received the B.A.Sc (Bachelor of Applied Sciences) degree in Instrumentation from Shaheed Rajguru College of Applied Sciences for Women, Delhi University, New Delhi, India in 2010, and the M.Sc. degree in Bio-electronics and Instrumentation, Jamia Hamdard University, New Delhi, India in 2012. After completing my M.Sc. degree I joined the Micro Electro Mechanical System (MEMS) Laboratory under Mechanical Engineering Department, Birla Institute of Technology & Science, Pilani Campus, Pilani in August 2012 as a Research Fellow. My research interest includes areas of MEMS and microfluidic devices.

Biography of Supervisor

Dr. Sachin U. Belgamwar received his B.E. degree in Mechanical Engineering from Anuradha Engineering College, Chikhli, Amaravati University, India in 1999 and the M.E. and Ph.D Degree in Mechanical Engineering from Birla Institute of Technology and Science, Pilani, India, in 2001 and 2014 respectively. After working for six years in different engineering colleges, he joined the Mechanical Engineering Department, Birla Institute of Technology and Science, BITS-Pilani, Pilani Campus, Pilani, India in January 2007 as a Lecturer. Currently he is working as Assistant Professor in Mechanical Engineering Department and he also holds the position of Faculty-in-Charge, First Degree (FD) Admission at Birla Institute of Technology and Science, Pilani Campus, India.

Biography of Co-Supervisor

Prof. Niti Nipun Sharma completed his B.E. (Mechanical) from REC, Srinagar (now NIT, Srinagar) and M.E. (Mechanical) and Ph.D. both from BITS, Pilani. He is a faculty in Mechanical Engineering Department for over 17 years now currently serving as full Professor in Mechanical Engineering Department. Prof. Sharma served as visiting professor in EPFL, Switzerland during May-August 2014. He is first recipient of Kris Ramachandran best faculty award in 2010 at BITS, Pilani. Prof. Sharma specialized in Robotics and was a part of team which developed 'ACYUT', the humanoid from BITS. He later during his Ph.D. worked on dynamics of nanorobots proposed a simple method to include modeling of Brownian motion attributable to thermal agitation to predict the dynamics of Nanorobots. His methodology of analyzing synergism in local and global motion of non-rigid kind of nanoparticles due to thermal agitation from surrounding medium has recently been shown to model radiation of nanoparticle validating with Planck's Radiation Law.

Three patents, over 100 technical papers in high impact factor journals and peer reviewed National and International conferences, around two dozen invited/keynote talks in India and abroad and with ten funded projects from nodal agencies like DBT, UGC, CSIR-CEERI, NPMASS and Industries, currently Prof. Sharma is working in Interdisciplinary areas of MEMS and Nanotechnology.

He is Guest Editor, Journal of Bionanoscience (Springer), Associate Editor of International Journal of Smart Sensors and Intelligent Systems, has reviewed many articles for IEEE Tr. Systems, Man and Cybernetics, IEEE Tr. Education, has been on-board of many Technical Committees of reputed National and International Conference. He was co-chair for Int. Conf. on Emerging Technologies (ETMN-2013), International Conference on Emerging Mechanical Technology Macro to Nano (EMTM2N-2007), co-organized 2nd ISSS-MEMS-2007 conference with CEERI, Pilani and organized Northern Region NPMASS MEMS Software Training Program from 19-24 Feb. 2011.

Prof. Sharma also holds the post of Dean, Academic Registration & Counselling Division at BITS, Pilani since 2010 to 2015. Currently he is Professor and Pro-President at Manipal University Jaipur. He is also Associate Dean at Faculty of Engineering.